HEC MONTRÉAL
École affiliée à l'Université de Montréal

Goods Distribution with Electric Vehicles

par
Samuel Pelletier

Thèse présentée en vue de l'obtention du grade de Ph. D. en administration
(option Sciences de la décision)

Mai 2019

© Samuel Pelletier, 2019

HEC MONTRÉAL
École affiliée à l'Université de Montréal

Cette thèse intitulée :

Goods Distribution with Electric Vehicles

Présentée par :

Samuel Pelletier

a été évaluée par un jury composé des personnes suivantes :

Jean-François Cordeau
HEC Montréal
Président-rapporteur

Gilbert Laporte
HEC Montréal
Directeur de recherche

Ola Jabali
Politecnico di Milano
Codirectrice de recherche

Fausto Errico
École de technologie supérieure
Membre du jury

Grit Walther
RWTH Aachen University
Examinatrice externe

Justin Leroux
HEC Montréal
Représentant du directeur de HEC Montréal

Résumé

Au cours de la dernière décennie, le recours aux véhicules électriques de transport de marchandises (VÉTM) est devenu une option intéressante pour réduire les externalités négatives d'opérations logistiques. Bien qu'offrant des économies concernant les coûts d'énergie et de maintenance, l'utilisation de VÉTM s'accompagne de défis en ce qui a trait à leur coût d'acquisition, à leur autonomie et capacité limitées, et au temps requis pour le rechargement de leur batterie. Les décisions liées à l'achat, au routage et à l'ordonnancement du rechargement des VÉTM doivent donc être prises avec soin. Cette thèse tente de fournir des outils d'aide à la décision pour supporter le recours aux VÉTM en fonction de leurs caractéristiques clés. La contribution scientifique principale de cette thèse est d'introduire, de modéliser et de résoudre des problèmes de transport pratiques associés à l'intégration des VÉTM en logistique urbaine. La thèse est divisée en cinq articles comme suit.

Nous commençons, dans le premier article de la thèse, par une revue de la littérature sur l'utilisation des véhicules électriques pour la distribution des marchandises. Nous explorons ensuite, dans le deuxième article, l'état des lieux des batteries utilisées dans les véhicules électriques, ainsi que les méthodes permettant de modéliser la dégradation et le comportement de telles batteries. En fonction des conclusions tirées dans les deux premiers articles, nous introduisons trois problèmes d'optimisation concernant l'utilisation de VÉTM du point de vue opérationnel et stratégique: le problème d'ordonnancement du rechargement des

VÉTM, le problème de tournées de véhicules électriques avec consommation énergétique incertaine, et le problème de transition de la flotte électrique.

Les troisième et quatrième articles visent à résoudre des problèmes opérationnels résultant du fait qu'en milieu urbain, les VÉTM sont généralement rechargés dans un dépôt central et utilisent rarement des bornes de recharge en cours de route. Le problème d'ordonnancement du rechargement des VÉTM étudié dans le troisième article consiste à déterminer un horaire de rechargement au dépôt qui permette à une flotte de VÉTM d'accomplir leurs routes de livraison, tout en minimisant la somme des coûts associés à l'énergie, à la puissance maximale de rechargement requise, et à la santé des batteries. Nous focalisons ensuite, dans le quatrième article, sur l'élaboration d'itinéraires de livraison pour une flotte de VÉTM. Plus précisément, il s'agit d'un problème de tournées de véhicules électriques dans lequel est considérée l'incertitude reliée à la consommation énergétique des véhicules. Cette incertitude est prise en compte en faisant appel à des notions d'optimisation robuste, et une méthode heuristique basée sur l'approche de recherche à large voisinage est proposée pour résoudre le problème.

Alors que les deux articles précédents portent sur des décisions opérationnelles, le cinquième article de la thèse explore un problème associé aux VÉTM qui requiert des décisions plus stratégiques. Plusieurs entreprises et municipalités, que ce soit volontairement ou pour se conformer à des exigences légales, devront faire une transition vers des flottes plus électriques dans les années à venir. L'objectif du cinquième article est de concevoir un problème d'optimisation dont la résolution permettra à ces organisations de déterminer un plan à long terme qui respectera toutes leurs cibles d'électrification à moindres coûts.

Mots-clés

Véhicules électriques; transport de marchandises; problème de tournées de véhicules; transport vert; logistique urbaine; détérioration de batteries; modélisation de batteries; ordonnancement du rechargement; gestion de flotte.

Méthodes de recherche

Recherche opérationnelle; programmation linéaire mixte; optimisation robuste; métaheuristiques.

Abstract

Over the last decade, electric freight vehicles (EFVs) have emerged as interesting candidates to be used in logistics operations as a means of improving air quality. Although offering the advantage of lower energy and maintenance costs, these vehicles typically have autonomy and payload limitations, require much larger initial investments than internal combustion engine vehicles, and involve long recharging times. Therefore, fleet managers must make careful decisions about purchasing, charging and routing EFVs. The objective of this thesis is to provide a set of comprehensive decision tools supporting the use of EFVs while rigorously accounting for their pivotal characteristics. The main scientific contribution of this thesis is to introduce, model and solve practical transportation problems associated with the integration of EFVs in urban environments. The thesis is split into five papers as follows.

We begin with a review of the literature related to the use of electric vehicles for goods distribution in the first paper of the thesis. In the second paper of the thesis, we investigate how fundamental battery degradation and behaviour characteristics can be modeled in a tractable way. Based on the findings of the two first papers, we introduce three new optimization problems pertaining to EFVs from both an operational and a strategic planning perspective: the EFV charge scheduling problem (EFV-CSP), the electric vehicle routing problem with energy consumption uncertainty (EVRP-ECU), and the electric fleet transition problem (EFTP).

The third and fourth papers aim to solve operational-level problems resulting from the fact that EFVs are typically charged at a central depot and rarely use charging stations en route in urban environments. In the third paper, we consider the implications of this issue on charging decisions through the EFV-CSP, in which the charging schedule at the depot must be planned so as to allow a fleet of EFVs to complete their routes at minimal cost. We develop a comprehensive mathematical model for the EFV-CSP that incorporates a large variety of features associated with the use of EFVs. In the fourth paper, we turn our focus to the routing implications of only charging EFVs at the depot by introducing the EVRP-ECU, in which EFVs must be routed considering the realization of energy consumption uncertainties. We use a robust optimization approach to take into account such energy consumption uncertainties, and a large neighbourhood search metaheuristic is proposed to solve the problem.

While the previous two papers concern operational-level decision problems, the fifth article of the thesis considers a strategic planning problem associated with EFVs. Several companies and municipalities, either voluntarily or to comply with legal requirements, need to transition to electric fleets in upcoming years. The aim of the fifth paper is to introduce and solve a fleet replacement problem, i.e., the EFTP, that will allow such organizations to determine long-term transition plans respecting all their electrification targets in a cost-effective way.

Keywords

Electric vehicles; goods distribution; vehicle routing problems; green transportation; city logistics; battery degradation; battery modeling; charge scheduling; fleet management.

Research methods

Operations research; mixed integer programming; robust optimization; meta-heuristics.

Contents

Résumé iii

Abstract vii

List of Tables xvii

List of Figures xxi

List of acronyms xxiii

Acknowledgements xxvii

General Introduction 1

1 50th anniversary invited article – Goods distribution with electric vehicles: Review and research perspectives 13

Abstract 14

1.1 Introduction 14

1.2 Technological background 17

1.2.1 Electric vehicle types 17

1.2.1.1 Battery electric vehicles 17

1.2.1.2 Hybrid electric vehicles 18

1.2.1.3 Fuel cell electric vehicles 19

1.2.2 Batteries 20

1.2.2.1 Battery lifespan 24
1.2.2.2 Battery charging 25
1.3 Market penetration 28
1.3.1 Market Shares 28
1.3.2 Cost competitiveness 30
1.3.3 Incentives 33
1.3.3.1 Financial incentives 33
1.3.3.2 Prioritized access incentives 34
1.4 Electric vehicles in transportation science 35
1.4.1 Fleet size and mix 36
1.4.2 Vehicle routing 40
1.4.3 Optimal paths 46
1.5 Research perspectives 50
1.5.1 Strategic perspectives 51
1.5.2 Tactical perspectives 53
1.5.3 Operational perspectives 54
1.6 Conclusions 56
References 57

2 Battery degradation and behaviour for electric vehicles: Review and numerical analyses of several models **77**
Abstract 77
2.1 Introduction 78
2.1.1 Motivation for battery degradation modeling 79
2.1.2 Motivation for battery behaviour modeling 80
2.1.3 Aim and organization of this paper 84
2.2 Lithium-ion batteries 85
2.2.1 How lithium-ion batteries function 86
2.2.2 Performance assessment 88

2.3 Lithium-ion battery degradation 89
2.3.1 Degradation mechanisms and aggravating factors 91
2.3.2 Useful battery lifetime degradation models 94
2.4 Instantaneous battery behaviour modeling 105
2.4.1 Discharging 109
2.4.2 Charging 118
2.4.3 Simplifications 124
2.4.3.1 Time discretization 124
2.4.3.2 Constant open-circuit voltage 125
2.4.3.3 Peukert equation 130
2.5 Conclusions 132
2.6 Appendix A – Glossary 135
2.7 Appendix B – Parameter values 138
References 139

3 Charge scheduling for electric freight vehicles **155**
Abstract 155
3.1 Introduction 156
3.2 The EFV charge scheduling problem 160
3.2.1 Problem description 161
3.2.2 The battery charging process 162
3.2.3 Mathematical formulation 167
3.2.4 Two optimal solutions to the EFV-CSP 171
3.2.5 Deriving an equivalent solution in continuous time from the discrete time model 174
3.3 Incorporating battery degradation considerations 176
3.3.1 Cyclic aging 176
3.3.2 Calendar aging 183
3.4 Computational experiments and managerial insights 184

3.4.1 Description of the base-case scenario . . . 185
3.4.2 Base case results . . . 188
3.4.3 The impact of facility-related demand charges . . . 190
3.4.4 The impact of longer routes . . . 191
3.4.5 The impact of the grid restriction . . . 194
3.4.6 Using the model to select an energy rate plan . . . 196
3.4.7 The impact of battery size . . . 197
3.4.8 The impact of non-increasing cycling degradation costs . . . 199
3.5 Conclusions . . . 201
3.6 Appendix A – Glossary of abbreviations . . . 204
3.7 Appendix B – Incorporating general wear cost functions into the EFV-CSP . . . 204
References . . . 207

4 The electric vehicle routing problem with energy consumption uncertainty 213
Abstract . . . 213
4.1 Introduction . . . 214
4.2 Related literature . . . 216
4.3 The electric vehicle routing problem with energy consumption uncertainty . . . 219
4.3.1 Problem description . . . 220
4.3.2 Estimating the expected values of the arcs' uncertain energy consumption parameters . . . 221
4.3.3 Incorporating uncertainty . . . 224
4.3.4 Mathematical formulation . . . 226
4.3.5 Uncertainty sets . . . 228
4.4 Exact methods . . . 230
4.4.1 Reformulation . . . 231

4.4.2 Cutting-plane method 233
4.5 Two-phase metaheuristic 235
4.5.1 Initial solution construction 239
4.5.2 Removal operators 239
4.5.3 Insertion operators 241
4.5.4 Local search 242
4.5.5 Acceptance criterion 244
4.5.6 Checking robustness 245
4.5.7 Set partitioning phase 247
4.6 Computational experiments 249
4.6.1 Test instances and parameter tuning 250
4.6.2 Performance of the two-phase method on small EVRP-ECU instances 253
4.6.3 Performance of the two-phase method on large EVRP-ECU instances 255
4.6.4 Performance of the two-phase method on CVRP and RCVRP instances 259
4.6.5 The trade-off between cost and risk 263
4.6.6 The impact of correlation in routes 264
4.6.7 The impact of specific parameters in the energy consumption model 265
4.7 Conclusions 269
4.8 Appendix A – Detailed results for the CVRP and RCVRP benchmark instances 271
References 274

5 The electric fleet transition problem **283**
Abstract 283
5.1 Introduction 284

5.2 Literature review . . . 287
5.3 Deterministic problem description and formulation . . . 290
5.3.1 Mathematical formulation . . . 293
5.4 Stochastic formulation . . . 297
5.5 Computational experiments . . . 301
5.5.1 Description of the base-case scenario . . . 302
5.5.2 Base case results . . . 310
5.5.3 Sensitivity analysis for the deterministic EFTP . . . 311
5.5.3.1 En route charging configurations . . . 313
5.5.3.2 Charging infrastructure requirements for articulated electric buses . . . 316
5.5.3.3 Electrification targets . . . 319
5.5.3.4 Demand charges . . . 320
5.5.3.5 Energy prices . . . 322
5.5.3.6 Battery prices . . . 323
5.5.3.7 EV maintenance savings . . . 325
5.5.3.8 Robustness of choice to replace 40 ft diesel buses with electric buses . . . 326
5.5.3.9 Salvage values . . . 327
5.5.3.10 Depot upgrades for CNG buses . . . 330
5.5.3.11 Miscellaneous extensions . . . 333
5.5.4 The stochastic EFTP . . . 334
5.6 Conclusions . . . 337
References . . . 339

General Conclusion **343**

Bibliography **349**

List of Tables

1.1 Characteristics of BEVs, HEVs and FCEVs 20

1.2 Projections for other promising BEV battery technologies at pack level 23

1.3 BEV lithium-ion battery pack cost projections 2010-2030 24

2.1 Projections for current and other promising BEV battery technologies . 90

2.2 Overview of lithium-ion battery anode aging mechanisms 92

2.3 Key elements of presented battery degradation models 96

3.1 Variable and parameter definitions of the EFV-CSP model 168

3.2 Route parameters for the numerical example 171

3.3 Optimal solution 1: Keeping the FRD charge low 173

3.4 Optimal solution 2: Keeping the energy costs low 173

3.5 SOC intervals for cyclic aging model when $n_d = 10$ 179

3.6 Rates (\$/kWh) and monthly FRD charge (\$/kW) under the TOU-EV-4 plan 187

3.7 Battery wear cost function 188

3.8 Costs obtained when minimizing energy, degradation and FRD costs . 189

3.9 Costs obtained when minimizing energy and FRD costs 189

3.10 Costs obtained when minimizing energy and degradation costs 191

3.11 Costs obtained when minimizing energy, degradation and FRD costs for the scenario with one longer route per day 192

3.12 Costs obtained when minimizing energy, degradation and FRD costs for the scenario with two longer routes per day 193
3.13 Rates ($/kWh) and monthly FRD charge ($/kW) under the TOU-EV-3-B plan 194
3.14 The impact of the grid restriction on costs under plan TOU-EV-3-B . . 195
3.15 Cost comparison of the TOU-EV plan options 196
3.16 Comparison of costs obtained when minimizing energy, FRD and degradation costs with two different battery sizes 198
3.17 Non-increasing battery degradation costs 199
3.18 Costs and average periodic SOC before and after mitigating calendar aging 200

4.1 Vehicle, cost and expected energy consumption model parameter values 251
4.2 Uncertainty set parameter values 252
4.3 Two-phase heuristic parameter values 253
4.4 Results for the small instances with uncertainty sets U_k^3 and $\beta = 0.05$. 256
4.5 Results for the small instances with uncertainty sets U_k^4 and $\beta = 0.05$. 256
4.6 Results for the small instances with uncertainty sets U_k^5 and $\beta = 0.05$. 256
4.7 Results for the large instances with sets U_k^3, U_k^4 and U_k^5, and with $\beta = 0.05$ 258
4.8 Feasibility of best found nominal solutions and the price of robustness 259
4.9 Summarized results for the CVRP and RCVRP benchmark instances . 262
4.10 Best found solutions with different uncertainty sets and different protection levels 265
4.11 Best found solutions with sets U_k^5, $\beta = 0.01$, and different correlation levels 266
4.12 Nominal and worst-case energy consumption model parameter values used to assess the impact of specific parameters 267

4.13 Best found solutions with uncertainty sets U_k^5, $\beta = 0.01$, and different energy consumption model parameters' worst-case values used to compute $\hat{a}_{ij}$ and $\hat{b}_{ij}$ 269

4.14 Results for the set A of CVRP instances from Augerat (1995) and the associated RCVRP instances from Gounaris et al. (2013) 271

4.15 Results for the set B of CVRP instances from Augerat (1995) and the associated RCVRP instances from Gounaris et al. (2013) 272

4.16 Results for the set P of CVRP instances from Augerat (1995) and the associated RCVRP instances from Gounaris et al. (2013) 272

4.17 Results for the sets E, M, and F of CVRP instances and the associated RCVRP instances from Gounaris et al. (2013) 273

4.18 Results for the Christofides et al. (1979) and Golden et al. (1998) CVRP instances and the associated RCVRP instances from Gounaris et al. (2016) 273

5.1 Optimal transition plan for the base-case scenario 312

5.2 Optimal transition plans under different en route charging assumptions 316

5.3 Optimal transition plans under more stringent charging infrastructure requirements for articulated electric buses 318

5.4 Optimal transition plans under different electrification targets to be met by 2035 320

5.5 Optimal transition plans under different electrification target to be met by 2025 321

5.6 Optimal transition plans under different demand charges 322

5.7 Optimal transition plans under different oil price scenarios 324

5.8 Optimal transition plans under different battery price scenarios 325

5.9 Optimal transition plans under different EV maintenance savings assumptions 326

5.10 Optimal transition plans under base case bus-to-charger ratios, worst-case scenarios for EVs in terms of demand charges, battery prices, and maintenance savings, and without electrification requirements 328
5.11 Optimal transition plans under doubled base case bus-to-charger ratios, worst-case scenarios for EVs in terms of demand charges, battery prices, and maintenance savings, and without electrification requirements 329
5.12 Optimal transition plans under different salvage value assumptions . . 330
5.13 Optimal transition plans when depot upgrades are required prior to operating CNG buses 332
5.14 Optimal transition plans under miscellaneous extensions to the base-case scenario 334
5.15 Optimal solution to the assumed stochastic counterpart of the EFTP . . 337

List of Figures

2.1 Schematic representation of lithium-ion battery function 87
2.2 Overview of lithium-ion battery cathode aging mechanisms 93
2.3 Using capacity fade curves under varying conditions 99
2.4 Capacity loss for different storage SOC values at 25 degrees Celsius . . 100
2.5 Capacity loss for two different year long storage SOC profiles (SOC in blue, capacity lost in red) 101
2.6 Cycle life versus DOD 103
2.7 Cycle life versus fast charging rate 104
2.8 Simple battery equivalent circuit model, with current $i(t)$ direction reflecting discharging. 106
2.9 Plots of Equations (2.10), (2.11) and (2.12) 107
2.10 Typical constant current discharge curve 108
2.11 Schematic calculation of required battery power 111
2.12 Average energy shares in dependence of average trip speed 112
2.13 Numerical solutions of (2.24) for two different power profiles 114
2.14 Numerical example of voltage, current and SOC profiles according to speed profile 117
2.15 CC-CV charging scheme 119
2.16 Comparison of CC-CV charging profile for different current values in CC phase 121
2.17 Charging power during CC-CV charging scheme 123

2.18 Numerical solutions of (2.24) using a time step of 1 second for the same two power profiles of Figure 2.13. 126
2.19 Numerical solutions of (2.24) using a time step of 1 second and a constant open-circuit voltage for the same two power profiles of Figure 2.13. 128
2.20 Numerical solutions of (2.24) using a time step of 1 second for a constant power demand P_B when assuming a constant open-circuit voltage and a SOC dependent one 129

3.1 Comparison of CC-CV charging profiles for a lithium-ion battery cell with different current values in the CC phase 164
3.2 Piecewise linear approximation of a CC-CV charging process 166
3.3 Example of time-dependent energy costs 175
3.4 Illustration of $ACC(DOD)$ function for a lithium-ion battery 178
3.5 Results of accelerated calendar aging tests at various SOCs and temperatures 201

List of acronyms

AFS Alternative fuel station

AFV Alternative fuel vehicle

BEV Battery electric vehicle

CC Constant current

CNG Compressed natural gas

CV Constant voltage

CVRP Capacitated vehicle routing problem

DOD Depth of discharge

EFTP Electric fleet transition problem

EFV Electric freight vehicle

EFV-CSP Electric freight vehicle charge scheduling problem

EV Electric vehicle

EVRP Electric vehicle routing problem

EVRP-ECU EVRP with energy consumption uncertainty

FCEV Fuel cell electric vehicle

FRD Facility-related demand

GVW Gross vehicle weight

HEV Hybrid electric vehicle

ICE Internal combustion engine

ICEV Internal combustion engine vehicle

LEZ Low emission zone

LNS Large neighbourhood search

PEV Plug-in electric vehicle

PHEV Plug-in hybrid electric vehicle

RCVRP Robust capacitated vehicle routing problem

REEV Range extended electric vehicle

SOC State of charge

UCC Urban consolidation center

US DOE U.S. Department of Energy

US EIA U.S. Energy Information Administration

VRP Vehicle routing problem

To my parents, who believed in me when I no longer did.

Acknowledgements

It has truly been an honor and a privilege to work under the direction of Professors Ola Jabali and Gilbert Laporte. I cannot thank them enough for their guidance, availability, expertise, and trust. They consistently provided the perfect balance of supervision and freedom to allow me to fully develop as a researcher, and gave me the opportunity to present my work in several scientific conferences around the world. I will forever be grateful to them for their mentorship. I also thank Professor Vedat Verter for his support and valuable input as an external member of my Ph.D. committee.

Thanks are also due to Professors Jorge E. Mendoza and Marco Veneroni, with whom I had the pleasure of collaborating on two of the papers in this thesis. Their scientific advice has been of great value to me. I also wish to thank Professors Jean-François Cordeau, Fausto Errico and Grit Walther for agreeing to be a part of my thesis jury and providing valuable feedback on the contents of this thesis.

I am very grateful for the environment at HEC Montréal and at the Interuniversity Research Centre on Enterprise Networks, Logistics and Transportation (CIRRELT) in which I was fortunate enough to pursue my Ph.D. studies. It is impossible to enumerate all of the people I wish to mention from both of these institutions, but I sincerely thank every single staff member, professor, colleague and friend for their support.

I also wish to acknowledge the financial support offered by my advisors, the

Natural Sciences and Engineering Research Council, the Fonds de recherche du Québec – Nature et technologies, and the Institut de l'énergie Trottier. This project would have taken several additional years to complete without their generous support, for which I am very thankful.

Finally, I offer my deepest appreciation to my family and friends. I thank my parents Gérald and Antonia for their never-ending love and support. Few classical studies professors know more about goods distribution with electric vehicles than my mom – she read each article in this thesis. Thanks to my brother Joe and my friends Rick, Lis, Alex, Kev, Stef, Duke, Yan, and Pat for always being there to get my mind off my research. To Cat, thank you for your constant support and encouragement. You make waking up and coming home each day so wonderful.

General Introduction

In recent years, increasing attention has been paid to the use of electric freight vehicles (EFVs) as a means to yield green goods distribution practices. Global vehicle manufacturers began producing passenger electric vehicles around 2010, and global sales have been steadily increasing since then. However, the market for EFVs has not taken off as well, due to several factors. Indeed, there exist performance and financial issues associated with their integration into distribution schemes. These vehicles typically have autonomy and payload limitations, involve much larger initial investments than internal combustion engine vehicles (ICEVs), and operate on batteries that take a relatively long time to recharge and for which recharging infrastructures remain limited. On the other hand, companies using EFVs instead of conventional vehicles benefit from much lower energy and maintenance costs, a greener corporate image, and several local incentives for prioritized access that can yield significant cost and time savings. Moreover, there are important social benefits associated with a larger use of EFVs in urban logistics, namely reductions in local air and noise pollution.

At its core, the objective of this thesis is to leverage the power of operations research to support the use of EFVs by both capitalizing on the opportunities they present, and mitigating the obstacles they face when they are used in goods distribution operations. This is achieved first, by conducting an extensive literature review, and subsequently, by introducing and solving practical optimization problems involving EFVs at both operational and strategic planning levels based

on the identified background information. In what follows we briefly discuss the existing research that is relevant to the field of goods distribution with electric vehicles before introducing the five scientific papers that constitute this thesis.

Existing research

Due to the potential societal benefits associated with EFVs, several researchers have tackled optimization problems involving their use, in which case the specifities of the vehicles must be taken into account. Although the relevant literature is reviewed in each of the papers that constitute this thesis, the following is a non-exhaustive summary of the main transportation science literature on EFVs as it relates to vehicle routing, fleet size and mix, optimal paths, charging infrastructure design, depot charge scheduling, and fleet replacement. Moreover, because new studies have appeared after our papers were published, we refer to some of them in what follows as a means of updating the main literature review of the thesis, undertaken in the paper appearing in Chapter 1.

Vehicle Routing

Many authors have worked on electric vehicle routing problems (EVRPs) to deal with the routing issues associated with EFVs (especially those stemming from their limited range), and have proposed models and algorithms for the optimization of routes that incorporate en route recharging. There are thus both customer nodes and charging station nodes in the graphs associated with many EVRPs. The main objective in these studies is to determine feasible delivery routes for a fleet of EFVs so as to serve all customers and minimize costs or the number of vehicles used.

As the field has expanded over the last few years, the features considered in such routing problems are becoming increasingly realistic. The models proposed in earlier studies (e.g., Erdoğan and Miller-Hooks, 2012; Schneider et al., 2014) included several simplifying assumptions pertaining to energy consumption, charging processes, and charging infrastructures, but subsequent studies have included other features, for example,

- partial charging (Bruglieri et al., 2017; Keskin and Çatay, 2018);
- non-linear charging functions (Montoya et al., 2017; Froger et al., 2019);
- networks with multiple types of chargers (Felipe et al., 2014);
- realistic energy consumption models (Preis et al., 2014; Basso et al., 2019);
- capacitated charging stations (Froger et al., 2017);
- shared charging stations by several organizations (Koç et al., 2019);
- two-echelon delivery schemes (Breunig et al., 2019; Jie et al., 2019);
- time-dependent waiting times at charging stations (Keskin et al., 2019).

Some authors have also studied EVRPs from a more strategic planning perspective by incorporating both routing and charging infrastructure location decisions in their models, e.g., Yang and Sun (2015), Hof et al. (2017), Schiffer and Walther (2017a, 2017b, 2018), Schiffer et al. (2018). Electric vehicles in pickup and delivery as well as dial-a-ride operations have also been recently considered by Goeke (2019) and Bongiovanni et al. (2019), respectively. The traveling salesman problem has also been approached with electric vehicles and en route recharging in mind (e.g., Roberti and Wen, 2016). Others have instead considered hybrid electric vehicle routing problems, where in addition to having the possibility of charging en route, the vehicles can change propulsion modes as well (e.g., Abdallah, 2013; Mancini, 2017). As a testimony to the popularity of the field of electric

vehicle routing, there are even new surveys on electric vehicle routing problems that have been published since our 2016 paper (i.e., Chapter 1 of this thesis). We therefore refer readers to Bektaş et al. (2018) and Erdelić and Carić (2019) for more recent discussions on EVRP variants.

Fleet size and mix

The fleet size and mix studies pertaining to the use of EFVs are similar to the routing studies, but with the additional feature of having the possibility of using different types of vehicles. The objective thus becomes to determine both the delivery routes and the fleet composition. Vehicles may have different characteristics pertaining to energy storage capacity, energy consumption, load capacity, and fixed and variable costs. While some fleet size and mix studies incorporating EFVs either do not consider battery charging (van Duin et al., 2013), assume charging can occur anywhere (Gonçalves et al., 2011) or only at the depot (Lebeau et al., 2015), others have considered the possibility for the vehicles to stop at charging stations during their routes, and have taken into account the actual location of the stations (e.g., Goeke and Schneider, 2015; Sassi et al., 2015; Hiermann et al., 2016; Villegas et al., 2018; Macrina et al., 2019; Hiermann et al., 2019). The different problems considered also vary in similar fashion to the EVRP variants (e.g., simplified or realistic energy consumption models, partial or full charging, etc.).

Optimal paths

Although most optimal path studies incorporating electric vehicles are undertaken with passenger vehicles in mind, they are nevertheless relevant to the issue

of optimal routing of EFVs. Indeed, several studies have focused on the case of a single electric vehicle traveling from an origin to a destination by trying to determine an optimal path with respect to energy consumption, cost or time without the possibility of charging along the way (e.g., Artmeier et al., 2010; Eisner et al., 2011; Sachenbacher et al., 2011). The problem is therefore a constrained shortest path problem, in which the battery charge is bounded by its capacity. Moreover, energy recuperation is often considered in such studies, and certain edges of the graph may therefore have negative costs in terms of energy consumption. Fontana (2013) has also considered uncertainties related to travel time and energy consumption when determining optimal paths for electric vehicles without en route recharging.

On the other hand, some optimal path studies with electric vehicles have integrated the idea of allowing the battery to be recharged along the path. Zündorf (2014) attempted to minimize the sum of travel and charging times to get from an origin to a destination with an electric vehicle, while considering different types of charging stations and non-linear charging functions. Sweda et al. (2016) have studied the problem of determining optimal charging policies along a predetermined path which are cost effective and improve battery longevity. This problem was extended in Sweda et al. (2017) by taking into account the uncertainty surrounding charging station availability, and the selection of the path. Arslan et al. (2014) have integrated plug-in hybrid electric vehicles into the minimum cost path problem, in which case the vehicles can stop at both charging and refueling stations along the path. Strehler et al. (2017) also considered hybrid electric vehicles in their energy-efficient path problem, and added the possibility of converting fossil fuel to electricity while driving along edges.

Charging infrastructure design

A larger charging infrastructure is considered to be a factor that could significantly increase the adoption of electric vehicles in road transportation, however the large investments required to provide this infrastructure makes locating the right number of stations at the right places crucial (Touati-Moungla and Jost, 2012). For this reason, quite a few studies have considered the problem of optimally locating or designing electric vehicle charging infrastructures (Dong et al., 2014; Frade et al., 2011; González et al., 2014; He et al., 2013; Mak et al., 2013; Nie and Ghamami, 2013; Wang et al., 2016; Xu et al., 2013; Rogge et al., 2018; Yıldız et al., 2019). As for the optimal path studies, many charging infrastructure studies are not explicitly performed with EFVs in mind, but are still relevant since larger and faster charging infrastructures would facilitate the use of EFVs outside of urban environments (e.g., for mid- and long-haul goods distribution).

Depot charge scheduling

The issue of depot charge scheduling for EFVs has received less attention than the routing component, but it nevertheless raises interesting challenges whose solution could facilitate the integration of EFVs in goods distribution schemes. Many companies using EFVs prefer charging the vehicles at their own facilities because of a combination of factors, in which case the specifities of the commercial electricity rate plan offered at the depot should be accounted for. Two relevant studies in the context of depot charge scheduling for EFVs are those of Sassi and Oulamara (2014a, 2014b), in which a fleet of electric and conventional vehicles must be assigned to a set of predetermined routes so as to maximize the usage of the electric vehicles and minimize the cost of the charging schedule.

Fleet replacement

Fleet replacement studies treat problems in which decisions regarding purchasing and salvaging of fleet vehicles must be made over the course of a discretized planning horizon. Feng and Figliozzi (2013) developed a deterministic fleet replacement optimization model for fleets with electric and diesel trucks in which vehicles can be purchased and resold on a yearly basis. The objective is to minimize the discounted sum of all costs while answering each year's travel demand in miles. Ahani et al. (2016) subsequently revisited this problem, but modified the objective so as to minimize the sum of deterministic total costs and of the weighted variance of total costs when purchase and energy costs are assumed to be uncertain. Bakır (2017) considered a multi-period deterministic long-haul trucking context in which alternative fuel vehicles (AFVs) must be introduced into a fleet of diesel trucks. Islam (2018) introduced a fleet replacement model for transit agencies similar to that of Feng and Figliozzi (2013), with the addition of emissions constraints, an electrification target at the end of the planning horizon, and the need for charging infrastructure investments. A few fleet replacement studies also assume that fleet vehicles are leased for a fixed period of time rather than purchased, thus removing reselling decisions (e.g., Ansaripoor et al., 2016; Kleindorfer et al., 2012).

Scientific articles in this thesis

This thesis is a collection of five contributions that were written as scientific papers. The first four papers have been published, and the fifth is still under review. The five papers are briefly described in what follows, and publication details are given for each paper at the beginning of their associated chapter in the thesis.

Paper 1: 50th anniversary invited article – Goods distribution with electric vehicles: Review and research perspectives

In the first paper of the thesis, we conduct an extensive review of the literature related to the use of EFVs for goods distribution in order to provide transportation researchers with an overview of the technological background and market penetration information needed to conduct research in this area, to present a survey of the existing research in this emerging field, and to offer perspectives for future research. The technological background portion of the paper presents the pros and cons pertaining to different types of electric vehicles, as well as the main issues associated with the batteries such vehicles rely on. The market penetration analysis describes non-technological issues surrounding the adoption of EFVs, the key factors that influence their cost competitiveness, and the types of incentives that can be offered to companies employing them. The main transportation science literature on EFVs available at the time is summarized, and research perspectives are discussed at the strategic, tactical and operational levels.

Paper 2: Battery degradation and behaviour for electric vehicles: Review and numerical analyses of several models

Electric vehicles operate on batteries that have a limited life, as well as specific charging and discharging patterns that need to be considered in the context of their use for goods distribution. While many transportation problems associated with the integration of EFVs in distribution management problems had already been investigated at the time of writing the second paper, there was room for further research on specifically how to model battery degradation and behaviour in such problems. The aim of the second paper of the thesis is therefore to provide

tractable models for transportation scientists that will allow predicting the lifetime degradation and instantaneous charging and discharging behaviour of electric vehicle batteries. Empirical approaches are determined to be most tractable for taking into account battery degradation considerations, while equivalent circuit models are found to be a practical method for considering fundamental battery behaviour during charging and discharging.

Paper 3: Charge scheduling for electric freight vehicles

In the third paper, we consider a charge scheduling problem for EFVs. In an urban environment, EFVs are typically charged at a central depot and rarely use charging stations en route. Therefore, the charging schedule at the depot must be planned ahead of time so as to allow the vehicles to complete their routes at minimal cost. Vehicle fleet operators are subject to commercial electricity rate plans, which should be accounted for in order to provide an accurate estimation of the energy-related costs and restrictions. In addition, high vehicle utilization rates can accelerate battery aging, thereby requiring degradation mitigation considerations. We therefore develop a comprehensive mathematical model that incorporates a large variety of features associated with the use of EFVs. These include a realistic charging process, time-dependent energy costs, battery degradation, grid restrictions, and facility-related demand charges. Extensive numerical experiments are conducted in order to draw managerial insights regarding the impact of such features on the charging schedules of EFVs.

Paper 4: The electric vehicle routing problem with energy consumption uncertainty

The fourth paper tackles an electric vehicle routing problem with uncertainties surrounding the energy consumption of the vehicles. As previously mentioned, in urban areas, EFVs must often perform the entirety of their delivery routes without recharging. However, their energy consumption is subject to a fair amount of uncertainty, which is due to exogenous factors such as the weather and road conditions, endogenous factors such as driver behaviour, and several energy consumption parameters that are difficult to measure precisely. We therefore propose a robust optimization framework to take into account these energy consumption uncertainties in the context of an electric vehicle routing problem. The objective is to determine minimum cost delivery routes capable of providing strong guarantees that a given vehicle will not run out of charge during its route. Small instances are solved to optimality using robust optimization techniques, and we develop a two-phase heuristic method based on large neighbourhood search to solve larger instances of the problem. Computational experiments illustrate the quality of the methodology and the influence of several parameters on best found solutions.

Paper 5: The electric fleet transition problem

The final paper adopts a more strategic planning perspective. Several organizations need to transition to greener fleets in the next decades, and have chosen electric vehicles to achieve this goal. Such transitions are often established by temporal targets, which dictate the number of electric vehicles that should be in the fleet by a given time period. In the final paper of the thesis, we present a fleet

replacement problem which allows organizations to determine long-term vehicle replacement plans respecting their fleet electrification targets in a cost-effective way. We model the deterministic and stochastic forms of the problem as an integer linear program and a mixed integer linear program, respectively. Although we consider a public transit context for the case study presented in the paper because we had access to real data from a transit agency, the problem is intentionally formulated so as to be applicable to both goods distribution and public transit contexts.

Chapter 1

50th anniversary invited article – Goods distribution with electric vehicles: Review and research perspectives

Chapter information

This article is the result of a collaboration with my thesis advisors. It was published in *Transportation Science*: S. Pelletier, O. Jabali, G. Laporte. 2016. 50th anniversary invited article – Goods distribution with electric vehicles: Review and research perspectives. *Transportation Science* **50**(1) 3–22.

Abstract

Since the mid-2000s, electric vehicles have gained popularity in several countries even though their market share is still relatively low. However, most gains have been made in the area of passenger vehicles and most technical and scientific studies have been devoted to this case. By contrast, the potential of electric vehicular technology for goods distribution has received less attention. The issues related to the use of electric vehicles for goods distribution reveal a wide range of relevant research problems. The aims of this survey paper are to provide transportation researchers an overview of the technological and marketing background needed to conduct research in this area, to present a survey of the existing research in this field, and to offer perspectives for future research.

Keywords: electric vehicular technology; batteries; vehicle routing; market penetration; incentives; green transportation; city logistics.

1.1. Introduction

Green logistics encompasses the set of practices aimed at controlling environmental externalities in logistics operations (Psaraftis, 2016). The study of this relatively new field has increased in popularity since 2010, as witnessed by the growing number of publications on green transportation (Demir et al., 2014) and city logistics (Gonzalez-Feliu et al., 2014), as well as conference presentations. Research on green transportation has focused on the pollution-routing problem (Bektaş and Laporte, 2011), which seeks to design optimal vehicle routes in which routing costs and polluting emissions are jointly minimized. City logistics proposes ways of reducing pollution in urban environments, such as forbidding or

restricting the use of heavy vehicles in city centers. Research in these fields focuses on the design of distribution policies that will help diminish the environmental impact of goods distribution. Since 2010, we have witnessed an increased interest in topics such as vehicle fleet composition in green logistics (e.g., Kopfer and Kopfer, 2013; Kopfer et al., 2014; Koç et al., 2014; Goeke and Schneider, 2015; Sassi et al., 2015a; Lebeau et al., 2015). In the same vein, increasing attention is being paid to the use of electric vehicles (EVs) as a means to yield green distribution practices.

The market share of electric cars is insignificant in most countries, with the possible exceptions of Norway and the Netherlands (Mock and Yang, 2014). Electric vans and trucks are even more rare because of several real or perceived factors related to cost, driving range, payload, reliability, and availability. Electric trucks operate on batteries that have a limited life and are characterized by high costs as well as specific degradation and charging patterns, which must be taken into account in fleet size and mix decisions. In addition, because the number of electric recharging stations is still small compared with that of conventional fuel stations, the limited range of EVs becomes a critical constraint in purchasing and operational decisions. However, when coupled with interesting incentives, EVs can sometimes become an attractive option for goods distribution. As Taefi et al. (2016, p. 497) point out, "many initiatives are driven by companies' awareness of regulations for less environmentally-friendly vehicles becoming more restrictive in the future". Deployment of electric freight vehicles should therefore not be automatically associated with profitability, but rather with exploration and preparation in anticipation of expected future developments.

Several project reports provide examples of practices with EVs for goods distribution, most of these in Europe. In North America, large companies using EVs include FedEx, General Electric, Coca-Cola, UPS, Frito-Lay, Staples, Enterprise, Hertz, and others (Electrification Coalition, 2013). Many U.S. companies operat-

ing electric trucks received financial support from the American Recovery and Reinvestment Act to reduce the vehicles' purchase costs (US DOE, 2013b). One of project FREVUE's reports (Nesterova et al., 2013) provides overviews of European companies and projects using these vehicles. The same report also points to two-phase delivery as an interesting logistics concept for electric freight vehicles, where goods are first brought to a logistics facility near the denser urban area by conventional trucks before being transferred to the EVs for last mile deliveries. When multiple organizations use the same facility, this is known as an urban consolidation center (UCC), defined as "a logistics facility situated in relatively close proximity to the geographic area that it serves (...), to which many logistics companies deliver goods destined for the area, from which consolidated deliveries are carried out within that area, in which a range of other value-added logistics and retail services can be provided" (Allen et al., 2007, p. 61). Examples of a UCC using EVs are available in Vermie (2002); Allen et al. (2007); van Duin et al. (2010); E-Mobility NSR (2013); and Nesterova et al. (2013).

Issues related to the use of EVs for goods distribution reveal a wide range of relevant research problems. This paper is designed to provide transportation researchers an overview of the technological background and market penetration information needed to conduct research in this area, to present a survey of the existing research in this emerging field, and to offer perspectives for future research. It is organized as follows. Section 1.2 describes the vehicle technology, including vehicle types and batteries. Section 1.3 provides information on the market penetration of EVs as well as their cost competitiveness and adoption incentives. Section 1.4 provides an overview of existing research on EVs in transportation science. It covers three topics: fleet size and mix, vehicle routing, and optimal paths. Section 1.5 suggests several promising research perspectives. It is organized around strategic, tactical, and operational transportation science issues. The paper closes with some thoughts on the current state of the field and

the future of electric vehicle use in Section 1.6.

1.2. Technological background

This section provides a classification of electric vehicle technology under two main headings: electric vehicle types and batteries.

1.2.1 Electric vehicle types

EVs are generally divided into battery electric vehicles (BEVs), hybrid electric vehicles (HEVs), and fuel cell electric vehicles (FCEVs). An advantage of BEVs and HEVs is their ability to use their electric motor for regenerative braking to recuperate kinetic energy (Larminie and Lowry, 2003). FCEVs can also allow for regenerative braking if a battery is used to assist the fuel cell (Emadi et al., 2005). While this paper focuses on goods distribution with BEVs, the main characteristics of each of these electric vehicle types are discussed below and summarized in Table 1.1.

1.2.1.1 Battery electric vehicles

A BEV is propelled by an electric motor and only uses the power provided by its battery pack, which can be charged from the electricity grid (Electrification Coalition, 2013). The benefits associated with BEVs include the absence of tailpipe emissions, high tank-to-wheel efficiency, as well as much less operating noise than internal combustion engine vehicles (ICEVs). Technical disadvantages include a relatively low achievable range and the considerable amount of time required for charging their batteries (Pollet et al., 2012). Their motors can produce

great torque at low speeds and are much more efficient than ICEVs (MacLean and Lave, 2003). BEVs also require less maintenance than ICEVs, partly because they do not have as many moving parts and do not need oil changes (Feng and Figliozzi, 2013). Maintenance costs are further reduced because the frictionless regenerative braking allows for less brake wear (Lee et al., 2013). Typical ranges vary from 100 to 200 kilometers for freight BEVs (Nesterova et al., 2013; AustriaTech, 2014) and have been reported to diminish with time due to battery aging (Taefi et al., 2016). Other factors that temporarily reduce vehicle range include extreme temperatures, high speeds, quick acceleration, carrying heavy loads, and upward slopes (US DOE, 2012b). A lithium-ion battery pack, the leading battery technology for BEVs, requires a battery management system to ensure that it is used in a safe and reliable way (Waag et al., 2014). Battery weight generally reduces maximum payload for freight BEVs compared to equivalent ICEVs (E-Mobility NSR, 2013).

1.2.1.2 Hybrid electric vehicles

HEVs use an internal combustion engine (ICE) and an electric motor for propulsion as well as a battery pack for electrical energy storage (US DOE, 2013a). They can be classified according to the function of their electric motor, their powertrain architecture or their capacity to be plugged into an electricity grid to charge their batteries (Chan, 2007).

While the electric motor in micro-hybrids is mainly used as a start/stop system to reduce fuel consumption, it can also be used to provide modest and strong propulsion assistance to the ICE in mild and full hybrids, respectively, with the latter category also providing limited electric propulsion, i.e., with the ICE turned off (Karden et al., 2007).

Full HEVs can be further classified according to their powertrain architectures

(Tie and Tan, 2013). In a series configuration, the ICE is only used to power a generator and the electric motor is the only propulsion component coupled to the final drive shaft. A parallel configuration allows for both the ICE and the electric motor to be coupled to the final drive shaft and used simultaneously or individually (Chan, 2007). While the former offers a simpler design, the latter is more efficient due to fewer energy conversions, and does not require its components to be sized for maximum power demands (Chan, 2007). A series-parallel configuration combines both previous architectures (i.e., inclusion of a generator and ICE coupled to the drive shaft), while a complex configuration grants additional operating modes via the possibility of using the generator as a supplementary electric motor (Chan, 2007).

Finally, a full HEV with a battery that can be charged from the electricity grid is referred to as a plug-in HEV (PHEV) (Tie and Tan, 2013). PHEVs use larger batteries than standard HEVs (but smaller than BEVs) and can achieve an electric range in the lines of 30 to 60 kilometers with lithium-ion batteries (Chan, 2007). A series PHEV is sometimes referred to as a range extended electric vehicle (REEV) (CALSTART, 2013b). The term plug-in electric vehicle (PEV) is also used to designate electric vehicle types that can be charged with electricity from the grid, i.e., BEVs and PHEVs (Electrification Coalition, 2013).

1.2.1.3 Fuel cell electric vehicles

In an FCEV, a fuel cell stack generates electricity from the chemical energy of hydrogen, from which the output is water, which then powers the motor or charges a battery (Chan, 2007). The hydrogen must be stored on-board either in gaseous or liquid states, or through physical or chemical adsorption (den Boer et al., 2013). FCEVs can be refueled in a few minutes and can achieve ranges of several hundred kilometers with compressed gaseous hydrogen storage tanks (Eberle and von Helmolt, 2010). FCEVs also offer reduced operating noise (Emadi et al., 2005),

but are less efficient than BEVs from a tank-to-wheel perspective (den Boer et al., 2013). Fuel cells have efficiencies of approximately 50% in terms of the proportion of the hydrogen's energy being converted to electricity (US DOE, 2013a) and could also be used as auxiliary power units in conventional trucks (Emadi et al., 2005). The cost of FCEVs is an important market barrier (Shulock et al., 2011), as is the fuel cell's durability which is currently 10,000 operating hours at best (den Boer et al., 2013). A battery or ultracapacitor pack is usually used in a FCEV to store the regenerative braking energy and to assist the fuel cell stack during load variations that it cannot handle by itself (Emadi et al., 2005). Ultracapacitors, which have a much higher power density than batteries, might also be used alongside batteries in BEVs and HEVs (Khaligh and Li, 2010).

Table 1.1 – Characteristics of BEVs, HEVs and FCEVs
(Source: Chan, 2007)

EV types	BEVs	HEVs	FCEVs
Propulsion	Electric motor	Electric motor and ICE	Electric motor
Energy storage	Battery pack (possibility to combine with ultracapacitor)	Fuel tank and battery pack (possibility to combine with ultracapacitor)	Fuel cell stack and battery/ultracapacitor pack for power assistance
Characteristics	High tank-to-wheel efficiency Relatively short driving range High cost Zero tailpipe emissions	Higher fuel economy than ICEVs Long driving range Higher cost than ICEVs Several configurations	High tank-to-wheel efficiency Satisfying driving range High cost Zero tailpipe emissions
Issues	Battery properties and management Charging infrastructure Purchase cost	Multiple energy sources control, optimization and management Charging infrastructure (for PHEVs)	Fuel cell cost, duration and reliability Hydrogen infrastructure

1.2.2 Batteries

Currently available options for batteries in EVs are lead-acid batteries, nickel-metal-hydride batteries, sodium-nickel-chloride batteries (also called ZEBRA batteries), and lithium-ion batteries (Yong et al., 2015). Because lithium-ion batteries have a high specific energy, high specific power, long cycle life, and low mem-

ory effect (Lukic et al., 2008), they are the most commonly used alternative for modern passenger and freight BEVs (den Boer et al., 2013). Lithium-ion batteries are also the leading option for PHEVs, but nickel-metal-hydride batteries are still used in non-plug-in HEVs, which do not require such a high specific energy (Cluzel and Douglas, 2012). Lead-acid batteries have an even lower specific energy and are thus limited to low performance BEVs and micro-HEVs (Gerssen-Gondelach and Faaij, 2012). ZEBRA batteries have a good specific energy and have been used in earlier freight BEVs (Nesterova et al., 2013), but their low specific power and very high operating temperature are important drawbacks compared to lithium-ion batteries (Gerssen-Gondelach and Faaij, 2012).

Several materials can be used in lithium-ion batteries. Each type has pros and cons as to attributes such as energy, power, safety, and lifespan. In current lithium-ion batteries, the cathode typically consists of a lithium metal oxide or lithium iron phosphate compound; graphite is commonly used for the anode (Cluzel and Douglas, 2012). Battery weight in particular is a key consideration for goods distribution with BEVs since it forces trade-offs to be made between payload and range. The amount of energy that a battery can deliver varies according to certain operating conditions (e.g., temperature and discharge current), and hence so does its energy content per unit of mass (Larminie and Lowry, 2003). Nevertheless, approximate values can be helpful for comparison purposes with other fuel types. Current lithium-ion cells for BEVs have a specific energy ranging from 100 to 180 Wh/kg, depending on the materials used (Cluzel and Douglas, 2012). While future lithium-ion cells' specific energy could reach 300 Wh/kg, development of technologies such as lithium-sulfur (Li-S) and lithium-air (Li-air) batteries should allow reaching values above 500 Wh/kg (Bruce et al., 2012). Zinc-air (Zn-air) batteries are another option in development that could improve specific energy (Yong et al., 2015).

Furthermore, the cells must be assembled into modules and then into a bat-

tery pack. The pack's specific energy is thus lower due to the additional packaging components. The pack can have a specific energy up to 40% lower than the cells, typically ranging between 80 and 120 Wh/kg for BEVs (Dinger et al., 2010). Lithium-ion battery packs for BEVs could reach 200 Wh/kg by 2025 (Gerssen-Gondelach and Faaij, 2012). Duleep et al. (2011) expect lithium-sulfur batteries to be commercialized between 2025 and 2030 with at least three times the specific energy of 2010 lithium-ion batteries. Projections for other potential BEV battery types are provided in Table 1.2 but these do not imply that their issues will necessarily be resolved by 2025. Lithium-air batteries in particular are much less developed and thus considered to be a longer term solution (Gerssen-Gondelach and Faaij, 2012). Several battery electric truck manufacturers have opted for some form of lithium iron phosphate compound for the cathode in their vehicles' lithium-ion battery (e.g., Balqon Corporation, 2013; Boulder Electric Vehicle, 2013). Lithium iron phosphate batteries typically provide good safety and lifespan attributes compared to other options (Dinger et al., 2010), as well as a specific energy ranging from 80 Wh/kg to 100 Wh/kg at the pack level (Thackeray et al., 2012).

Diesel fuel, on the other hand, has a specific energy of approximately 12,500 Wh/kg (ACEA, 2013). Even taking into account the fuel tank's weight in ICEVs and the fact that battery electric trucks can be three to four times more efficient than similar diesel trucks from a tank-to-wheel perspective (Gallo and Tomić, 2013; Lee et al., 2013), the difference in energy actually being used to turn the wheels per kilogram of the on-board energy storage system remains significant.

While specific power is considered an issue for other potential battery technologies for BEVs (see Table 1.2), this is not so much the case for lithium-ion batteries since they can already offer similar power capabilites as ICEs (Dinger et al., 2010). The specific power of current lithium-ion cells can take many values according to design trade-offs between specific power and specific energy

(e.g., PHEVs require significant power from smaller batteries), thus ranging from roughly 200 W/kg to 2,000 W/kg (Cluzel and Douglas, 2012). Lithium-ion battery packs in current BEVs should provide approximately 400 W/kg, with 500 W/kg expected by 2025 (Gerssen-Gondelach and Faaij, 2012).

Table 1.2 – Projections for other promising BEV battery technologies at pack level (Source: Gerssen-Gondelach and Faaij, 2012)

Battery type		Li-S	Zn-air	Li-air
Specific energy (Wh/kg)	2025	400	250	500
	Beyond 2025	500	350	1,000
Specific power (W/kg)	2025	300	Unknown	Unknown
	Beyond 2025	400	Unknown	Unknown
Cost ($/kWh)	2025	Highly uncertain	Highly uncertain	Highly uncertain
	Beyond 2025	250–500	100–300	350–700
Issues		Safety Cycle life	Specific power Charge/discharge efficiency	Specific power Cycle life Safety

The lithium-ion battery pack is also the main reason for the substantial cost premium of BEVs (Electrification Coalition, 2013). However, significant improvements in battery costs are expected due to manufacturing and technological advancements (Hensley et al., 2012). Battery cost estimates vary considerably, but cost intervals are given in Table 1.3 for BEV lithium-ion battery packs by using lower and upper bounds from a few sources. Gerssen-Gondelach and Faaij (2012) have also made a few long-term cost projections for other promising battery types (see Table 1.2). Batteries in larger freight BEVs may be somewhat less costly since forecasts are usually for passenger BEV batteries, and costs per kWh in larger packs decrease because of certain fixed packing costs (Cluzel and Douglas, 2012). Furthermore, a recent study suggests that battery costs have been decreasing even faster than estimated in most of the literature (Nykvist and Nilsson, 2015). Nevertheless, considering that the packs in current battery electric trucks can have energy capacities of 100 kWh (e.g., Smith Electric Vehicles, 2015;

Electric Vehicles International, 2015) and sometimes much more (e.g., Balqon Corporation, 2013), the battery still represents a large portion of the vehicle's cost.

Table 1.3 – BEV lithium-ion battery pack cost projections 2010-2030

Period	Estimate ($/kWh)	Sources
2010–2011	650–1000	Khaligh and Li (2010) Shulock et al. (2011)
2012–2013	500–800	IEA and EVI (2013) Cluzel and Douglas (2012) Duleep et al. (2011)
2015	400–700	Shulock et al. (2011) Gerssen-Gondelach and Faaij (2012)
2020	300–500	Shulock et al. (2011) Mosquet et al. (2011) Gerssen-Gondelach and Faaij (2012)
2025	225–400	Gerssen-Gondelach and Faaij (2012) Cluzel and Douglas (2012)
2030	200–300	Gerssen-Gondelach and Faaij (2012) Cluzel and Douglas (2012)

1.2.2.1 Battery lifespan

Lithium-ion batteries' health can be negatively influenced by the way they are used and stored, with the former corresponding to cycle aging and the latter to calendar aging (Barré et al., 2013). The two main consequences of such deterioration are capacity fade, which reduces the vehicle's achievable range, and impedance raise, which reduces the battery's available power output (Barré et al., 2013). The end of life of the battery is usually considered to occur when its maximum capacity has decreased to 80% of its original value (McMorrin et al., 2012).

The main factors that influence calendar aging are time, temperature, and the state of charge (SOC) (Barré et al., 2013). SOC refers to the current battery charge as a percentage of maximum capacity. Keeping the battery at a high SOC for

long periods or in high temperatures will accelerate battery degradation (Barré et al., 2013). Current lithium-ion cells for BEVs usually have a calendar life ranging from five to 10 years according to the cell chemistry and the way they are managed (Cluzel and Douglas, 2012).

Cycle aging is a result of the way and frequency at which the battery is charged and discharged. For example, battery deterioration can be accelerated if it is frequently cycled with a large depth of discharge (DOD) (Millner, 2010), which corresponds to the cycling SOC swing. Most lithium-ion batteries in current battery electric trucks should provide 1,000 to 2,000 cycles from 90% SOC to 10% SOC, with 4,000 cycles expected in the near future (den Boer et al., 2013). Some freight BEV manufacturers using lithium iron phosphate batteries have already surpassed 2,000 cycles, although this depends on the DOD considered since cycle life and DOD have a nonlinear relationship (Millner, 2010). For example, Balqon Corporation (2015) refers to 2,500 and 5,000 cycles when discharging 80% and 70% of the battery, respectively. Using the battery outside of its specified voltage range (i.e., overcharging and overdischarging) can also speed up degradation (Lam, 2011), as can using high charging and discharging rates (Omar et al., 2014; Wang et al., 2011). In practice, many manufacturers restrict the usable SOC window due to the negative effects that can occur at low and high SOC (Marra et al., 2012).

1.2.2.2 Battery charging

The most common way of charging batteries is conductive charging, thus implying the need for a cable and a vehicle connector (Yilmaz and Krein, 2013). Charging modes are defined by the communication protocol between the vehicle and the charging equipment. Overviews of modes and connector standards are available in Cluzel et al. (2013) and Naberezhnykh et al. (2012). Charging levels can be divided according to the power rate used. Different classifications are used

according to the availability of power levels in a given country (Haghbin et al., 2010). Yilmaz and Krein (2013) refer to three levels based on the SAE Standard J1772: level 1 (1.4 kW to 1.9 kW), level 2 (4 kW to 19.2 kW), and level 3 (50 kW to 100 kW), also known as fast charging. While level 1 charging only requires a vehicle connector and a standard grounded outlet, levels 2 and 3 need special charging equipment as well as higher voltage circuits, and are the viable options in public charging infrastructures (Yilmaz and Krein, 2013). Some chargers also have the ability to send energy back into the grid (Yilmaz and Krein, 2013).

Charging times vary according to the capacity of the batteries and the equipment used, thus ranging from as little as 30 minutes to several hours (US DOE, 2012b). Furthermore, they are not linear during the entire process. Several different charging methods can be used. The most frequent is the constant current/constant voltage (CC/CV) approach in which the battery is charged with a constant current while its voltage increases to a maximum value, followed by gradually reducing the current until it drops below a minimum threshold while maintaining the voltage at its limit (Moura, 2011). The SOC increases linearly with time during the CC phase and then rises more slowly during the CV phase (Zhang, 2006; Marra et al., 2012).

In most cases where BEVs are used for goods distribution, they are mainly charged at depots overnight and do not use public charging stations outside the drivers' breaks (Nesterova et al., 2013; Naberezhnykh et al., 2012; Taefi et al., 2016). This can be explained by the need to use driver time efficiently and by security concerns (Naberezhnykh et al., 2012). Also, charging during off-peak hours can allow for reduced electricity rates (Yilmaz and Krein, 2013), and fast charging infrastructures necessary for charging during delivery routes are insignificant in most countries (IEA and EVI, 2013). Fast charging stations could be installed at the depot, but the necessary equipment is much more expensive than level 2 charging equipment (US DOE, 2012b). The impact of the high power

demand from the grid is another issue (Dharmakeerthi et al., 2014). This could limit the number of BEVs that could be simultaneously charged with high power levels (Etezadi-Amoli et al., 2010), potentially requiring investments for transformer upgrades (Electrification Coalition, 2010). As mentioned previously, the effect of using higher charging rates on battery health is another drawback, which is why it is generally recommended to minimize the number of times the battery is fast charged (Hatton et al., 2009).

While conductive charging is the most common method for charging EVs, there are a few other options, such as inductive charging and battery swapping. Another option for powering larger EVs is catenary wires.

Inductive charging involves transferring the power to the battery magnetically via an on-board charger, thus eliminating the need for charge cords (Yilmaz and Krein, 2013). Stationary inductive charging would be used to charge the battery while the vehicle is stopped, such as in parking lots or at bus stops, while in-road inductive charging could allow for charging the battery or powering the motor even while the vehicle is in motion (den Boer et al., 2013). Infrastructure costs and the power required for several trucks traveling near each other could limit applications for in-road charging in freight transportation (CALSTART, 2013a).

Battery swapping involves using automated battery swapping stations that remove the battery and insert a fully charged one (CALSTART, 2013b). Technical barriers include the cost associated with the large amount of batteries needed, infrastructure costs for the swapping stations, the required standardization of vehicles and batteries, and the risk of battery damage (Mak et al., 2013; Hatton et al., 2009; CALSTART, 2013b; den Boer et al., 2013). The stations would also need to recharge many batteries at the same time, which could impact the electric grid (Mak et al., 2013).

Using catenary wires as a power supply would only be a viable option on

heavily used freeways. Under this option, overhead wires are charged with electricity, and a truck uses a device to slide along the wires and retrieve the power (CALSTART, 2013b). The energy used for electric drive is not stored on-board, thus allowing additional payload and unlimited electric range when connected to the wires (den Boer et al., 2013). However, infrastructure costs, business models for access, and visual pollution constitute important barriers for a wider adoption in freight transportation (CALSTART, 2013b).

1.3. Market penetration

Global manufacturers began producing passenger BEVs and PHEVs in 2010 (Tuttle and Kockelman, 2012), but smaller manufacturers had been producing EVs in several classes much earlier (Sierzchula et al., 2012), some of which have been tested in the logistics sector (e.g., Vermie, 2002). However, relatively few have produced heavy duty vehicles. Also, in several cases, models on the market are conversions of ICEVs where the engine has been replaced by the necessary electric components (US DOE, 2012b).

1.3.1 Market Shares

Global sales of passenger BEVs and PHEVs reached 300,000 in 2014 and were approximately 10,000 in 2009, 45,000 in 2011, 110,000 in 2012, and 210,000 in 2013. Only a few national markets exceeded a 1% market share of all passenger vehicles in 2013 and 2014 (Mock and Yang, 2014; IEA and EVI, 2015). According to Berman and Gartner (2013) of Navigant, approximately 37,000 BEVs and PHEVs were expected to be sold for fleet purposes in 2013. Some of these vehicles are used in the delivery of lighter goods. For example, battery electric cars have been tested

in pizza delivery operations in Hamburg (E-Mobility NSR, 2013).

According to Jerram and Gartner (2013) of Navigant, the market for plug-in electric trucks and vans has not taken off as well as that for passenger vehicles. These vehicles have generally only penetrated niche applications while remaining dependent on government incentives. This is partially attributed to key industry players going out of business, to the conservative nature of fleet operators when it comes to new technologies, to a renewed interest in natural gas, and to the high purchase cost of EVs. The executive summary of Navigant's report also states that the global stock of HEV, PHEV, and BEV commercial trucks (class 2 to 8) was around 20,000 at the time of publication, with the majority of sales forecasts being for non-plug-in HEVs. A more recent report estimated global 2014 sales of BEV, HEV, and PHEV trucks and buses to be less than 16,000 (Navigant, 2015).

Den Boer et al. (2013) indicated that approximately 1,000 battery electric distribution trucks were being used around the world as of 2013. Parish and Pitkanen (2012) concluded that the fleet of battery electric trucks in North America as of 2012 was below 500, with most sales being made in U.S. states with strong incentives for these vehicles (e.g., California and New York). Their report also mentions that roughly 4,500 hybrid trucks (including HEVs, PHEVs, and hydraulic hybrid vehicles) were sold in North America as of 2012, with few long-haul class 8 applications.

According to the Electrification Coalition (2013), the small amount of models for heavier PEVs is another reason for their limited market penetration. Most of these vehicles are offered by small start-up firms. The report states that even if fleet operators tend to focus more on total cost of ownership than purchase costs, they are rather risk averse. Therefore, new small manufacturers offering electric trucks have difficulty penetrating the market. The substantial cost associated with installing several charging stations in a depot was also identified as an

adoption barrier. The price and installation of the equipment needed for higher power levels can be several thousands of dollars per station (Lee et al., 2013).

One of the reports of the European project FREVUE (Nesterova et al., 2013) lists similar factors for the limited use of electric freight vehicles in city logistics, notably doubts about technology readiness, high purchase costs, and the limited number of available models. The report also states that the rapid technology improvements themselves can be a market barrier since a BEV purchased today could quickly lose its residual value and become obsolete. The scarcity of information about the residual value of freight BEVs was also identified as an adoption barrier. Furthermore, the report mentions that companies experimenting with freight BEVs had trouble accessing maintenance services. E-Mobility NSR (2013) also reported this problem; this can be another factor of doubt since fleet mechanics do not have much experience with battery electric trucks, thus highlighting the need to develop maintenance repair networks (Gallo and Tomić, 2013).

However, the Electrification Coalition (2010) has identified factors making BEVs attractive for commercial applications, notably their lower operational and maintenance costs combined with high use rates of fleet vehicles, route predictability, commercial and industrial electricity rates, and corporate image. Even so, a wider adoption of BEVs in distribution applications can only be achieved if these prove to be cost-effective when compared to using conventional ICEVs for the same application.

1.3.2 Cost competitiveness

Because of the different cost structures between ICEVs and BEVs, the only way to appropriately compare their cost competitiveness is to study their whole life

costs (McMorrin et al., 2012). While the energy costs of BEV delivery trucks can be nearly four times lower than diesel trucks, the downside is that their purchase costs can be three times higher (Feng and Figliozzi, 2013). Maintenance costs for BEVs have been reported as 20% to 30% lower than those of ICEVs in some cases (Taefi et al., 2016), although the exact savings can take many different values depending on several factors, e.g., vehicle use rate, driving style and conditions, and level of regenerative braking use (Gallo and Tomić, 2013). Also, maintenance savings should increase with the ICEVs' age (Electrification Coalition, 2010); combined with lower energy costs, this makes BEVs more interesting from a strategic planning perspective. The evaluation of freight BEV costs should also include the possibility of having to replace batteries, which can age quickly due to intensive use.

One way to decrease the cost premium of BEVs and increase their payload is to right-size the battery, although the smaller battery would need to be used more intensively, which could accelerate battery deterioration (Van Amburg and Pitkanen, 2012). Another option for reducing upfront costs while also addressing concerns about battery life is to lease the battery for a monthly fee based on energy consumed or distance traveled (McMorrin et al., 2012). However, some fleets would prefer owning the batteries and eventually selling them in a second-hand market; this is currently difficult due to the uncertainty surrounding battery residual values, which also complicates determining appropriate battery leasing fees (Van Amburg and Pitkanen, 2012).

While numerous studies have analyzed whole life costs for battery electric cars (e.g., Tuttle and Kockelman, 2012; Prud'homme and Koning, 2012; Thiel et al., 2010; Delucchi and Lipman, 2001; Offer et al., 2010), the business case of commercial BEVs has been less studied.

Davis and Figliozzi (2013) have compared whole life costs of battery electric delivery trucks with that of conventional ICEVs serving urban delivery routes.

They considered two types of BEVs and one type of ICEV. They simulated many route instances, varied by using different values for several parameters. Residual value of the vehicles was assumed to be 20% of their purchase cost. Results show that although the BEVs' total cost of ownership (TCO) was highest in the majority of scenarios, certain factors can allow them to be economically competitive with ICEVs, e.g., high use rates, congestion, frequent customer stops during which an ICEV would idle, other elements amplifying the BEVs' superior tank-to-wheel efficiency, financial incentives or reductions in battery costs, and a planning horizon above 10 years. With a battery replacement after 150,000 miles at a cost of \$600/kWh, the diesel truck always had a lower TCO.

Feng and Figliozzi (2013) have developed a fleet replacement optimization model for fleets with one BEV truck type and one ICEV truck type. The objective is to minimize the discounted sum of all costs over a planning horizon of 30 years while answering each year's travel demand in miles. Several scenarios with varying vehicle use rates and ICEV fuel efficiency were analyzed. Resale values were determined by using depreciation rates ranging from 15% to 25%, depending on annual use. Optimal solutions showed that BEVs were only purchased at the start of the horizon when used for at least 16,000 miles per year in scenarios assuming a low fuel efficiency for the ICEVs; this would be the case in scenarios assuming a high fuel efficiency for the ICEVs if the BEVs' purchase cost could be reduced by 9% to 27%, depending on use. Including a battery replacement at a cost of \$400/kWh was found to significantly decrease the BEVs' current business case.

Lighter commercial BEVs such as vans and quadricycles should be more cost competitive with their equivalent ICEV counterparts over long planning horizons thanks to their smaller batteries and thus lower purchase costs, as demonstrated by a few studies (e.g., Macharis et al., 2013; Crist, 2012). However, despite the fact that long planning horizons can significantly increase the competitiveness of

electric delivery vehicles, in practice, freight transport vehicles are rarely used more than 10 years by the same owner. They are usually sold after a few years based on a lifecycle cost analysis (WTO, 2014), a task which is hindered by the uncertain information about the residual value of freight BEVs. Ultimately, the appropriateness of BEVs for goods distribution depends on the context of their intended use, but high purchase costs have been shown to be a major cost effectiveness barrier. As a result, at this stage incentives are likely to be needed to increase the commercial use of BEVs (Taefi et al., 2016).

1.3.3 Incentives

Several national governments have already established measures aimed at increasing the commercial use of BEVs. Local policies can also be useful for promoting BEVs for goods distribution. A few interesting examples of such incentives are provided below.

1.3.3.1 Financial incentives

Financial incentives are used to reduce the ownership costs of BEVs and their charging equipment (IEA and EVI, 2013). One form is purchase subsidies granted on buying the vehicle (Mock and Yang, 2014). For example, the New York Truck Voucher Incentive Program provides 80% of the incremental cost of battery electric trucks, up to $60,000 (New York State Energy Research and Development Authority, 2015), and the city of Amsterdam covers €40,000 for the purchase of such trucks (den Boer et al., 2013). Another example is the UK Plug-in Van Grant, which covers 20% of the cost of battery electric vans, up to £8,000 (McMorrin et al., 2012). Companies can also receive such subsidies for participating in demonstration or performance evaluation projects. In Germany, up to 50%

of the investment can be covered by participating in such projects (Taefi et al., 2016). Furthermore, some countries such as Norway, the Netherlands, the UK, and France offer subsidies for installation of the charging equipment (AustriaTech, 2014). Finally, tax exemptions are another financial incentive used for lowering ownership costs of BEVs. These include exemptions from VAT, vehicle registration taxes, fuel consumption taxes, and company car taxes (AustriaTech, 2014). Overviews of BEV tax exemptions are available in ACEA (2015), US DOE (2012a), and Mock and Yang (2014).

1.3.3.2 Prioritized access incentives

Local incentives for prioritized access often yield significant cost and time savings (Cluzel et al., 2013). One mechanism for freight BEVs is to grant them access to high occupancy lanes or bus lanes, as has been done in Utrecht, Lisbon, and Trondheim (Nesterova et al., 2013). However, some experiments with such access incentives have identified issues such as conflicts with buses and insufficient coverage of the road network by the lanes (AustriaTech, 2014). BEVs can also be exempted from certain road tolls, as is the case in Norway (Hannisdahl et al., 2013). Another concept is low emission zones (LEZs) in city centers to reduce polluting and noise emissions. Many LEZs in which EVs are permitted can be found in Dutch cities, and restrict the use of polluting commercial vehicles over 3,500 kg gross vehicle weight (GVW) in these areas (AustriaTech, 2014). In Rome, diesel freight vehicles pay €570 annually for access to the city center, while electric freight vehicles pay €300 (AustriaTech, 2014). Another example is the London Congestion Charge; the daily rate for accessing central London is £10, but electric freight vehicles are fully exempted (McMorrin et al., 2012). Rather than exempt them from a charge, BEVs can also be offered extended delivery time windows (Nesterova et al., 2013). For example, trials have taken place in Barcelona and Dublin where freight BEVs could enter the city center at night because of their

noiseless operation (AustriaTech, 2014). In 's-Hertogenbosch, they are exempted from the city center's exclusion of freight vehicles during the afternoon (AustriaTech, 2014). BEVs can also be exempted from restrictions on the maximum weight of vehicles allowed in city centers, as is the case in Amsterdam (E-Mobility NSR, 2013). Finally, preferential parking is another way to encourage the use of commercial BEVs, either in allocating free spaces or designated loading and unloading areas (AustriaTech, 2014). For example, in Bremen, a dedicated loading area exclusively for Euro 5 diesel vehicles and BEVs up to 7,500 kg GVW is used near the city center (MDS Transmodal Limited, 2012).

1.4. Electric vehicles in transportation science

From an operational research point of view, BEVs and ICEVs share several features, namely a restricted autonomy and a limited capacity. However, the autonomy of BEVs is more limited, the availability of recharging stations for BEVs is rather restricted, and their recharging time is considerably longer, compared to that of ICEVs. Moreover, BEVs have a number of characteristics that differentiate them from ICEVs: They can sometimes recharge at customer locations, possibly while service is being carried out; they can generate energy by decelerating; and battery efficiency depends on recharging policies. Finally, relations and incentives may have an impact on the adoption of BEVs. Below we review the main transportation science literature on BEVs as to fleet size and mix, vehicle routing, and optimal paths.

1.4.1 Fleet size and mix

The fleet size and mix literature related to BEVs is relatively recent and limited. We are aware of the following contributions in this area.

Van Duin et al. (2013) have sought to determine the ideal fleet of BEVs for cargo distribution to a set of customers in Amsterdam's city center from a transhipment facility. The aim is to determine an optimal fleet of BEVs and delivery routes to offer a desired service level at minimal costs to a set of customers with delivery time windows, service times, and demands. The autonomy, payloads, purchase costs, and operational costs of the BEVs are taken into account. Tours must also respect a maximum duration. The authors used a sequential insertion heuristic to solve a real instance in which the number of customers varies according to the day of the week, ranging from 155 to 219. Ten fleet configurations were tested, and the one with the lowest average cost per delivery and service level over 99% was recommended for implementation.

Gonçalves et al. (2011) have studied the vehicle routing problem (VRP) with pickup and delivery with a heterogeneous fleet of BEVs and ICEVs. The objective is to minimize total fixed and variable costs. Charging times are fixed and depend on vehicle range, and charging can be done at any time during the routes. They tested the model in the case of a Portuguese battery distributor that delivers batteries and recuperates them from its customers. Customers are also visited for other reasons (e.g., technical assistance). Three scenarios were evaluated, i.e., one using a fleet of two types of ICEVs, one using a fleet of two types of ICEVs and one type of uncapacitated BEVs, and one using exclusively one type of BEVs. Results obtained using CPLEX showed that using BEVs is a more costly alternative due to the high investment required.

Bae et al. (2011) have cast the EV and ICEV fleet size and mix problem as a

two-player two-stage game between a regulatory agency and an operator. The regulatory agency imposes environmental standards and can offer tax and price incentives to encourage the acquisition of EVs. It may also specify maximum emission constraints. The fleet operator works in a competive environment and seeks to offer good quality service while minimizing its costs. The authors developed and solved an equilibrium model for this game. They concluded that while subsidies may increase the operator's profit, they may also result in higher prices for the customers. However, these customers will benefit from a reduction in pollution if more EVs are used. In addition, energy price shocks and the resulting intensification in price competition will put late EV adopters at a disadvantage. Still, as the benefits of EVs become clearer, their adoption should increase, leading to more price competition and benefits to the customers. Finally, a wider initial quality difference in products and services between firms should result in a greater response from latecomers.

Lebeau et al. (2015) have studied the Fleet Size and Mix VRP with Time Windows for Electric Vehicles (FSMVRPTW-EV). The fleet is composed of BEVs and ICEVs each having their own fixed costs, operating costs, payload, volume capacity, energy capacity, and energy consumption. The objective is to minimize the sum of all fixed, operating, and driver costs. Each customer has a demand, a time window, and a service time. The depot also has a service time representing loading time so that vehicles can accomplish several routes. The BEVs can be fast charged up to 80% SOC at the depot during loading with a linear charging rate. They solved the problem using a modified Clarke and Wright savings and tested their method on 21 generated instances each with 25, 10 or 5 customers and one of seven different fleet configurations. Results indicated that BEVs were most competitive in the small vans segment.

Contrary to the previously discussed studies which either did not consider battery charging (van Duin, Tavasszy, and Quak 2013), assumed charging could

occur anywhere (Gonçalves et al., 2011) or only at the depot between routes (Lebeau et al., 2015), other fleet size and mix studies incorporating BEVs have considered the possibility for the vehicles to stop at charging stations during their routes and have taken into account the actual location of the stations.

Hiermann et al. (2016) have formulated the Electric Fleet Size and Mix Vehicle Routing Problem with Time Windows and Recharging Stations (E-FSMVRPTW). Each vehicle type has a specific fixed cost, load capacity, battery capacity, energy consumption rate per unit of distance, and recharging rate per unit of time. Whenever a vehicle stops to charge at a station or the depot, the battery is charged to full capacity. The objective is to minimize the sum of all fixed costs and traveled distance. The authors have developed a resolution approach combining adaptive large neighbourhood search (ALNS) to a cyclic neighbourhood search. A labeling algorithm is also proposed to find optimal positions charging stations. They have proposed benchmark test instances, and the results for small instances with up to 15 customers show that their method outperforms CPLEX. They have also modified their approach to compare it to benchmark results of related problems, showing it to be very competitive.

Goeke and Schneider (2015) have addressed the Electric VRP with Time Windows and Mixed Fleet (E-VRPTWMF), in which the fleet is composed of a certain number of homogeneous BEVs and homogeneous ICEVs. A linear charging rate is used, and charging is always done to maximum battery capacity when stopping at a station or the depot during routes. The authors use an energy consumption model that considers vehicle mass, speed, and road grade. Three objective functions were proposed, i.e., one minimizing total traveled distance, one minimizing total energy and labor costs, and one minimizing the previous costs with additional battery depreciation costs. They solved the E-VRPTWMF using ALNS and a local search procedure to improve repaired solutions. Numerical tests on new instances with 10 to 200 customers demonstrated the benefits of consider-

ing the carried load in the energy consumption, and indicated that minimizing distance cannot achieve the same cost efficiency when considering labor, energy, and battery costs.

Sassi et al. (2015a) have formulated the Heterogenous Electric Vehicle Routing Problem with Time Dependent Charging Costs and a Mixed Fleet (HEVRP-TDMF). The BEVs have varying battery capacities and operating costs, and the fleet also has ICEVs. Charging can be done en route at charging stations or at the depot, and each station is assigned an operating time window. Depot charging must also respect the grid's time-dependent capacity constraints; this can be done overnight with level 1 charging. Charging costs vary according to the station and time of day. Each charger has a maximum power that it can provide, and the power level used is a decision variable. Furthermore, each BEV has a set of compatible charging stations, and partial charging is allowed. The objective is to minimize the sum of routing, charging, fixed, and waiting costs. A construction heuristic is proposed, as well as an Inject-Eject Routine-Based Local Search that can be used with three insertion methods. Numerical experiments on instances with 300 to 550 nodes showed their approach generated the best solutions with the regret search insertion method. The authors subsequently proposed local search metaheuristics based on large neighbourhood search (LNS) for the same problem in Sassi et al. (2015b, c), with the exception that overnight charging and the grid's capacity are not considered in Sassi et al. (2015b).

As discussed previously, Feng and Figliozzi (2013) have also studied the BEV and ICEV fleet size and mix problem; readers may refer to Section 1.3.2 for more information on their findings.

1.4.2 Vehicle routing

Since the mid-2000s, there has been a growing interest in the integration of environmental aspects in the study of the VRP and its variants. For recent surveys, see Demir et al. (2014) and Lin et al. (2014). Below we survey some recent contributions in this area in the context of BEVs.

Erdoğan and Miller-Hooks (2012) have formulated the Green VRP (GVRP) in which routes and refueling of alternative-fuel powered vehicles (AFVs) at alternative fuel stations (AFSs) are determined simultaneously, similar to a few of the fleet size and mix papers discussed previously. The objective is the minimization of traveled distance considering a limited driving autonomy and the locations of AFSs, as well as constraints on the number of tours and their duration. Vehicles are assumed to be uncapacitated. Refueling is always done to maximum capacity and takes a constant amount of time. The authors used a modified Clarke and Wright savings heuristic and a density-based clustering algorithm to find initial solutions, followed by a postoptimization phase. Numerical experiments were performed using parameters for biodiesel vehicles. Small instances with 20 customers were designed, as well as a large instance with up to 500 customers. Results indicate that as the number of AFSs increases, costs diminish, more customers can be served, and the total distance traveled decreases.

Omidvar and Tavakkoli-Moghaddam (2012) have added delivery time windows, customer demands, and vehicle capacity constraints to the GVRP, while also integrating the effect of congestion. The working day is discretized into intervals with different congestion levels, speeds, and travel times. The AFVs can refuel at AFSs along their routes and can stay at customer locations during congestion periods. The objective is the minimization of the sum of vehicle, distance, travel, and emission cost. The authors proposed a simulated annealing (SA) algo-

rithm and a genetic algorithm to solve the problem. They tested their methods on small instances and compared them to optimal solutions obtained with CPLEX. Results showed that their algorithms always find optimal or near-optimal solutions. Larger instances indicated that the SA algorithm yielded better results than the genetic algorithm at the expense of larger computational times.

Montoya et al. (2016) have also studied the GVRP. Their objective is to minimize total distance traveled to serve a set of customers considering vehicle range limitations, maximum route duration, and available AFS infrastructure. Service times and refueling times are assumed to be constant, and no time windows are considered, as in Erdoğan and Miller-Hooks (2012). The authors solved the problem by means of a modified multispace sampling heuristic that includes three randomized Traveling Salesman Problem (TSP) heuristics within a route-first cluster-second approach, as well as an autonomy reparation procedure to ensure route feasibility. They compared their results to those obtained by Erdoğan and Miller-Hooks (2012) and Schneider et al. (2014) and found their approach to be competitive as well as relatively simple.

Schneider et al. (2014) have studied the GVRP with customer time windows and demands as well as capacity constraints, while focusing exclusively on BEVs, thus formulating in the Electric VRP with Time Windows (E-VRPTW). A linear charging rate was assumed and batteries must always be fully charged. The authors considered a hierarchical objective function whose first term is the fleet size minimization and whose second term is the minimization of total traveled distance. They have developed a metaheuristic combining variable neighbourhood search (VNS) with tabu search (TS), and have proposed benchmark instances for the E-VRPTW. Their approach outperforms CPLEX for all small instances (i.e., up to 15 customers). Experiments on larger instances with 100 customers and 21 charging stations showed the benefits of adding the VNS component to TS, as well as using SA as the acceptance criterion of the VNS.

A few other authors have worked on nearly identical problems to the E-VRPTW formulated by Schneider et al. (2014) in which differences mainly concern the assumptions about the charging process.

In Afroditi et al. (2014), the same objective as in Schneider et al. (2014) is considered. The batteries must be fully charged whenever a BEV stops at a charging station or the depot, but a fixed charging time is assumed. An equation taken from Davis and Figliozzi (2013) is also proposed to model the vehicles' energy consumption at constant speed. No resolution method is proposed for solving the problem but a few promising future research directions are put forward.

Bruglieri et al. (2015) have considered a variant of the E-VRPTW in which the battery level reached during charging is a decision variable. Energy consumption and recharging are assumed to be linear with respect to distance and time, respectively. The objective is to minimize the weighted sum of vehicles used, travel time, waiting time, and recharging time. They solved the problem using variable neighbourhood search branching (VNSB). They also used CPLEX on a few small E-VRPTW benchmark instances, showing that, compared to the model in Schneider et al. (2014), their model improves total waiting, travel, and recharging times, while finding similar total distances and number of vehicles. They also solved these instances with their VNSB approach, showing that the method can find optimal or near-optimal solutions faster than CPLEX.

Keskin and Çatay (2016) have also worked on the E-VRPTW in which partial recharges are allowed when stopping at a recharging station, and a linear charging rate is used to determine the associated charging time. The objective is to minimize total traveled distance. They have solved the problem using ALNS and SA as the acceptance criterion. They have tested their method with the E-VRPTW instances from Schneider et al. (2014). Results show that allowing partial recharges usually allows achieving better solutions than forcing the battery to always be fully charged. This holds whether the partial recharge option is modeled

as a continuous decision variable or a fixed amount, although improvements are more significant for the former.

Preis et al. (2014) have studied E-VRPTW using an energy consumption model taking into account rolling resistance, air resistance, gradient resistance, and energy recuperation. The carried load is also considered in the energy consumed. Charging is always done to maximum capacity and takes a fixed amount of time. The objective is to minimize the total energy consumption. They have solved the problem using TS and tested their method on 160 generated instances with 10 to 100 customers and three charging stations, as well as with varying altitude scenarios. Smaller instances solved to optimality show their method provides an average gap of 2.5%. Numerical results also demonstrate that minimizing distance alone can prevent energy consumption savings, especially in graphs with larger altitude differences.

Desaulniers et al. (2016) have developed exact resolution methods for four variants of the E-VRPTW according to whether a single or multiple recharges are allowed per route and whether batteries can be partially charged or must be fully charged. They propose a set partitioning formulation that requires a set of feasible routes and aims to minimize the total travel costs of the selected routes. They have proposed two branch-price-and-cut algorithms for each variant according to whether the labeling algorithm used to generate the set of feasible routes is monodirectional or bidirectional. They tested their methods on modified instances of Schneider et al. (2014), thus generating 87 instances with 25, 50 or 100 customers and 21 charging stations. Results demonstrate that their algorithms can solve almost all instances with 25 or 50 customers to optimality and several of those with 100 customers.

Conrad and Figliozzi (2011) have formulated the Recharging VRP (RVRP), in which charging can be done at certain customer locations rather than stations. A fixed time penalty is incurred when a vehicle charges, and this can be done while

servicing customers. The amount charged is a fixed proportion of the battery's capacity. Vehicle capacity constraints and customer time windows are considered. The objective function is hierarchical, the first term being to minimize the number of routes and the second being to minimize the total costs associated with distance, time, and recharging. The authors solved the problem with a modified version of the iterative construction and improvement heuristic for the Capacitated VRP (CVRP) with Time Windows from Figliozzi (2010). They conducted experiments on instances containing 40 customers, showing an increase in distance traveled and in the number of vehicles for lower vehicle ranges and longer charging times.

Abdallah (2013) has integrated PHEVs in the problem, thus formulating the PHEV Routing Problem with Time Windows (PHEVRPTW). The aim is to minimize the distance-based travel costs when running on gasoline. At each node, there is the possibility to charge the vehicle's battery to achieve a greater electric range, or to continue and use the ICE if the battery dies. Partial charging is considered. The author first solves the problem by using Lagrangian relaxation to find solution lower bounds, and then applies TS.

Barco et al. (2017) have studied a public transportation VRP variant with BEVs, while also coordinating the charging schedule of the vehicles to minimize costs and battery degradation. Customer node demands therefore represent passengers who must be picked up and dropped off at another node. An energy consumption model is applied to the VRP graph so that all edges represent minimum consumption paths. The objective is to minimize the energy consumption of all routes while answering all transport demands. The charging schedule problem then minimizes the charging and battery degradation costs to perform the routes in the VRP's solution. Battery degradation costs result from factors such as the charging power level, the average SOC, and the DOD. A differential evolution algorithm is applied to solve the charging schedule problem, while the optimiza-

tion tool XPRESS was used to solve the VRP.

Felipe et al. (2014) have formulated the Green Vehicle Routing Problem with Multiple Technologies and Partial Recharges (GVRP-MTPR). Partial recharges and overnight depot charging are allowed. The fleet consists of homogeneous BEVs, and charging consists of a fixed stopping time and a variable charging time. A charging speed and cost is associated with each charging technology, and each station has a set of offered technologies. A fixed charging cost is also used to represent battery aging. The objective is to minimize the total charging costs. A nearest neighbour construction heuristic is proposed, as well as neighbourhood structures to be used within deterministic local search algorithms and an SA algorithm. The authors tested their methods on new instances for the GVRP-MTPR, as well as on instances from Schneider et al. (2014) and Erdoğan and Miller-Hooks (2012). Results showed their algorithms to be competitive and that their SA heuristic performs better for large instances. Numerical analyses also demonstrated the cost benefit of considering several charging technologies and allowing partial recharges.

Finally, Juan et al. (2014) have studied the VRP with Multiple Driving Ranges (VRPMD), in which the fleet is composed of vehicle types with different driving ranges. The objective is to minimize the total distance-based travel costs. The authors solve the problem using a multiround heuristic. In each round, a CVRP with all unserved nodes and unused vehicles must be solved, while constraining routes to be inferior to the range of the most autonomous vehicle still available. They tested their approach on 20 CVRP benchmark instances and considered three vehicle classes: ICEVs and PHEVs (unlimited range), medium-range BEVs, and short-range BEVs. Comparing solutions found with imposed fleet congifurations to best known solutions showed that BEVs could be used with small increases in distance costs.

1.4.3 Optimal paths

Several studies have focused on the case of a single electric vehicle traveling from an origin to a destination by trying to determine an optimal path with respect to energy consumption, cost or time. Others consider a predetermined path and attempt to find an optimal recharging policy for minimizing total recharging costs. While the previous sections were mostly concerned with fleets of delivery vehicles, most optimal path studies incorporating EVs concern passenger vehicles. Nevertheless, below we present a few of these studies because they are relevant to the issue of optimal routing.

Artmeier et al. (2010) consider energy-optimal routing of BEVs that can recuperate energy using regenerative braking. The authors therefore allow certain edges of the graph to have negative costs in terms of energy consumption. This is a constrained shortest path problem in which the battery charge is bounded by its capacity. The aim of the problem is to determine an origin-destination path, given an initial battery SOC, so that the remaining charge on arriving at the destination is highest. The authors proposed algorithms with a worst case cubic complexity for this problem. Numerical experiments were performed on a road network near Munich containing 776,419 nodes. Eisner et al. (2011) and Sachenbacher et al. (2011) have subsequently developed more efficient methods for the same problem.

Fontana (2013) incorporated some stochastic features into the problem. The focus is not only on energy consumption but also on travel time. The objective is to determine an origin-destination path of least duration as well as the vehicle speed, while respecting an energy consumption limit and considering uncertainties as to time and energy consumption. A solution methodology is proposed that combines Lagrangian relaxation, techniques from robust optimization, and

A* search. Real-world data were used to construct instances based on trips in Massachusetts and Michigan with different energy consumption requirements. Estimates for lower bounds obtained by Lagrangian relaxation suggest that their algorithms can find near-optimal solutions within a few seconds.

Other optimal path studies with BEVs integrated the idea of allowing the battery to be recharged along the path. A few of these are discussed below.

Sweda and Klabjan (2012) have considered the problem of determining a minimum cost origin destination path for BEVs that can charge along the path, such that the battery charge always remains within a usable SOC window. The problem is formulated as a dynamic program, and the terms used in the optimality equations refer to the cost of recharging, the cost of traveling between two nodes, and the value function on reaching the next node. A backward recursion algorithm is applied to find an optimal path. However, certain conditions must be satisfied for the state space to be discrete and the approach to be applicable. Therefore, the authors also propose an approximate dynamic programming algorithm.

Sweda et. al. (2016) have studied the problem of finding optimal charging policies along a predetermined path which are cost effective and improve battery longevity. The objective is to minimize the total cost of recharging. These costs consist of a fixed stopping cost, a recharging cost per unit of energy, and an overcharging cost incurred when charging beyond a threshold over which degradation occurs and charging time increases; the threshold occurs on entering the CV phase of a CC/CV charging scheme. The authors derive optimal charging policies for general paths where charging is allowed at prespecified nodes, and for two specific path types, i.e., paths where charging can be done anywhere, and paths with equidistant charging locations. An optimal policy is determined through a forward recursion algorithm for the general paths. The number of stops for the other path types are obtained by solving a closed-form expression

before determining the corresponding optimal policy. The authors have also developed two heuristics according to whether the priority is to avoid overcharging or stopping frequently.

Arslan et al. (2014) have integrated PHEVs into the minimum cost path problem. In this case, the vehicles can stop at both charging and refueling stations along the path. Because a shortest path is not necessarily the minimum cost path, a depreciation cost is used to penalize long distances. Additionally, a fixed cost is incurred for each stop. Battery degradation costs depend on the swing in SOC on charging. The objective is to minimize the total travel cost associated with electricity, gasoline, battery degradation, vehicle depreciation, and stopping. The authors propose three solution techniques, i.e., a mixed integer quadratic constrained program, a dynamic programming based heuristic, and a shortest path heuristic. Numerical experiments were conducted using generated instances with up to 100 nodes and a California network with 339 nodes. Results showed that their heuristic methods can quickly find optimal or near-optimal solutions for large instances.

Kobayashi et al. (2011) consider slow and fast charging stations in the minimum cost path for BEVs. Their method first identifies potential stations when the vehicle cannot complete the path from its origin with its current charge. Dijkstra's algorithm is then used to find a least travel cost route using the identified stations. Depending on the driver's priority, traveling costs focus on distance traveled or on traveling and charging time. The vehicles must be fully charged when stopping at a station. Numerical experiments were conducted on a Japanese map with 2,500 hypothetical charging stations, while prioritizing travel time. Results showed that the method is effective but requires more computational time than conventional methods due to the step of finding potential stations.

Alesiani and Maslekar (2014) look to determine optimal paths for a fleet of BEVs, each vehicle having its own origin-destination pair. Furthermore, the au-

thors incorporate the idea of allocating charging stations to the vehicles so as to avoid having many vehicles simultaneously at the same one. The goal is to minimize total costs related to energy consumption and charging times resulting from concurrency at the stations, while respecting constraints with regard to battery capacity, the number of charging stops per route, and the number of vehicles that can be charged at the stations. Energy recuperation is also considered. The problem is solved with a modified evolutionary genetic algorithm. Numerical experiments show that this approach allows a better distribution of the vehicles among the stations.

Siddiqi et al. (2011a,b) only consider fast charging stations along the path. The objective is to minimize total distance traveled while respecting constraints on travel times, charging times, and charging costs. The multiconstrained optimal path (MCOP) formulation is transformed into an unconstrained optimization problem using a penalty function method, which is then solved with an algorithm based on simulated evolution (Siddiqi et al., 2011b), or on particle swarm optimization (Siddiqi et al., 2011a). Numerical experiments based on a Saudi Arabian city with 108 nodes show the competitiveness of their method. Siddiqi et al. (2012) further studied the problem using a simulated evolution based algorithm but on a multi-objective shortest path formulation of the problem in which the goal is to minimize three objective functions, i.e., charging time, path length, and travel time, respectively.

Finally, Zündorf (2014) attempts to minimize the sum of travel and charging times to get from an origin to a destination while considering different types of stations, i.e., regular charging stations, battery swapping stations, and super chargers. The super chargers use higher power levels that can charge the battery up to a maximum of 80% SOC with a single linear charging function. The regular charging stations can charge the battery to full capacity, but the charging process is modeled as a piecewise linear and concave function to represent the increase

in charging times which occurs around 80% SOC in a CC/CV charging scheme. The battery swapping stations require a small amount of time for swapping. Exact and heuristic methods were developed and tested on several graphs varying in size and in the stations they contain.

1.5. Research perspectives

While electric delivery vehicles can significantly decrease greenhouse gas emissions in areas with clean electricity generation sources, this environmentally-based business case can be harder to make with more coal intensive production, in which case local pollution is simply replaced by upstream emissions (Lee et al., 2013). However, the effects of displacing polluting and noise emissions from dense urban areas to more remote areas where power plants are located should not be ignored (Ji et al., 2012). Compared with ICEVs, BEVs create less local pollution, produce less noise, and are thus generally perceived as a more sustainable means of goods distribution when used in regions with relatively clean energy sources. As noted in Section 1.3.3, the societal advantages of using BEVs translates into a number of incentive schemes designed to increase their competitiveness.

From a cost perspective, BEVs require lower maintenance costs and incur lower operating costs, but have high purchasing costs. However, the lower energy costs ultimately depend on the price of electricity in the market of operation. At present, adoption of BEVs for goods distribution depends somewhat on incentives, thus indicating that this form of transportation is not yet economically viable. Therefore, the cost competitiveness of BEVs depends significantly on future technological developments related to these vehicles, coupled with governmental investment in adequate infrastructure and incentives. Nonetheless, a number of

important features can already be identified as necessary when studying freight distribution with EVs.

Based on the review presented in the previous sections, we present a number of important interrelated modeling issues that are relevant to the emerging research area of goods distribution with BEVs. In Sections 1.5.1–1.5.3, we discuss research perspectives at the strategic, tactical and operational levels.

1.5.1 Strategic perspectives

The strategic perspectives of BEVs ownership in goods distribution mostly relate to fleet composition issues, i.e., the best choice of fleet size and mix when considering a potential mix of ICEVs and BEVs. Ownership of BEVs should encompass purchase cost, as well as operational and maintenance costs.

A substantial part of the purchase cost of BEVs is related to the battery cost. The battery size and weight influence the BEVs' payload, and thus impact their effective capacity. The size of the battery also influences the BEVs' driving range. Therefore, choosing the correct battery type is paramount in fleet acquisition questions. The relation between range, payload, battery degradation, and cost could be investigated in fleet size and mix problems considering BEVs with different battery sizes (i.e., with the option to use smaller batteries to decrease costs and increase payload, but at the expense of reduced range and more intensive battery use). Note that significant reductions in battery costs and weights are also expected in the future. Thus, it is worth examining the impact that such developments may have on fleet composition. Furthermore, battery aging will gradually reduce the maximum range over time. Other factors influencing battery lifetimes are discussed below.

The use of BEVs and ICEVs essentially implies addressing the potential dis-

tance ranges that these vehicles can traverse without recharging or refueling, respectively. The issue of refueling ICEVs has been addressed in certain studies (e.g., Bousonville et al., 2011; Suzuki, 2009; Khuller et al., 2007) but has generally been rightfully ignored by the transportation science community since there are an abundance of fuel stations for conventional vehicles, the refueling times are negligible, and refueling stations offer similar services. However, these conditions do not hold for BEVs. Indeed, the recharging infrastructure is scarce, and refueling times can be heavily affected by the type of service offered by the particular recharging station. Two main categories of charging stations exist, i.e., slow (level 2) and fast (level 3); the latter is more costly. Furthermore, fast charging dictates high power demand levels from the electricity grid. Thus, the charging infrastructure depends on the local electricity grid capabilities.

Naturally, charging capacities are subject to technological developments and should be considered. However, the decision to purchase BEVs should explicitly account for the existing infrastructure since this influences the strategic capacity of BEVs in terms of potential range. Furthermore, a fleet operator may consider investing in recharging infrastructures (e.g., at depots, customer locations or even along long-haul paths), in which case both the cost of the charging equipment and the grid capacity should be considered.

A measure for the battery life is the number of times a battery can be deeply discharged. This should be carefully considered in fleet investment decisions. Moreover, the fleet size and mix issues should not be limited to BEVs, but should also include HEVs and FCEVs. Finally, well-to-wheel investigations should be performed in fleet composition problems when analyzing energy consumption and emission costs. This is important for BEVs since their energy efficiency and environmental superiority depend on the way the electricity is generated. Similarly, the production and disposal of batteries should also be accounted for when assessing the ecological performance of BEVs, especially considering that many

new battery types are expected to be commercialized in the future.

1.5.2 Tactical perspectives

Once purchased, BEVs necessitate a number of tactical decisions mainly pertaining to charging policies, which in return influence battery lifespan. While there are several ways of recharging batteries, the most common is conductive charging. Therefore, considering the current state of the conductive charging technology, one important decision relates to where the BEVs can recharge. This can be a combination of charging at the depot, at a customer location or at a charging station.

In reality, when BEVs are used for goods distribution, it is common not to use the public infrastructure and to fully charge them overnight at the depot (Nesterova et al., 2013; Naberezhnykh et al., 2012; Taefi et al., 2016). While charging at customers' location is an option, it requires a joint agreement with customers, with respect to charging times and rates.

Recharging along a path, be it at a public station or a customer location, would make sense if fast charging could be performed at these stations. The slow recharging infrastructure would require several hours to fully recharge a freight BEV, and therefore would be less relevant considering a daily shift in short-haul transportation. Additionally, fast charging infrastructures remain relatively scarce in most countries except Japan (IEA and EVI, 2013). Therefore, for most countries it seems logical that vehicles should mostly recharge at the depot. Furthermore, fast charging may reduce battery lifespan. The cost of recharging should also be accounted for when addressing the issue of charging policies, since electricity is often cheaper during night and off-peak hours.

Finally, a potential tactical decision relates to leasing batteries. Battery leas-

ing is currently available for a few electric vans but not for electric trucks. The existence of such an option for trucks may help their market penetration.

1.5.3 Operational perspectives

Considering the tactical recharging policy, operational decisions should be made in an attempt to optimize the battery life while not compromising the operational cost of serving customers. Therefore, deciding when and how much to recharge is a critical operational issue since this directly impacts the long-term performance of BEVs via battery health.

Earlier models worked with fixed charging times or assumed that the battery must always be charged to its full capacity. More recent models allow the battery to be partially charged and consider several charging technologies. Nonlinear or piecewise linear approximations of charging functions (e.g., Zündorf, 2014) could be used in future studies when the batteries can be fully charged. Another alternative could be to consider battery dynamics more explicitly during charging, for example by linking the battery's terminal voltage to its SOC and current via an equivalent circuit model (e.g., Marra et al., 2012). Such circuit models could also be used to account for battery dynamics during discharging, for example by monitoring its terminal voltage and electrical current according to power demands (Larminie and Lowry, 2003). The SOC of the battery could thus be treated as an amount of charge rather than energy, with its variation determined according to the electrical current (Marra et al., 2012).

Synchronization of charging times and drivers' schedules (e.g., lunch break time windows during which there is the possibility of charging) could also be incorporated into VRPs. Such problems could also work with longer planning horizons (e.g., a whole week) to consider the impact of the BEVs' SOC at the

end of each day on subsequent days, in addition to the possibility of charging overnight in the depot, as has been proposed in a few recent problems (e.g., Felipe et al., 2014; Sassi et al., 2015a).

Future models could also explicitly target battery charge times and schedules as a means to develop battery management strategies to extend their lifetime. Only a few papers studying routing problems have explicitly addressed battery life, e.g., they consider some of the negative impacts resulting from high charging power levels, the average SOC, overcharging, and large SOC swings (e.g., Barco et al., 2017; Sweda et. al., 2016; Arslan et al., 2014). Elaborate battery health models can surely be further developed in future transportation planning problems.

Regenerative braking should also be treated differently for trucks and small vehicles since a much greater amount of energy quickly arises when a large truck goes downhill or must come to a quick stop, especially when carrying heavy loads. Therefore, the percentage of kinetic energy that can be recovered may decrease for large freight BEVs if the battery cannot handle the high power input when going downhill or if the regenerative braking cannot stop the vehicle quickly enough. Energy recuperation in vehicle routing and shortest path problems should therefore be modeled depending on the size and load of the trucks.

The competitiveness of BEVs is amplified when considering congestion, which is particularly realistic in urban distribution. For example, traffic may increase a BEV's range due to frequent stop-and-go movements and hence more energy being recuperated via regenerative braking. On the other hand, some uncontrollable factors may temporarily reduce a BEV's range, e.g., extreme temperatures and driving style (US DOE 2012b). These may be captured by designing stochastic models to quantify their impact on the achievable range.

Furthermore, certain incentives associated with freight BEVs (e.g., zones which can be accessed exclusively or free of charge by BEVs; possibility for night deliv-

eries with BEVs due to their silent operation) could be integrated into routing problems. The potential for BEVs in two-phase deliveries could also lead to integrating BEVs in multiechelon VRPs. Finally, additional research could be conducted to investigate the appropriateness of battery electric trucks for different types of transportation tasks (e.g., chilled cargo).

1.6. Conclusions

The integration of BEVs in goods distribution depends on a number of factors related to cost, technology, infrastructure, electricity sources, and financial incentives. Because future trends in these areas are highly uncertain, the problems that must be solved by the transportation science community are likely to evolve over time, thus creating important research challenges. However, we believe that modeling these features and developing adequate solution procedures to the resulting models is vital, as it facilitates study of the current problems and of future scenarios, within a rigorous framework.

Given the current state of technology, BEVs are more appropriate for city distribution than for longhaul applications because of the battery limitations. Typical daily distances traveled by urban delivery trucks are often lower than the range of commercial BEVs (Feng and Figliozzi, 2013), which has been shown to be suitable for the urban routing patterns of some logistic service providers, even if the reduced payload of the vehicles remained a concern expressed by some drivers (Ehrler and Hebes, 2012). Therefore, BEVs are more suitable for last-mile deliveries in urban areas involving the transportation of relatively light goods, frequent stop-and-go movements, limited route lengths as well as low travel speeds (Nesterova et al., 2013; E-Mobility NSR, 2013). Their reduced pollution and noise are also more relevant in urban areas and thus more likely to be re-

warded by incentives. These factors should certainly be of concern to researchers working in the area of city logistics.

Finally, we highlight the fact that BEVs compete not only against ICEVs but also with other cleaner alternatives such as compressed natural gas, over which the superiority of BEVs can be hard to establish when considering economic risks, costs, and benefits (Valenta, 2013). Furthermore, significant improvements in ICEV efficiencies can be expected in the future (Mosquet et al., 2011). This fact should not be ignored in the fleet size and mix research.

Acknowledgements

This research was partly supported by the Canadian Natural Sciences and Engineering Research Council [Grants 463834-2014, 436014-2013, and RGPIN-2015-06189]. This support is gratefully acknowledged. The authors thank the associate editor and the referees for their valuable comments.

References

Abdallah, T. 2013. The plug-in hybrid electric vehicle routing problem with time windows. Master's thesis, University of Waterloo, Canada.

ACEA (European Automobile Manufacturers Association). 2013. Differences Between Diesel and Petrol. URL `http://www.acea.be/news/article/differences-between-diesel-and-petrol`. Last accessed June 2015.

ACEA (European Automobile Manufacturers Association). 2015. Overview of purchase and tax incentives for electric vehicles in the EU in

2015. URL http://www.acea.be/uploads/publications/Electric_vehicles_overview_2015.pdf. Last accessed June 2015.

Afroditi, A., M. Boile, S. Theofanis, E. Sdoukopoulos, D. Margaritis. 2014. Electric vehicle routing problem with industry constraints: Trends and insights for future research. *Transportation Research Procedia* **3** 452–459.

Alesiani, F., N. Maslekar. 2014. Optimization of charging stops for fleet of electric vehicles: A genetic approach. *IEEE Intelligent Transportation Systems Magazine* **6**(3) 10–21.

Allen, J., G. Thorne, M. Browne. 2007. *BESTUFS Good Practice Guide on Urban Freight Transport* (BESTUFS, Rijswijk, The Netherlands).

Arslan, O., B. Yıldız, O.E. Karaşan. 2014. Minimum cost path problem for plug-in hybrid electric vehicles. *Transportation Research Part E: Logistics and Transportation Review* **80** 123–141.

Artmeier, A., J. Haselmayr, M. Leucker, M. Sachenbacher. 2010. The shortest path problem revisited: Optimal routing for electric vehicles. R. Dillmann, J. Beyerer, U. Hanebeck, T. Schultz, eds., *KI 2010: Advances in Artificial Intelligence*. Lecture Notes in Computer Science, Vol. 6359 (Springer-Verlag, Berlin Heidelberg), 309–316.

AustriaTech. 2014. Electric fleets in urban logistics: Improving urban freight efficiency in small and medium-sized historic towns. Published as part of the ENCLOSE project, funded by Intelligent Energy Europe (IEE), Vienna, Austria. URL http://www.austriatech.at/files/get/834747f18fdcc9538376c9314a4d7652/austriatech_electricfleets_broschuere.pdf. Last accessed June 2016.

Bae, S.H., J. Sarkis, C.S. Yoo. 2011. Greening transportation fleets: Insights from a two-stage game theoretic model. *Transportation Research Part E: Logistics and Transportation Review* **47**(6) 793–807.

Balqon Corporation. 2013. M100 product specifications. URL `http://www.balqon.com/wp-content/uploads/2013/09/m100_brochure_2013.pdf`. Last accessed June 2016.

Balqon Corporation. 2015. Mule M100 electric truck. URL `http://www.balqon.com/electric-vehicles/mule-m100/`. Last accessed June 2016.

Barco, J., A. Guerra, L. Muñoz, N. Quijano. 2017. Optimal routing and scheduling of charge for electric vehicles: A case study. *Mathematical Problems in Engineering*, Article ID 8509783.

Barré, A., B. Deguilhem, S. Grolleau, M. Gérard, F. Suard, D. Riu. 2013. A review on lithium-ion battery ageing mechanisms and estimations for automotive applications. *Journal of Power Sources* **241** 680–689.

Bektaş, T., G. Laporte. 2011. The pollution-routing problem. *Transportation Research Part B: Methodological* **45**(8) 1232–1250.

Berman, B., J. Gartner. 2013. Report executive summary: Selecting electric vehicles for fleets. Navigant Research. URL `http://www.navigantresearch.com/wp-assets/uploads/2013/02/RB-SEVF-13-Executive-Summary.pdf`. Last accessed June 2015.

Boulder Electric Vehicle. 2013. 1000-series master brochure. URL `http://www.boulderev.com/docs/1000%20Master%20Brochure.pdf`. Last accessed June 2016.

Bousonville, T., A. Hartmann, T. Melo, H. Kopfer. 2011. Vehicle routing and refueling: The impact of price variations on tour length. E. Sucky, B. Asdecker, A.

Dobhan, S. Haas, J. Wiese, eds., *Logistikmanagement – Herausforderungen, Chancen, und Lösungen, Band 2 (Proceedings of LM 11)* (University of Bamberg Press, Bamberg, Germany), 83–101.

Bruce, P.G., S.A. Freunberger, L.J. Hardwick, J-M. Tarascon. 2012. Li-O2 and Li-S batteries with high energy storage. *Nature materials* **11**(1) 19–29.

Bruglieri, M., F. Pezzella, O. Pisacane, S. Suraci. 2015. A variable neighborhood search branching for the electric vehicle routing problem with time windows. *Electronic Notes in Discrete Mathematics* **47** 221–228.

CALSTART. 2013a. I-710 Project zero-emission truck commercialization study final report. URL `http://www.calstart.org/Libraries/I-710_Project/I-710_Project_Zero-Emission_Truck_Commercialization_Study_Final_Report.sflb.ashx`. Last accessed June 2015.

CALSTART. 2013b. Technologies, challenges and opportunities: I-710 Zero-emission freight corridor vehicle systems (Revised Version Final V1). URL `http://www.calstart.org/Libraries/I-710_Project/Technologies_Challenges_and_Opportunities_I-710_Zero-Emission_Freight_Corridor_Vehicle_Systems.sflb.ashx`. Last accessed June 2015.

Chan, C.C. 2007. The state of the art of electric, hybrid, and fuel cell vehicles. *Proceedings of the IEEE* **95**(4) 704–718.

Cluzel, C., C. Douglas. 2012. Cost and performance of EV batteries. Element Energy, Axeon and EaStCHEM, commissioned by The Committee on Climate Change. URL `http://www.element-energy.co.uk/wordpress/wp-content/uploads/2012/06/CCC-battery-cost_-Element-Energy-report_March2012_Finalbis.pdf`. Last accessed June 2016.

Cluzel, C., B. Lane, E. Standen. 2013. Pathways to high penetration of electric vehicles. Element Energy and Ecolane, commissioned The Committee on Cli-

mate Change. URL http://www.theccc.org.uk/wp-content/uploads/2013/12/CCC-EV-pathways_FINAL-REPORT_17-12-13-Final.pdf. Last accessed June 2015.

Conrad, R.G., M.A. Figliozzi. 2011. The recharging vehicle routing problem. T. Doolen, E. Van Aken, eds., *Proceedings of the 2011 Industrial Engineering Research Conference* (Institute of Industrial Engineers, Norcross, GA), 2785–2792.

Crist, P. 2012. Electric vehicles revisited: Costs, subsidies and prospects. *International Transport Forum Discussion Papers* (OECD Publishing, Paris, France), No. 2012/03.

Davis, B.A., M.A. Figliozzi. 2013. A methodology to evaluate the competitiveness of electric delivery trucks. *Transportation Research Part E: Logistics and Transportation Review* **49**(1) 8–23.

Delucchi, M.A., T.E. Lipman. 2001. An analysis of the retail and lifecycle cost of battery-powered electric vehicles. *Transportation Research Part D: Transport and Environment* **6**(6) 371–404.

Demir, E., T. Bektaş, G. Laporte. 2011. A comparative analysis of several vehicle emission models for road freight transportation. *Transportation Research Part D: Transport and Environment* **16**(5) 347–357.

Demir, E., T. Bektaş, G. Laporte. 2014. A review of recent research on green road freight transportation. *European Journal of Operational Research* **237**(3) 775–793.

den Boer, E., S. Aarnink, F. Kleiner, J. Pagenkopf. 2013. Zero emission trucks: An overview of state-of-the-art technologies and their potential. CE Delft and DLR, commissioned by the International Council on Clean Transportation (ICCT). URL http://www.cedelft.eu/?go=home.downloadPub&id=1399&file=CE_Delft_4841_Zero_emissions_trucks_Def.pdf. Last accessed June 2016.

Desaulniers, G., F. Errico, S. Irnich, M. Schneider. 2016. Exact algorithms for electric vehicle-routing problems with time windows. *Operations Research* **64**(6) 1388–1405.

Dharmakeerthi, C.H., N. Mithulananthan, T.K. Saha. 2014. Impact of electric vehicle fast charging on power system voltage stability. *International Journal of Electrical Power & Energy Systems* **57** 241–249.

Dinger, A., R. Martin, X. Mosquet, M. Rabl, D. Rizoulis, M. Russo, G. Sticher. 2010. Batteries for electric cars: Challenges, opportunities, and the outlook to 2020. The Boston Consulting Group. URL `https://www.bcg.com/documents/file36615.pdf`. Last accessed June 2016.

Duleep, G., H. van Essen, B. Kampman, M M. Grünig. 2011. Impacts of electric vehicles – deliverable 2: Assessment of electric vehicle and battery technology. CE Delft, ICF International, and Ecologic, commissioned by the European Commission. URL `http://www.cedelft.eu/?go=home.downloadPub&id=1153&file=4058_D2defreportHvE_1314726004.pdf`. Last accessed June 2016.

Eberle, U., R. von Helmolt. 2010. Sustainable transportation based on electric vehicle concepts: A brief overview. *Energy & Environmental Science* **3**(6) 689–699.

Ehrler, V., P. Hebes. 2012. Electromobility for city logistics - the solution to urban transport collapse? An analysis beyond theory. *Procedia-Social and Behavioral Sciences* **48** 786–795.

Eisner, J., S. Funke, S. Storandt. 2011. Optimal route planning for electric vehicles in large networks. W. Burgard, D. Roth, eds., *Proceedings of the Twenty-Fifth AAAI Conference on Artificial Intelligence* (AAAI, Menlo Park, CA), 1108–1113.

Electric Vehicles International. 2015. EVI Medium Duty Truck Specification Sheet. URL http://www.evi-usa.com/LinkClick.aspx?fileticket=SyZhwUVqNJs%3d&tabid=83. Last accessed June 2016.

Electrification Coalition. 2010. Fleet electrification roadmap. URL http://www.electrificationcoalition.org/sites/default/files/EC-Fleet-Roadmap-screen.pdf. Last accessed May 2015.

Electrification Coalition. 2013. State of the plug-in electric vehicle market. URL http://www.electrificationcoalition.org/sites/default/files/EC_State_of_PEV_Market_Final_1.pdf. Last accessed June 2016.

Emadi, A., K. Rajashekara, S.S. Williamson, S.M. Lukic. 2005. Topological overview of hybrid electric and fuel cell vehicular power system architectures and configurations. *IEEE Transactions on Vehicular Technology* **54**(3) 763–770.

E-Mobility NSR. 2013. Comparative analysis of European examples of schemes for freight electric vehicles – Compilation report. URL http://e-mobility-nsr.eu/fileadmin/user_upload/downloads/info-pool/E-Mobility_-_Final_report_7.3.pdf. Last accessed January 2019.

Erdoğan, S., E. Miller-Hooks. 2012. A green vehicle routing problem. *Transportation Research Part E: Logistics and Transportation Review* **48**(1) 100–114.

Etezadi-Amoli, M., K. Choma, J. Stefani. 2010. Rapid-charge electric-vehicle stations. *IEEE Transactions on Power Delivery* **25**(3) 1883–1887.

Felipe, Á., M.T. Ortuño, G. Righini, G. Tirado. 2014. A heuristic approach for the green vehicle routing problem with multiple technologies and partial recharges. *Transportation Research Part E: Logistics and Transportation Review* **71** 111–128.

Feng, W., M. Figliozzi. 2013. An economic and technological analysis of the key factors affecting the competitiveness of electric commercial vehicles: A case

study from the USA market. *Transportation Research Part C: Emerging Technologies* **26** 135–145.

Figliozzi, M.A. 2010. An iterative route construction and improvement algorithm for the vehicle routing problem with soft time windows. *Transportation Research Part C: Emerging Technologies* **18**(5) 668–679.

Fontana, M.W. 2013. Optimal routes for electric vehicles facing uncertainty, congestion, and energy constraints. Ph.D. thesis, Massachusetts Institute of Technology, Massachusetts.

Gallo, J.-B., J. Tomić. 2013. Battery electric parcel delivery truck testing and demonstration. California Hybrid, Efficient and Advanced Truck Research Center (CalHEAT). URL `http://www.calstart.org/Libraries/CalHEAT_2013_Documents_Presentations/Battery_Electric_Parcel_Delivery_Truck_Testing_and_Demonstration.sflb.ashx`. Last accessed June 2015.

Gerssen-Gondelach, S.J., A.P.C. Faaij. 2012. Performance of batteries for electric vehicles on short and longer term. *Journal of Power Sources* **212** 111–129.

Goeke, D., M. Schneider. 2015. Routing a mixed fleet of electric and conventional vehicles. *European Journal of Operational Research* **245**(1) 81–99.

Gonçalves, F., S.R. Cardoso, S. Relvas, A.P.F.D. Barbosa-Póvoa. 2011. Optimization of a distribution network using electric vehicles: A VRP problem. D. Cardoso, J. Clímaco, eds., *IO2011-15 Congresso da Associação Portuguesa de Investigação Operacional* (INESC, Coimbra, Portugal), 103–114.

Gonzalez-Feliu, J., F. Semet, J-L. Routhier, eds. 2014. *Sustainable urban logistics: Concepts, methods and information systems* (Springer-Verlag, Berlin Heidelberg).

Haghbin, S., K. Khan, S. Lundmark, M. Alakula, O. Carlson, M. Leksell, O. Wallmark. 2010. Integrated chargers for EV's and PHEV's: Examples and new so-

lutions. *2010 XIX International Conference on Electrical Machines (ICEM)* (IEEE, Piscataway, NJ), 1–6.

Hannisdahl, O.H., H.V. Malvik, G.B. Wensaas. 2013. The future is electric! The EV revolution in Norway – explanations and lessons learned. *2013 World Electric Vehicle Symposium and Exhibition (EVS27)* (IEEE, Piscataway, NJ), 1–13.

Hatton, C.E., S.K. Beella, J.C. Brezet, Y. Wijnia. 2009. Charging stations for urban settings – The design of a product platform for electric vehicle infrastructure in Dutch cities. *Proceedings of the 24th International Battery, Hybrid and Fuel Cell Electric Vehicle Symposium (EVS24)* (European Association for Battery, Hybrid and Fuel Cell Electric Vehicles, Brussels), 514–526.

Hensley, R., J. Newman, M. Rogers. 2012. Battery technology charges ahead. McKinsey & Company. URL `http://www.mckinsey.com/insights/energy_resources_materials/battery_technology_charges_ahead`. Last accessed June 2015.

Hiermann, G., J. Puchinger, S. Ropke, R.F. Hartl. 2016. The electric fleet size and mix vehicle routing problem with time windows and recharging stations. *European Journal of Operational Research* **252**(3) 995–1018.

International Energy Agency (IEA), Electric Vehicles Initiative (EVI). 2013. Global EV outlook - Understanding the electric vehicle landscape to 2020. URL `https://www.iea.org/publications/freepublications/publication/GlobalEVOutlook_2013.pdf`. Last accessed June 2016.

International Energy Agency (IEA), Electric Vehicles Initiative (EVI). 2015. Global EV outlook 2015 update. URL `http://www.iea.org/evi/Global-EV-Outlook-2015-Update_2page.pdf`. Last accessed June 2015.

Jerram, L., J. Gartner. 2013. Report executive summary - Hybrid electric, plug-in hybrid, and battery electric light duty, medium duty, and heavy

duty trucks and vans: Global market analysis and forecasts. Navigant Research. URL http://www.navigantresearch.com/wp-assets/uploads/2013/12/HTKS-13-Executive-Summary.pdf. Last accessed June 2015.

Ji, S., C.R. Cherry, M.J. Bechle, Y. Wu, J.D. Marshall. 2012. Electric vehicles in China: Emissions and health impacts. *Environmental science & technology* **46**(4) 2018–2024.

Juan, A.A., J. Goentzel, T. Bektaş. 2014. Routing fleets with multiple driving ranges: Is it possible to use greener fleet configurations? *Applied Soft Computing* **21** 84–94.

Karden, E., S. Ploumen, B. Fricke, T. Miller, K. Snyder. 2007. Energy storage devices for future hybrid electric vehicles. *Journal of Power Sources* **168**(1) 2–11.

Keskin, M., B. Çatay. 2016. Partial recharge strategies for the electric vehicle routing problem with time windows. *Transportation Research Part C: Emerging Technologies* **65** 111–127.

Khaligh, A., Z. Li. 2010. Battery, ultracapacitor, fuel cell, and hybrid energy storage systems for electric, hybrid electric, fuel cell, and plug-in hybrid electric vehicles: State of the art. *IEEE Transactions on Vehicular Technology* **59**(6) 2806–2814.

Khuller, S., A. Malekian, J. Mestre. 2007. To fill or not to fill: The gas station problem. L. Arge, M. Hoffmann, E. Welzl, eds., *ESA'07 Proceedings of the 15th Annual European Symposium on Algorithms*. Lecture Notes in Computer Science, Vol. 4698 (Springer-Verlag, Berlin Heidelberg), 534–545.

Kobayashi, Y., N. Kiyama, H. Aoshima, M. Kashiyama. 2011. A route search method for electric vehicles in consideration of range and locations of charging stations. *2011 IEEE Intelligent Vehicles Symposium (IV)* (IEEE, Piscataway, NJ), 920–925.

Koç, C., T. Bektaş, O. Jabali, G. Laporte. 2014. The fleet size and mix pollution-routing problem. *Transportation Research Part B: Methodological* **70** 239–254.

Kopfer, H.W., H. Kopfer. 2013. Emissions minimization vehicle routing in dependence of different vehicle classes. H-J. Kreowski, B. Scholz-Reiter, K-D. Thoben, eds., *Dynamics in Logistics – Proceedings of LDIC 2012*. Lecture Notes in Logistics (Springer-Verlag, Berlin Heidelberg), 49–58.

Kopfer, H.W., J. Schönberger, H. Kopfer. 2014. Reducing greenhouse gas emissions of a heterogeneous vehicle fleet. *Flexible Services and Manufacturing Journal* **26** 221–248.

Lam, L. 2011. A practical circuit-based model for state of health estimation of li-on battery cells in electric vehicles. Master's thesis, Delft University of Technology, The Netherlands.

Larminie, J., J. Lowry. 2003. *Electric Vehicle Technology Explained* (Wiley, Chichester, UK).

Lebeau, P., C. De Cauwer, J. Van Mierlo, C. Macharis, W. Verbeke, T. Coosemans. 2015. Conventional, hybrid, or electric vehicles: Which technology for an urban distribution centre? *The Scientific World Journal*, Article ID 302867.

Lee, D.Y., V.M. Thomas, M.A. Brown. 2013. Electric urban delivery trucks: Energy use, greenhouse gas emissions, and cost-effectiveness. *Environmental science & technology* **47**(14) 8022–8030.

Lin, C., K.L. Choy, G.T.S. Ho, S.H. Chung, H.Y. Lam. 2014. Survey of green vehicle routing problem: Past and future trends. *Expert Systems with Applications* **41**(4) 1118–1138.

Lukic, S.M., J. Cao, R.C. Bansal, F. Rodriguez, A. Emadi. 2008. Energy storage systems for automotive applications. *IEEE Transactions on Industrial Electronics* **55**(6) 2258–2267.

Macharis, C., P. Lebeau, J. Van Mierlo, K. Lebeau. 2013. Electric versus conventional vehicles for logistics: A total cost of ownership. *2013 World Electric Vehicle Symposium and Exhibition (EVS27)* (IEEE, Piscataway, NJ), 1–10.

MacLean, H.L., L.B. Lave. 2003. Evaluating automobile fuel/propulsion system technologies. *Progress in Energy and Combustion Science* **29**(1) 1–69.

Mak, H.Y., Y. Rong, Z.J.M. Shen. 2013. Infrastructure planning for electric vehicles with battery swapping. *Management Science* **59**(7) 1557–1575.

Marra, F., G.Y. Yang, C. Traholt, E. Larsen, C.N. Rasmussen, S. You. 2012. Demand profile study of battery electric vehicle under different charging options. *2012 IEEE Power and Energy Society General Meeting* (IEEE, Piscataway, NJ), 3428–3434.

McMorrin, F., R. Anderson, I. Featherstone, C. Watson. 2012. Plugged-in fleets: A guide to deploying electric vehicles in fleets. The Climate Group, Cenex, and Energy Saving Trust. URL `http://www.theclimategroup.org/_assets/files/EV_report_final_hi-res.pdf`. Last accessed June 2015.

MDS Transmodal Limited. 2012. DG move – European Commission: Study on urban freight transport. URL `http://ec.europa.eu/transport/themes/urban/studies/doc/2012-04-urban-freight-transport.pdf`. Last accessed June 2015.

Millner, A. 2010. Modeling lithium ion battery degradation in electric vehicles. *2010 IEEE Conference on Innovative Technologies for an Efficient and Reliable Electricity Supply (CITRES)* (IEEE, Piscataway, NJ), 349–356.

Mock, P., Z. Yang. 2014. Driving electrification: A global comparison of fiscal incentive policy for electric vehicles. The International Council on Clean Transportation (ICCT). URL `http://www.theicct.org/sites/default/`

files/publications/ICCT_EV-fiscal-incentives_20140506.pdf. Last accessed June 2015.

Montoya, A., C. Guéret, J.E. Mendoza, J.G. Villegas. 2016. A modified multi space sampling heuristic for the green vehicle routing problem. *Transportation Research Part C: Emerging Technologies* **70** 113–128.

Mosquet, X., M. Devineni, T. Mezger, H. Zablit, A. Dinger, G. Sticher, M. Gerrits, M. Russo. 2011. Powering autos to 2020 – The era of the electric car? The Boston Consulting Group. URL http://www.bcg.com/documents/file80920.pdf. Last accessed June 2015.

Moura, S.J. 2011. Techniques for battery health conscious power management via electrochemical modeling and optimal control. Ph.D thesis, University of Michigan, Michigan.

Naberezhnykh, D., J. Wardle, J. Lowes, C. Herron, T. Brightman, T. Parker. 2012. Electric vehicle charging points for freight vehicles in central London (Version – Final 1.0). Prepared for Central London FQP by Transport & Travel Research Ltd, in partnership with TRL and Zero Carbon Futures. URL http://www.centrallondonfqp.org/app/download/12240926/CLFQP_EVCP_strategy+report_Final+v1+0.pdf. Last accessed January 2019.

Navigant Research. 2015. Electric drive trucks and buses – Market data for medium and heavy duty commercial all-electric, plug-in hybrid electric, and hybrid electric vehicles. URL https://www.navigantresearch.com/research/electric-drive-trucks-and-buses. Last accessed June 2015.

Nesterova, N., H. Quak, S. Balm, I. Roche-Cerasi, T. Tretvik. 2013. Project FREVUE deliverable D1.3: State of the art of the electric freight vehicles implementation in city logistics. TNO and SINTEF. European Commission Seventh framework programme.

New York State Energy Research and Development Authority. 2015. New York truck voucher incentive program – NYSEV-VIF all-electric vehicle eligibility list. URL `https://truck-vip.ny.gov/NYSEV-VIF-vehicle-list.php`. Last accessed June 2015.

Nykvist, B., M. Nilsson. 2015. Rapidly falling costs of battery packs for electric vehicles. *Nature Climate Change* **5** 329–332.

Offer, G.J., D. Howey, M. Contestabile, R. Clague, N.P. Brandon. 2010. Comparative analysis of battery electric, hydrogen fuel cell and hybrid vehicles in a future sustainable road transport system. *Energy Policy* **38**(1) 24–29.

Omar, N., M.A. Monem, Y. Firouz, J. Salminen, J. Smekens, O. Hegazy, H. Gaulous, G. Mulder, P. Van den Bossche, T. Coosemans, J. van Mierlo. 2014. Lithium iron phosphate based battery – Assessment of the aging parameters and development of cycle life model. *Applied Energy* **113** 1575–1585.

Omidvar, A., R. Tavakkoli-Moghaddam. 2012. Sustainable vehicle routing: Strategies for congestion management and refueling scheduling. *2012 IEEE International Energy Conference and Exhibition (ENERGYCON)* (IEEE, Piscataway, NJ), 1089–1094.

Parish, R., W. Pitkanen. 2012. Demand assessment of first-mover hybrid and electric truck fleets. CALSTART. URL `http://www.calstart.org/Libraries/Publications/Demand_Assessment_of_First-Mover_Hybrid_and_Electric_Truck_Fleets.sflb.ashx`. Last accessed June 2015.

Pollet, B.G., I. Staffell, J.L. Shang. 2012. Current status of hybrid, battery and fuel cell electric vehicles: From electrochemistry to market prospects. *Electrochimica Acta* **84** 235–249.

Preis, H., S. Frank, K. Nachtigall. 2014. Energy-optimized routing of electric vehicles in urban delivery systems. S. Helber, M. Breitner, D. Rösch, C. Schön, J-M.

Graf von der Schulenburg, P. Sibbertsen, M. Steinbach, S. Weber, A. Wolter, eds., *Operations Research Proceedings 2012* (Springer International Publishing, Switzerland), 583–588.

Prud'homme, R., M. Koning. 2012. Electric vehicles: A tentative economic and environmental evaluation. *Transport Policy* **23** 60–69.

Psaraftis, H.N., ed. 2016. *Green Transportation in Logistics: The Quest for Win-Win Solutions*. International Series in Operations Research & Management Science, Vol. 226 (Springer International Publishing, Switzerland).

Sachenbacher, M., M. Leucker, A. Artmeier, J. Haselmayr. 2011. Efficient energy-optimal routing for electric vehicles. W. Burgard, D. Roth, eds., *Proceedings of the Twenty-Fifth AAAI Conference on Artificial Intelligence* (AAAI, Menlo Park, CA), 1402–1407.

Sassi, O., W.R. Cherif-Khettaf, A. Oulamara. 2015a. Vehicle routing problem with mixed fleet of conventional and heterogenous electric vehicles and time dependent charging costs. *International Journal of Mathematical, Computational, Statistical, Natural and Physical Engineering* **9**(3) 148–158.

Sassi, O., W.R. Cherif-Khettaf, A. Oulamara. 2015b. Iterated tabu search for the mix fleet vehicle routing problem with heterogenous electric vehicles. H.A. Le Thi, T. Pham Dinh, N.T. Nguyen, eds., *Modelling, Computation and Optimization in Information Systems and Management Sciences*. Advances in Intelligent Systems and Computing, Vol. 359 (Springer International Publishing, Switzerland), 57–68.

Sassi, O., W.R. Cherif-Khettaf, A. Oulamara. 2015c. Multi-start iterated local search for the mixed fleet vehicle routing problem with heterogenous electric vehicles. G. Ochoa, F. Chicano, eds., *Evolutionary Computation in Combinatorial*

Optimization. Lecture Notes in Computer Science, Vol. 9026 (Springer International Publishing, Switzerland), 138–149.

Schneider, M., A. Stenger, D. Goeke. 2014. The electric vehicle-routing problem with time windows and recharging stations. *Transportation Science* **48**(4) 500–520.

Shulock, C., E. Pike, A. Lloyd R. Rose. 2011. Vehicle electrification policy study – Task 1 report: Technology status. The International Council on Clean Transportation (ICCT). URL `http://theicct.org/sites/default/files/publications/ICCT_VEPstudy_Mar2011_no1.pdf`. Last accessed June 2015.

Siddiqi, U.F., Y. Shiraishi, S.M. Sait. 2011a. Multi-constrained route optimization for electric vehicles (EVs) using particle swarm optimization (PSO). *IEEE 2011 11th International Conference on Intelligent Systems Design and Applications (ISDA)* (IEEE, Piscataway, NJ), 391–396.

Siddiqi, U.F., Y. Shiraishi, S.M. Sait. 2011b. Multi-constrained route optimization for electric vehicles using SimE. *2011 International Conference of Soft Computing and Pattern Recognition (SoCPaR)* (IEEE, Piscataway, NJ), 376–383.

Siddiqi, U.F., Y. Shiraishi, S.M. Sait. 2012. Multi-objective optimal path selection in electric vehicles. *Artificial Life and Robotics* **17**(1) 113–122.

Sierzchula, W., S. Bakker, K. Maat, B. van Wee. 2012. The competitive environment of electric vehicles: An analysis of prototype and production models. *Environmental Innovation and Societal Transitions* **2** 49–65.

Smith Electric Vehicles. 2015. Smith Newton United States spec sheet. URL `http://www.smithelectric.com/wp-content/themes/barebones/pdfs/SmithNewtonUS_SpecSheet_2011.pdf`. Last accessed June 2016.

Suzuki, Y. 2009. A decision support system of dynamic vehicle refueling. *Decision Support Systems* **46**(2) 522–531.

Sweda, T.M., I.S. Dolinskaya, D. Klabjan. 2016. Optimal recharging policies for electric vehicles. *Transportation Science* **51**(2) 457–479.

Sweda, T.M., D. Klabjan. 2012. Finding minimum-cost paths for electric vehicles. *2012 IEEE International Electric Vehicle Conference (IEVC)* (IEEE, Piscataway, NJ), 1–4.

Taefi, T.T., J. Kreutzfeldt, T. Held, R. Konings, R. Kotter, S. Lilley, H. Baster, N. Green, M.S. Laugesen, S. Jacobsson, M. Borgqvist, C. Nyquist. 2016. Comparative analysis of European examples of freight electric vehicles schemes – A systematic case study approach with examples from Denmark, Germany, the Netherlands, Sweden and the UK. H. Kotzab, J. Pannek, K-D. Thoben, eds., *Dynamics in Logistics – Proceedings of LDIC 2014*. Lecture Notes in Logistics (Springer International Publishing, Switzerland), 495–504.

Thackeray, M.M., C. Wolverton, E.D. Isaacs. 2012. Electrical energy storage for transportation – approaching the limits of, and going beyond, lithium-ion batteries. *Energy & Environmental Science* **5**(7) 7854–7863.

Thiel, C., A. Perujo, A. Mercier. 2010. Cost and CO2 aspects of future vehicle options in Europe under new energy policy scenarios. *Energy Policy* **38**(11) 7142–7151.

Tie, S.F., C.W. Tan. 2013. A review of energy sources and energy management system in electric vehicles. *Renewable and Sustainable Energy Reviews* **20** 82–102.

Tuttle, D.P., K.M. Kockelman. 2012. Electrified vehicle technology trends, infrastructure implications, and cost comparisons. *Journal of the Transportation Research Forum* **51**(1) 35–51.

U.S. Department of Energy. 2012a. All laws and incentives sorted by type. Office of Energy Efficiency and Renewable Energy, Alternative Fuels Data Center. URL http://www.afdc.energy.gov/laws/matrix/incentive. Last accessed June 2015.

U.S. Department of Energy. 2012b. Plug-in electric vehicle handbook for fleet managers. Office of Energy Efficiency and Renewable Energy, National Renewable Energy Laboratory (NREL). URL http://www.afdc.energy.gov/pdfs/pev_handbook.pdf. Last accessed June 2016.

U.S. Department of Energy. 2013a. Clean cities guide to alternative fuel and advanced medium- and heavy-duty vehicles. Office of Energy Efficiency and Renewable Energy, National Renewable Energy Laboratory (NREL). URL http://www.afdc.energy.gov/uploads/publication/medium_heavy_duty_guide.pdf. Last accessed June 2015.

U.S. Department of Energy. 2013b. Smith and Navistar electric and plug-in hybrid electric vehicle testing. Office of Energy Efficiency and Renewable Energy, National Renewable Energy Laboratory (NREL) URL http://www.nrel.gov/transportation/fleettest_electric_smith_navistar.html. Last accessed June 2015.

Valenta, M. 2013. Business case of electric vehicles for truck fleets. Ph.D. thesis, Argosy University, Colorado.

Van Amburg, B., W. Pitkanen. 2012. Best fleet uses, key challenges and the early business case for e-trucks: Findings and recommendations of the e-truck task force. CALSART. URL http://www.calstart.org/Libraries/E-Truck_Task_Force_Documents/Best_Fleet_Uses_Key_Challenges_and_the_Early_Business_Case_for_E-Trucks_Findings_and_Recommendations_of_the_E-Truck_Task_Force.sflb.ashx. Last accessed June 2015.

van Duin, J.H.R., H. Quak, J. Muñuzuri. 2010. New challenges for urban consolidation centres: A case study in the Hague. *Procedia-Social and Behavioral Sciences* **2**(3) 6177–6188.

van Duin, J.H.R., L.A. Tavasszy, H.J. Quak. 2013. Towards e(lectric)-urban freight: First promising steps in the electric vehicle revolution. *European Transport*, Issue 54, Paper no.9.

Vermie, T. 2002. ELCIDIS – Electric vehicle city distribution final report. European Commission. URL `http://www.elcidis.org/elcidisfinal.pdf`. Last accessed June 2015.

Waag, W., C. Fleischer, D.U. Sauer. 2014. Critical review of the methods for monitoring of lithium-ion batteries in electric and hybrid vehicles. *Journal of Power Sources* **258** 321–339.

Wang, J., P. Liu, J. Hicks-Garner, E. Sherman, S. Soukiazian, M. Verbrugge, H. Tataria, J. Musser, P. Finamore. 2011. Cycle-life model for graphite-LiFePO4 cells. *Journal of Power Sources* **196** 3942–3948.

Work Truck Online (WTO). 2014. Determining the optimal lifecycle for truck fleets. URL `http://worktruckonline.com/channel/operations/article/story/2014/11/determining-the-optimal-lifecycle-for-truck-fleets.aspx`. Last accessed June 2015.

Yilmaz, M., P.T. Krein. 2013. Review of battery charger topologies, charging power levels, and infrastructure for plug-in electric and hybrid vehicles. *IEEE Transactions on Power Electronics* **28**(5) 2151–2169.

Yong, J.Y., V.K. Ramachandaramurthy, K.M. Tan, N. Mithulananthan. 2015. A review on the state-of-the-art technologies of electric vehicle, its impacts and prospects. *Renewable and Sustainable Energy Reviews* **49** 365–385.

Zhang, S.S. 2006. The effect of the charging protocol on the cycle life of a Li-ion battery. *Journal of Power Sources* **161**(2) 1385–1391.

Zündorf, T. 2014. Electric vehicle routing with realistic recharging models. Master's thesis, Karlsruhe Institute of Technology, Germany.

Chapter 2

Battery degradation and behaviour for electric vehicles: Review and numerical analyses of several models

Chapter information

This article is the result of a collaboration with my thesis advisors and Professor Marco Veneroni. It was published in *Transportation Research Part B: Methodological*: S. Pelletier, O. Jabali, G. Laporte, M. Veneroni. 2017. Battery degradation and behaviour for electric vehicles: Review and numerical analyses of several models. *Transportation Research Part B: Methodological* **103** 158–187.

Abstract

The use of electric vehicles for goods distribution opens up a wide range of research problems. Battery electric vehicles (BEVs) operate on batteries that have

a limited life, as well as specific charging and discharging patterns which need to be considered in the context of their use for goods distribution. While many transportation problems associated with the integration of freight electric vehicles in distribution management problems have been investigated, there is room for further research on specifically how to model battery degradation and behaviour in such problems. The aim of this paper is to provide tractable models for transportation scientists that will allow predicting the lifetime degradation and instantaneous charging and discharging behaviour of BEV batteries.

Keywords: electric vehicles; battery degradation; battery behaviour; battery modeling; green transportation.

2.1. Introduction

In recent years we have witnessed an increased interest in topics related to vehicle fleet composition, route planning and speed optimization in green logistics (see, e.g., Koç et al., 2014, 2016; Stasko and Gao, 2012; Kopfer and Kopfer, 2013; Kopfer et al., 2014; Goeke and Schneider, 2015; Sassi et al., 2015; Bektaş and Laporte, 2011; Demir et al., 2014; Gonzalez-Feliu et al., 2014; Psaraftis, 2016). The research carried out in these fields focuses on the design of distribution policies that will help decrease the environmental impact of goods distribution. An important research area lies in the development of models that can accurately predict exhaust emissions of conventional vehicles (e.g., Demir et al., 2011; Kirschstein and Meisel, 2015; Kamarianakis et al., 2011). In the same vein, increasing attention is being paid to the use of battery electric vehicles (BEVs) as a means of yielding green distribution practices (Pelletier et al., 2016; Schiffer and Walther, 2017b; Montoya et al., 2016; Bay and Limbourg, 2015).

Beyond the uncertainties surrounding the environmental impacts of freight

electric vehicles, there exist performance and financial issues associated with their integration into distribution schemes. Although offering the advantage of much lower energy and maintenance costs, these vehicles typically have autonomy and payload limitations, and involve much larger initial investments than internal combustion engine vehicles. A common denominator to these financial and technical limitations is the vehicle's battery. The most common kind of batteries used in modern passenger and freight BEVs are lithium-ion batteries (den Boer et al., 2013), which in addition to being costly and restricting the payload and range of freight BEVs, have a limited lifespan and specific charging and discharging behaviours.

2.1.1 Motivation for battery degradation modeling

When BEVs are used for goods distribution, they are usually charged at companies' facilities overnight and do not use public charging stations other than during drivers' breaks (Nesterova et al., 2013; Naberezhnykh et al., 2012; Taefi et al., 2016). This is because the long service time of most public charging stations create cargo security concerns as well as an inefficient use of the drivers' time (Naberezhnykh et al., 2012). Charging automotive lithium-ion batteries can take hours depending on the equipment used and on the capacity of the battery (US DOE, 2012), making fast charging infrastructures necessary for recharging during delivery routes; these, however, are scarce in most countries (IEA and EVI, 2013). En route recharging facilities are only useful in contexts where BEV routes are highly constrained by the battery capacity. Since one of the effects of lithium-ion battery degradation is a loss of battery capacity and hence a decrease in the vehicle's achievable range (Barré et al., 2013), and since such autonomy declines have been reported in actual freight BEV deployments (Taefi et al., 2016), long term operational flexibility can be preserved by taking steps to ensure that the

battery is not excessively aged when this can be avoided.

Lithium-ion battery packs for BEVs are a major cost component of these vehicles (Electrification Coalition, 2013). The cost of BEV lithium-ion battery packs per kWh were up to $800 in 2012 (Cluzel and Douglas, 2012; Duleep et al., 2011) and should remain above $300/kWh in the next ten years (Gerssen-Gondelach and Faaij, 2012). However, it has recently been suggested that they have been decreasing faster than predicted and could already be about $400/kWh (Nykvist and Nilsson, 2015). Still, since lithium-ion battery packs in electric trucks can have approximate energy capacities of 100 kWh and more (e.g., Smith Electric Vehicles, 2015; Electric Vehicles International, 2015; Balqon Corporation, 2013), a significant portion of the vehicle's cost can still be attributed to the battery. Several factors regarding storage and operating conditions can influence the lifespan of these batteries (Barré et al., 2013). Having to replace the battery in electric delivery trucks over the course of their lifetime has been shown to significantly decrease their attractiveness (Davis and Figliozzi, 2013; Feng and Figliozzi, 2013; Lee et al., 2013). It therefore also seems logical from a cost perspective to try to incorporate certain battery health considerations into distribution schemes with BEVs.

2.1.2 Motivation for battery behaviour modeling

Several recent studies have successfully handled the routing issues associated with the integration of BEVs in distribution management problems, such as limited range and payload, and the possibility of recharging en route at stations or at the depot. Regarding battery modeling, most studies have treated the battery as having a fixed energy capacity. Such papers have modeled the charging process either as a fixed charging time penalty (Afroditi et al., 2014; Preis et al., 2014; Conrad and Figliozzi, 2011), as an energy recharging rate per unit of time (e.g.,

Lebeau et al., 2015; Hiermann et al., 2016; Goeke and Schneider, 2015; Schneider et al., 2014; Bruglieri et al., 2015; Felipe et al., 2014), or with piecewise linear approximations based on experimental data (Zündorf, 2014; Montoya et al., 2017). During discharging, the energy capacity of the battery is either assumed to decline linearly according to the distance traveled (e.g., Hiermann et al., 2016; Schneider et al., 2014; Bruglieri et al., 2015; Felipe et al., 2014; Sassi et al., 2015), or by an amount determined according to an energy consumption model based on road forces acting on the vehicle (e.g., Lebeau et al., 2015; Goeke and Schneider, 2015; Preis et al., 2014; Bay and Limbourg, 2015).

It is clear that several routing problems associated with the use of freight BEVs have been solved, thus demonstrating that operations research can help to successfully integrate these vehicles into distribution operations by modeling and solving relevant problems (e.g., optimal paths, fleet size and mix, vehicle routing) which take into account the specific characteristics of these vehicles (Pelletier et al., 2016). Moreover, some of these problems have recently been tackled from a more strategic planning perspective through the development of models requiring simultaneous routing and charging infrastructure siting decisions (e.g., Schiffer and Walther, 2017a,b; Yang and Sun, 2015). However, we believe that there is a need for further development regarding how to model the battery's discharging and recharging processes in a tractable way, which is still capable of taking certain fundamental battery behaviour characteristics into account.

For example, a battery's capacity should ideally be treated as a measure of electrical charge rather than energy (Sauer, 2009). The battery's state of charge (SOC) should therefore refer to the current proportion of electrical charge inside the battery with respect to the maximum possible charge it can hold (Bergveld, 2001), as opposed to the current amount of energy inside the battery with respect to a maximum energy capacity, as is typically the case in transportation planning problems. As a result, the instantaneous variation of the battery's SOC can be

defined as the electrical current coming in or out of the battery divided by its maximum capacity (Moura et al., 2011), since current is a measure of electrical charge per unit of time. Furthermore, the power output of a battery corresponds to the product of its terminal voltage and current (Khajepour et al., 2014), both of which are subject to variations while discharging, according to the power profile associated with the driving cycle (Campbell, 2011). Even when assuming that a BEV travels at constant speed and hence requires a constant battery power output, the battery's terminal voltage (as it partly depends on the SOC) would decrease while discharging and its current would need to increase in order to maintain the required power output (Sauer, 2009). The battery's SOC variation with time therefore depends on the electrical current profile associated with the driving cycle.

Moreover, there exists a difference between available and maximum capacity. The latter varies with temperature and will fade over the battery's life, but the former also decreases when the battery is discharged with larger currents (Lam, 2011). This is because in order to avoid certain degradation mechanisms, the discharging process must be stopped if the battery's terminal voltage decreases to a certain cut-off value (Wenzl, 2009). Since the battery's terminal voltage can be modeled as a function of both the current and the SOC (Larminie and Lowry, 2003), the end of the discharging process can occur at several SOC values due to different voltage drops resulting from different discharging currents (Chen and Rincón-Mora, 2006). Thus, if the SOC is defined with respect to the maximum capacity under a reference temperature, the end of discharge will be reached at a SOC higher than 0%, since larger currents cause larger voltage drops, and hence the maximum capacity will only be fully delivered under an infinitely small discharging current (Lam, 2011). This also implies that a battery discharged with a large current which has reached its cut-off voltage could actually be further discharged if the current was reduced (Bergveld, 2001). In the same vein, the

available energy during a specific discharging cycle will also depend on the terminal voltage and on the current profile required to provide the power output, with the total delivered energy obtained by integrating their product over discharge time (Khajepour et al., 2014). Many studies on the use of BEVs in goods transportation assume that the battery has a fixed energy capacity which either decreases linearly with respect to time or according to an energy consumption model. However, this is not representative of the battery's true discharging behaviour. In this paper, we define the SOC with respect to the maximum charge capacity. To this end, we use a simple battery model that allows monitoring the battery's terminal voltage, SOC and discharge current according to the required battery power profile, which itself depends on a mechanical energy consumption model.

In addition, the battery in an electric vehicle is usually charged with a constant current-constant voltage (CC-CV) scheme or a constant power-constant voltage scheme (CP-CV) (Liu, 2013). In the CC-CV scheme, the charging current is held constant during the first phase (CC) and hence the SOC increases linearly with time until the battery's terminal voltage increases to a specific maximum value. Allowing the battery to reach a higher voltage will cause overcharging degradation to occur (Lam, 2011). Therefore, the terminal voltage is then held constant at its maximum value in the second phase (CV), thus causing the current to decrease exponentially and the SOC to increase concavely (Marra et al., 2012). In the CP-CV scheme, the CC phase is then replaced by a CP phase during which the current decreases with time while the terminal voltage increases to maintain the constant charging power (Liu, 2013). In both cases, the battery's SOC cannot be assumed to increase linearly throughout the process, and models that link the battery's terminal voltage to the charging current and SOC must be employed to represent realistic charging schemes that do not deteriorate the battery through overcharging. Only Zündorf (2014) and Montoya et al. (2017) have considered a

charging scheme in which the SOC does not increase at the same rate throughout the process. However, both studies use piecewise linear approximations based on experimental data to model the CC-CV charging scheme. Here we propose a method that allows modeling the CC-CV process by monitoring the battery's terminal voltage and current through the use of a battery circuit model. We also provide an existing battery circuit model which can be calibrated using only the datasheet of the battery, therefore allowing to model realistic charging schemes without the need for experimental data.

Finally, there also exist some interesting battery empirical degradation models (none of which has yet been used in existing transportation planning problems for BEVs) that consider the battery's charge throughput (i.e., the amount of electrical charge coming in and out of the battery), as well as the charging and discharging rate to estimate the battery's capacity fade, both of which require the knowledge of the battery's electrical current. The models provided in this paper for the discharging and charging behaviour of the battery allow the monitoring of the battery's current.

2.1.3 Aim and organization of this paper

For the reasons stated above, in the context of transportation planning problems with BEVs, there is a need for more elaborate modeling approaches to represent the battery's degradation over its lifetime, as well as to account for its instantaneous charging and discharging behaviours. As it stands, the relevant models are scattered over a wide variety of journals spanning several fields of research. The objective of this paper is to synthetize the knowledge pertaining to the study of electric vehicles from an operations research perspective and to provide tractable models to predict the behaviour of their batteries. We also provide several numerical examples in order to illustrate the use of some models. Moreover, based

on our description of battery dynamics, on the models and on the related numerical results presented in this paper, we derive several insights that should be of benefit to transportation planners who manage electric vehicle fleets, and to the growing community of transportation scientists involved in the development of models and algorithms for goods distribution by BEVs, several of which rely explicitly on battery degradation and instantaneous behaviour functions. With this goal in mind, Section 2.2 provides a brief description of lithium-ion batteries, their current status and expected future projections. Section 2.3 describes the mechanisms that cause degradation to occur and lists a few interesting aging models that allow the prediction of capacity fading over battery lifetime. Section 2.4 investigates how the fundamental instantaneous charging and discharging behaviour of the battery can be taken into account by appropriately aggregating a number of existing models and principles. Finally, conclusions and insights are drawn in Section 2.5. Appendix A contains a glossary of the technical terms used in this study.

2.2. Lithium-ion batteries

Lead-acid batteries, nickel-metal hydride batteries, sodium-nickel-chloride batteries (also called ZEBRA batteries), and lithium-ion batteries are all alternatives for electric vehicles (Yong et al., 2015). However, since compared to the other options, lithium-ion batteries have a high specific energy, high specific power, good lifespan attributes and low memory effect (Lukic et al., 2008), they are currently the preferred option for modern BEVs and plug-in hybrid electric vehicles (PHEVs).

2.2.1 How lithium-ion batteries function

The purpose of any rechargeable battery is essentially to employ reduction and oxidation (redox) reactions in order to store energy during charging, and subsequently use it to accomplish work during discharging (Moura, 2011). Automotive lithium-ion batteries are made of many electrochemical lithium-ion cells which are first assembled into modules and then into a battery pack to reach the desired capacity and voltage (Cluzel and Douglas, 2012). The same lithium-ion technology is behind the batteries of passenger and freight BEVs, the latter using packs with more cells or larger cells (den Boer et al., 2013; Cluzel and Douglas, 2012). In each cell, lithium ions are displaced between two intercalation electrodes during charging and discharging while electrons flow through an external circuit. This process is summarized in Figure 2.1.

The electrodes are the components looking to react with each other (i.e., provoking the redox reactions), while the electrolyte allows ions to move back and forth between these within the battery (Tarascon and Armand, 2001). The electrolyte also contains a separator to ensure that the electrodes do not come into direct contact (to prevent a short circuit) while still allowing the lithium ions to traverse its pores (Cluzel and Douglas, 2012). While discharging, electrons and lithium cations (i.e., positive ions) simultaneously leave the negative electrode (i.e., the anode) and enter the positive one (i.e., the cathode), with the electrons traversing an external electric circuit and the ions traversing the electrolyte solution; the process is reversed when the battery is charged (Cluzel and Douglas, 2012). The oxidation reaction (i.e., the loss of electrons) therefore occurs at the anode and the reduction reaction (i.e., a gain of electrons) occurs at the cathode when the battery is being discharged. The electrolyte is essential for these reactions to occur (i.e., for electrical current to be generated) since it allows positive lithium ions to move from one electrode to the other. This neutralizes the charges

that form during the loss and gain of electrons at each side and thus allows the chemical reactions to carry on (Aravindan et al., 2011). Current collectors are also connected to each electrode via a binder in order to link the active materials of the cell to the external circuit (Lam, 2011).

In summary, the idea is to force lithium ions into a disfavored higher energy state at the anode during charging (by transforming the provided electrical energy into chemical energy), and only allow them to return to a preferred lower energy state at the cathode during discharging. At this stage an external electrical circuit is connected and the discharging redox reactions can occur (by transforming the stored chemical energy into electrical energy), thus taking advantage of the movement of electrons in the process to accomplish work.

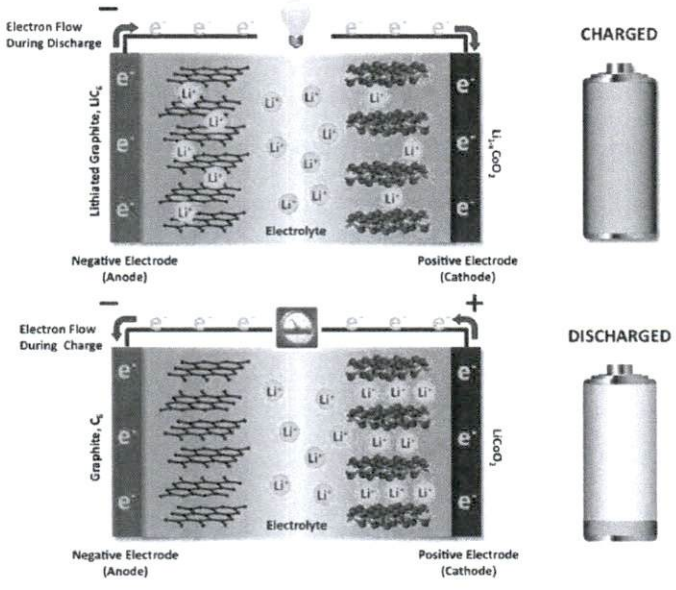

Figure 2.1 – Schematic representation of lithium-ion battery function
(Source: Thackeray et al., 2012)

2.2.2 Performance assessment

There exist several different kinds of lithium-ion batteries, varying according to the materials used in their cells and ultimately presenting pros and cons regarding attributes such as energy, power, safety, lifespan and cost (Dinger et al., 2010). The cathode is usually made of some lithium metal oxide (e.g., Figure 2.1 depicts a lithium cobalt oxide cathode) or lithium iron phosphate compound, while the anode typically consists of graphite; the electrolyte is often a lithium salt in an organic solvent (Cluzel and Douglas, 2012). Cathodes can also consist of a combination of different chemical compounds for performance and cost reasons (Thackeray et al., 2012).

Manufacturers of BEVs for goods distribution typically use cathodes made of a lithium iron phosphate compound (e.g, Boulder Electric Vehicle, 2013; Balqon Corporation, 2015), which have desirable safety and lifespan characteristics compared with other technologies, at the expense of a somewhat lower specific energy (Dinger et al., 2010). Some electric truck manufacturers have attempted to increase the performance of their vehicles by adding other metals such as magnesium to the conventional lithium iron phosphate cathode (e.g., Electric Vehicles International, 2015), or by using nanoscale materials (e.g., A123, 2015). Much research is still conducted to develop better component materials and combinations aimed at improving the performance of lithium-ion batteries (Thackeray et al., 2012).

In goods distribution with BEVs, battery weight requires trade-offs to be made between payload and range. As previously mentioned, the total energy that a battery can deliver depends on the load conditions, and hence so does its specific energy (Larminie and Lowry, 2003). However, approximate values for energy and power contents per unit of mass are still useful for comparison purposes with

other fuels. The specific energy of current automotive lithium-ion cells ranges from roughly 100 to 180 Wh/kg and depends on the materials used (Cluzel and Douglas, 2012). Although this is expected to increase in the future, the development of batteries with lithium metal anodes such as lithium-sulfur (Li-S) and lithium-air (Li-air) batteries should eventually reach specific energy values above 500 Wh/kg (Bruce et al., 2012). Another technology under development with the potential to increase specific energy is Zinc-air (Zn-air) batteries (Yong et al., 2015). Note that the final battery pack can have a specific energy that is significantly lower than the cells because of packaging components, thus estimated to be between 80 and 120 Wh/kg for BEVs in 2010 (Dinger et al., 2010). Projections made in 2012 from Gerssen-Gondelach and Faaij (2012) for BEV lithium-ion battery packs and other promising BEV battery types (Li-S, Li-air and Zn-air) are provided in Table 2.1. Specific power is not considered as a major issue for lithium-ion batteries since they are already competitive with internal combustion engines (Dinger et al., 2010). Current lithium-ion cells provide specific power values ranging approximately from 200 W/kg to 2000 W/kg (Cluzel and Douglas, 2012), while lithium-ion battery packs in modern BEVs supply about 400 W/kg, with 500 W/kg predicted for 2025 (Gerssen-Gondelach and Faaij, 2012). Current ranges for freight BEVs typically vary from 100 to 200 km (Nesterova et al., 2013; AustriaTech, 2014), and depend on factors such as load, slopes, speed, and acceleration (US DOE, 2012).

2.3. Lithium-ion battery degradation

The health of lithium-ion batteries can be adversely affected by their operating and storage conditions, with deterioration occuring during charging and discharging corresponding to cycle aging, and also during storage corresponding to calendar aging (Barré et al., 2013). Battery degradation in electric vehicles leads to

Table 2.1 – Projections for current and other promising BEV battery technologies (Source: Gerssen-Gondelach and Faaij, 2012)

		Li-ion	Li-S	Zn-air	Li-air
Specific energy (Wh/kg)	2015	150	Not applicable	Not applicable	Not applicable
	2025	200	400	250	500
	Beyond 2025	250	500	350	1000
Specific power (W/kg)	2015	400	Not applicable	Not applicable	Not applicable
	2025	500	300	Unknown	Unknown
	Beyond 2025	500	400	Unknown	Unknown
Cost ($/kWh)	2015	400–600	Not applicable	Not applicable	Not applicable
	2025	300–400	Highly uncertain	Highly uncertain	Highly uncertain
	Beyond 2025	250–300	250–500	100–300	350–700

capacity fade, thereby shortening the vehicle's achievable range, and impedance raise, which reduces the battery's available power output (Barré et al., 2013). A BEV battery is typically considered to have reached the end of its life when its available capacity or maximum power under reference conditions has decreased by 20% of its original value, although the loss of capacity is typically the determining factor given that the initial power capabilities of the battery are superior to what the vehicle requires (Lam, 2011). Lithium-ion cells in modern BEVs should have a five to ten year calendar life depending on the materials they are made of and on how they are managed (Cluzel and Douglas, 2012), and should be able to supply 1,000 to 2,000 cycles when cycled with large SOC variations in electric trucks, with 4,000 cycles expected soon (den Boer et al., 2013).

The objective of this section is twofold: to investigate what causes the performance of lithium-ion batteries to fade over their lifespan, and to determine whether such aging can be modeled in a tractable way. In order to fulfil this objective, Section 2.3.1 describes the primary mechanisms causing degradation to occur in lithium-ion batteries, as well as operating conditions which tend to enhance the effect of such mechanisms. Section 2.3.2 then presents a few practical models which allow predicting the degradation resulting from certain stress

factors over the course of a battery's lifetime.

2.3.1 Degradation mechanisms and aggravating factors

A significant portion of the deterioration of current lithium-ion cells with a graphite anode stems from chemical side reactions that occur between the anode and the electrolyte at their interface, resulting in the formation of a solid electrolyte interphase (SEI) on the anode's surface and the simultaneous consumption of lithium ions during the reaction, thus causing power and capacity fade respectively (Vetter et al., 2005; Tan et al., 2013; Zheng et al., 2015a). In the battery's first cycles, the formation of the SEI on the anode is desirable since it prevents excessive electrolyte decomposition and anode corrosion in the future while still allowing lithium ions to traverse it (Vetter et al., 2005). However, the SEI film slowly continues to grow and rearrange itself as well as to consume lithium over the course of the battery's life, and the battery's performance therefore continues to deteriorate (Vetter et al., 2005; Tan et al., 2013; Zheng et al., 2015a). Solid surface layers may also form at the interface of the cathode and the electrolyte (Vetter et al., 2005), although they are much thinner than those formed on the anode (Hausbrand et al., 2015). The reactions occurring at the interfaces of the electrodes and the electrolyte can also reduce the electrolyte's capability to allow lithium ions to flow through it as well as release unwanted gaseous side products (Moura, 2011). Overviews of anode and cathode aging mechanisms are provided in Table 2.2 and Figure 2.2, respectively.

There exist certain operating and storage conditions that tend to enhance lithium-ion battery degradation mechanisms. Keeping the cell at a high SOC or in high temperatures as well as using high charging or discharging rates can accelerate degradation resulting from electrolyte decomposition and the SEI development on the graphite anode (Vetter et al., 2005; Barré et al., 2013; Zheng et al.,

Table 2.2 – Overview of lithium-ion battery anode aging mechanisms (Source: Vetter et al., 2005)

Cause	Effect	Leads to	Reduced by	Enhanced by
Electrolyte decomposition (→ SEI) (Continuous side reaction at low rate)	Loss of lithium Impedance rise	Capacity fade Power fade	Stable SEI (additives) Rate decreases with time	High temperatures High SOC
Solvent co-intercalation, gas evolution and subsequent cracking formation in particles	Loss of active material (graphite exfoliation) Loss of lithium	Capacity fade	Stable SEI (additives) Carbon pre-treatment	Overcharge
Decrease of accessible surface area due to continuous SEI growth	Impedance rise	Power fade	Stable SEI (additives)	High temperatures High SOC
Changes in porosity due to volume changes, SEI formation and growth	Impedance rise Overpotentials	Power fade	External pressure Stable SEI (additives)	High cycling rate High SOC
Contact loss of active material particles due to volume changes during cycling	Loss of active material	Capacity fade	External pressure	High cycling rate High DOD
Decomposition of binder	Loss of lithium Loss of mechanical stability	Capacity fade	Proper binder choice	High SOC High temperatures
Current collector corrosion	Overpotentials Impedance rise Inhomogeneous distribution of current and potential	Power fade Enhances other aging mechanisms	Current collector pre-treatment	Overdischarge Low SOC
Metallic lithium plating and subsequent electrolyte decomposition by metallic lithium	Loss of lithium (loss of electrolyte)	Capacity fade (power fade)	Narrow potential window	Low temperature High cycling rate Poor cell balance Geometric misfits

2015b,c). Larger SOC variations during cycling may accelerate power fade via the growth of the SEI and possible damage to the cathode materials (Belt et al., 2003). A larger depth of discharge (DOD, i.e., cycling SOC swing) can also cause contact losses between certain components on the anode side due to volume variations of anode materials during cycling (Vetter et al., 2005).

Overcharging the battery (i.e., allowing its terminal voltage to exceed the specified cut-off value) can result in the formation of dendrite on the anode (i.e., metallic lithium deposits), thus wasting more cyclable lithium (Ouyang et al., 2015). If continuously expanded, the dendrite can even puncture the separator and result in severe overheating (Moura, 2011). Lithium plating on the anode can also develop as a result of low temperatures (Vetter et al., 2005; Barré et al., 2013)

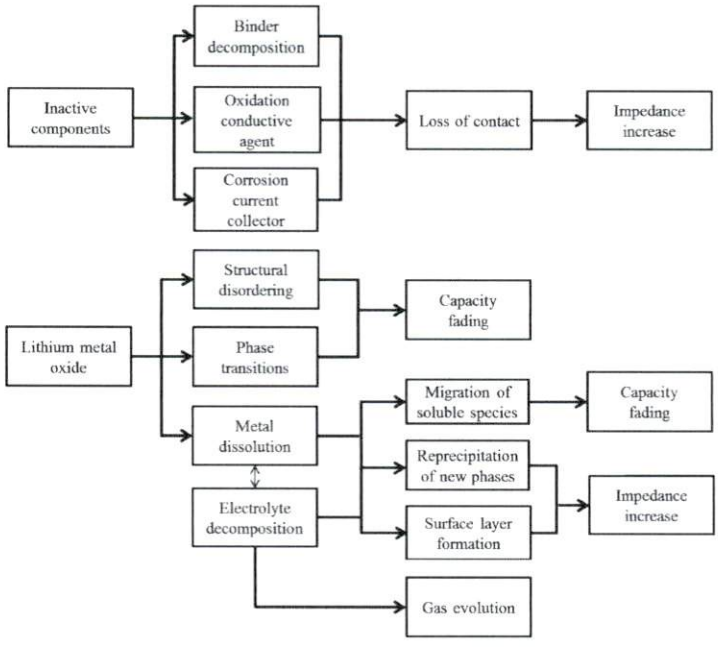

Figure 2.2 – Overview of lithium-ion battery cathode aging mechanisms (Source: Wohlfahrt-Mehrens et al., 2004)

and high charging rates (Trippe et al., 2014). A loss of active cathode materials can also occur when the battery is overcharged (Lam, 2011).

Graphite anodes can be subject to mechanical degradation (e.g., cracks and fissures) when using high charging rates in high SOC levels (Agubra and Fergus, 2013). Furthermore, certain conditions (e.g., high temperatures, low and high SOC levels) can result in the dissolution of the active materials of certain cathodes into the electrolyte as ions which can eventually end up growing the SEI film on the anode (Vetter et al., 2005; Amine et al., 2005).

Current collectors on the electrodes may also contribute to certain degradation mechanisms; for example, there could be dissolution of the anode's copper current collector when the battery is discharged to low voltage levels (i.e., near or beyond the cut-off voltage), subsequently forming dendrites on the anode which may also eventually puncture the separator (Arora et al., 1998). Current collector

corrosion resulting from excessively low voltage levels can also lead to diminished contact with the anode's materials (Vetter et al., 2005).

In summary, lithium-ion battery degradation occurs during both storage and cycling because of several chemical and mechanical processes which ultimately lead to capacity fade through the loss of cyclable lithium and other active materials, and to power fade through the formation of interface films and the loss of electrical contact between certain materials (Barré et al., 2013). The presence and extent of the different degradation mechanisms ultimately depend on the specific cell chemistry as well as storage and operating conditions; however, these mechanisms tend to interact with each other, which makes battery degradation prediction and modeling a difficult task (Vetter et al., 2005). Nevertheless, there seem to be certain recurrent factors which accelerate aging in most lithium-ion batteries, such as overcharging, overdischarging, high and low temperatures, high SOC during storage, large DOD, and high charging or discharging rates. These may be more easily incorporated into transportation planning problems without an expertise in electrochemistry. While some factors can be taken into account with simple model constraints (e.g., limiting the usable voltage or SOC window to avoid overcharging and overdischarging), the effect of others may require more elaborate degradation models (e.g., storage conditions, charging and discharging rates, temperature, DOD).

2.3.2 Useful battery lifetime degradation models

There exist different ways to estimate lithium-ion battery degradation depending on which performance attribute is being studied (capacity fade or resistance increase), which type of battery life is being considered (calendar or cycle life), and the overall modeling approach. Some of these approaches use electrochemical models, which rely heavily on theory to understand and predict the actual reac-

tions causing degradation within the battery, while others use a more empirical approach to model battery aging, thus trying to establish relationships between battery aging and certain factors by using experimental data (Bashash et al., 2011). Both electrochemical and empirical approaches have their drawbacks, notably that the former are very complex and too theoretical to be practically applied, while the latter require significant amounts of data and are only valid under specific experimental conditions (Xu, 2013). Semi-empirical models seek to combine the advantages of both previous approaches by combining theoretical principles with experimental results to attribute values to the fitting parameters of the models, thus being simpler than electrochemical models, while being applicable to broader conditions than empirical models (Xu, 2013).

Due to the very detailed and complex nature of electrochemical models, empirical and semi-empirical models seem like the most likely candidates in the context of transportation planning. The goal of this section is not to exhaustively survey such models, but rather to identify the most relevant ones for transportation planning problems. Table 2.3 highlights the key elements of the models discussed in what follows. Differences among the models include the stress factors they consider (e.g., charge or discharge rate, charge or energy throughput, DOD, temperature, storage SOC), the type of aging they study (cycle aging or calendar aging), and their output. The parameters for most of the models of Table 2.3 are determined for lithium iron phosphate batteries, which are of main interest for electric vehicles. The exceptions are the models of Hoke et al. (2011), calibrated for lithium nickel cobalt aluminium oxide batteries, of Xu (2013), calibrated for lithium manganese oxide batteries, and of Han et al. (2014), which provide an approach allowing to calibrate the model for any battery type based on information typically supplied by battery manufacturers. Also, since power capabilities of modern lithium-ion batteries are not problematic in BEVs, the following examples will mostly focus on capacity fade models. Note that such empirical and

semi-empirical methods measure the available capacity under reference conditions over the lifespan of the battery, thus eliminating the previously discussed variation of available capacity which can occur under different operating conditions.

Table 2.3 – Key elements of presented battery degradation models

Source	Stress factors considered	Type of aging considered	Model output
Wang et al. (2011)	Temperature, C-rate, charge throughput	Cycle aging	Remaining capacity
Peterson et al. (2010)	Energy throughput	Cycle aging	Remaining capacity
Sarasketa-Zabala et al. (2014b)	DOD, charge throughput	Cycle aging	Remaining capacity
Sarasketa-Zabala et al. (2014a)	Temperature, SOC	Calendar aging	Remaining capacity
Xu (2013)	DOD, SOC, C-rate, temperature, time	Cycle and calendar aging	Remaining capacity
Hoke et al. (2011)	Temperature, SOC, DOD, energy throughput	Cycle and calendar aging	Daily battery degradation cost
Omar et al. (2014)	Temperature, C-rate, DOD	Cycle aging	Number of achievable cycles before end of life
Han et al. (2014)	SOC	Cycle aging	Wear cost per unit of energy transferred to/from battery as function of SOC

Wang et al. (2011) have developed a semi-empirical degradation model for the cycle life of lithium iron phosphate cells, thus establishing a mathematical relationship linking capacity loss to the discharge C-rate, temperature and charge throughput. A discharge rate of one C is a measure of the discharging current associated with the delivered capacity when a fully charged battery reaches its cut-off voltage in one hour, and serves as the reference for expressing other discharging currents (Sauer, 2009). For example, if the one-hour discharge capacity of a battery is 10 ampere-hours, then $C = 10$ amperes (A), $5C = 50$ A, and $0.2C = 2$ A. The charge throughput is the total amount of electrical charge processed through the cell. The model of Wang et al. (2011) provides a simple formula to account for different discharge rates via Equation (2.1), in which Q_{loss} is the percentage of capacity loss, B is the pre-exponential factor (which depends on the C-rate), R is the gas constant, T is the absolute temperature, and A_h is the total charge

throughput of the cell:

$$Q_{loss} = B \cdot \exp\left(\frac{-31700 + 370.3 \cdot C_{Rate}}{R \cdot T}\right) \cdot (A_h)^{0.55}. \tag{2.1}$$

Peterson et al. (2010) have developed an empirical degradation model for the cycle life of lithium iron phosphate cells as well, and have established a linear relationship between capacity fade and the discharged energy throughput (Wh) under a realistic PHEV driving duty cycle. Their results also show the difference in the degradation occurring in driving conditions (i.e., with a time-varying discharge current) and in static conditions (i.e., with a constant discharge current). This is important since empirical models are often validated under specific experimental operating conditions which may not adequately represent the dynamic load profiles to which electric vehicles are subject in reality. Models developed for static operating conditions therefore assume that the stress factors (e.g., charging and discharging rate, cycling DOD, average SOC and temperature) will be identical over the entire lifespan of the battery. Applying a degradation model that has not been developed for dynamic operating conditions in a transportation planning problem thus requires making certain assumptions, such as the effect of time-varying stress factors during a certain horizon corresponds to the effect of their average values, and the effects of stress factors in different horizons are independent of each other.

Thus, ideally battery degradation models should be validated with data obtained under dynamic operating conditions, such as the semi-empirical ones proposed by Sarasketa-Zabala et al. (2014a) and Sarasketa-Zabala et al. (2014b) for calendar and cycling aging, respectively. These models establish mathematical relationships to link capacity loss to temperature and SOC for the calendar life model (Equation (2.2)), as well as to DOD and charge throughput for the cycle life model (Equations (2.3) and (2.4)). Both models were developed with experimental data of lithium iron phosphate cells, and validated under dynamic con-

ditions. In the following calendar aging model, T is the storage temperature, t is the storage time in days, and α_1, β_1, α_2, and β_2 are fitting parameters:

$$Q_{loss} = \alpha_1 \cdot \exp\left(\beta_1 \cdot T^{-1}\right) \cdot \alpha_2 \cdot \exp\left(\beta_2 \cdot SOC\right) \cdot t^{0.5}. \tag{2.2}$$

The cycle aging model is expressed through the following capacity fade equations, in which DOD is the depth of discharge, Ah is the total charge processed through the battery, and α_3, β_3, α_4, β_4, γ_1, γ_2, and γ_3 are fitting parameters. Equation (2.3) is for a DOD ranging from 10% to 50%, while (2.4) is for all other DOD values. Parameter k is a correction factor for dynamic operating conditions and is thus equal to 1 if the cycling DOD is constant. The only problem arising in applying this cycle life model is that the swing of SOC during charging and discharging (DOD) is assumed to always occur around a middle SOC of 50%. However, the authors plan to combine the calendar and cycle life models into a unified degradation model which would be valid under varying operating conditions, and extend the cycle life model for other middle states of charge:

$$Q_{loss} = \left(\gamma_1 \cdot DOD^2 + \gamma_2 \cdot DOD + \gamma_3\right) \cdot k \cdot Ah^{0.87} \quad \text{for} \quad 10\% \leq DOD \leq 50\% \tag{2.3}$$

$$Q_{loss} = \left(\alpha_3 \cdot \exp(\beta_3 \cdot DOD) + \alpha_4 \cdot \exp(\beta_4 \cdot DOD)\right) \cdot k \cdot Ah^{0.65} \quad \text{for} \quad DOD < 10\% \quad \text{and} \quad DOD > 50\%. \tag{2.4}$$

Another interesting aspect of their work is the method for accounting for variations in operating conditions; they use the residual capacity resulting from previous conditions to determine the position on the capacity fade curve associated with the new conditions, as proposed by Wenzl et al. (2013). This is illustrated in Figure 2.3 for calendar life degradation with varying storage temperatures. For example, in Figure 2.3, the battery is initially stored at 10°C for approximately 600 days before the storage temperature changes to 40°C. Thus, the capacity fade curve for 10°C is first followed until the temperature switches to 40°C (arrow 1 in the figure). When this happens, a horizontal shift from the capacity fade curve for

10°C to the one for 40°C is performed in order to use the one for 40°C according to the accumulated capacity fade under the previous temperature. The capacity fade curve for 40°C is then followed during the total storage time at this temperature (arrow 2 in the figure). In the same vein, when the storage temperature then switches from 40°C to 20°C, the horizontal shift to the capacity fade curve for 20°C takes into account the accumulated degradation under all previous temperatures. Such an approach therefore requires making the assumption that the degradation resulting from new operating conditions is independent of the way the accumulated capacity fade was reached (Wenzl et al., 2013).

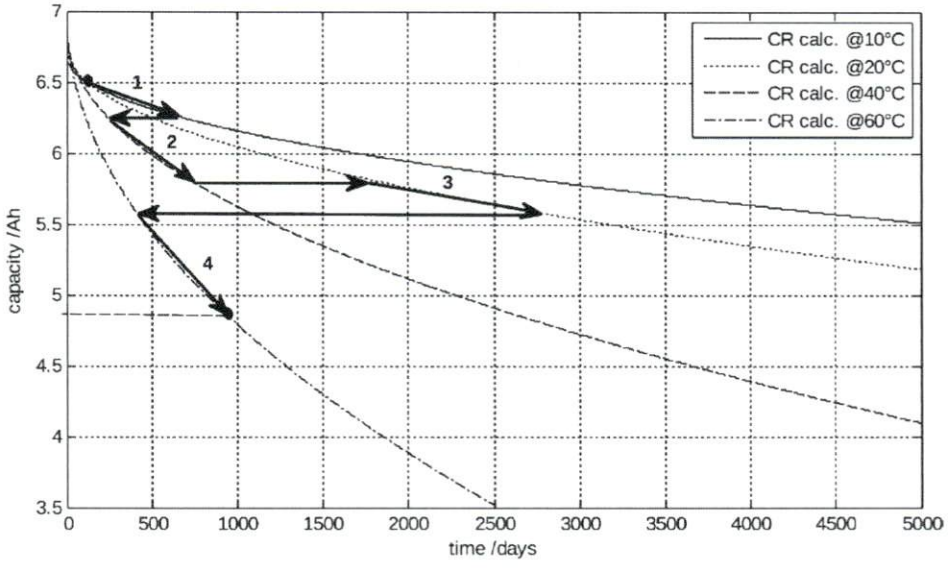

Figure 2.3 – Using capacity fade curves under varying conditions
(Source: Wenzl et al., 2013)

Using Equation (2.2) with parameter values from Sarasketa-Zabala et al. (2013), the capacity fade curves for different storage temperatures and SOC can be determined. The resulting capacity fade curves for a temperature of 25 degrees Celsius and SOC values ranging from 20% to 100% are presented in Figure 2.4. Clearly, capacity loss increases with storage SOC.

These capacity fade curves are used to determine the capacity loss for a new

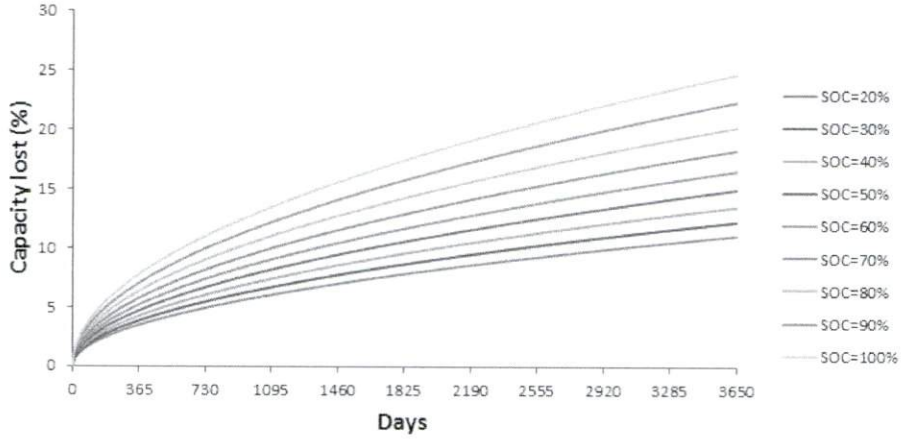

Figure 2.4 – Capacity loss for different storage SOC values at 25 degrees Celsius

lithium iron phosphate battery associated with the year long storage SOC profiles presented in Figure 2.5, assuming a constant temperature of 25 degrees Celsius. The battery SOC is maintained at values greater than or equal to 50% for the entire year in the profile on the left, while it is maintained at values below 50% for the entire year in the profile on the right. Whenever the storage SOC changes, the residual capacity resulting from all previous conditions determines the position on the capacity fade curve of the new SOC value which will be followed until the next SOC variation. The resulting capacity fade curves for the dynamic storing conditions are reported in Figure 2.5. The model predicts that the battery subjected to the profile on the left would have lost more than 6% of its initial capacity at the end of the year, while the battery subjected to the profile on the right would have lost less than 4% of its initial capacity. This is not insignificant considering that the end of life of the battery is considered to be when the capacity decreases to approximately 20% of its initial value. In fact, Lunz et al. (2012) estimated that by always trying to charge electric vehicles as closely as possible to their departure time, the battery's lifetime could be increased by approximately 40% compared to always fully charging the vehicles upon arrival. It therefore

seems logical, from a fleet management perspective, to charge electric vehicles as closely as possible to departure times when this can be done without affecting operational flexibility.

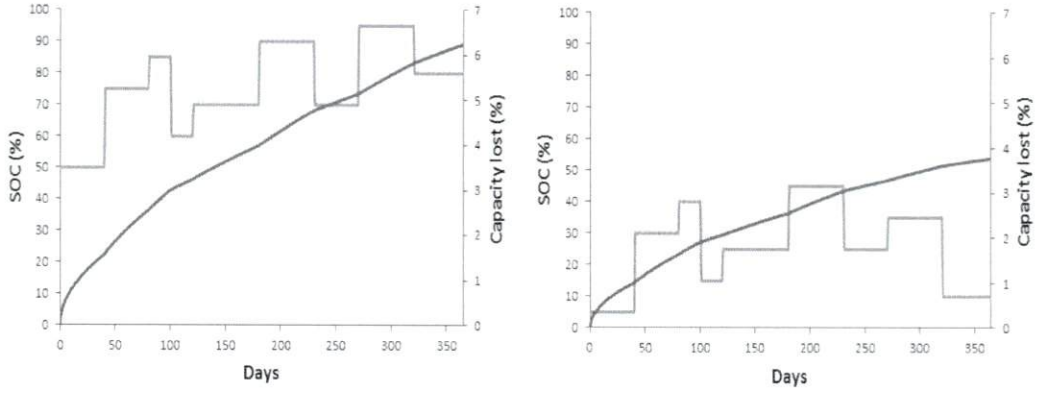

Figure 2.5 – Capacity loss for two different year long storage SOC profiles (SOC in blue, capacity lost in red)

Another approach for considering battery degradation (whether calendar or cycle aging) under varying conditions, is to consider the effect arising from operating conditions regarding a stress factor during a certain horizon relative to the total lifespan of the battery, if those same conditions were maintained throughout the battery's life. This approach was used by Hoke et al. (2011) to determine the loss of life ratios for the individual effects of temperature, average SOC, and cycling DOD on capacity fade, and for the effect of temperature on power fade. Using the assumption that the effects of these stress factors are independent, the maximum between the total capacity fade costs and power fade costs is then chosen as the degradation cost associated with the planning horizon. Thus, the battery degradation cost c_{deg} over the considered horizon is obtained with Equations (2.5) and (2.6), in which c_{bat} is the purchase cost of the battery, $c_{Q,T}$, $c_{Q,SOC}$, and $c_{Q,DOD}$ are capacity fade costs associated with temperature, SOC, and DOD respectively, and $c_{P,T}$ is the power fade cost associated with temperature. $\Delta L_{y,x}$ is

the lifespan lost during the considered horizon due to fading characteristic y (i.e., capacity Q or power P) under the present conditions regarding stress factor x (i.e., T, SOC, or DOD), and $L_{y,x}$ is the total battery lifespan if the present conditions regarding stress factor x were maintained until fading characteristic y reached its end of life value. Readers may refer to the paper of Hoke et al. (2011) for more information on the determination of the different $c_{y,x}$ costs:

$$c_{deg} = \max\{c_{Q,T} + c_{Q,SOC} + c_{Q,DOD}, c_{P,T}\} \tag{2.5}$$

$$c_{y,x} = c_{bat} \cdot \frac{\Delta L_{y,x}}{L_{y,x}}. \tag{2.6}$$

Similar approaches (i.e., determining battery degradation costs via the product of relative loss of life and the battery's price) have also been used in a few transportation planning problems. Barco et al. (2017) applied a version of the model of Hoke et al. (2011) to their VRP with electric vehicles in the context of public transportation. Arslan et al. (2014) studied a minimum cost path problem for PHEVs in which they first determine the number of cycles which could be achieved for each DOD according to the battery's cycle life curve with respect to DOD, and then multiply the battery purchase cost by the inverse of the number of cycles for each possible DOD. Hence, they determine the parameters for the following quadratic degradation cost function in monetary units for any charging SOC swing δ_i at a node i along the path, in which a and b are parameters which depend on the specific cycle life versus DOD curve of the battery: $c_{deg} = a \cdot \delta_i^2 + b \cdot \delta_i$.

For example, assume the approach described above was employed with the cycle life curve with respect to DOD given by Equation (2.7), which is used by Hoke et al. (2011) and has been determined based on data for lithium nickel cobalt

aluminium oxide batteries. The cycle life CL is then

$$CL(DOD) = \left(\frac{DOD}{145.71}\right)^{-1/0.6844}. \tag{2.7}$$

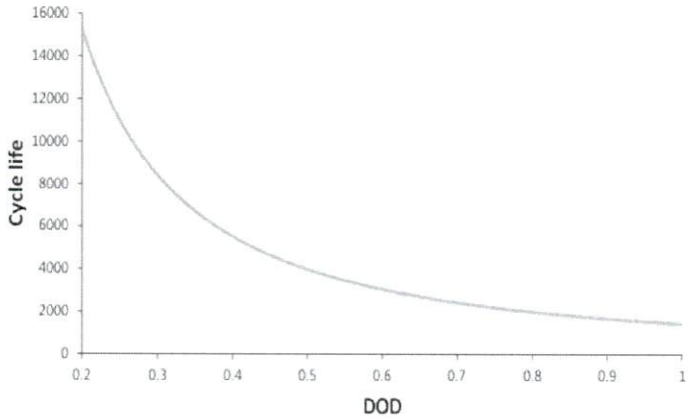

Figure 2.6 – Cycle life versus DOD

The resulting cycle life versus DOD curve is given in Figure 2.6, showing a non-linear relationship between the number of achievable cycles and DOD. As the DOD increases, the number of achievable cycles decreases. Now assume this battery is worth \$10,000 and that on a given day, it is subjected to a SOC swing of 80%. At this DOD, Equation (2.7) suggests that the battery could supply approximately 2008 cycles. The approach from Arslan et al. (2014) would therefore assume that the corresponding battery degradation cost for that day's cycle is $\$(\frac{1}{2008} \cdot 10,000)$.

This methodology could also be extended to include more elaborate cycle life models. For example, Omar et al. (2014) developed the following empirical relationship between the number of cycles that could be achieved by lithium iron phosphate batteries and the charging rate used:

$$CL(I_{ch}) = 5963 \cdot \exp(-0.6531 \cdot I_{ch}) + 321.4 \cdot \exp(0.03168 \cdot I_{ch}), \tag{2.8}$$

where $CL(I_{ch})$ is the number of times the cell can be fast charged at a constant C-

rate of I_{ch} and fully discharged at a C-rate of one before its reference capacity has decreased to 80% of its original value. Figure 2.7 illustrates $CL(I_{ch})$ for charging rates ranging from 1 to 10; the number of available cycles is clearly reduced when charging the battery with larger charging current rates. A similar relationship is also developed in Omar et al. (2014) to link cycle life to the discharging rate used.

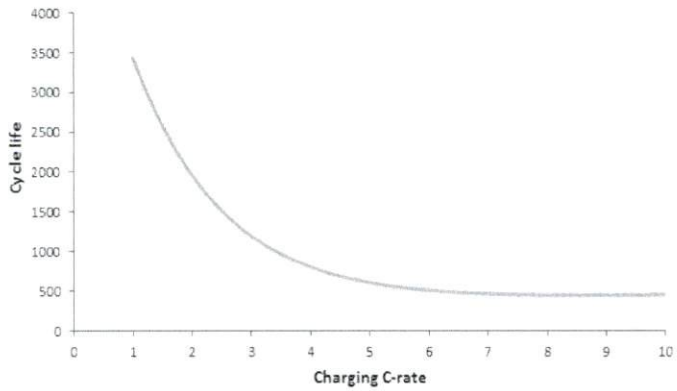

Figure 2.7 – Cycle life versus fast charging rate

A methodology similar to that of Arslan et al. (2014) could be employed in an electric vehicle routing problem with different charging options (e.g., Sassi et al., 2015; Felipe et al., 2014) in order to determine a degradation cost per cycle associated with quickly charging the battery under a high charging rate. Moreover, Omar et al. (2014) also determined an empirical relationship between the number of cycles that could be achieved by the battery before the end of its life with respect to DOD using a load profile representing dynamic operating conditions such as those encountered by electric vehicles. The cycle life versus DOD curve could be employed to calibrate the model proposed by Han et al. (2014), which uses the battery's acquisition cost and cycle life versus DOD data to develop a function representing wear costs per unit of energy going in or out of the battery according to the battery's SOC in order to account for different degradation rates occurring at different SOC levels.

Another interesting way of accounting for more specific cycling conditions than charge throughput is to use rainflow cycle counting to determine what should constitute cycles under irregular SOC driving profiles (Liu, 2013), as was done by Xu (2013) in his semi-empirical degradation model for capacity fade. The model extends that of Millner (2010) by accounting for irregular SOC profiles and isolating cycle and calendar aging. It considers stress factors such as DOD, SOC, C-rate, temperature and time. In order to determine the stress factors associated with each cycle in irregular SOC profiles, the rainflow cycle-counting method is applied to identify cycles and their respective amplitude (DOD), mean value (average SOC), begin time, and end time. Each cycle's C-rate and temperature are then determined, and their mean SOC and associated temperature are subsequently averaged to compute the horizon's overall SOC and temperature averages to be used in the calendar aging model alongside time. The fitting parameters of the model are determined with experimental data for lithium manganese oxide batteries.

2.4. Instantaneous battery behaviour modeling

Modeling the battery as an equivalent electrical circuit is a tractable way to link the battery's terminal voltage, SOC and current. The simplest of these circuit models is illustrated in Figure 2.8; it consists of modeling the battery as an open-circuit voltage ($V_{OC}(SOC(t))$) source connected in series with an internal battery resistance $R(SOC(t))$ (in ohms).

The open-circuit voltage of the battery corresponds to its voltage when there is no external load connected to it, i.e., when no current is flowing through the battery (Li and Ke, 2011). The battery's instantaneous actual voltage (or terminal voltage, $V_{term}(t)$) will be inferior and superior to its open-circuit voltage when it

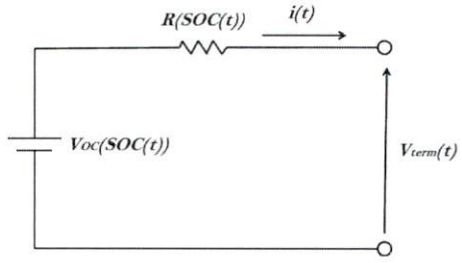

Figure 2.8 – Simple battery equivalent circuit model, with current $i(t)$ direction reflecting discharging.

is being discharged and recharged, respectively, because of the current flowing out of it or into it (Larminie and Lowry, 2003). The open-circuit voltage and the internal resistance of the battery depend on factors such as SOC and temperature (Larminie and Lowry, 2003). The battery's terminal voltage at time t can thus be obtained with Equation (2.9) from Larminie and Lowry (2003), in which $SOC(t)$ is the battery's SOC at time t, and $i(t)$ is the current flowing through the battery at time t, with the convention that the battery current is positive during discharging and negative during charging:

$$V_{term}(t) = V_{OC}(SOC(t)) - R(SOC(t)) \cdot i(t). \tag{2.9}$$

One way of establishing relationships between these circuit elements and such factors is to design empirical equations and find their fitting parameters with experimental data obtained by charging and discharging the battery in certain operating conditions, or simply to implement such experimental results as lookup tables. For example, Xu (2013) uses a circuit as in Figure 2.8 for lithium iron phosphate cells with empirical Equations (2.10)–(2.12); see Figure 2.9 for an example of these relations. The model also distinguishes between the resistance during discharging (R_d) and charging (R_c), and considers these as functions of SOC. The parameters in Equations (2.10)–(2.12) from Xu (2013) are determined experimentally by Lam et al. (2011) and given in Appendix B:

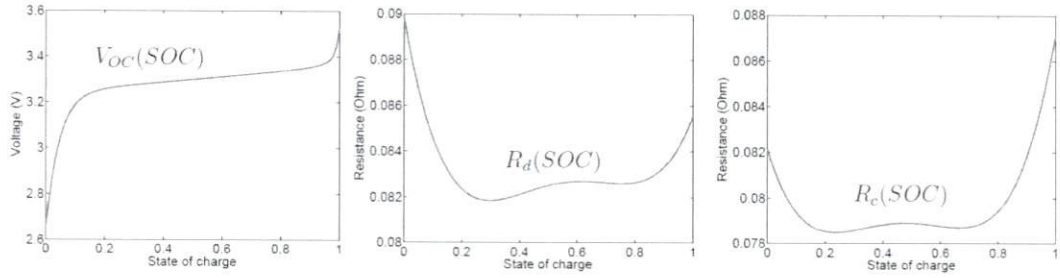

Figure 2.9 – From left to right: plots of Equations (2.10), (2.11) and (2.12), which describe open-circuit voltage, discharging resistance and charging resistance, respectively, as functions of SOC.

$$V_{OC}(SOC) = a_1 e^{-a_2 SOC} + a_3 + a_4 SOC + a_5 e^{-\frac{a_6}{1-SOC}} \tag{2.10}$$

$$R_d(SOC) = b_{1d} SOC^4 + b_{2d} SOC^3 + b_{3d} SOC^2 + b_{4d} SOC + b_{5d} \tag{2.11}$$

$$R_c(SOC) = b_{1c} SOC^4 + b_{2c} SOC^3 + b_{3c} SOC^2 + b_{4c} SOC + b_{5c}. \tag{2.12}$$

With this model, assuming that the battery's SOC varies with time (i.e., $SOC(t)$), the instantaneous terminal voltage during discharging ($V_{term,d}(t)$) and charging ($V_{term,c}(t)$) is expressed through Equations (2.13) and (2.14) respectively, which are adapted from Xu (2013):

$$V_{term,d}(t) = V_{OC}(SOC(t)) - R_d(SOC(t)) \cdot i(t) \tag{2.13}$$

$$V_{term,c}(t) = V_{OC}(SOC(t)) - R_c(SOC(t)) \cdot i(t). \tag{2.14}$$

Another approach is to use pre-established mathematical relationships to model fundamental relationships between terminal voltage, SOC and current (Li and Ke, 2011). The model of Tremblay et al. (2007), which is based on Shepherd's equation (Shepherd, 1965), is an example. It has the advantage of only requiring three points on the constant current discharge curve typically included in the battery's data sheets (as illustrated in Figure 2.10) to extract the model's parameters and it allows to develop a generic battery behaviour model for four battery

types (including lithium-ion batteries). The approach of Tremblay et al. (2007) considers the following relationship between the open-circuit voltage and SOC:

$$V_{OC}(SOC(t)) = E_0 - \frac{K}{SOC(t)} + A\exp(-BQ(1 - SOC(t))). \tag{2.15}$$

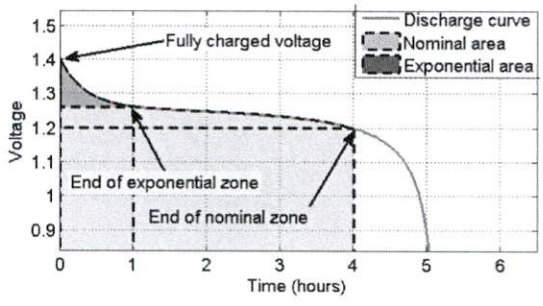

Figure 2.10 – Typical constant current discharge curve
(Source: Tremblay et al., 2007)

In Equation (2.15), E_0 is the battery constant voltage, K is the polarisation voltage, Q is the maximum battery capacity in ampere-hours, $SOC(t)$ is the present charge at time t with respect to maximum capacity Q, A is the exponential zone amplitude (in volts), and B is the exponential zone time constant inverse. Readers may refer to Tremblay et al. (2007) for the practical method to extract the parameters from the discharge curve. The model assumes that the internal resistance R in Equation (2.9) is constant, that all parameters are identical during charging and discharging, that the temperature has no effect on the parameters, and that the minimum open-circuit voltage is zero.

Using this expression in (2.9) we obtain Equation (2.16), which constitutes an alternative to (2.13) and (2.14) to describe the terminal voltage, for both charging and discharging:

$$V_{term}(t) = E_0 - \frac{K}{SOC(t)} + A\exp(-BQ(1 - SOC(t))) - R \cdot i(t). \tag{2.16}$$

There exist several additional ways of modeling the battery as an equivalent circuit, which vary according to trade-offs between accuracy and complex-

ity (Chen and Rincón-Mora, 2006). For example, the model in Figure 2.8 assumes that the terminal voltage reacts instantaneously to a sudden variation of the applied load, while in reality during such sudden current variations there are both an instantaneous variation and a gradual one. These dynamic voltage responses under step current variations can be captured by adding parallel resistor-capacitor (RC) components to the circuit of Figure 2.8 (e.g., Chen and Rincón-Mora, 2006; Liu, 2013). The circuit components must be determined through experimental tests allowing a characterization of the battery's response to sudden load variations, by either assuming that the circuit components are constant or depend on factors such as SOC and temperature (see, e.g., Rahmoun and Biechl, 2012; Zheng et al., 2009).

In models based on pre-estmathematical relationships such as the one of Tremblay et al. (2007) previously discussed, such dynamic voltage responses during sudden current variations can be incorporated by using a low pass filtered current flowing through a polarisation resistance, as proposed by Tremblay and Dessaint (2009), thereby modeling a similar battery transient behaviour to that of a circuit model with an RC component. These authors further improved the model of Tremblay et al. (2007) by developing separate relationships for the four battery types during discharging and charging due to certain differences in voltage behaviours.

2.4.1 Discharging

In the context of routing electric vehicles for goods distribution, during discharging it is the required battery power that will determine the current to be supplied by the battery. In scenarios assuming a constant speed or infrequent and slow speed variations, the errors resulting from disregarding dynamic voltage responses are less significant (Larminie and Lowry, 2003). In such circumstances,

a tractable circuit like that of Figure 2.8 seems like a practical way to account for fundamental battery discharging behaviour.

During discharging, the required mechanical power (P_M) (in watts) can be found based on the road forces acting on the vehicle. Using the model of Barth et al. (2005), P_M can be calculated as follows:

$$P_M = Mav + Mgv\sin(\theta) + 0.5C_dA\rho v^3 + MgC_r\cos(\theta)v, \tag{2.17}$$

where M is the vehicle's total mass (kg), a is the acceleration (m/s^2), v is the speed (m/s), g is the gravitational constant, C_d is the aerodynamic drag coefficient, A is the frontal area of the vehicle (m^2), ρ is the air density (kg/m^3), C_r is the rolling resistance coefficient, and θ is the road angle. Equation (2.17) essentially states that the total mechanical power required must allow accelerating the vehicle with a and overcoming grade, aerodynamic, and rolling resistances. The associated power output (or input in the case that regenerative braking is also considered) by the electric motor and battery can then be found according to their output (or input) efficiencies (Goeke and Schneider, 2015), as illustrated in Figure 2.11. Wu et al. (2015) have used a similar approach to compare estimated instantaneous power and total trip energy consumption to real in-use EV data and have found the model to be accurate despite its simplicity.

Asamer et al. (2016) have also studied the energy consumption estimation of electric vehicles based on a similar mechanical model by computing P_M as

$$P_M = Mavf + Mgv\sin(\theta) + 0.5C_dA\rho v^3 + MgC_r\cos(\theta)v, \tag{2.18}$$

where all terms are the same as in (2.17), except for f which represents a mass factor greater than one used to account for the rotational inertia of a BEV's rotating

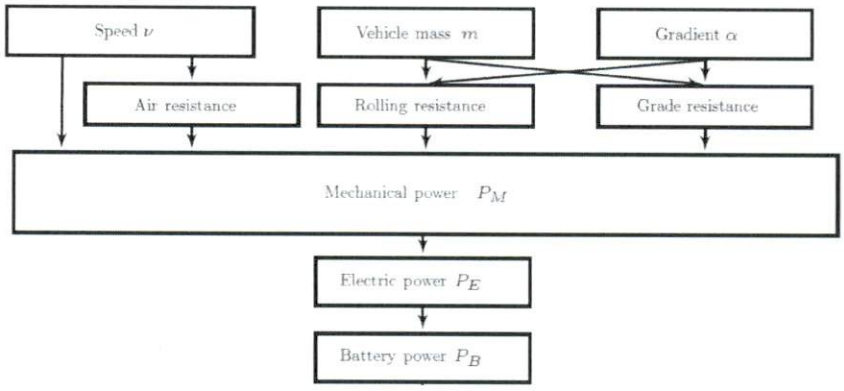

Figure 2.11 – Schematic calculation of required battery power
(Source: Goeke and Schneider, 2015)

parts. The authors then compute the required battery power P_B as follows:

$$P_B = \begin{cases} \frac{P_M}{\eta_M} + P_0, & \text{if } P_M \geq 0 \\ P_M \eta_G + P_0, & \text{if } P_M < 0, \end{cases} \tag{2.19}$$

where P_0 is a constant power demand for auxiliary loads (e.g., heating, air conditioning), η_M is the total efficiency of the drive train during energy consumption, and η_G is the total efficiency of the drive train during energy recuperation. The model presented in Asamer et al. (2016) also considers that if $P_M < 0$, then the term $P_M \eta_G$ is zero if the vehicle's speed is below a certain threshold V_{min} (i.e., energy recuperation is not possible when the vehicle's speed is too low). The authors first used the above model with default parameter values to estimate the energy consumption of a BEV for hundreds of trips with varying speed and elevation profiles, as well as the energy share related to each of the model's components (i.e., rolling resistance, grade resistance, aerodynamic resistance, acceleration, and auxiliary energy). The real total energy consumption was also measured for each trip. They subsequently computed average measured and estimated energy consumption for different average trip speeds. Their results are presented in Figure 2.12 and show that the energy consumption per 100 kilometers is highest at

low and high speeds, with acceleration and auxiliary loads responsible for most of the energy consumption at low speeds (because of more acceleration phases and longer travel times), and aerodynamic resistance being responsible for most of the energy consumption at high speeds. The authors also performed a sensitivity analysis to determine which of the mechanical model parameters should be calibrated as precisely as possible, finding that the rolling resistance coefficient and the drive train efficiency during energy consumption have the largest impact on the accuracy of the model. The uncertainty of other parameter values were also found to have a significant impact on the model's accuracy, but only under specific conditions (e.g., auxiliary loads at low speeds, air density at high speeds, vehicle mass in uphill environments, drive train efficiency during energy recuperation in downhill environments).

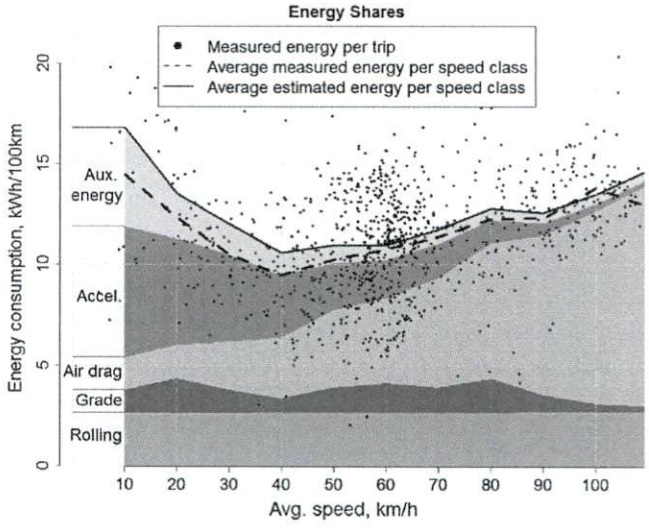

Figure 2.12 – Average energy shares in dependence of average trip speed (Source: Asamer et al., 2016)

Once the power profile required from the battery with respect to time is known (i.e., $P_B(t)$), it can be linked to its instantaneous terminal voltage $V_{term}(t)$ and cur-

rent $i(t)$ with Equation (2.20) from Larminie and Lowry (2003):

$$P_B(t) = V_{term}(t) \cdot i(t). \tag{2.20}$$

Recalling that the terminal voltage can itself be modeled with Equations (2.15) and (2.16), Equation (2.20) can be reformulated as (2.21):

$$P_B(t) = (V_{OC}(SOC(t)) - R \cdot i(t)) \cdot i(t). \tag{2.21}$$

As in Moura et al. (2011), we define the rate of change of SOC with respect to time as

$$\dot{SOC}(t) = \frac{d}{dt} SOC(t) = -\frac{i(t)}{3600 \cdot Q}. \tag{2.22}$$

Note that since the maximum capacity Q is assumed to be in ampere-hours, it must be converted to coulombs by multiplying it by 3600, since current is expressed in coulombs per second. One can then solve the quadratic formula (2.23) resulting from Equation (2.21) and thus find Equation (2.24) for the instantaneous SOC rate of change, $\dot{SOC}(t)$, as in Moura et al. (2011):

$$P_B(t) = V_{OC}(SOC(t)) \cdot i(t) - R \cdot i(t)^2 \tag{2.23}$$

$$\dot{SOC}(t) = -\frac{V_{OC}(SOC(t)) - \sqrt{V_{OC}(SOC(t)^2 - 4P_B(t)R}}{2 \cdot 3600QR}. \tag{2.24}$$

The expression of SOC with respect to time for the associated power profile can then be determined by solving the differential Equation (2.24) with an initial SOC value, see Figure 2.13.

The same approach could also be used with a model considering the internal resistance R as a function of SOC (e.g., with Equations (2.11) and (2.12)); it would yield comparable results to those shown in Figure 2.13. If using a degradation model considering charge throughput, the expression for the electrical current with respect to time (which can easily be found knowing the expression of $SOC(t)$) can be integrated over travel time to find the total charge throughput.

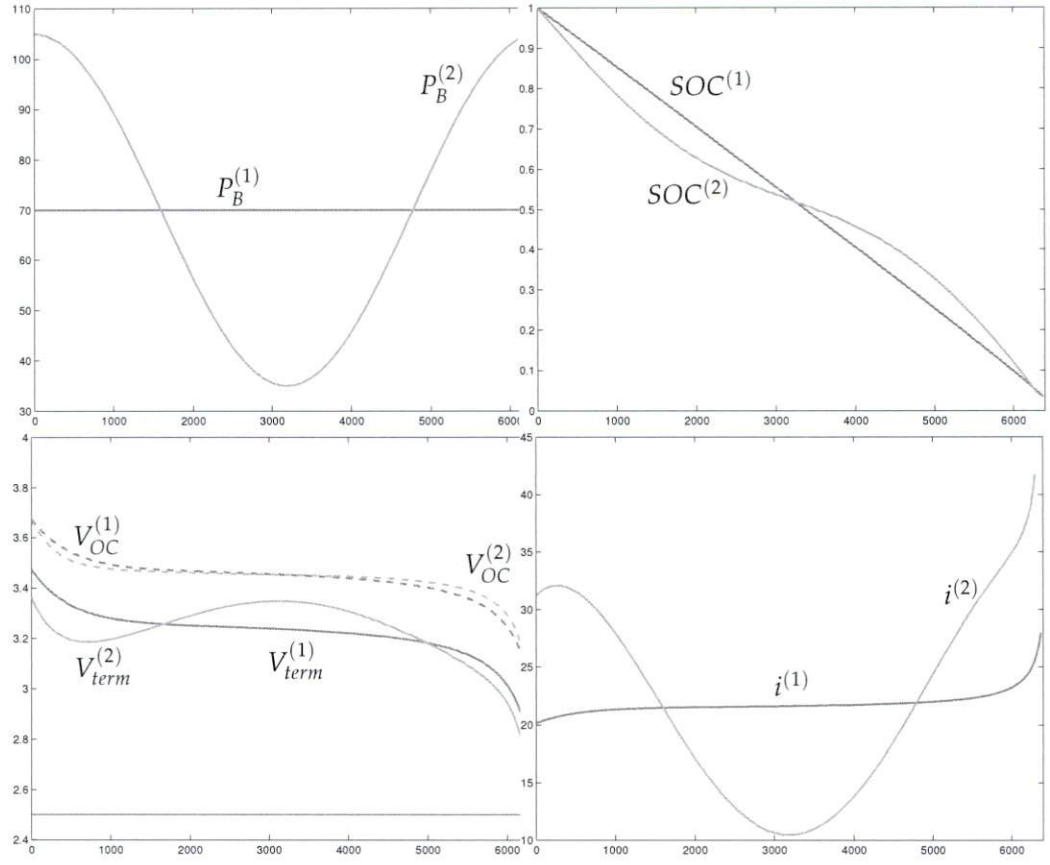

Figure 2.13 – Numerical solutions of (2.24) for two different power profiles: a constant one, $P_B^{(1)}$, and an oscillating one, $P_B^{(2)}$ (top left diagram). In clockwise order starting from the top right diagram, for $j = 1, 2$, the corresponding states of charge $SOC^{(j)}$, currents $i^{(j)}$, open-circuit voltage $V_{OC}^{(j)}$ and terminal voltage $V_{term}^{(j)}$, as given by Equations (2.15) and (2.16) (right). The horizontal line in the voltage plot marks the cut-off voltage (V_{min} =2.5 V), the horizontal axis represents time (in seconds).

If the degradation model also involves the discharging rate, one can then make the assumption that the C-rate corresponds to the one associated with the average current supplied (i.e., the charge throughput divided by the travel time). The expression for current with respect to time can also be discretized into segments during which the current does not vary significantly. The capacity fade curves associated with the average C-rate of each segment could then be used as in Figure 2.3 by replacing the horizontal axis with charge throughput and with variations in operating conditions being caused by changing C-rates rather than temperatures.

In addition, since the battery can never operate at a terminal voltage lower than a certain cut-off value V_{min}, it is possible to approximate the maximum available discharging power and discharging current at any given moment t according to $SOC(t)$ with the relation linking terminal voltage, SOC and current. The maximum available instantaneous discharging current $i_{max}(t)$ is the one that would result in the battery's terminal voltage $V_{term}(t)$ dropping to its known cut-off value V_{min}. With the model of Figure 2.8 and assuming that resistance R is constant, the following equations from Liu (2013) allow approximating the maximum available instantaneous discharging current $i_{max}(t)$:

$$\begin{aligned} V_{term}(t) &= V_{OC}(SOC(t)) - R \cdot i(t) \\ V_{min} &= V_{OC}(SOC(t)) - R \cdot i_{max}(t) \\ i_{max}(t) &= \frac{V_{OC}(SOC(t)) - V_{min}}{R}. \end{aligned}$$

Recall that with the model of Figure 2.8, during discharging the instantaneous battery power is a concave quadratic function with respect to the instantaneous battery current for a given SOC, so its maximum value is reached at stationary point $i(t)^* = \frac{V_{OC}(SOC(t))}{2R}$, corresponding to a battery power $\frac{V_{OC}(SOC(t))^2}{4R}$. However, this maximum value can only be reached if $i(t)^*$ is smaller than $i_{max}(t)$. Assuming that the maximum allowable discharging current $i_{max,limit}$ specified by

the manufacturer is known and must always be respected, the real maximum available instantaneous discharging power can be defined as

$$P_{B_{max}}(t) = \begin{cases} \frac{V_{OC}(SOC(t))^2}{4R}, & \text{if } \min\{i(t)^*, i_{max}(t), i_{max,limit}\} = i(t)^* \\ (V_{OC}(SOC(t)) - R \cdot i_{max}(t)) \cdot i_{max}(t), & \text{if } \min\{i(t)^*, i_{max}(t), i_{max,limit}\} = i_{max}(t) \\ (V_{OC}(SOC(t)) - R \cdot i_{max,limit}) \cdot i_{max,limit}, & \text{if } \min\{i(t)^*, i_{max}(t), i_{max,limit}\} = i_{max,limit}. \end{cases}$$

Finally, it should be noted that the parameters of electrical circuit models are typically determined for single electrochemical cells, while battery packs are made of several parallel strings of cells connected in series. Assuming all cells in the pack are identical and that power P_{pack}, terminal voltage V_{pack}, and current i_{pack} at the pack level are evenly distributed among the cells (i.e., P_{cell}, V_{cell}, and i_{cell}), the relationships between these elements at the pack and cell level are given by Equations (2.25)–(2.27) from Xu (2013). N_p indicates the number of parallel strings and N_s indicates the number of cells connected in series per string:

$$P_{cell} = \frac{P_{pack}}{N_s \cdot N_p} \tag{2.25}$$

$$V_{cell} = \frac{V_{pack}}{N_s} \tag{2.26}$$

$$i_{cell} = \frac{i_{pack}}{N_p}. \tag{2.27}$$

Some cell models use parameters that can be directly extended to the pack level according to the cell's data sheets and the number of parallel strings in the pack and cells connected in series per string (e.g., MathWorks, 2015).

Assuming all parameters in Equation (2.17) besides speed, acceleration and road grade remain constant during a trip, the approach described in this section can thus be used to obtain the terminal voltage, current, and SOC profile of the battery based on the speed and elevation profile of a given trip. Figure 2.14 provides an example of these profiles for the simulated speed profile in the top left diagram. The road grade and auxiliary power demand are assumed to be zero.

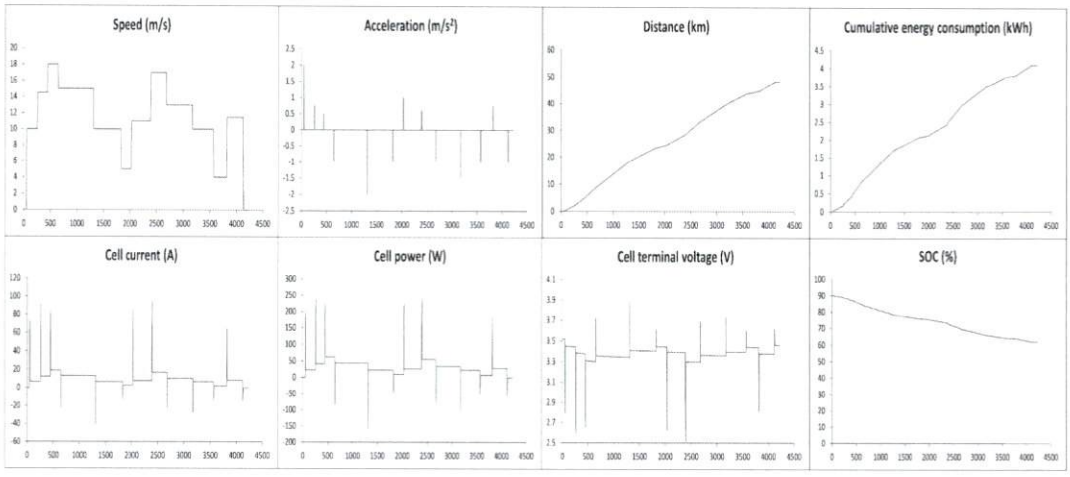

Figure 2.14 – Numerical example of voltage, current and SOC profiles according to speed profile. The horizontal axis represents time (in seconds)

The required mechanical power is calculated with Equation (2.17), and the required battery power is calculated with Equation (2.19). The parameters for the mechanical power model are taken from Peterson et al. (2010). The battery model of Tremblay et al. (2007) is used with parameter values from Marra et al. (2012) for a battery composed of 110 lithium iron phosphate cells connected in series, each with a charge capacity of 40 ampere-hours. The required battery power is assumed to be evenly divided among the cells, as expressed through Equation (2.25). The battery pack has a nominal energy capacity of 14 kWh. As can be seen in Figure 2.14, the cell current, power, and terminal voltage change at a slow and relatively constant rate when the vehicle travels at constant speed, but suddenly increase or decrease during acceleration and deceleration phases. The required power from each cell clearly is at its highest levels when the vehicle is accelerating. The total traveled distance for the simulated speed profile is approximately 48 kilometers, and the battery's SOC varies from initial SOC of 90% to a final SOC of 62%.

2.4.2 Charging

Avoiding overcharging degradation can essentially be achieved by modeling the recharging process as a CC-CV process (or CP-CV) rather than one linear charging function with time, since the CV phase eliminates the risk of reaching exceedingly high voltage levels which can damage the battery. However, this requires a method to monitor the non-linearly increasing SOC during the CV phase. In the context of transportation planning problems, Sweda et. al. (2016) propose using an overcharging cost function that considers the extra amount of time required for charging the battery in the CV phase of a CC-CV charging scheme. The actual function is based on the experience of a Nissan Leaf driver and is used to determine optimal recharging policies along a certain path. Another method that has been employed in such problems is to use piecewise linear approximations for the charging curve according to experimental data. This technique was applied by Zündorf (2014) in his minimum cost path problem with different types of charging stations. On the other hand, the battery models just described can be used to model the charging behaviour explicitly since they allow monitoring the battery's terminal voltage and current throughout the process of CC-CV and CP-CV charging schemes (e.g., Marra et al., 2012). In what follows we model the CC-CV explicitly by using a battery circuit model as in Figure 2.8.

As discussed in Section 2.1.2, in a CC-CV charging process, the charging current is held constant during the first phase until the battery's voltage reaches a predefined maximum value V_{CV}; the SOC will therefore increase linearly with time, and the battery's terminal voltage can be monitored according to its relation with SOC and current. Once the terminal voltage reaches its specified threshold, the charging process switches to the CV phase, during which the terminal voltage is held constant; the electrical current decreases exponentially with time until a minimal cut-off current value is reached, and the SOC's rate of change therefore

continuously decreases. This is illustrated in Figure 2.15.

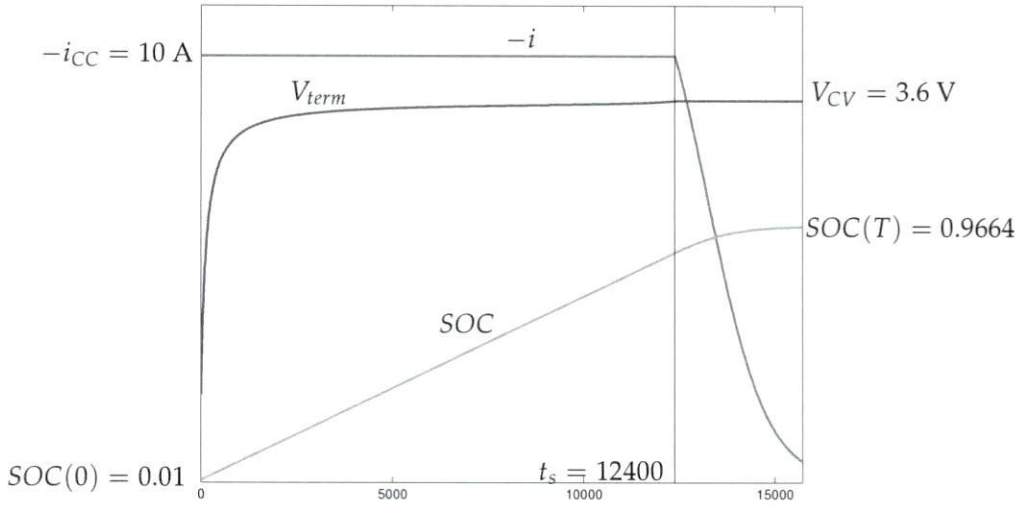

Figure 2.15 – CC-CV charging scheme. The horizontal axis shows the time, the vertical axis is not in scale, in order to simultaneously illustrate the behaviour of current, voltage, and state of charge. The CC phase ($t < t_s$) is obtained explicitly from (2.28). The CV phase ($t > t_s$) is obtained as a numerical solution of Equations (2.30)–(2.32).

Thus, during the CC phase (i.e., until the terminal voltage reaches its specified threshold V_{CV}), the state of charge is given by

$$SOC(t) = SOC(0) - \frac{i_{CC} \cdot t}{3600 \cdot Q} \qquad \forall t \mid V_{term}(t) < V_{CV}, \tag{2.28}$$

where $SOC(0)$ is the known SOC at the moment the charging process begins, and i_{CC} is the known constant charging current (the battery current is assumed to be negative during charging).

The terminal voltage must be monitored during the CC phase in order to switch to CV charging when it reaches its known threshold V_{CV} and thus ensure the battery is not overcharged. This can be achieved by incorporating the expression for $SOC(t)$ from (2.28) and the constant charging current i_{CC} into Equation (2.9), thus giving Equation (2.29) in which $V_{OC}(SOC(t))$ can be determined with

(2.15) if the resistance R is assumed to be constant:

$$V_{term}(t) = V_{OC}(SOC(t)) - R \cdot i_{CC} \qquad \forall t \mid V_{term}(t) < V_{CV}. \tag{2.29}$$

The same could be done by assuming that the internal resistance R varies with SOC as well, in which case Equations (2.10) and (2.12) could be used for $V_{OC}(SOC(t))$ and $R(SOC(t))$.

Let t_s denote the time t for which $V_{term}(t) = V_{CV}$, which marks the switching time between CC and CV phase. The value of SOC upon entering this phase is simply $SOC(t_s) = SOC(0) - i_{CC} \cdot t_s/3600 \cdot Q$. The relationship linking the terminal voltage to the battery's SOC and current (now a decreasing function of time, $i(t)$) allows one to establish a differential equation which can be solved to find SOC as a function of time during the CV phase, according to the initial value $SOC(t_s)$ and the maintained voltage value V_{CV}. Recalling the relationship between the rate of change of SOC and electrical current (2.22) results in the following equations for the CV phase:

$$i(t_s) = i_{CC} \tag{2.30}$$

$$\begin{aligned} V_{CV} &= V_{OC}(SOC(t)) - R \cdot i(t) \quad \forall t \geq t_s \\ &= V_{OC}(SOC(t)) + R \cdot 3600 \cdot Q \cdot \dot{SOC}(t) \end{aligned} \tag{2.31}$$

$$\dot{SOC}(t) = \frac{V_{CV} - V_{OC}(SOC(t))}{R \cdot 3600 \cdot Q}. \tag{2.32}$$

Once the expression for $SOC(t)$ has been determined, the one for $i(t)$ can be easily deduced during the CV phase and the charging process can be terminated once it falls below a certain current threshold i_{min}. One can intuitively understand why the SOC increases concavely during the CV phase by recalling that the battery's open-circuit voltage increases with SOC and that a larger current implies a larger difference between the battery's open-circuit and terminal voltage (with the latter superior to the former during charging). The battery's terminal voltage is held constant during CV, so that following an infinitesimal time increment af-

ter entering the CV phase, the SOC will increase by the amount corresponding to the current used in the CC phase. Since the SOC will have increased, so will the open-circuit voltage, but since the terminal voltage must remain constant, the current will have to decrease (Bergveld, 2001). Hence following another infinitesimal time increment, the SOC will have further increased, but at a slower pace due to the current decrease, thus requiring the current to further diminish, and so on until the current reaches its termination value.

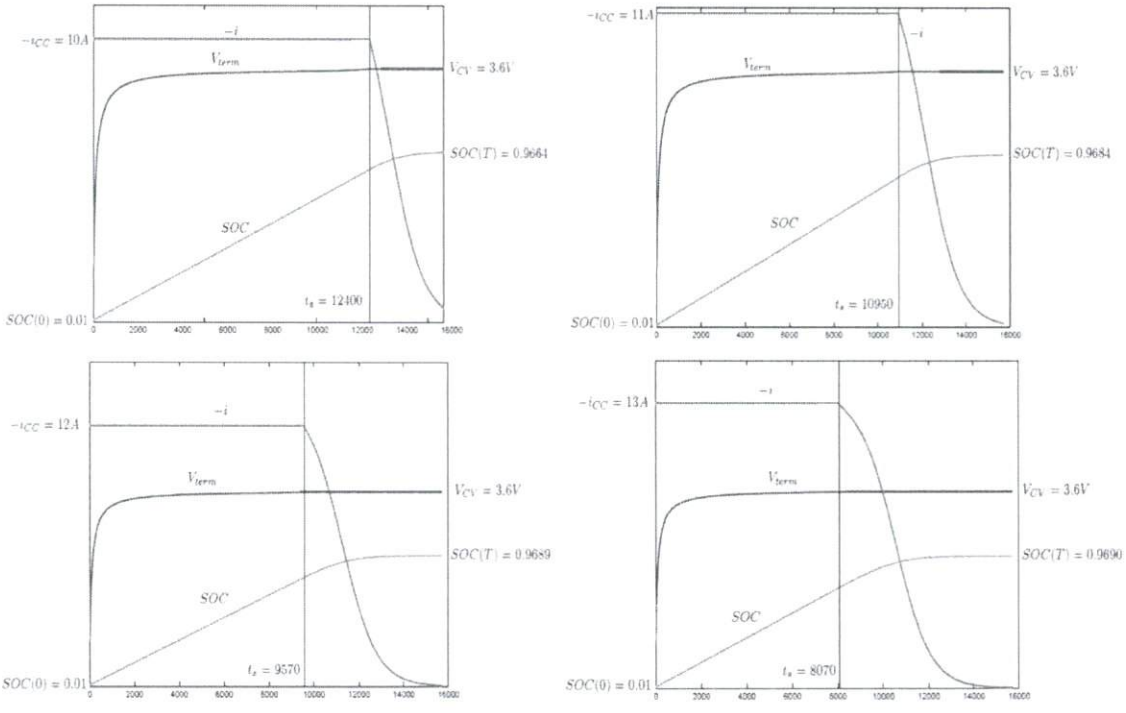

Figure 2.16 – Comparison of CC-CV charging profile for different current values in CC phase

Figure 2.16 illustrates the impact the current i_{CC} has on the CC-CV charging profile of a given battery cell. The top left diagram in Figure 2.16 reproduces the same CC-CV charging scheme as in Figure 2.15 for $-i_{CC} = 10$ A, while the other three are for i_{CC} values of 11 A, 12 A, and 13 A. The final time T is the same in all simulations. As can be seen in Figure 2.16, as the value of $-i_{CC}$ increases, the time

t_s at which the CV phase is entered is reached faster and at a lower SOC. Indeed, $SOC(t_s)$ is worth approximately 87%, 85%, 81% and 74% when $-i_{CC}$ is 10 A, 11 A, 12 A, and 13 A respectively. There is therefore a trade-off between the elapsed time and the SOC at the end of the CC phase according to the charging rate used. Moreover, it is interesting to note that although the value of i_{CC} influences the respective length of each phase, the final SOC value at time T is almost the same in all cases. In sum, a larger current rate during the CC phase will shorten the CC phase but lengthen the CV phase. This also means that in the context of fast charging, which only performs the CC phase (i.e., charging is terminated when the terminal voltage reaches V_{CV}), there exists a tradeoff between the charging time and the maximum reachable SOC according the charging current used.

Another advantage of considering the charging process in such a way is that it allows for monitoring the power being retrieved from the grid more accurately, and hence for the development of more realistic grid capacity constraints in routing problems which allow central depot recharging. For example, the power on the grid side can be monitored by linking the instantaneous grid charging power $P_{grid}(t)$ to the required battery power $P_B(t)$ according to the charging efficiency η (Marra et al., 2012). Since the current is held constant while the terminal voltage increases during the CC phase, and since $P_B(t) = V_{term}(t) \cdot i_{cc}$ during this phase, both P_B and P_{grid} will increase (in absolute values) with time until reaching the CV phase. This is illustrated in Figure 2.17 for a CC-CV scheme with an initial charging power level of 3.7 kW and an initial SOC of 60%.

This also enables us to determine the charging current i_{CC} that will be applied to the battery during the CC phase if the charger offers an adjustable initial power level $P_{grid}(0)$. Denoting $V_0 := V_{OC}(SOC(0))$, the following equations describe the relation between $P_{grid}(t)$ and $P_B(t)$, as well as how to find i_{CC}, assuming the initial

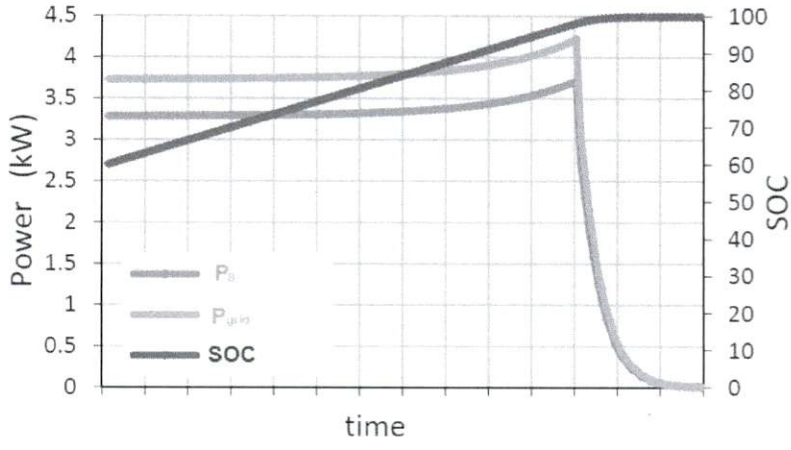

Figure 2.17 – Charging power during CC-CV charging scheme (Source: Marra et al., 2012)

SOC and charging power to be known (i.e., $SOC(0)$ and $P_{grid}(0)$):

$$P_B(t) = \eta \cdot P_{grid}(t) \tag{2.33}$$
$$P_B(0) = \eta \cdot P_{grid}(0) = V_{term}(0) \cdot i_{CC} = (V_0 - R \cdot i_{CC}) \cdot i_{CC}$$
$$i_{CC} = \frac{V_0 - \sqrt{V_0^2 - 4P_B(0)R}}{2R}.$$

On the other hand, in the absence of an increase in the grid's power output throughout the charging process, the battery can be charged under a CP-CV charging process (Marra et al., 2012). According to the constant power output from the grid and the charging efficiency, the power applied to the battery during the CP phase can be found with Equation (2.33), and the functions for SOC and current (which decreases with time since the terminal voltage increases but the power must remain constant) can be found with Equation (2.24) for a constant power P_B instead of $P_B(t)$, assumed to be negative during charging. Once the terminal voltage reaches its threshold, the same method as for the CV phase in the CC-CV scheme can be applied to express SOC as a function of time.

2.4.3 Simplifications

Evidently, there exist several different ways of modeling the behaviour of a battery during discharging and charging, ultimately varying according to trade-offs between accuracy and complexity. Nevertheless, some simplifications can also be made. A few of these are now discussed.

2.4.3.1 Time discretization

In order to avoid having to deal with continuous temporal functions for SOC and current that must be determined by solving differential equations, time can always be discretized into short intervals during which it is assumed that the battery's power, terminal voltage and current remain constant. This eliminates the need both for solving differential equations and for integrating current to find charge throughputs. Knowing the initial SOC at the start of the horizon and the length Δt of each time step, the SOC at the beginning of each time step k could thus be determined according to the current of the previous one, as expressed in Equation (2.34) from Dekkiche (2008):

$$SOC_{k+1} = SOC_k - \frac{\Delta t}{3600 \cdot Q} \cdot i_k. \tag{2.34}$$

Similarly, the charge throughput of a period will correspond to the product of its current and duration. With a simple circuit model in which the battery is considered as a SOC-dependent open-circuit voltage connected in series with a constant internal resistance, the terminal voltage of each time step will correspond to

$$V_{term_k} = V_{OC}(SOC_k) - R \cdot i_k. \tag{2.35}$$

As a result, for a given SOC_k and discharging or charging battery power P_k, the

current of each time step will be

$$i_k = \frac{V_{OC}(SOC_k) - \sqrt{V_{OC}(SOC_k)^2 - 4P_kR}}{2R}. \tag{2.36}$$

In the case of a CC-CV charging scheme, during the CV phase of charging, the current of each period would then determined according to the constant terminal voltage V_{CV} and the SOC at the start of the period:

$$\begin{aligned} V_{CV} &= V_{OC}(SOC_k) - R \cdot i_k \\ i_k &= \frac{V_{OC}(SOC_k) - V_{CV}}{R}. \end{aligned}$$

Figure 2.18 recreates the discharging numerical example of Figure 2.13 with a time step of $\Delta t = 1$ second using Excel. The numerical solution obtained is very similar to that obtained by solving the differential Equation (2.24) with the `ode45` solver in MATLAB (which, it should be noted, solves the differential equation by discretizing time with an adaptive time step). The mean absolute difference between the SOC values at each time step of one second obtained with Excel and the ones produced by the differential equation solver at the corresponding time points is below 0.2% for both the constant and variable battery power profiles. The same result holds with a time step of 10 seconds.

2.4.3.2 Constant open-circuit voltage

Although it seems relevant to closely monitor the battery's terminal voltage, current, and SOC during charging in the context of goods distribution with electric vehicles in order to determine realistic charging times, this seems somewhat less reasonable in a transportation planning problem to simulate the battery's voltage, current and SOC in real time. Doing so while simultaneously optimizing delivery routes and respecting their associated operational constraints may lead to a problem that is simply too large for practical purposes. However, since some

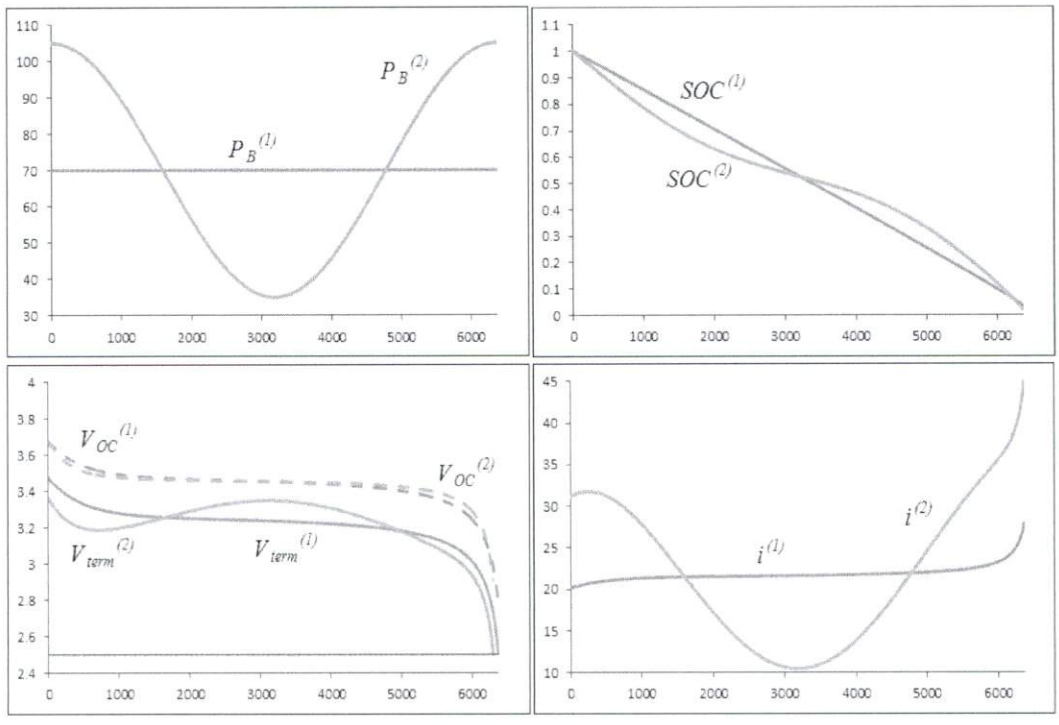

Figure 2.18 – Numerical solutions of (2.24) using a time step of 1 second for the same two power profiles of Figure 2.13.

lithium-ion batteries such as those with a lithium iron phosphate cathode have a relatively flat open-circuit voltage curve for a large SOC range, while the battery is discharging one could assume that it has a fixed open-circuit voltage, e.g., its average value with respect to SOC. A circuit model with a constant internal resistance can then be used to further simplify the analysis. The rate of change of the battery's SOC, as given by Equation (2.24), would therefore no longer depend on the SOC itself and could be more easily integrated to find a continuous function of SOC with respect to time.

Figure 2.19 recreates the numerical example of Figure 2.13 with a time step of $\Delta t = 1$ second and assuming a constant open-circuit voltage of 3.45 volts. With such a simplification, as can be seen in Figure 2.19, if the discharging power is

assumed to be constant, the discharging current will also be constant for the required power output, which may simplify determining the value of certain degradation model variables such as charge throughput and discharging C-rate. Without assuming a constant open-circuit voltage (i.e., in Figure 2.18), the SOC value when the terminal voltage reaches its cut-off value is 3.5% (at the final time of 6370 seconds) and 4.2% (after 6295 seconds) for the constant and variable power profiles respectively. When assuming a constant open-circuit voltage, the terminal voltage never reaches its cut-off value before the final time of 6370 seconds; the SOC reached at the time when the terminal voltage would have reached its cut-off value with the SOC dependent open-circuit voltage is approximately 4.2% (at the final time of 6370 seconds) and 5.0% (after 6295 seconds) for the constant and variable power profiles respectively. The simplification can therefore still track the SOC fairly accurately.

However, the fact that for the same power profiles, assuming the open-circuit voltage is constant influences whether the terminal voltage reaches its cut-off value illustrates a drawback of this simplification. Indeed, it could result in the overestimation of the battery's available capacity and overdischarging degradation (i.e., operating the battery at a terminal voltage lower than the cut-off value). In reality, as the battery discharges, its SOC decreases and so does its open-circuit voltage. Eventually, the open-circuit voltage reaches values that are too low to allow supplying the battery current needed to meet the power demand without resulting in a voltage drop that would cause the battery's terminal voltage to fall below its cut-off voltage, and discharging must therefore be terminated. Assuming a constant open-circuit voltage, however, will lead to overestimating the terminal voltage of the battery towards the end of its discharge cycle, since the constant value will then be larger than its real SOC dependent value. Figure 2.20 illustrates this drawback. For the given constant power demand (top left), the blue and green lines are the resulting open-circuit voltage, terminal voltage, SOC,

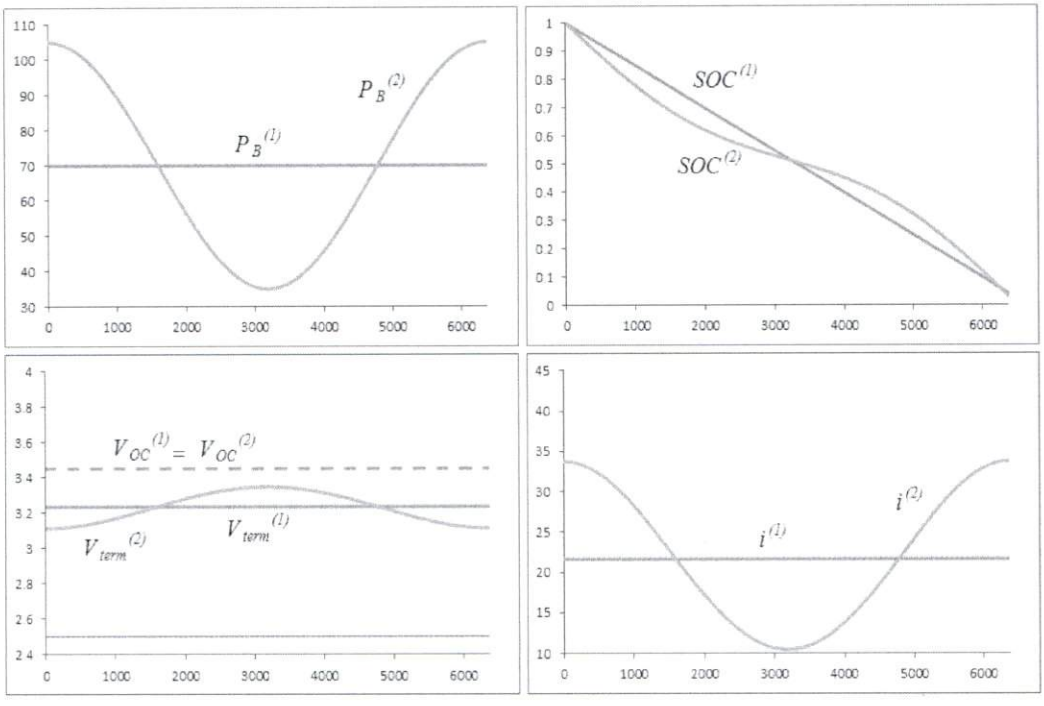

Figure 2.19 – Numerical solutions of (2.24) using a time step of 1 second and a constant open-circuit voltage for the same two power profiles of Figure 2.13.

and current profiles when assuming a constant and SOC dependent open-circuit voltage respectively. For the SOC dependent open-circuit voltage, the terminal voltage reaches its cut-off value of 2.5 volts when the SOC is approximately 18%, and the battery can no longer supply the current needed for the power demand without operating beneath the cut-off voltage, so discharging must be halted. For the constant open-circuit voltage, the battery's terminal voltage never reaches its cut-off value and can therefore discharge all the way to a SOC of 0%, but in reality it will have been operating at a terminal voltage below its cut-off value since the SOC was 18%.

Moreover, this simplification cannot be used for modeling the battery's CC-CV charging scheme. Recall that during charging, SOC is always increasing, and

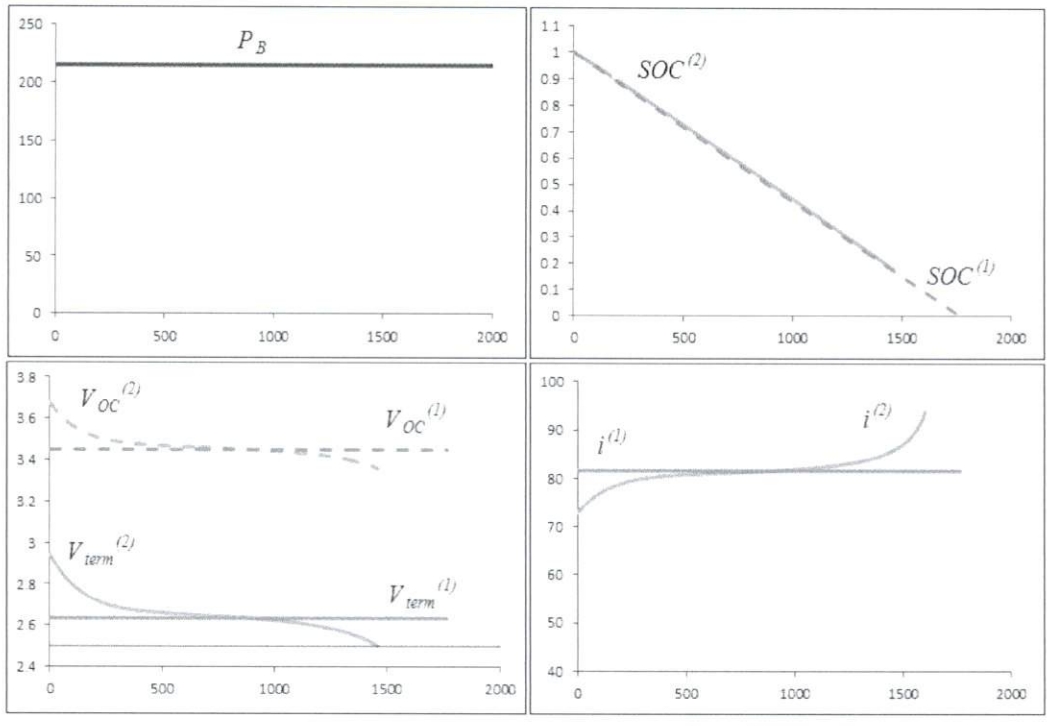

Figure 2.20 – Numerical solutions of (2.24) using a time step of 1 second for a constant power demand P_B (top left diagram) when assuming a constant open-circuit voltage (blue lines, $j = 1$) and a SOC dependent one (green lines, $j = 2$). In clockwise order starting from the top right diagram, for $j = 1, 2$, the corresponding states of charge $SOC^{(j)}$, currents $i^{(j)}$, open-circuit voltage $V_{OC}^{(j)}$ (3.45 V for $j = 1$; as given by Equation (2.15) for $j = 2$) and terminal voltage $V_{term}^{(j)}$ (as given by Equation (2.35)). The horizontal line in the voltage plot marks the cut-off voltage (V_{min} =2.5 V), the horizontal axis represents time (in seconds).

that the open-circuit voltage increases with SOC. During the CC phase, the current is held at a constant value until the terminal voltage reaches its specified maximum value. However, the only reason the terminal voltage increases during the CC phase is due to the open-circuit voltage. Indeed, the only variable of the right hand side of Equation (2.29) (which describes the terminal voltage during the CC phase) is the SOC dependent open-circuit voltage. Similarly, during the CV phase, the only reason the current decreases is due to the increasing open-

circuit voltage, since the only variable of the right hand side of Equation (2.32), which describes the rate of change of the SOC (i.e., current divided by capacity) during the CV phase, is the SOC dependent open-circuit voltage. Therefore, assuming a constant open-circuit voltage does not allow modeling a realistic charging process for the battery.

2.4.3.3 Peukert equation

If the load can be regarded as a constant discharge current, the Peukert equation offers a practical method to account for variations in available capacity according to the discharging current. The following discussion is based on principles and equations from Larminie and Lowry (2003) and Khajepour et al. (2014). A battery's Peukert capacity C_p is assumed to be the available capacity in amperehours of a battery under a constant discharge current of 1 A. The battery's constant Peukert coefficient k is used to establish a relationship between its Peukert capacity and any constant discharge current i and associated discharge time t_{cut} (i.e., the elapsed time in hours from a fully charged state before the terminal voltage reaches its cut-off value when discharged with constant current i):

$$C_p = i^k \cdot t_{cut}.$$

The coefficient k can be found with two known capacity ratings (C_1 and C_2) for the battery and their associated discharge time in hours (t_{cut_1} and t_{cut_2}). First, the discharge current (i_1 and i_2) for each capacity rating can be computed:

$$i_1 = \frac{C_1}{t_{cut_1}}, \qquad i_2 = \frac{C_2}{t_{cut_2}}.$$

We can then use this information to find the Peukert coefficient k since the right-hand side of both following equations must be equivalent:

$$C_p = i_1^k \cdot t_{cut_1}, \qquad C_p = i_2^k \cdot t_{cut_2}.$$

The coefficient k is thus

$$k = \frac{\log t_{cut_2} - \log t_{cut_1}}{\log i_1 - \log i_2}.$$

The available capacity $C_a(i)$ in ampere-hours and discharge time $t_{cut}(i)$ in hours for any constant discharge current i can then be estimated through the following equations:

$$t_{cut}(i) = \frac{C_p}{i^k}$$
$$C_a(i) = t_{cut}(i) \cdot i = \frac{C_p}{i^{k-1}}.$$

It is also possible to assume that with a time-varying discharge current $i(t)$, the available capacity would be the one associated with the average discharge current. Another approach for a time-varying discharge current is to assume that the level of discharge of the battery can be estimated with respect to the constant Peukert capacity C_p according to the integral of $i^k(t)$ over time. Assuming a positive current during discharge, if the instantaneous level of discharge $D(t)$ is defined as a value ranging from 0 (i.e., fully charged state) to 1 (i.e., when the cut-off voltage has been reached), and if the initial level of discharge D_0 is known, then $D(t)$ can be defined as

$$D(t) = D_0 + \frac{\int_0^t i^k(t)}{3600 \cdot C_p}.$$

The Peukert capacity is multiplied by 3600 to convert it to the same unit as $i^k(t)$ (coulombs). The instantaneous variation of the level of discharge is thus

$$\frac{dD(t)}{dt} = \frac{i^k(t)}{3600 \cdot C_p}.$$

However, using the Peukert equation for a time-varying discharge current as described above underestimates the available capacity of the battery (Doerffel and Sharkh, 2006). Moreover, without monitoring the battery's terminal voltage, the current can no longer be determined by dividing the required battery

power by its terminal voltage. Therefore, using this simplification to determine the battery's available capacity without monitoring its voltage would require a knowledge of the current profile in advance, rather than determining it by dividing the required battery power by its terminal voltage. Nevertheless, if the load can be regarded as constant discharge current (e.g., for a constant power demand when assuming a constant open-circuit voltage), this is a simple but interesting capacity modeling approach since it provides a method to estimate variations of available capacity without having to monitor the terminal voltage of the battery. The coefficient k for lithium-ion batteries typically varies between 1.00 and 1.09, where a value of 1.00 indicates that there is no loss of capacity under higher discharge currents (Omar et al., 2012). Estimations of available capacity based on the Peukert relationship can also be further extended to incorporate the effect of other factors (e.g., temperature and cycle life) on the Peukert coefficient (Omar et al., 2013).

2.5. Conclusions

The goal of this article was not to advance the science of battery monitoring and degradation, but rather to model these features so as to provide applicable knowledge to the growing community of researchers involved in the planning of goods distribution by electric vehicles. Several lithium-ion battery degradation mechanisms and specific storage and operating conditions that affect their lifespan were described, as well as a few useful degradation models. In addition, some existing battery models and principles were investigated and aggregated in order to account for fundamental battery behaviour during discharging and charging. We have shown that battery degradation and behaviour are quite complex phenomena to model, and that several different modeling approaches are available. We have concluded that empirical approaches allow for the development of capacity

fade equations which are more easily employed without an expertise in electrochemistry. In the same vein, modeling the battery as an equivalent circuit appears to be a tractable way to describe basic battery characteristics during charging and discharging.

Moreover, our simultaneous investigation of both battery degradation and behaviour leads to a few intuitive insights which should be of interest from a fleet management perspective in the context of goods distribution with electric vehicles. For example, since calendar aging occurs faster when the battery is stored at a higher SOC, in terms of battery health, the charging of fleet vehicles should always be performed as closely as possible to their departure time. Another insight concerns the charging time and the required SOC upon departure. If different charging rate options are available at the depot for the CC phase during CC-CV charging, the use of a higher charging rate will cause the SOC to increase more quickly during the CC phase, but the terminal voltage will reach its maximum value at a lower SOC. Since the purpose of using a higher charging current is to quickly charge the battery, in such cases it seems logical to terminate charging after the CC phase. Hence, if the CV phase is not performed, there exists a trade-off between the elapsed time and the SOC at the end of the CC phase according to the charging rate used.

We also believe that some of our findings can be used in the context of goods distribution with electric vehicles to develop charging and discharging policies which ensure that battery health is preserved both in the short and long term, the latter being treated from a more strategic perspective. For instance, operating the battery outside its specified voltage range will quickly cause severe overcharging and overdischarging degradation, and should therefore always be avoided (Lam, 2011). However, storing the battery overnight at a higher rather than a lower SOC has a much smaller effect, and hence does not need to be as tightly constrained. The same could be said about cycling the battery with a large DOD or with large

charging and discharging rates. The incorporation of such stress factors in transportation planning problems is not so straightforward, but the use of calendar and cycle aging models should allow for the development of certain habits that can prolong battery life.

Finally, it is worth mentioning that although battery behaviour can be described by the different models we have discussed, incorporating these models into transportation planning problems is not a trivial task. An interesting research avenue lies in the integration of some of the methods discussed in this paper into a vehicle routing problem setting. To obtain tractable models in such a setting, a first step could be to discretize time in order to facilitate the application of some of the discussed behaviour and degradation models, thus implying the need to account for multi-period planning horizons. Moreover, electric vehicle routing problems with a strong emphasis on the vehicles' charging schedule should incorporate more realistic charging processes (e.g., CC-CV), and ideally consider the charging schedule's impact on the batteries' health, both of which imply the presence of non-linearities which pose modeling and algorithmic challenges.

Acknowledgements

This research was partly supported by the Canadian Natural Sciences and Engineering Research Council under grants 463834-2014, 436014-2013 and 2015-06189. This support is gratefully acknowledged. Thanks are also due to Olivier Tremblay for sharing his knowledge of battery modeling with us, and to the referees for their valuable comments.

2.6. Appendix A – Glossary

Anode: The electrode of a cell at which the oxidation reaction (i.e., loss of electrons) occurs during discharging.

Available capacity (C_a): The amount of charge that can be discharged from a fully charged battery before the terminal voltage reaches its cut-off value. The available capacity is reduced when the battery is discharged with larger currents. Capacity is expressed in ampere-hours (Ah), with one Ah equivalent to a current of one A supplied during one hour (i.e., A = C/s = $\frac{1}{3600}$ Ah/s). If the terminal voltage reaches its cut-off value at time t_{cut} when discharged from a fully charged state at time t_0, the available capacity in Ah is

$$C_a = \int_{t_0}^{t_{cut}} \frac{i(t)}{3600} \cdot dt.$$

Available energy (E_a): The amount of energy that can be supplied from a fully charged battery before the terminal voltage reaches its cut-off value, expressed in watt-hours (Wh). If the terminal voltage reaches its cut-off value at time t_{cut} when discharged from a fully charged state at time t_0, the available energy is

$$E_a = \int_{t_0}^{t_{cut}} P_B(t) \cdot dt = \int_{t_0}^{t_{cut}} V_{term}(t) \cdot i(t) \cdot dt.$$

Battery current ($i(t)$): The electrical current flowing through the battery at time t, assumed to be positive during discharging and negative during charging in this article. The battery current is expressed in amperes (A), with one A equivalent to one coulomb (C) per second.

Battery electric vehicle (BEV) : A vehicle that is propelled by an electric motor and only uses the power provided by its battery that can be charged from the electricity grid.

Battery power ($P_B(t)$): The instantaneous power supplied by or to the battery, equivalent to the product of the battery's instantaneous terminal voltage and current, and expressed in watts (W):

$$P_B(t) = V_{term}(t) \cdot i(t).$$

Cathode: The electrode of a cell at which the reduction reaction (i.e., gain of electrons) occurs during discharging.

C-rate: A discharge rate of one C is a measure of the discharging current associated with the available capacity when a fully charged battery reaches its cut-off voltage in one hour, and serves as the reference for expressing other discharging currents. If the one-hour discharge capacity of a battery is 10 Ah, then $C = 10$ A, $5C = 50$ A, and $0.2C = 2$ A.

Cut-off voltage (V_{min}): The minimum allowable terminal voltage value. Discharging must be halted when the terminal voltage, which decreases while the battery is discharged, reaches this value.

Depth of discharge (DOD): The proportion of electrical charge discharged or charged during a cycle with respect to the maximum possible charge the battery can hold.

Electrolyte: The medium that allows ions to be displaced between the anode and the cathode within a cell while electrons flow through an external electrical circuit.

Hybrid electric vehicle (HEV): A vehicle that uses an internal combustion en-

gine and an electric motor for propulsion, as well as a battery for electrical energy storage.

Lithium-ion battery: Several lithium-ion cells connected in series and parallel to reach the desired voltage and capacity.

Lithium-ion cell: An electrochemical device in which lithium ions are displaced back and forth between two electrodes in order to transform the stored chemical energy into electrical energy during discharging, and the provided electrical energy into chemical energy during charging.

Maximum charge voltage (V_{CV}): The maximum allowable terminal voltage value during charging, expressed in volts (V) and indicating when the charging scheme switches from the constant current phase to the constant voltage phase.

Memory effect: The gradual loss of available capacity when certain types of batteries are frequently recharged without being fully discharged.

Open-circuit voltage ($V_{OC}(SOC(t))$): The voltage between the battery terminals when there is no load connected (i.e., when no current is flowing through the battery), expressed in volts. The open-circuit voltage depends on the SOC of the battery at time t.

Plug-in hybrid electric vehicle (PHEV): A hybrid electric vehicle with a battery that can be charged from the electricity grid.

Specific energy: The approximate amount of energy stored per unit of battery mass, expressed in watt-hours per kilogram (Wh/kg).

Specific power: The approximate amount of available power per unit of battery mass, expressed in watts per kilogram (W/kg).

State of charge ($SOC(t)$): The proportion of electrical charge inside the battery at time t with respect to the maximum possible charge Q it can hold.

Terminal voltage ($V_{term}(t)$): The voltage between the battery terminals at time t when a load is connected (i.e., when a current is flowing through the battery), expressed in volts. The terminal voltage is superior and inferior to the open-circuit voltage while charging and discharging, respectively.

2.7. Appendix B – Parameter values

In this section, we list the numerical values used to produce Figures 2.9, 2.13, and 2.15.

Figure 2.9 uses parameter values from Lam et al. (2011); (left) is the plot of Equation (2.10) with parameters

$$a_1 = -0.5863, \quad a_2 = 21.90, \quad a_3 = 3.414, \quad a_4 = 0.1102, \quad a_5 = -0.1718, \quad a_6 = 0.008;$$

(center) is the plot of Equation (2.11) with parameters

$$b_{1d} = 0.1298, \quad b_{2d} = -0.2892, \quad b_{3d} = 0.2273, \quad b_{4d} = -0.07216, \quad b_{5d} = 0.0898;$$

(right) is the plot of Equation (2.12) with parameters

$$b_{1c} = 0.1369, \quad b_{2c} = -0.2518, \quad b_{3c} = 0.1609, \quad b_{4c} = -0.041, \quad b_{5c} = 0.0821.$$

Figure 2.13 (top left): Final time: $T = 6370$ seconds, $P_B^{(1)}(t) \equiv 70$ W, $P_B^{(2)}(t) = 70(1 + 0.5\cos(2\pi t/T))$ W; (top right): numerical solution of Equation (2.24) with

$R = 0.01$ ohms, $Q = 40$ Ah, and $V_{OC}(SOC)$ given by (2.15) with $E_0 = 3.5$ V, $K = 0.025$ V, $A = 0.2$ V, $B = 0.375$ $(\text{Ah})^{-1}$ (parameter values from Marra et al., 2012); (bottom left) is the plot of (2.15) and (2.16); (bottom right) the current is obtained from (2.23), as in (2.36).

Figure 2.15: (CC-phase): $i_{cc} = -10$ A, $SOC(t)$ is obtained from (2.28), $V_{term}(t)$ from (2.29), with V_{OC} given by (2.15) with $R = 0.01$ ohms. (CV-phase): SOC is obtained from (2.32) with $Q = 40$ Ah and $V_{CV} = 3.6$ V.

The numerical solutions of the ordinary differential Equations (2.24) and (2.32) are obtained with the `ode45` solver in MATLAB.

References

A123 systems. 2015. Energy storage for commercial and off-highway vehicles. URL `http://www.a123systems.com/solutions-transportation-commercial-vehicles.htm`. Last accessed June 2016.

Afroditi, A., M. Boile, S. Theofanis, E. Sdoukopoulos, D. Margaritis. 2014. Electric vehicle routing problem with industry constraints: Trends and insights for future research. *Transportation Research Procedia* **3** 452–459.

Agubra, V., J. Fergus. 2013. Lithium ion battery anode aging mechanisms. *Materials* **6**(4) 1310–1325.

Amine, K., J. Liu, I. Belharouak. 2005. High-temperature storage and cycling of C-LiFePO4/graphite Li-ion cells. *Electrochemistry Communications* **7**(7) 669–673.

Aravindan, V., J. Gnanaraj, S. Madhavi, H.-K. Liu. 2011. Lithium-ion conducting electrolyte salts for lithium batteries. *Chemistry European Journal* **17** 14326–14346.

Arora, P., R.E. White, M. Doyle. 1998. Capacity fade mechanisms and side reactions in lithium-ion batteries. *Journal of the Electrochemical Society* **145**(10) 3647–3667.

Arslan, O., B. Yıldız, O.E. Karaşan. 2014. Minimum cost path problem for plug-in hybrid electric vehicles. *Transportation Research Part E: Logistics and Transportation Review* **80** 123–141.

Asamer, J., A. Graser, B. Heilmann, M Ruthmair. 2016. Sensitivity analysis for energy demand estimation of electric vehicles. *Transportation Research Part D: Transport and Environment* **46** 182–199.

AustriaTech. 2014. Electric fleets in urban logistics: Improving urban freight efficiency in small and medium-sized historic towns. Published as part of the ENCLOSE project, funded by Intelligent Energy Europe (IEE), Vienna, Austria. URL `http://www.austriatech.at/files/get/834747f18fdcc9538376c9314a4d7652/austriatech_electricfleets_broschuere.pdf`. Last accessed June 2016.

Balqon Corporation. 2013. M100 product specifications. URL `http://www.balqon.com/wp-content/uploads/2013/09/m100_brochure_2013.pdf`. Last accessed June 2016.

Balqon Corporation. 2015. Mule M100 electric truck. URL `http://www.balqon.com/electric-vehicles/mule-m100/`. Last accessed June 2016.

Barco, J., A. Guerra, L. Muñoz, N. Quijano. 2017. Optimal routing and scheduling of charge for electric vehicles: A case study. *Mathematical Problems in Engineering*, Article ID 8509783.

Barré, A., B. Deguilhem, S. Grolleau, M. Gérard, F. Suard, D. Riu. 2013. A review on lithium-ion battery ageing mechanisms and estimations for automotive applications. *Journal of Power Sources* **241** 680–689.

Barth, M., T. Younglove, G. Scora. 2005. Development of a heavy-duty diesel modal emissions and fuel consumption model. Tech.rep. UCB-ITS-PRR-2005-1, California PATH Program, Institute of Transportation Studies, University of California at Berkeley.

Bashash, S., S.J. Moura, J.C. Forman, H.K. Fathy. 2011. Plug-in hybrid electric vehicle charge pattern optimization for energy cost and battery longevity. *Journal of Power Sources* **196** 541–549.

Bay, M., S. Limbourg. 2015. TSP model for electric vehicle deliveries, considering speed, loading and road grades. Presentation given at the Sixth international workshop on Freight Transportation and Logistics (ODYSSEUS 2015), Ajaccio, France.

Bektaş, T., G. Laporte. 2011. The pollution-routing problem. *Transportation Research Part B: Methodological* **45**(8) 1232–1250.

Belt, J.R., C.D. Ho, C.G. Motloch, T.J. Miller, T.Q. Duong. 2003. A capacity and power fade study of Li-ion cells during life cycle testing. *Journal of Power Sources* **123**(2) 241–246.

Bergveld, H.J. 2001. Battery management systems: Design by modelling. Ph.D thesis, University of Twente, The Netherlands.

Boulder Electric Vehicle. 2013. 1000-series master brochure. URL `http://www.boulderev.com/docs/1000%20Master%20Brochure.pdf`. Last accessed June 2016.

Bruce, P.G., S.A. Freunberger, L.J. Hardwick, J-M. Tarascon. 2012. Li-O2 and Li-S batteries with high energy storage. *Nature materials* **11**(1) 19–29.

Bruglieri, M., F. Pezzella, O. Pisacane, S. Suraci. 2015. A variable neighborhood search branching for the electric vehicle routing problem with time windows. *Electronic Notes in Discrete Mathematics* **47** 221–228.

Campbell, R. 2011. Battery characterization and optimization for use in plug-in hybrid electric vehicles: Hardware-in-the-loop duty cycle testing. Master's thesis, Queen's University, Canada.

Chen, M., G.A. Rincón-Mora. 2006. Accurate electrical battery model capable of predicting runtime and I–V performance. *IEEE Transactions on Energy Conversion* **21**(2) 504–511.

Cluzel, C., C. Douglas. 2012. Cost and performance of EV batteries. Element Energy, Axeon and EaStCHEM, commissioned by The Committee on Climate Change. URL `http://www.element-energy.co.uk/wordpress/wp-content/uploads/2012/06/CCC-battery-cost_-Element-Energy-report_March2012_Finalbis.pdf`. Last accessed June 2016.

Conrad, R.G., M.A. Figliozzi. 2011. The recharging vehicle routing problem. T. Doolen, E. Van Aken, eds., *Proceedings of the 2011 Industrial Engineering Research Conference* (Institute of Industrial Engineers, Norcross, GA), 2785–2792.

Davis, B.A., M.A. Figliozzi. 2013. A methodology to evaluate the competitiveness of electric delivery trucks. *Transportation Research Part E: Logistics and Transportation Review* **49**(1) 8–23.

Dekkiche, A. 2008. Modèle de batterie générique et estimation de l'état de charge. Master's thesis, École de technologie supérieure, Canada.

Demir, E., T. Bektaş, G. Laporte. 2011. A comparative analysis of several vehicle emission models for road freight transportation. *Transportation Research Part D: Transport and Environment* **16**(5) 347–357.

Demir, E., T. Bektaş, G. Laporte. 2014. A review of recent research on green road freight transportation. *European Journal of Operational Research* **237**(3) 775–793.

den Boer, E., S. Aarnink, F. Kleiner, J. Pagenkopf. 2013. Zero emission trucks: An overview of state-of-the-art technologies and their potential. CE Delft

and DLR, commissioned by the International Council on Clean Transportation (ICCT). URL http://www.cedelft.eu/?go=home.downloadPub&id=1399&file=CE_Delft_4841_Zero_emissions_trucks_Def.pdf. Last accessed June 2016.

Dinger, A., R. Martin, X. Mosquet, M. Rabl, D. Rizoulis, M. Russo, G. Sticher. 2010. Batteries for electric cars: Challenges, opportunities, and the outlook to 2020. The Boston Consulting Group. URL https://www.bcg.com/documents/file36615.pdf. Last accessed June 2016.

Doerffel, D., S.A. Sharkh. 2006. A critical review of using the Peukert equation for determining the remaining capacity of lead-acid and lithium-ion batteries. *Journal of Power Sources* **155**(1) 395–400.

Duleep, G., H. van Essen, B. Kampman, M M. Grünig. 2011. Impacts of electric vehicles – deliverable 2: Assessment of electric vehicle and battery technology. CE Delft, ICF International, and Ecologic, commissioned by the European Commission. URL http://www.cedelft.eu/?go=home.downloadPub&id=1153&file=4058_D2defreportHvE_1314726004.pdf. Last accessed June 2016.

Electric Vehicles International. 2015. EVI Medium Duty Truck Specification Sheet. URL http://www.evi-usa.com/LinkClick.aspx?fileticket=SyZhwUVqNJs%3d&tabid=83. Last accessed June 2016.

Electrification Coalition. 2013. State of the plug-in electric vehicle market. URL http://www.electrificationcoalition.org/sites/default/files/EC_State_of_PEV_Market_Final_1.pdf. Last accessed June 2016.

Felipe, Á., M.T. Ortuño, G. Righini, G. Tirado. 2014. A heuristic approach for the green vehicle routing problem with multiple technologies and partial recharges. *Transportation Research Part E: Logistics and Transportation Review* **71** 111–128.

Feng, W., M. Figliozzi. 2013. An economic and technological analysis of the key factors affecting the competitiveness of electric commercial vehicles: A case study from the USA market. *Transportation Research Part C: Emerging Technologies* **26** 135–145.

Gerssen-Gondelach, S.J., A.P.C. Faaij. 2012. Performance of batteries for electric vehicles on short and longer term. *Journal of Power Sources* **212** 111–129.

Goeke, D., M. Schneider. 2015. Routing a mixed fleet of electric and conventional vehicles. *European Journal of Operational Research* **245**(1) 81–99.

Gonzalez-Feliu, J., F. Semet, J-L. Routhier, eds. 2014. *Sustainable urban logistics: Concepts, methods and information systems* (Springer-Verlag, Berlin Heidelberg).

Han, S., S. Han, H. Aki. 2014. A practical battery wear model for electric vehicle charging applications. *Applied Energy* **113** 1100–1108.

Hausbrand, R., G. Cherkashinin, H. Ehrenberg, M. Gröting, K. Albe, C. Hess, W. Jaegermann. 2015. Fundamental degradation mechanisms of layered oxide Li-ion battery cathode materials: Methodology, insights and novel approaches. *Materials Science and Engineering B* **192** 3–25.

Hiermann, G., J. Puchinger, S. Ropke, R.F. Hartl. 2016. The electric fleet size and mix vehicle routing problem with time windows and recharging stations. *European Journal of Operational Research* **252**(3) 995–1018.

Hoke, A., A. Brissette, D. Maksimović, A. Pratt, I. Labs, K. Smith. 2011. Electric vehicle charge optimization including effects of lithium-ion battery degradation. *2011 IEEE Vehicle Power and Propulsion Conference (VPPC)* (IEEE, Piscataway, NJ), 1–8.

International Energy Agency (IEA), Electric Vehicles Initiative (EVI). 2013. Global EV outlook – Understanding the electric vehicle landscape to 2020.

URL https://www.iea.org/publications/freepublications/publication/GlobalEVOutlook_2013.pdf. Last accessed June 2016.

Kamarianakis, Y., H.O. Gao, B.A. Holmén, D.B. Sonntag. 2011. Robust modeling and forecasting of diesel particle number emissions rates. *Transportation Research Part D: Transport and Environment* **16**(6) 435–443.

Khajepour, A., S. Fallah, A. Goodarzi. 2014. *Electric and Hybrid Vehicles – Technologies, Modeling, and Control: A Mechatronic Approach* (Wiley, Chichester, UK).

Kirschstein, T., F. Meisel. 2015. GHG-emission models for assessing the eco-friendliness of road and rail freight transports. *Transportation Research Part B: Methodological* **73** 13–33.

Koç, C., T. Bektaş, O. Jabali, G. Laporte. 2014. The fleet size and mix pollution-routing problem. *Transportation Research Part B: Methodological* **70** 239–254.

Koç, C., T. Bektaş, O. Jabali, G. Laporte. 2016. The impact of depot location, fleet composition and routing on emissions in city logistics. *Transportation Research Part B: Methodological* **84** 81–102.

Kopfer, H.W., H. Kopfer. 2013. Emissions minimization vehicle routing in dependence of different vehicle classes. H-J. Kreowski, B. Scholz-Reiter, K-D. Thoben, eds., *Dynamics in Logistics – Proceedings of LDIC 2012*. Lecture Notes in Logistics (Springer-Verlag, Berlin Heidelberg), 49–58.

Kopfer, H.W., J. Schönberger, H. Kopfer. 2014. Reducing greenhouse gas emissions of a heterogeneous vehicle fleet. *Flexible Services and Manufacturing Journal* **26** 221–248.

Lam, L. 2011. A practical circuit-based model for state of health estimation of li-on battery cells in electric vehicles. Master's thesis, Delft University of Technology, The Netherlands.

Lam, L., P. Bauer, E. Kelder. 2011. A practical circuit-based model for Li-ion battery cells in electric vehicle applications. *2011 IEEE 33rd International Telecommunications Energy Conference (INTELEC)* (IEEE, Piscataway, NJ), 1–9.

Larminie, J., J. Lowry. 2003. *Electric Vehicle Technology Explained* (Wiley, Chichester, UK).

Lebeau, P., C. De Cauwer, J. Van Mierlo, C. Macharis, W. Verbeke, T. Coosemans. 2015. Conventional, hybrid, or electric vehicles: Which technology for an urban distribution centre? *The Scientific World Journal*, Article ID 302867.

Lee, D.Y., V.M. Thomas, M.A. Brown. 2013. Electric urban delivery trucks: Energy use, greenhouse gas emissions, and cost-effectiveness. *Environmental science & technology* **47**(14) 8022–8030.

Li, S., B. Ke. 2011. Study of battery modeling using mathematical and circuit oriented approaches. *2011 IEEE Power and Energy Society General Meeting* (IEEE, Piscataway, NJ), 1–8.

Liu, W. 2013. *Introduction to Hybrid Vehicle System Modeling and Control* (Wiley, Hoboken, NJ).

Lukic, S.M., J. Cao, R.C. Bansal, F. Rodriguez, A. Emadi. 2008. Energy storage systems for automotive applications. *IEEE Transactions on Industrial Electronics* **55**(6) 2258–2267.

Lunz, B., Z. Yan, J.B. Gerschler, D.U. Sauer. 2012. Influence of plug-in hybrid electric vehicle charging strategies on charging and battery degradation costs. *Energy Policy* **46** 511–519.

Marra, F., G.Y. Yang, C. Traholt, E. Larsen, C.N. Rasmussen, S. You. 2012. Demand profile study of battery electric vehicle under different charging options. *2012 IEEE Power and Energy Society General Meeting* (IEEE, Piscataway, NJ), 3428–3434.

MathWorks. 2015. Battery model implementation. URL http://www.mathworks.com/help/physmod/sps/powersys/ref/battery.html. Last accessed June 2016.

Millner, A. 2010. Modeling lithium ion battery degradation in electric vehicles. *2010 IEEE Conference on Innovative Technologies for an Efficient and Reliable Electricity Supply (CITRES)* (IEEE, Piscataway, NJ), 349–356.

Montoya, A., C. Guéret, J.E. Mendoza, J.G. Villegas. 2016. A modified multi space sampling heuristic for the green vehicle routing problem. *Transportation Research Part C: Emerging Technologies* **70** 113–128.

Montoya, A., C. Guéret, J.E. Mendoza, J.G. Villegas. 2017. The electric vehicle routing problem with nonlinear charging function. *Transportation Research Part B: Methodological* **103** 87–110.

Moura, S.J. 2011. Techniques for battery health conscious power management via electrochemical modeling and optimal control. Ph.D thesis, University of Michigan, Michigan.

Moura, S.J., H.K. Fathy, D.S. Callaway, J.L. Stein. 2011. A stochastic optimal control approach for power management in plug-in hybrid electric vehicles. *IEEE Transactions on Control Systems Technology* **19**(3) 545–555.

Naberezhnykh, D., J. Wardle, J. Lowes, C. Herron, T. Brightman, T. Parker. 2012. Electric vehicle charging points for freight vehicles in central London (Version – Final 1.0). Prepared for Central London FQP by Transport & Travel Research Ltd, in partnership with TRL and Zero Carbon Futures. URL http://www.centrallondonfqp.org/app/download/12240926/CLFQP_EVCP_strategy+report_Final+v1+0.pdf. Last accessed January 2019.

Nesterova, N., H. Quak, S. Balm, I. Roche-Cerasi, T. Tretvik. 2013. Project FREVUE deliverable D1.3: State of the art of the electric freight vehicles imple-

mentation in city logistics. TNO and SINTEF. European Commission Seventh framework programme.

Nykvist, B., M. Nilsson. 2015. Rapidly falling costs of battery packs for electric vehicles. *Nature Climate Change* **5** 329–332.

Omar, N., M. Daowd, P. van den Bossche, O. Hegazy, J. Smekens, T. Coosemans, J. van Mierlo. 2012. Rechargeable energy storage systems for plug-in hybrid electric vehicles — Assessment of electrical characteristics. *Energies* **5** 2952–2988.

Omar, N., P. van den Bossche, T. Coosemans, J. van Mierlo. 2013. Peukert revisited — Critical appraisal and need for modification for lithium-ion batteries. *Energies* **6** 5625–5641.

Omar, N., M.A. Monem, Y. Firouz, J. Salminen, J. Smekens, O. Hegazy, H. Gaulous, G. Mulder, P. Van den Bossche, T. Coosemans, J. van Mierlo. 2014. Lithium iron phosphate based battery – Assessment of the aging parameters and development of cycle life model. *Applied Energy* **113** 1575–1585.

Ouyang, M., D. Ren, L. Lu, J. Li, X. Feng, X. Han, G. Liu. 2015. Overcharge-induced capacity fading analysis for large format lithium-ion batteries with LiyNi1/3Co1/3Mn1/3O2 + LiyMn2O4 composite cathode. *Journal of Power Sources* **279** 626–635.

Pelletier, S., O. Jabali, G. Laporte. 2016. 50th anniversary invited article – Goods distribution with electric vehicles: Review and research perspectives. *Transportation Science* **50**(1) 3–22.

Peterson, S.B., J. Apt, J.F. Whitacre. 2010. Lithium-ion battery cell degradation resulting from realistic vehicle and vehicle-to-grid utilization. *Journal of Power Sources* **195** 2385–2392.

Preis, H., S. Frank, K. Nachtigall. 2014. Energy-optimized routing of electric vehicles in urban delivery systems. S. Helber, M. Breitner, D. Rösch, C. Schön, J-M. Graf von der Schulenburg, P. Sibbertsen, M. Steinbach, S. Weber, A. Wolter, eds., *Operations Research Proceedings 2012* (Springer International Publishing, Switzerland), 583–588.

Psaraftis, H.N., ed. 2016. *Green Transportation in Logistics: The Quest for Win-Win Solutions*. International Series in Operations Research & Management Science, Vol. 226 (Springer International Publishing, Switzerland).

Rahmoun, A., H. Biechl. 2012. Modelling of Li-ion batteries using equivalent circuit diagrams. *Electrical review* **88**(7b) 152–156.

Sarasketa-Zabala, E., I. Gandiaga, L.M. Rodriguez-Martinez, I. Villarreal. 2014a. Calendar ageing analysis of a LiFePO4/graphite cell with dynamic model validations: Towards realistic lifetime predictions. *Journal of Power Sources* **272** 45–57.

Sarasketa-Zabala, E., I. Gandiaga, L.M. Rodriguez-Martinez, I. Villarreal. 2014b. Cycle ageing analysis of a LiFePO4/graphite cell with dynamic model validations: Towards realistic lifetime predictions. *Journal of Power Sources* **275** 573–587.

Sarasketa-Zabala, E., I. Laresgoiti, I. Alava, M. Rivas, I. Villarreal, F. Blanco. 2013. Validation of the methodology for lithium-ion batteries lifetime prognosis. *2013 World Electric Vehicle Symposium and Exhibition (EVS27)* (IEEE, Piscataway, NJ), 1–12.

Sassi, O., W.R. Cherif-Khettaf, A. Oulamara. 2015. Vehicle routing problem with mixed fleet of conventional and heterogenous electric vehicles and time dependent charging costs. *International Journal of Mathematical, Computational, Statistical, Natural and Physical Engineering* **9**(3) 148–158.

Sauer, D.U. 2009. BATTERIES | Charge–Discharge Curves. J. Garche, C. Dyer, P. Moseley, Z. Ogumi, D. Rand, B. Scrosati, eds., *Encyclopedia of Electrochemical Power Sources* (Elsevier, Amsterdam, The Netherlands), 443–451.

Schiffer, M., G. Walther. 2017a. An adaptive large neighborhood search for the location routing problem with intraroute facilities. *Transportation Science* **52**(2) 331–352.

Schiffer, M., G. Walther. 2017b. The electric location routing problem with time windows and partial recharging. *European Journal of Operational Research* **260**(3) 995–1013.

Schneider, M., A. Stenger, D. Goeke. 2014. The electric vehicle-routing problem with time windows and recharging stations. *Transportation Science* **48**(4) 500–520.

Shepherd, C.M. 1965. Design of primary and secondary cells II. An equation describing battery discharge. *Journal of the Electrochemical Society* **112**(7) 657–664.

Smith Electric Vehicles. 2015. Smith Newton United States spec sheet. URL `http://www.smithelectric.com/wp-content/themes/barebones/pdfs/SmithNewtonUS_SpecSheet_2011.pdf`. Last accessed June 2016.

Stasko, T.H., H.O. Gao. 2012. Developing green fleet management strategies: Repair/retrofit/replacement decisions under environmental regulation. *Transportation Research Part A: Policy and Practice* **46** 1216–1226.

Sweda, T.M., I.S. Dolinskaya, D. Klabjan. 2016. Optimal recharging policies for electric vehicles. *Transportation Science* **51**(2) 457–479.

Taefi, T.T., J. Kreutzfeldt, T. Held, R. Konings, R. Kotter, S. Lilley, H. Baster, N. Green, M.S. Laugesen, S. Jacobsson, M. Borgqvist, C. Nyquist. 2016. Comparative analysis of European examples of freight electric vehicles schemes –

A systematic case study approach with examples from Denmark, Germany, the Netherlands, Sweden and the UK. H. Kotzab, J. Pannek, K-D. Thoben, eds., *Dynamics in Logistics – Proceedings of LDIC 2014*. Lecture Notes in Logistics (Springer International Publishing, Switzerland), 495–504.

Tan, L., L. Zhang, Q. Sun, M. Shen, Q. Qu, H. Zheng. 2013. Capacity loss induced by lithium deposition at graphite anode for LiFePO 4/graphite cell cycling at different temperatures. *Electrochimica Acta* **111** 802–808.

Tarascon, J-M., M. Armand. 2001. Issues and challenges facing rechargeable lithium batteries. *Nature* **414**(6861) 359–367.

Thackeray, M.M., C. Wolverton, E.D. Isaacs. 2012. Electrical energy storage for transportation – approaching the limits of, and going beyond, lithium-ion batteries. *Energy & Environmental Science* **5**(7) 7854–7863.

Tremblay, O., L.-A. Dessaint, A.-I. Dekkiche. 2007. A generic battery model for the dynamic simulation of hybrid electric vehicles. *2007 Vehicle Power and Propulsion Conference* (IEEE, Piscataway, NJ), 284–289.

Tremblay, O., L.-A. Dessaint. 2009. Experimental validation of a battery dynamic model for EV applications. *World Electric Vehicle Journal* **3**(2) 289–298.

Trippe, A.E., R. Arunachala, T. Massier, A. Jossen, T. Hamacher. 2014. Charging optimization of battery electric vehicles including cycle battery aging. *2014 IEEE PES Innovative Smart Grid Technologies Europe (ISGT Europe)* (IEEE, Piscataway, NJ), 1–6.

U.S. Department of Energy. 2012. Plug-in electric vehicle handbook for fleet managers. Office of Energy Efficiency and Renewable Energy, National Renewable Energy Laboratory (NREL). URL `http://www.afdc.energy.gov/pdfs/pev_handbook.pdf`. Last accessed June 2016.

Vetter, J., P. Novák, M.R. Wagner, C. Veit, K.-C. Möller, J.O. Besenhard, M. Winter, M. Wohlfahrt-Mehrens, C. Vogler, A. Hammouche. 2005. Ageing mechanisms in lithium-ion batteries. *Journal of Power Sources* **147** 269–281.

Wang, J., P. Liu, J. Hicks-Garner, E. Sherman, S. Soukiazian, M. Verbrugge, H. Tataria, J. Musser, P. Finamore. 2011. Cycle-life model for graphite-LiFePO4 cells. *Journal of Power Sources* **196** 3942–3948.

Wenzl, H. 2009. BATTERIES | Capacity. J. Garche, C. Dyer, P. Moseley, Z. Ogumi, D. Rand, B. Scrosati, eds., *Encyclopedia of Electrochemical Power Sources* (Elsevier, Amsterdam, The Netherlands), 395–400.

Wenzl, H., A. Haubrock, H.-P. Beck. 2013. Degradation of lithium ion batteries under complex conditions of use. *Zeitschrift fur Physikalische Chemie* **227**(1) 57–72.

Wohlfahrt-Mehrens, M., C. Vogler, J. Garche. 2004. Aging mechanisms of lithium cathode materials. *Journal of Power Sources* **127** 58–64.

Wu, X., D. Freese, A. Cabrera, W.A Kitch. 2015. Electric vehicles energy consumption measurement and estimation. *Transportation Research Part D: Transport and Environment* **34** 52–67.

Xu, B. 2013. Degradation-limiting optimization of battery energy storage systems operation. Master's thesis, ETH Zürich, Switzerland.

Yang, J., H. Sun. 2015. Battery swap station location-routing problem with capacitated electric vehicles. *Computers & Operations Research* **28** 217–232.

Yong, J.Y., V.K. Ramachandaramurthy, K.M. Tan, N. Mithulananthan. 2015. A review on the state-of-the-art technologies of electric vehicle, its impacts and prospects. *Renewable and Sustainable Energy Reviews* **49** 365–385.

Zheng, H., L. Tan, L. Zhang, Q. Qu, Z. Wan, Y. Wang, M. Shen, H. Zheng. 2015a. Correlation between lithium deposition on graphite electrode and the capacity loss for LiFePO4/graphite cells. *Electrochimica Acta* **173** 323–330.

Zheng, M., B. Qi, X. Du. 2009. Dynamic model for characteristics of Li-ion battery on electric vehicle. *4th IEEE Conference on Industrial Electronics and Applications (ICIEA 2009)* (IEEE, Piscataway, NJ), 2867–2871.

Zheng, Y. Y.-B. He, K. Qian, B. Li, X. Wang, J. Li, S.W. Chiang, C. Miao, F. Kang, J. Zhang. 2015b. Deterioration of lithium iron phosphate/graphite power batteries under high-rate discharge cycling. *Electrochimica Acta* **176** 270–279.

Zheng, Y. Y.-B. He, K. Qian, B. Li, X. Wang, J. Li, C. Miao, F. Kang. 2015c. Effects of state of charge on the degradation of LiFePO4/graphite batteries during accelerated storage test. *Journal of Alloys and Compounds* **639** 406–414.

Zündorf, T. 2014. Electric vehicle routing with realistic recharging models. Master's thesis, Karlsruhe Institute of Technology, Germany.

Chapter 3

Charge scheduling for electric freight vehicles

Chapter information

This article is the result of a collaboration with my thesis advisors. It was published in *Transportation Research Part B: Methodological*: S. Pelletier, O. Jabali, G. Laporte. 2018. Charge scheduling for electric freight vehicles. *Transportation Research Part B: Methodological* **115** 246–269.

Abstract

We consider a fleet of electric freight vehicles (EFVs) that must deliver goods to a set of customers over the course of multiple days. In an urban environment, EFVs are typically charged at a central depot and rarely use public charging stations during delivery routes. Therefore, the charging schedule at the depot must be planned ahead of time so as to allow the vehicles to complete their routes at minimal cost. Vehicle fleet operators are subject to commercial electricity rate

plans, which should be accounted for in order to provide an accurate estimation of the energy-related costs and restrictions. In addition, high vehicle utilization rates can accelerate battery aging, thereby requiring degradation mitigation considerations. We develop and solve a comprehensive mathematical model that incorporates a large variety of features associated with the use of EFVs. These include a realistic charging process, time-dependent energy costs, battery degradation, grid restrictions, and facility-related demand charges. Extensive numerical experiments are conducted in order to draw managerial insights regarding the impact of such features on the charging schedules of EFVs.

Keywords: electric freight vehicles; charge scheduling; green transportation; battery degradation; city logistics.

3.1. Introduction

Electric freight vehicles (EFVs) are fast becoming a viable alternative for short- and mid-haul goods distribution (Davis and Figliozzi, 2013; Lee et al., 2013; Pelletier et al., 2016; Quak et al., 2016; Franceschetti et al., 2017). Because they help reduce air and noise pollution they are often regarded as an attractive option in the context of city logistics. Most recent studies have dealt with the routing issues associated with EFVs, especially those that stem from their limited range, and have proposed models and algorithms for the optimization of routes that incorporate en route recharging (e.g., Felipe et al., 2014; Schneider et al., 2014; Bruglieri et al., 2015; Goeke and Schneider, 2015; Hiermann et al., 2016; Montoya et al., 2017). Some authors have also approached such optimization problems from a more strategic planning perspective by incorporating both routing and charging infrastructure location decisions in their models (e.g., Yang and Sun, 2015; Schiffer and Walther, 2017a,b, 2018; Schiffer et al., 2018).

The issue of depot charge scheduling for electric vehicles has received less attention than the routing component, but it nevertheless raises interesting challenges whose solution could facilitate the integration of EFVs in goods distribution schemes. Indeed, many companies using EFVs prefer charging the vehicles at their own facilities (Morganti and Browne, 2018). This is due to a combination of factors, such as limited fast charging infrastructures in most regions, as well as long charging times associated with slow charging stations that lead to cargo security concerns and inefficient use of drivers' time when charging along delivery routes (Naberezhnykh et al., 2012; Nesterova et al., 2013; E-Mobility NSR, 2013). In addition, lower energy costs may be attained through commercial off-peak electricity rates when charging at the depot during specific periods of the day. Moreover, EFVs are more likely to be used in urban areas because of low driving speeds and frequent stop-and-starts, where their superior energy efficiency becomes relatively advantageous compared with that of diesel vehicles, and where financial incentives are more likely to be available. Since typical urban delivery routes are shorter than the range of currently available EFVs (Feng and Figliozzi, 2013), there is often no need to consider charging outside the depot. While some studies have focused on charge scheduling for EFVs (e.g., Sassi and Oulamara, 2014a,b), several important issues have not yet been addressed.

Before the publication of the recent paper by Montoya et al. (2017), charging of EFVs in a routing context was either treated as a fixed time penalty (e.g., Conrad and Figliozzi, 2011; Afroditi et al., 2014; Preis et al., 2014), or was assumed to be linear with respect to time (e.g., Felipe et al., 2014; Schneider et al., 2014; Bruglieri et al., 2015; Lebeau et al., 2015; Goeke and Schneider, 2015; Hiermann et al., 2016), which does not always correspond to reality. Indeed, in order to prevent overcharging the battery (i.e., operating the battery at voltage values beyond a value specified by the manufacturer), the charging function usually comprises both a linear and a non-linear component with respect to time when large charging cur-

rents are employed. Moreover, certain charging practices of electric vehicles have been shown to adversely influence the lifespan of their batteries (Bashash et al., 2011; Lunz et al., 2012). Since the battery still remains a major cost component of EFVs (Pelletier et al., 2016), it is relevant to take this consideration into account when making charge scheduling decisions. This is particularly important since high use rates have frequently been identified as a means of increasing the cost competitiveness of EFVs because of their high purchase costs and low operational costs (Davis and Figliozzi, 2013; Lee et al., 2013). However, recent studies (e.g., Taefi, 2016; Taefi et al., 2016) have concluded that this may not be the case if costly battery replacements result from intensive usage in high utilization scenarios. In addition, such scenarios often involve using the vehicles in multi-shift contexts, whereby vehicles may need to perform multiple routes throughout day and night (EFVs are sometimes allowed to perform night-time deliveries in cities because they are silent, Taefi, 2016). As a result, fleet operators may have to install expensive chargers at the depot in order to charge the vehicles between consecutive delivery routes during specific periods of the day, and to benefit from off-peak electricity rates. A company would probably own a limited number of chargers, typically fewer than the fleet size, thus leading to tight charging schedules. Moreover, commercial electricity rate plans are often subject to both time-dependent energy costs and facilities-related demand (FRD) charges, the latter depending on the maximum power demand registered over the course of the billing period (see, e.g., Southern California Edison, 2017). Therefore, regardless of whether the operational context requires fast chargers or not, optimizing the charging schedule can help in determining the best alternative between paying a higher FRD charge and incurring lower energy costs (e.g., by charging many vehicles when electricity is cheap), or rather keeping such FRD fees low at the expense of spreading out the charging activites throughout the day, notably when electricity is more costly.

Two relevant studies in the context of depot charge scheduling for EFVs are

those of Sassi and Oulamara (2014a,b). In the first of these papers, a fleet of electric and conventional vehicles must be assigned to a set of predetermined routes so as to maximize the usage of the electric vehicles and minimize the cost of the charging schedule. Charging can only take place at the depot when the vehicles are not performing routes. The planning horizon is discretized into periods during which the charging power remains fixed and must stay within a certain interval indicating the minimum and maximum charging power of the homogeneous chargers at the depot. Charging costs and grid capacities are time-dependent. Sassi and Oulamara (2014b) have extended this problem by considering different types of chargers at the depot and a limited number of each type. They also proposed different objective functions depending on whether certain considerations are taken into account or not. These include being allowed to exceed the grid capacity by paying fixed hourly penalties, treating the number of chargers of each type at the depot as decision variables with deployment costs, and the presence of time-dependent greenhouse gas emissions costs depending on the electricity generation mix at that time.

As in Sassi and Oulamara (2014b), we focus on the depot charging schedule rather than on en route charging at public stations, but we model a more realistic charging process which avoids overcharging, and hence battery deterioration (Lam, 2011). Moreover, we work with a planning horizon of several days rather than with a single day, since the assumption that the vehicles will always be fully charged overnight does not hold in certain multi-shift operational contexts. In addition, we incorporate battery degradation considerations when determining an optimal charging schedule, as well as FRD charges. Finally, we draw several managerial insights through our numerical experiments. These relate to the impact of time-dependent energy costs, battery degradation, grid restrictions, FRD charges and battery size on the charging schedules of EFVs. Such insights are relatively absent from the aforementioned related studies.

The scientific aim of this paper is to model, construct and analyze charging schedules of EFVs that must operate fixed delivery routes over the course of a multiple-day planning horizon in a multi-shift operational context, thereby performing several routes per day, and using vehicles that can only be charged at a central depot. With this goal in mind, Section 3.2 describes the problem at hand and presents a first mathematical formulation without battery degradation considerations. Section 3.3 explains how certain battery health considerations can be incorporated into the model. Section 3.4 provides extensive computational results and derives managerial insights. The paper closes with conclusions in Section 3.5. Appendix A contains a glossary of the abbreviations used in the paper, including those related to energy and electricity units.

3.2. The EFV charge scheduling problem

The objective of this section is to introduce what we refer to as the EFV Charge Scheduling Problem (EFV-CSP). The section is organized as follows. We first provide a general description of the EFV-CSP in Section 3.2.1. In Section 3.2.2 we elaborate on the approach used to model the charging process of EFVs in discrete time. The mathematical formulation of the EFV-CSP is then given in Section 3.2.3, and examples of optimal solutions for a small instance of the problem are presented in Section 3.2.4. Finally, Section 3.2.5 provides comments on the derivation of solutions in continuous time from solutions obtained in discrete time.

As is often the case in optimization problems, several assumptions are made in the EFV-CSP, the most important of which are outlined here. First, it is assumed that the routes that must be performed by the vehicles are given but may differ from one day to another, and that the assignment of vehicles to routes is also known in advance. Working with fixed routes simplifies the problem con-

siderably and makes sense in multi-period routing contexts in which service consistency is valued (Kovacs et al., 2014). Note that our assumption of given routes implies that we can precompute the charge consumption a priori for each route. Second, while the charging activity of each vehicle can only occur at the depot, it can be carried out with several different chargers, i.e., we consider preemptive charging. Finally, since we formulate the EFV-CSP in discrete time, the charging schedule is determined on a period to period basis and we assume that no charging can occur during departure and arrival periods.

3.2.1 Problem description

The EFV-CSP is defined over a planning interval of several days which is discretized into a set $P = \{1, ..., n_p\}$ of n_p consecutive periods lasting δ hours each. The set $K = \{1, ..., m\}$ represents a fleet of m homogeneous EFVs, each equipped with a battery with a charge capacity of Q ampere-hours (Ah) and an energy capacity of E kilowatt-hours (kWh). We define the state of charge (SOC) of a battery as the amount of charge it contains divided by its maximum charge capacity Q. The set R contains all delivery routes that must be performed during the planning interval and is given as an input. Note that each vehicle may have several routes to perform. Each route $r \in R$ is associated with the following parameters: a departure period β_r, an arrival period α_r, the vehicle v_r that must perform it and the total SOC variation ΔSOC_r incurred by that vehicle. Let routes r and η_r be assigned to the same vehicle (i.e., $v_{\eta_r} = v_r$), where η_r is the route that immediately precedes route r. In other words, for each route $r \in R$, the route η_r is the route of vehicle v_r with the latest arrival period prior to β_r. Let f_k be the earliest route to be performed by vehicle k in the planning interval, and let set A_k represent all periods during which vehicle k returns from one of its routes, i.e., $A_k = \{\alpha_r | r \in R, v_r = k\}$. Assume that $\alpha_{\eta_r} = 1$ if $r = f_k$ for any vehicle $k \in K$.

At the depot, there is an energy cost of c_p in \$/kWh associated with each period $p \in P$, an FRD charge of F in \$/kW which depends on the maximum charging power retrieved from the grid throughout the planning interval, and a grid restriction G representing the maximum power in kilowatts (kW) that can be retrieved from the grid to charge the vehicles. Indeed, in addition to time-dependent energy costs and FRD fees, electricity rate plans for charging electric vehicles on company grounds may also include maximum power restrictions (see, e.g., Southern California Edison, 2017). We assume that there are different kinds of chargers installed at the depot, represented by the set S. A charger of type $s = 1$ is assumed to be a level 1 charger that comes with the vehicle upon its purchase; all vehicles can therefore use charger $s = 1$ whenever they are at the depot. The other chargers are faster but more costly. The acquisition, installation, and maintenance costs associated with such charging equipment are significant cost components of operating electric vehicles for goods distribution (Lee et al., 2013). It is therefore assumed that a limited number $\kappa_s < m$ of chargers of type $s \in S \backslash \{1\}$ are available. As in Sassi and Oulamara (2014b), we constrain the number of charging events of the vehicles. We define a charging event as plugging a charger into a vehicle at a given time and unplugging it later. To avoid impractical solutions in which vehicles are constantly being moved from one charger to another, we set a limit of C charging events between each arrival and departure for each vehicle. The objective of the EFV-CSP is to determine a charging schedule that allows the vehicles to complete all their routes at minimal cost.

3.2.2 The battery charging process

Electric vehicles are typically charged under a constant current (CC)-constant voltage (CV) scheme to avoid overcharging degradation (Lam, 2011). The charging current is held constant during the CC phase and the SOC thus increases

linearly with respect to time since the rate of change of the SOC is charging current divided by charge capacity. During the CC phase, the terminal voltage of the battery increases until it reaches a certain maximum value V_{CV}, which is specified by the manufacturer. When it does, the CV phase begins and the terminal voltage must be maintained at that maximum value in order to avoid the degradation resulting from overcharging the battery; the charging current then decreases with time throughout the CV phase.

The process can be understood through the battery behaviour model proposed by Tremblay et al. (2007). The terminal voltage is the voltage measured at the battery terminals when it is being charged or discharged, and is a function of SOC and current. The model essentially states that the terminal voltage V_{term} of a battery is the sum of its open-circuit voltage OCV and the voltage drop across its internal resistance R, the latter term depending on the charging current $i(t)$. The open-circuit voltage is the voltage measured at the battery terminals when it is at rest and is an increasing function of SOC. Using this model, the charging terminal voltage at time t can be approximated as

$$V_{term}(SOC(t), i(t)) = OCV(SOC(t)) + R \cdot i(t). \tag{3.1}$$

The terminal voltage is thus larger than the open-circuit voltage during charging. During the CC phase of a CC-CV charging process, the charging current (which depends on the kind of charger used) remains constant. As time elapses during the CC phase, the right-hand side of (3.1) therefore increases according to the relationship between open-circuit voltage and SOC, and hence so does the terminal voltage. As previously mentioned, the terminal voltage must never be allowed to rise above V_{CV}. Depending on the charging current used during the CC phase, V_{CV} will be reached at SOC values well below 100%. In order to continue charging the battery once V_{CV} is attained, the terminal voltage must be held at that maximum value throughout the CV phase. Following an infinitesimal time

increment after entering the CV phase, the SOC will then increase according to the current in the CC phase. Since the open-circuit voltage will increase with the SOC, the current will have to be decreased in order to ensure that the terminal voltage remains at V_{CV}. The process then repeats itself following other infinitesimal time increments until the battery is fully charged.

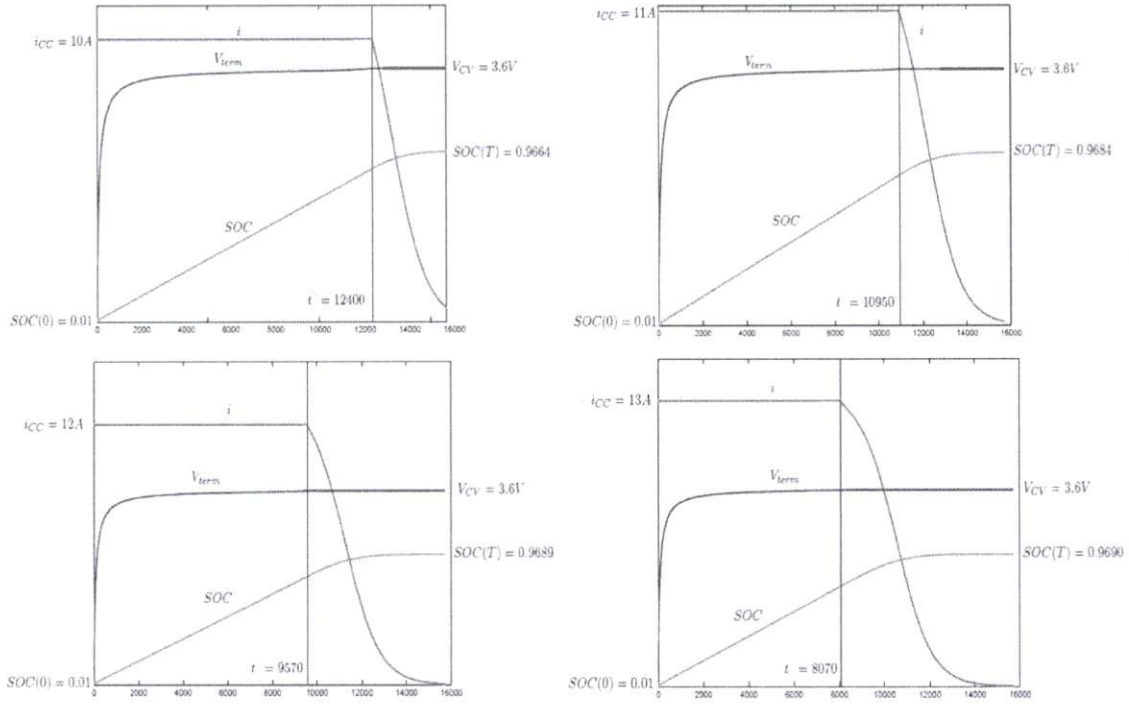

Figure 3.1 – Comparison of CC-CV charging profiles for a lithium-ion battery cell with different current values in the CC phase (Source: Pelletier et al., 2017)

Note that the charging rate used in the CC phase influences both the elapsed time and the SOC upon entering the CV phase. Indeed, a larger current will shorten the CC phase but will cause the CV phase to be entered at a lower SOC value, thereby prolonging the CV phase. Figure 3.1 illustrates this process by simulating the CC-CV charging scheme for a 40 Ah lithium-ion battery cell with different values for the current i_{CC} used during the CC phase and a maximum charge voltage V_{CV} of 3.6 volts (V). The final time T is set to 16,000 seconds in all

the simulations. As the value of i_{CC} increases, the time t at which the CV phase is entered decreases. However, the SOC at time t is approximately 87%, 85%, 81% and 74% when i_{CC} is 10, 11, 12, and 13 amperes (A), respectively. In sum, the larger is the current used during the CC phase, the more important it is to consider the non-linear component of the charging function (e.g., for very slow chargers, a linear approximation of the entire charging function can be sufficient since the CV phase is entered at a high SOC value).

In order to model the CC-CV process in discrete time, we use a piecewise linear approximation of the evolution of SOC over time, as in Montoya et al. (2017). We assume that each charger of type $s \in S$ has a specific CC-CV charging function which is piecewise linear with $b_s + 1$ breakpoints, fitted to the real CC-CV concave function. Let a_{si} be the SOC associated with breakpoint $i \in B_s$ of the charging function of charger type s, with the set of breakpoints $B_s = \{0, ..., b_s\}$. The approximation therefore assumes that the charging current is constant between each pair of consecutive breakpoints. Let I_{si} be the charging current (A) used in the piecewise approximation between breakpoints i and $i-1$ of charger type s, for all $i \in B_s \backslash \{0\}$, with I_{s1} therefore referring to the CC phase current of charger type s.

A piecewise linear approximation of the CC-CV charging process for a charger of type s with $b_s = 3$ is illustrated in Figure 3.2. This function represents how the SOC evolves with respect to time when the battery is charged with charger type s. As the figure shows, the piecewise approximation of the CC-CV process for this type of charger would have $b_s + 1 = 3 + 1 = 4$ breakpoints, represented by set $B_s = \{0, 1, 2, 3\}$. Each of these four breakpoints is associated with a specific SOC value (i.e., a_{s0}, a_{s1}, a_{s2}, and a_{s3}). Since $a_{s0} = 0$ and $a_{s4} = 1$ in this case, the figure illustrates a full charge from a SOC of zero to a SOC of one. The slope of the piecewise function between each pair of consecutive breakpoints corresponds to the charging current used between these breakpoints, divided by the

battery capacity. For example, according to the definition of parameter I_{si}, I_{s2} is the charging current applied by charger type s when the SOC is between a_{s1} and a_{s2}. Thus, I_{s2}/Q corresponds to the slope of the piecewise function between these two breakpoints in Figure 3.2, since the charging current divided by the charge capacity is the rate of change of the SOC. Indeed, with I_{si} in amperes and the battery charge capacity Q in Ah, I_{si}/Q indicates how much the SOC will increase per hour when the battery is charged with a current of I_{si}.

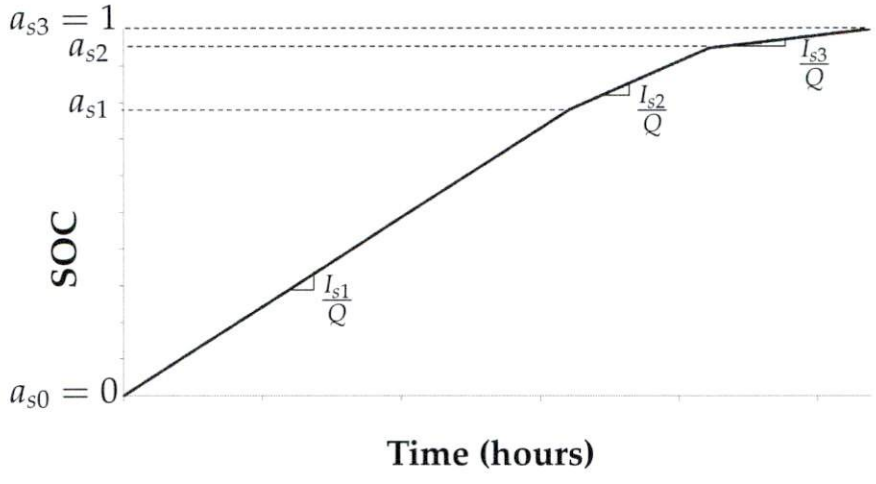

Figure 3.2 – Piecewise linear approximation of a CC-CV charging process

Finally, note that the charging power applied to the battery during charging is equal to the product of its terminal voltage and of the charging current; it therefore increases with time during the CC phase of charging until it reaches a maximum value upon entering the CV phase, and then decreases throughout the CV phase. To ensure the respect of potential grid restrictions, let parameter P_s be the largest charging power retrieved from the grid by the battery throughout the CC-CV charging process of charger type s.

3.2.3 Mathematical formulation

The following decision variables are required for the formulation of the EFV-CSP without battery degradation considerations. Real and positive variables soc_{pk} refer to the state of charge of vehicle k at the start of period p, while real and positive variables i_{pk} refer to the charging current applied to vehicle k during the entirety of period p. As in Sassi and Oulamara (2014a), for modeling convenience we assume that the entire charge consumption of a route occurs during the last period of that route. For example, if vehicle $k = 1$ leaves the depot during period $p = 1$ with a SOC of 90%, and returns to the depot during period $p = 5$ with a SOC of 50%, the model is designed so that $soc_{11} = soc_{21} = soc_{31} = soc_{41} = 90\%$ and $soc_{51} = 50\%$ (so the values of soc_{pk} are irrelevant while vehicle k is performing its route; they remain the same as the departure SOC until the vehicle returns). Each vehicle starts with a given initial SOC value (i.e., soc_{1k} is a constant for each vehicle). For battery health reasons, we assume the SOC must remain between certain minimum and maximum values SOC_{min} and SOC_{max}. The variable y indicates the maximum charging power retrieved from the grid during the planning interval.

The binary variables x_{pksi} take value 1 if vehicle k uses a charger of type s during period p with SOC values at the start and end of p between breakpoints $a_{s,i-1}$ and a_{si}, and take value 0 otherwise. It is assumed that if a charger is used by a vehicle during a period, that charger is unavailable to other vehicles for the entirety of the period. Finally, the binary variables z_{pk} take value 1 when the event of a new charge happens for vehicle k during period p, and take value 0 otherwise.

Table 3.1 summarizes all variable and parameter definitions discussed in this section. The following mixed integer linear programming formulation then rep-

resents the EFV-CSP:

Table 3.1 – Variable and parameter definitions of the EFV-CSP model

P	Set of periods in the planning interval
K	Set of EFVs
R	Set of routes
A_k	Set of all periods during which vehicle k returns from one of its routes
S	Set of types of chargers installed at the depot
B_s	Set of breakpoints used in the piecewise linear approximation of the CC-CV charging function of charger type s
n_p	Number of periods in P
δ	Length of each period in hours
m	Number of EFVs in K
Q	Battery charge capacity (Ah)
E	Battery energy capacity (kWh)
β_r	Departure period of route r
α_r	Arrival period of route r
v_r	Vehicle that must perform route r
ΔSOC_r	Charge consumption of route r
η_r	Route of vehicle v_r with the latest arrival period prior to β_r
f_k	Earliest route to be performed by vehicle k
c_p	Energy cost during period p (\$/kWh)
F	FRD charge (\$/kW)
G	Grid restriction (kW)
κ_s	Number of chargers of type s installed at the depot
C	Maximum number of charging events between each arrival and departure for each vehicle
a_{si}	SOC associated with breakpoint $i \in B_s$ of the piecewise linear approximation of the CC-CV charging function of charger type s
I_{si}	Charging current (A) used in the piecewise linear approximation of the CC-CV charging function of charger type s between breakpoints i and $i-1$, with $i \in B_s, i > 0$
P_s	Largest charging power (kW) retrieved from the grid throughout the CC-CV charging process of charger type s
soc_{pk}	Decision variable indicating the SOC of vehicle k at the start of period p
i_{pk}	Decision variable indicating the charging current (A) applied to vehicle k during period p
y	Decision variable indicating the maximum charging power (kW) retrieved from the grid during the planning interval
x_{pksi}	Binary decision variable worth 1 if vehicle k uses a charger of type s during period p with SOC values at the start and end of p between breakpoints $a_{s,i-1}$ and a_{si}, and 0 otherwise
z_{pk}	Binary decision variable worth 1 if vehicle k begins a charge during period p, and 0 otherwise

$$\text{minimize} \quad \sum_{k \in K} \sum_{p \in P} c_p \cdot E \cdot \frac{\delta \cdot i_{pk}}{Q} + F \cdot y \tag{3.2}$$

subject to

$$\sum_{p=\beta_r}^{\alpha_r} \sum_{s \in S} \sum_{i \in B_s \setminus \{0\}} x_{pv_rsi} = 0 \quad r \in R \tag{3.3}$$

$$soc_{\alpha_r, v_r} = soc_{\beta_r, v_r} - \Delta SOC_r \quad r \in R \tag{3.4}$$

$$\sum_{k\in K}\sum_{i\in B_s\setminus\{0\}} x_{pksi} \le \kappa_s \quad p \in P, s \in S\setminus\{1\} \tag{3.5}$$

$$\sum_{s\in S}\sum_{i\in B_s\setminus\{0\}} x_{pksi} \le 1 \quad k \in K, p \in P \tag{3.6}$$

$$0 \le i_{pk} \le \sum_{s\in S}\sum_{i\in B_s\setminus\{0\}} I_{si}\cdot x_{pksi} \quad k \in K, p \in P \tag{3.7}$$

$$soc_{p+1,k} \le a_{si} + 1 - x_{pksi} \quad k \in K, p \in P\setminus\{n_p\}, s \in S, i \in B_s\setminus\{0\} \tag{3.8}$$

$$soc_{pk} \ge a_{s,i-1} - 1 + x_{pksi} \quad k \in K, p \in P, s \in S, i \in B_s\setminus\{0\} \tag{3.9}$$

$$soc_{pk} = soc_{p-1,k} + \delta\cdot\frac{i_{p-1,k}}{Q} \quad k \in K, p \in P\setminus\{1\}, p \notin A_k \tag{3.10}$$

$$SOC_{min} \le soc_{pk} \le SOC_{max} \quad k \in K, p \in P \tag{3.11}$$

$$\sum_{k\in K}\sum_{s\in S}\sum_{i\in B_s\setminus\{0\}} P_s\cdot x_{pksi} \le y \quad p \in P \tag{3.12}$$

$$0 \le y \le G \tag{3.13}$$

$$z_{pk} \ge \sum_{i\in B_s\setminus\{0\}} x_{pksi} - \sum_{i\in B_s\setminus\{0\}} x_{p-1,ksi} \quad k \in K, p \in P\setminus\{1\}, s \in S \tag{3.14}$$

$$z_{1k} \ge \sum_{i\in B_s\setminus\{0\}} x_{1ksi} \quad k \in K, s \in S \tag{3.15}$$

$$\sum_{p=\alpha_{\eta r}}^{\beta_r-1} z_{pv_r} \le C \quad r \in R \tag{3.16}$$

$$x_{pksi} \in \{0,1\} \quad k \in K, s \in S, i \in B_s\setminus\{b_s\} \tag{3.17}$$

$$z_{pk} \in \{0,1\} \quad k \in K, p \in P. \tag{3.18}$$

The objective function (3.2) minimizes the total cost of the charging schedule. The first term corresponds to total energy costs. We conducted some numerical

simulations of the CC-CV process with the battery model of Tremblay et al. (2007) and noted that the cumulative energy (kWh) recharged in the battery is fairly constant regardless of the charging current used in the CC phase, and is linear with respect to SOC during the CC-CV process. We therefore compute the SOC variation during period p of vehicle k as the charging current i_{pk} (A) multiplied by the period length δ (hours) divided by the battery charge capacity Q (Ah), and we then determine the corresponding energy recharged in the battery by multiplying the resulting SOC variation by the energy capacity E (kWh). The second term in the objective function corresponds to the incurred FRD charges. Recall that the decision variable y indicates the maximum registered charging power retrieved from the grid over the course of the entire planning interval. Since parameter F is a fee in \$/kW which depends on the maximum charging power retrieved from the grid throughout the planning interval, the term $F \cdot y$ thus represents the incurred FRD charges.

Constraints (3.3) ensure that no charging takes place while a vehicle performs its route. Constraints (3.4) set the SOC of each vehicle during the arrival period of each route to their SOC during the departure period of that route, minus the SOC consumption of the route. Constraints (3.5) state that for each charger type, at most the number of units installed of that type may be used by the fleet (these constraints are not necessary for $s = 1$). Constraints (3.6) force each vehicle to use at most one charger per period. Constraints (3.7) ensure that the charging current applied to a vehicle during a period is at most the one associated with the corresponding segment of the CC-CV charger-specific piecewise linear function. Constraints (3.8) and (3.9) appropriately bound the SOC of each vehicle at the start and end of each period depending on the CC-CV charger-specific piecewise linear function (we recall that $a_{si} \leq 1, \forall s \in S, i \in B_s$). Constraints (3.10) link the SOC of a vehicle from period $p-1$ to period p according the charging current used during $p-1$ (as long as p is not an arrival period for that vehicle).

Constraints (3.11) bound the SOC of each vehicle during each period. Constraints (3.12) determine the maximum charging power used during the planning interval. Constraint (3.13) ensures that the grid restriction is respected. Constraints (3.14)–(3.16) mean that at most C new charging events take place between each arrival and departure (or between the start of the horizon and the first route if $r = f_k$). Finally, constraints (3.17)–(3.18) define the domains of the variables that are not already appropriately bounded by the other constraints. Note that variables z_{pk} can also be treated as continuous.

3.2.4 Two optimal solutions to the EFV-CSP

In order to help readers better understand the problem and its mathematical formulation, we now provide examples of optimal solutions for the following small instance of the EFV-CSP. The fleet consists of $m = 2$ vehicles, the planning interval contains $n_p = 16$ periods of length $\delta = 0.5$ hours each, there are $|R| = 4$ routes to be performed, and there are $|S| = 2$ types of chargers installed at the depot. Charger type $s = 1$ comes with the vehicle (i.e., $\kappa_1 = 2$), while charger type $s = 2$ is a faster charger purchased separately; we assume there is only one charger of type $s = 2$ (i.e., $\kappa_2 = 1$). We assume that energy costs c_p are \$0.10/kWh for $p = 1, ..., 5$, \$0.25/kWh for $p = 6, ..., 10$, and \$0.40/kWh for $p = 11, ..., 16$. The FRD charge F is set to \$0.40/kW. The route parameters are given in Table 3.2.

Table 3.2 – Route parameters for the numerical example

r	β_r	α_r	ΔSOC_r	v_r	η_r
1	4	6	0.45	1	–
2	6	7	0.45	2	–
3	11	12	0.30	1	1
4	14	15	0.50	2	2

For the sake of simplicity, we assume that $B_1 = B_2 = \{0, 1\}$, i.e., each type

of charger has only two breakpoints and the charging function is therefore linear. Since the piecewise approximation of each charging function has only one segment, index i is fixed to one everywhere in the model, e.g., in variables x_{pksi} and parameters I_{si}. Let $I_{11} = 8$ A, $I_{21} = 20$ A, $P_1 = 20$ kW, and $P_2 = 50$ kW. With period lengths of 30 minutes (i.e., $\delta = 0.5$ hours) and a battery charge capacity of $Q = 40$ Ah, each period spent charging with charger type $s = 1$ can increase the SOC by at most $(8 \cdot 0.5)/40 = 0.10$, and each period spent charging with charger type $s = 2$ can increase the SOC by at most $(20 \cdot 0.5)/40 = 0.25$. We assume that the grid restriction G can be ignored, and we set parameter C to 1, i.e., each vehicle can be charged at most once by a single charger between each of its routes (and before leaving for its first route). Each vehicle starts with a SOC of 0.25, and we set SOC_{min} to zero and SOC_{max} to 1.0. Energy costs are computed as in objective function (3.2) assuming an energy capacity of $E = 80$ kWh.

Tables 3.3 and 3.4 illustrate two optimal solutions to the instance described above and demonstrate different strategies to minimize total costs. The solution in Table 3.3 focuses on keeping the FRD charge low, while the solution in Table 3.4 focuses on keeping the energy costs low. Indeed, in the solution of Table 3.3, the FRD charge is smaller since the faster charger type $s = 2$ is never used (i.e., the rows x_{p121} and x_{p221} contain only zeros), and the two vehicles are never charged simultaneously with charger type $s = 1$ during a given period (i.e., there is no period p for which $x_{p111} = 1$ and $x_{p211} = 1$). The maximum charging power used over the entire horizon is thus kept at 20 kW by spreading the charging of the vehicles over more periods, notably those when the energy costs are higher. On the other hand, in the solution of Table 3.4, all the charging of both vehicles occurs during the first five periods of the planning horizon when energy is at its cheapest. However, in order to charge an amount during these first five periods that will allow the vehicles to perform all their routes, the faster charger of type $s = 2$ is used during each of these periods, thus increasing the FRD charge.

Table 3.3 – Optimal solution 1: Keeping the FRD charge low

Periods:	1	2	3	4	5	6	7	8	9	10	11	12	13	14	15	16
Energy costs:	0.10	0.10	0.10	0.10	0.10	0.25	0.25	0.25	0.25	0.25	0.40	0.40	0.40	0.40	0.40	0.40
Route 1 ($v_1 = 1$):				⟶	⟶	⟶										
Route 2 ($v_2 = 2$):						⟶	⟶									
Route 3 ($v_3 = 1$):											⟶	⟶				
Route 4 ($v_4 = 2$):														⟶	⟶	
Vehicle 1																
x_{p111}:	1	1	0	0	0	0	1	1	1	0	0	0	0	0	0	0
x_{p121}:	0	0	0	0	0	0	0	0	0	0	0	0	0	0	0	0
i_{p1}:	8	8	0	0	0	0	8	8	8	0	0	0	0	0	0	0
soc_{p1}:	0.25	0.35	0.45	0.45	0.45	0.00	0.00	0.10	0.20	0.30	0.30	0.00	0.00	0.00	0.00	0.00
z_{p1}:	1	0	0	0	0	0	1	0	0	0	0	0	0	0	0	
Vehicle 2																
x_{p211}:	0	0	1	1	1	0	0	0	0	1	1	1	1	0	0	0
x_{p221}:	0	0	0	0	0	0	0	0	0	0	0	0	0	0	0	0
i_{p2}:	0	0	8	8	8	0	0	0	0	8	8	8	8	0	0	0
soc_{p2}:	0.25	0.25	0.25	0.35	0.45	0.55	0.10	0.10	0.10	0.10	0.20	0.30	0.40	0.50	0.00	0.00
z_{p2}:	0	0	1	0	0	0	0	0	0	1	0	0	0	0	0	0
Charging power per period (kW):	20	20	20	20	20	0	20	20	20	20	20	20	20	0	0	0

Maximum charging power used (i.e., y variable): 20 kW

Energy costs ($):	21.60
FRD charge ($):	8.00
Total costs ($):	29.60

Table 3.4 – Optimal solution 2: Keeping the energy costs low

Periods:	1	2	3	4	5	6	7	8	9	10	11	12	13	14	15	16
Energy costs:	0.10	0.10	0.10	0.10	0.10	0.25	0.25	0.25	0.25	0.25	0.40	0.40	0.40	0.40	0.40	0.40
Route 1 ($v_1 = 1$):				⟶	⟶	⟶										
Route 2 ($v_2 = 2$):						⟶	⟶									
Route 3 ($v_3 = 1$):											⟶	⟶				
Route 4 ($v_4 = 2$):														⟶	⟶	
Vehicle 1																
x_{p111}:	0	0	0	0	0	0	0	0	0	0	0	0	0	0	0	0
x_{p121}:	1	1	0	0	0	0	0	0	0	0	0	0	0	0	0	0
i_{p1}:	20	20	0	0	0	0	0	0	0	0	0	0	0	0	0	0
soc_{p1}:	0.25	0.50	0.75	0.75	0.75	0.30	0.30	0.30	0.30	0.30	0.30	0.00	0.00	0.00	0.00	0.00
z_{p1}:	1	0	0	0	0	0	0	0	0	0	0	0	0	0	0	
Vehicle 2																
x_{p211}:	0	0	0	0	0	0	0	0	0	0	0	0	0	0	0	0
x_{p221}:	0	0	1	1	1	0	0	0	0	0	0	0	0	0	0	0
i_{p2}:	0	0	20	20	16	0	0	0	0	0	0	0	0	0	0	0
soc_{p2}:	0.25	0.25	0.25	0.50	0.75	0.95	0.50	0.50	0.50	0.50	0.50	0.50	0.50	0.50	0.00	0.00
z_{p2}:	0	0	1	0	0	0	0	0	0	0	0	0	0	0	0	0
Charging power per period (kW):	50	50	50	50	50	0	0	0	0	0	0	0	0	0	0	0

Maximum charging power used (i.e., y variable): 50 kW

Energy costs ($):	9.60
FRD charge ($):	20.00
Total costs ($):	29.60

3.2.5 Deriving an equivalent solution in continuous time from the discrete time model

In order to use an equality in constraints (3.10), we have allowed the charging current i_{pk} in constraints (3.7) of the discrete time model to be less than the value I_{si} associated with the segment of the CC-CV piecewise linear function which vehicle k is using during period p. Therefore, this may result in solutions in which certain charging events do not represent the CC-CV process in continuous time. In other words, the current could go up and down from one period to the next even if the SOC remained between the same two breakpoints. However, we mention here, as a side note, that a feasible solution that respects the CC-CV process in continuous time can always be constructed from the solution obtained in discrete time. Indeed, whenever i_{pk} does not take the maximum value it could during any period of a charging event, the same SOC variation from that charging event can be obtained within less time with the CC-CV process in continuous time. Moreover, energy plans involve a few fixed rates over the course of a full day, so the function of energy costs with respect to time during a charging event is always a step function. Assuming a solution within which i_{pk} does not always take the maximum value it could during a charging event, then the same energy costs as those in the discrete time solution can be obtained with the CC-CV process in continuous time for that charging event by disconnecting and reconnecting the cable at most the number of times the step function increases and subsequently decreases. Therefore, as long as the step function representing energy costs with respect to time during a charging event is quasiconvex, the same energy costs as those in the discrete time solution can be obtained in continuous time for that charging event without having to split it into multiple events (i.e., without disconnecting and reconnecting the charging cable at some point).

Since most energy plans involve two or three rates over the course of a full day (e.g., mid-peak in the morning, peak during the afternoon, mid-peak in the evening, off-peak at night, with peak rate $>$ mid-peak rate $>$ off-peak rate), it seems unlikely that the function of energy costs with respect to time will increase and subsequently decrease more than once during a charging event. For example, Figure 3.3 illustrates the time-dependent energy costs of a rate plan offered by Southern California Edison (2017). With this plan, a charging event would need to last more than 24 hours for the step function of energy costs to increase and subsequently decrease more than once during the charging event. In addition, some charger manufacturers (e.g., eMotorWerks, 2017) have even started to offer products allowing to stop and restart charging at specific times without having to unplug and plug the cable. In this case the same energy costs can be obtained in continuous time regardless of the shape of the energy costs function with respect to time during the charging event.

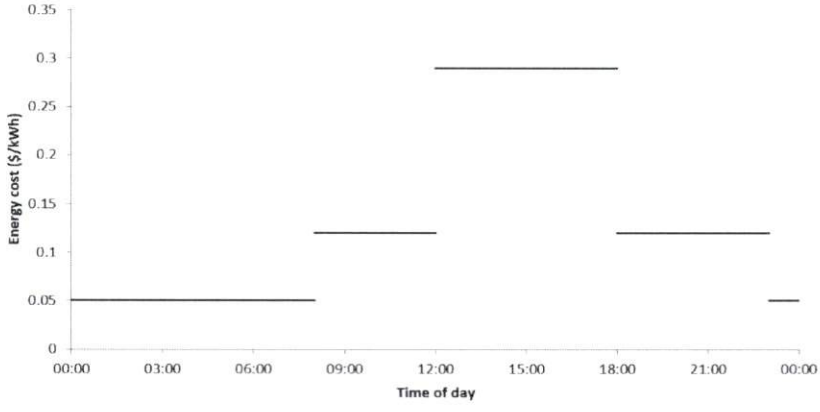

Figure 3.3 – Example of time-dependent energy costs

Finally, since the grid-related constraints (3.12)–(3.13) are modeled assuming the maximum charging power of each charger, the derived solution in continuous time will always respect the grid restriction and entail an FRD charge that is at most the one incurred in the discrete time solution.

3.3. Incorporating battery degradation considerations

Degradation occurs in electric vehicle batteries because of chemical and mechanical processes which ultimately lead to capacity and power fade (Barré et al., 2013). The degradation that occurs while cycling (i.e., charging or discharging) the battery is referred to as cyclic aging, while the degradation that occurs during storage is referred to as calendar aging. Battery degradation can either be estimated by using principles of electrochemistry, thereby modeling the reactions causing degradation within the battery, or by using a more empirical approach to predict battery aging according to experimental data (Bashash et al., 2011). Most transportation scientists would likely prefer a battery degradation model that can be understood without an expertise in electrochemisty and can be calibrated with easily obtainable battery specifications. Moreover, it seems desirable to use a model that transforms battery degradation directly into monetary battery wear costs. For these reasons, we propose using the model of Han et al. (2014) to take cyclic aging into account. This model uses an empirical approach to translate cyclic aging into monetary values and was applied in a vehicle-to-grid optimization problem solved with particle swarm optimization in the original paper. In Section 3.3.1 we detail the cyclic aging model as well as how to incorporate it into the EFV-CSP, and then in Section 3.3.2 we propose an intuitive approach to mitigate calendar aging when necessary via a second optimization phase.

3.3.1 Cyclic aging

Han et al. (2014) proposed a function representing wear costs per unit of energy going in or out of the battery according to the battery's SOC. This allows ac-

counting for different degradation rates occurring at different SOC values. The proposed model requires the following inputs: the battery's acquisition cost, as well as its cycle life versus depth of discharge (DOD) data. The DOD indicates the amount of electrical charge discharged and charged, divided by the maximum charge capacity of the battery, e.g., a DOD of 0.3 means that the SOC of the battery has increased or decreased by 0.3 depending on whether it was being charged or discharged. The cycle life versus DOD data typically provided by battery manufacturers indicates how many times the battery can be discharged and charged at that DOD before it reaches the end of its lifetime, assuming the battery is always discharged starting from a SOC of 1.0. Han et al. (2014) refer to this information as the Achievable Cycle Count and express it as a function of DOD (ACC-DOD). Let the function $ACC(DOD)$ refer to the ACC-DOD curve, i.e., $ACC(DOD)$ indicates how many times the battery can be discharged from a SOC of 1.0 to a SOC of $1.0 - DOD$, and then charged back from a SOC of $1.0 - DOD$ to a SOC of 1.0. For example, $ACC(0.4)$ would indicate the number of times the battery can be discharged from a SOC of 1.0 to a SOC of 0.6 and then charged back to 1.0 before the end of its lifespan. The $ACC(DOD)$ function of the lithium-ion battery used to calibrate the wear function in Han et al. (2014) is illutrated in Figure 3.4, where a curve is fitted to the ten data points.

However, in reality the battery will be cycled with different DOD values over its lifespan and at different starting SOC values (e.g., a DOD of 0.4 could be from 1.0 to 0.6, but also from 0.7 to 0.3, which would cause a different wear on the battery). Acknowledging this fact, Han et al. (2014) attribute a cost per kWh charged or discharged as a function of SOC based on the ACC-DOD data provided by the manufacturer. The authors propose a method for determining the wear cost function in both a continuous and a discrete manner. The discrete version can be derived as follows. A finite number of points from the ACC-DOD curve are required, and the SOC is discretized into corresponding intervals. Let

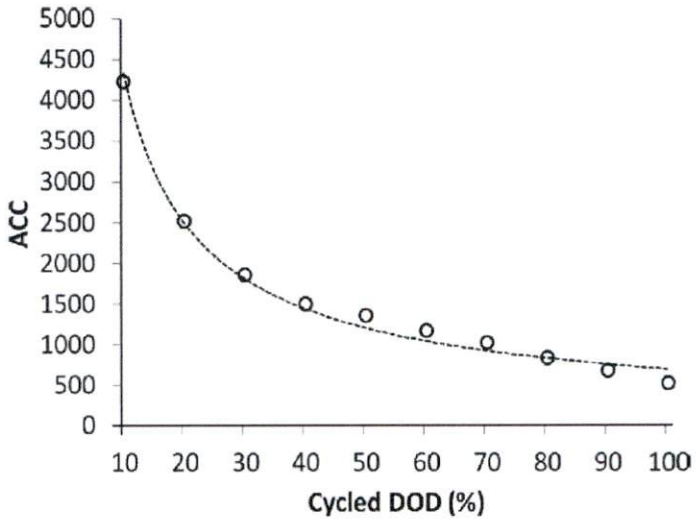

Figure 3.4 – Illustration of $ACC(DOD)$ function for a lithium-ion battery (Source: Han et al., 2014)

$D = \{1, ..., n_d\}$ represent the set of n_d SOC intervals used to calibrate the discrete wear cost function, with each interval $d \in D$ characterized by a lower SOC bound $\underline{S}_d$ and an upper SOC bound $\overline{S}_d$. Let L be the length of each SOC interval in D, i.e., $L = \overline{S}_d - \underline{S}_d \ \ \forall d \in D$. The wear cost function $W(\underline{S}_d)$ then indicates the cost per kWh charged or discharged in the SOC interval $[\underline{S}_d, \overline{S}_d]$ and satisfies

$$\text{Battery price} = 2 \cdot ACC(DOD) \cdot \sum_{d \in D: \underline{S}_d \geq 1.0 - DOD} (W(\underline{S}_d) \cdot \Delta q) \quad DOD \in \{L, 2L, 3L, ..., 1.0\}, \tag{3.19}$$

where Δq is the quantity of energy (kWh) in each SOC interval. Equation (3.19) must hold for each value of DOD used from the ACC-DOD curve. For example, if the manufacturer's ACC-DOD curve only provides points separated by 10% DOD intervals (or if the user wants the wear cost function for SOC intervals of 10%), then $n_d = 10$, $D = \{1, ..., 10\}$, and the lower and upper bounds of each SOC interval are given in Table 3.5.

Since the length of each interval is then $L = 0.1$, expression (3.19) yields 10 equations, i.e., one per $DOD \in \{0.1, 0.2, ..., 1.0\}$. By isolating the wear costs

Table 3.5 – SOC intervals for cyclic aging model when $n_d = 10$

d	1	2	3	4	5	6	7	8	9	10
$(\underline{S}_d, \overline{S}_d)$	(0.0, 0.1)	(0.1, 0.2)	(0.2, 0.3)	(0.3, 0.4)	(0.4, 0.5)	(0.5, 0.6)	(0.6, 0.7)	(0.7, 0.8)	(0.8, 0.9)	(0.9, 1.0)

$W(\underline{S}_d)$ in each of these, the following 10 equations can then be used to calibrate the wear cost function:

$$\begin{aligned} W(0.9) &= \frac{\text{Battery price}}{ACC(0.1) \cdot 2 \cdot \Delta q} \\ W(0.8) + W(0.9) &= \frac{\text{Battery price}}{ACC(0.2) \cdot 2 \cdot \Delta q} \\ &\vdots \qquad\qquad \vdots \\ W(0) + ... + W(0.9) &= \frac{\text{Battery price}}{ACC(1.0) \cdot 2 \cdot \Delta q}. \end{aligned}$$

We note that while the $ACC(DOD)$ curve is decreasing with respect to the DOD for any type of battery, the wear cost function is not necessarily increasing with the SOC. This is due to the computation in Equation (3.19), which does not exclusively depend on $ACC(DOD)$. The wear cost function used by Han et al. (2014) increases with the SOC, which means that cycling the battery in higher SOC intervals is more detrimental to the battery than in lower SOC intervals. We propose methodologies for incorporating monotonically increasing, monotonically decreasing and general wear costs functions with respect to SOC. Since all wear cost functions used in our numerical experiments are monotonic, for the sake of brevity we only describe the methodology for incorporating monotonic wear cost functions in what follows. However, in Appendix B we also propose a formulation that incorporates general wear cost functions into the EFV-CSP.

In the case of monotonically increasing or decreasing wear costs with respect to SOC, the following formulation can be used to incorporate degradation costs into the EFV-CSP. As mentioned above, let $D = \{1, ..., n_d\}$ represent the set of n_d SOC intervals used to calibrate the discrete wear cost function, with interval $d \in D$ characterized by lower SOC bound $\underline{S}_d$ and upper SOC bound $\overline{S}_d$. The

length of all the intervals is L, i.e., $L = \overline{S}_d - \underline{S}_d \ \ \forall d \in D$. Let W_d be the wear cost per kWh charged and discharged in the SOC interval d (computed through Equations (3.19)).

Define real variables soc^+_{dr} as the quantity of SOC interval $d \in D$ charged into vehicle v_r between arriving from route η_r (or the start of the horizon if $r = f_{v_r}$) and leaving for route r. The binary variables u_{dr} must take a value of 1 if interval d is used to charge vehicle v_r between arriving from route η_r (or the start of the horizon if $r = f_{v_r}$) and leaving for route r (i.e., if $soc^+_{dr} > 0$, then $u_{dr} = 1$). Note that several intervals in D can be used to charge all vehicles between two routes. Then the following constraints need to be added to the EFV-CSP regardless of whether the wear cost function is non-decreasing or non-increasing:

$$\sum_{d \in D} soc^+_{dr} = soc_{\beta_r, v_r} - soc_{\alpha_{\eta_r}, v_r} \quad r \in R \tag{3.20}$$

$$0 \leq soc^+_{dr} \leq L \cdot u_{dr} \quad d \in D, r \in R. \tag{3.21}$$

$$u_{dr} \in \{0,1\} \quad d \in D, r \in R. \tag{3.22}$$

Constraints (3.20) ensure that for each vehicle, the total energy charged over all SOC intervals in D between arriving from a route and leaving for its next route is equal to the total SOC variation resulting from charging the vehicle between arriving from the preceding route and leaving for the next. Constraints (3.21) state that the amount of energy used in each SOC interval is at most L if that interval is allowed to be used, and 0 otherwise.

If the wear function is non-decreasing with respect to SOC, then more degradation is incurred by cycling the battery in higher SOC intervals. The following constraints should thus be added to the problem in addition to constraints (3.20)–(3.22):

$$soc^+_{dr} \leq \overline{S}_d - soc_{\alpha_{\eta_r}, v_r} + 1 - u_{dr} \quad d \in D, r \in R. \tag{3.23}$$

Indeed, constraints (3.23) ensure that the variables u_{dr} can only take a value of 1 for SOC intervals with an upper bound that is larger than the SOC of vehicle v_r upon arriving from the previous route (or its SOC at the start of the horizon if it is the vehicle's first route). Since the wear costs increase with SOC in this case, the solution yielded by the model will always automatically fill out all lower SOC intervals, the lowest admissible interval being bounded by the difference between its upper bound and the SOC of the vehicle upon arriving from its previous route, rather than by the interval length L. Note that with a non-decreasing wear function with respect to SOC, in any optimal solution to the EFV-CSP, all the energy charged will subsequently be discharged, and any initial charge in the batteries of the vehicles will be completely discharged (assuming $\sum_{r \in R | v_r = k} \Delta SOC_r$ is greater than soc_{1k} for all $k \in K$). The objective function (3.2) can thus be replaced with

$$\text{minimize} \quad \sum_{k \in K} \sum_{p \in P} c_p \cdot E \cdot \frac{\delta \cdot i_{pk}}{Q} + F \cdot y + \sum_{r \in R} \sum_{d \in D} 2 \cdot W_d \cdot E \cdot soc^+_{dr}, \tag{3.24}$$

in which the total cyclic degradation costs (which should also include the cyclic degradation incurred during discharging) are computed using doubled wear costs on the amount of energy charged in each SOC interval. All discharging degradation other than that associated with discharging the initial charge in the batteries is thus computed at the time of charging. Note that with objective function (3.24), the initial charge in the batteries of the vehicles will still be completely discharged in any optimal solution.

On the other hand, if the wear cost function is non-increasing with respect to SOC, then more degradation is incurred by cycling the battery in lower SOC values. In this case, it is possible that some energy will be charged in an EFV-CSP optimal solution with the sole purpose of reaching (and subsequently staying in) more desirable SOC intervals. Therefore, some energy could be charged that will never be discharged, and the initial charge in the vehicles' batteries will not necessarily be completely discharged. As a result, we must compute the charging

and discharging cyclic degradation separately, and thus monitor the amount of energy charged and discharged in each SOC interval of the degradation model separately as well. To this end, we use two other sets of variables in addition to variables soc^{+}_{dr} and u_{dr}. Define real variables soc^{-}_{dr} as the quantity of SOC interval $d \in D$ discharged by vehicle v_r during route r. The binary variables π_{dr} must take a value of 1 if interval d is used to discharge the battery of vehicle v_r during route r (i.e., if $soc^{-}_{dr} > 0$, then $\pi_{dr} = 1$). The following constraints should be then added to the problem in addition to constraints (3.20)–(3.22):

$$soc^{+}_{dr} \leq soc_{\beta_r, v_r} - \underline{S}_d + 1 - u_{dr} \quad d \in D, r \in R \tag{3.25}$$

$$soc^{-}_{dr} \leq soc_{\beta_r, v_r} - \underline{S}_d + 1 - \pi_{dr} \quad d \in D, r \in R \tag{3.26}$$

$$\sum_{d \in D} soc^{-}_{dr} = \Delta SOC_r \quad r \in R \tag{3.27}$$

$$0 \leq soc^{-}_{dr} \leq L \cdot \pi_{dr} \quad d \in D, r \in R \tag{3.28}$$

$$\pi_{dr} \in \{0, 1\} \quad d \in D, r \in R. \tag{3.29}$$

Indeed, in this case the model will always try to fill out all higher SOC intervals first. For charging, constraints (3.25) bound the highest admissible interval by the difference between its lower bound and the departure SOC of the upcoming route rather than by the interval length L; constraints (3.26) do the same, but for discharging (i.e., the admissible SOC intervals discharged by a vehicle during a route must have a lower bound inferior or equal to the departure SOC). Constraints (3.27) ensure that for each vehicle, the total energy discharged over all SOC intervals in D during route r is equal to the total SOC variation resulting from performing route r. Constraints (3.28) state that the amount discharged in each SOC interval is at most L if that interval is allowed to be used, and 0 other-

wise. Finally, the objective function (3.2) should be replaced with

$$\text{minimize} \quad \sum_{k \in K} \sum_{p \in P} c_p \cdot E \cdot \frac{\delta \cdot i_{pk}}{Q} + F \cdot y + \sum_{r \in R} \sum_{d \in D} W_d \cdot E \cdot (soc_{dr}^{+} + soc_{dr}^{-}). \quad (3.30)$$

3.3.2 Calendar aging

The degradation occurring while the battery is stored always worsens with the increase in SOC. Lunz et al. (2012) showed that significant lifetime savings can be attained by charging electric vehicles as closely as possible to their departure times in order to avoid spending lengthy periods of time in higher SOC values. Although there exist some calendar aging models translating storage degradation in monetary terms that would easily lend themselves to problems akin to the EFV-CSP with periodic SOC variables, these rely on extensive long-term experimental data (e.g., Hoke et al., 2011) that may not be readily available for any given battery. Nevertheless, it would be desirable to at least mitigate calendar aging whenever possible without overly affecting the quality of the solution obtained without calendar aging considerations. Such a mitigation is especially desired if the cycling wear cost function is non-increasing with respect to SOC, since in this case the cycling aging model would be encouraged to keep the battery in high SOC intervals. Indeed, solely considering cyclic aging does not account for the time aspect of calendar aging, e.g., charging as closely as possible to departure times is preferable from a calendar aging perspective but makes no difference from a cyclic aging perspective.

One intuitive approach to mitigate calendar life aging in the EFV-CSP is to optimize the charging schedule in two phases: first by minimizing energy, FRD and cycling degradation costs, and then by minimizing the sum of the periodic SOC variables while constraining the aforementioned total costs or individual cost components to remain the same as (or within a maximum violation of) the

values found in the first phase. This should encourage the model to avoid keeping the batteries in high SOC values for lengthy periods when this can be avoided and thus take into account both the SOC and time aspects of calendar aging.

3.4. Computational experiments and managerial insights

We have performed an extensive computational study in order to assess the impact of different cost components in the formulation and to gain managerial insights into the proposed problem. More precisely, the aims of our experiments are: (1) to validate the proposed formulation, (2) to analyze the trade-off between energy, FRD and degradation costs under different scenarios, (3) to investigate the impact of the grid restriction on costs, (4) to illustrate how the model may be used to choose among different rate plans and battery sizes, and (5) to shed light on the importance of calendar aging considerations in certain contexts.

To this end, we have generated test instances and solved them under various scenarios. All test instances were solved using CPLEX 12.6 with a time limit of five hours and an optimality gap tolerance of 0.5%. The formulations were implemented in C++ and all experiments were conducted on a machine with eight Intel(R) Xeon(R) E7-8837 2.67 GHz processors with one TB of RAM running on Linux. The machine has 64 cores and each experiment was run using a single thread. We used a higher optimality gap tolerance than the default setting because our goal with these experiments is not to demonstrate the computational prowess of the model, but rather to derive meaningful managerial insights from reasonably good (in fact optimal or quasi-optimal) solutions. Except for the five tests in Section 3.4.8, for which the second phase of the approach proposed in Section 3.3.2 is performed, the remaining 225 tests generate a solution with an

optimality gap between 0% and 1.81% within the time limit. The average optimality gap of all 230 tests is 0.50%. (The worst gap for the above-mentioned five tests using the objective function of the second phase proposed in Section 3.3.2 is 3.35%.)

3.4.1 Description of the base-case scenario

We have generated test instances in which the vehicles are used in a multi-shift fashion throughout the day, thereby performing two routes per 24-hour interval (we allow both day and night routes). The fleet vehicles are assumed to be medium-duty electric trucks equipped with 80 kWh batteries, each consisting of several 3.2 V-40 Ah lithium-ion battery cells. We generated five test instances for each fleet size m of three, six and nine vehicles. The planning horizon begins at 6:00 and each vehicle is then assumed to have a SOC of 0.90. We worked with a planning horizon of three days and with period lengths of 30 minutes.

Let set $K_1 = \{1, 3, ...\}$ refer to the vehicles in K indexed by odd numbers, and let set $K_2 = \{2, 4, ...\}$ refer to the vehicles in K indexed by even numbers. For vehicles in K_1, the first route of each day occurs between 7:00 and 13:00, and the second route occurs between 19:00 and 1:00. The departure time is randomly generated between 7:00 and 9:00 for the first route, and between 19:00 and 21:00 for the second route. Similarly, the arrival time is randomly generated between 11:00 and 13:00 for the first route, and between 23:00 and 1:00 for the second route. For vehicles in K_2, the first route occurs between 12:00 and 18:00, and the second route occurs between 0:00 and 6:00, with departure and arrival times generated in a similar fashion. Davis and Figliozzi (2013), who also focus on depot charging, report that scenarios in which the daily distances traveled by electric trucks approach their maximum range can significantly help their business case. The SOC consumption of all routes is thus randomly generated between 0.4 and 0.47 so

that the vehicles discharge at least 80% of their battery on a daily basis. This is a reasonable representation of double-shift usage of the vehicles, considering typical daily miles traveled by urban delivery trucks are about 40 to 50 miles (Feng and Figliozzi, 2013).

Using some battery modeling considerations detailed in Pelletier et al. (2017) with battery cell parameters from Marra et al. (2012), we conducted numerical simulations of the CC-CV charging process for such battery cells with a maximum charge voltage of 3.65 V and two different charging currents during the CC phase: 3.5 A and 17.5 A. We set SOC_{min} to 0.05 and SOC_{max} to 0.99 for battery health reasons. We consider that the 3.5 A charger corresponds to an on-board charger that comes with the vehicle upon its purchase (i.e., each vehicle has one), and that the 17.5 A charger corresponds to a costly off-board fast charger (i.e., there are fewer 17.5 A chargers than there are vehicles in the fleet). Our simulations of the CC-CV charging process indicate that approximately 600 of the considered battery cells would need to be connected to form the battery pack so that a full charge from SOC_{min} to SOC_{max} corresponds to 80 kWh put into the battery, resulting in maximum charging powers of approximately 7.6 kW for the 3.5 A charger and 38 kW for the 17.5 A charger. These values are in line with maximum powers for AC level 2 (240 V) slow charging and DC level 1 (600 V) fast charging mentioned by Shareef et al. (2016) in their review of state-of-the-art charging technologies for electric vehicles.

With the 3.5 A charger, the batteries can be fully charged from SOC_{min} to SOC_{max} in just under 11 hours. The CV process is entered at a SOC of almost 0.98, so for the sake of simplicity we approximate the entire CC-CV process with two breakpoints: 0.05 and 0.99. With the 17.5 A charger, the batteries can be fully charged from SOC_{min} to SOC_{max} in just under three hours. The CV process is entered at a SOC of 0.78, and we approximate the CC-CV process associated with this charger with four breakpoints: 0.05, 0.78, 0.95, and 0.99. In all tested in-

stances, we use a depot charging infrastructure consisting of m slow chargers (i.e., 3.5 A) and $(m/3 - 1)$ fast chargers (i.e., 17.5 A). This infrastructure seems reasonable, since 1) considering the large costs associated with the acquisition, installation, and maintenance costs of fast chargers, a company would most likely want to get by with only a few (if any) of them, and 2) using several fast chargers simultaneously can potentially overload the grid, thus limiting the number of such chargers that may be installed at the depot. We allow each vehicle to perform two charging events (i.e., $C = 2$) between each pair of consecutive routes.

We used the time-dependent energy costs offered by Southern California Edison (2017) in their TOU-EV-4 plan for businesses charging electric vehicles on company grounds. The energy prices vary with time of day and season. Peak hours are from noon to 18:00; mid-peak hours are from 8:00 to noon and from 18:00 to 23:00; and off-peak hours are from 23:00 to 8:00. Summer rates are in place from the first Saturday of June to the first Saturday of October, while winter rates apply for the rest of the year. The energy rates and FRD charge of the TOU-EV-4 plan are summarized in Table 3.6. With the TOU-EV-4 plan, the maximum charging power must remain under 500 kW, so the grid restriction can be ignored under these circumstances. Assuming 22 working days per month, the FRD charge of \$13.20/kW would be equivalent to \$1.8/kW over a planning horizon of three days.

Table 3.6 – Rates (\$/kWh) and monthly FRD charge (\$/kW) under the TOU-EV-4 plan

	Summer	Winter
Peak (12:00–18:00)	0.29	0.11
Mid-peak (8:00–12:00, 18:00–23:00)	0.12	0.09
Off-peak (23:00–8:00)	0.05	0.06
FRD charges	13.20	13.20

Finally, regarding battery degradation, we consider a battery wear cost function calibrated with the cycle life data used in the original paper of Han et al.

(2014), resulting in a non-decreasing wear cost function. It is therefore preferable to avoid cycling such a battery in high SOC values. We calibrate the degradation costs for SOC intervals of 25% assuming battery costs of \$410/kWh (see Nykvist and Nilsson, 2015) and thus a battery price of \$32,800. We also multiply the obtained wear costs by two and use objective function (3.24), since the wear cost function is non-decreasing. The resulting costs (i.e., $2 \cdot W_d$) are reported in Table 3.7.

Table 3.7 – Battery wear cost function

SOC interval	Degradation costs
0–0.25	\$0.48/kWh
0.25–0.5	\$0.52/kWh
0.5–0.75	\$0.58/kWh
0.75–1	\$0.79/kWh

3.4.2 Base case results

The results for the problem setting described in Section 3.4.1 when all cost components (i.e., energy, degradation, and FRD) are jointly minimized are reported in Table 3.8. We also present in Table 3.9 the results obtained when only optimizing energy costs and the FRD charge. The columns "Energy (1)", "Deg. (2)" and "FRD (3)" report the obtained energy costs, degradation costs, and FRD charge, respectively. The column "Avg. SOC" reports the average SOC of the vehicles upon departing for their routes. The entries of Tables 3.8 and 3.9 show that incurring a slightly larger sum of energy costs and FRD charges can be worthwhile in order to cycle the battery in specific SOC intervals and thus lower battery degradation costs. Note that since the degradation costs used increase with SOC (see Table 3.7), the model tries to cycle the battery in low SOC intervals when the degradation costs are included in the optimization process, and the average departing SOC thus decreases significantly.

Table 3.8 – Costs obtained when minimizing energy, degradation and FRD costs

	Summer rates							Winter rates						
Instance	Energy (1)	Deg. (2)	FRD (3)	Total A (1)+(3)	Avg. SOC	Total B (1)+(2)+(3)	Time (s)	Energy (1)	Deg. (2)	FRD (3)	Total A (1)+(3)	Avg. SOC	Total B (1)+(2)+(3)	Time (s)
1-3V	39.53	220.75	27.36	66.89	0.62	287.64	0.06	34.06	213.31	27.36	61.42	0.56	274.73	842.42
2-3V	33.16	216.85	27.36	60.52	0.63	277.37	0.05	32.72	207.44	27.36	60.08	0.56	267.52	1044.34
3-3V	41.42	223.62	27.36	68.78	0.60	292.40	0.06	34.50	217.92	27.36	61.86	0.56	279.78	1424.99
4-3V	35.15	217.73	27.36	62.51	0.62	280.24	0.05	33.00	209.87	27.36	60.36	0.56	270.23	18000.00
5-3V	32.36	217.86	27.36	59.72	0.61	277.58	0.13	32.63	210.64	27.36	59.99	0.56	270.63	2512.42
1-6V	77.22	431.85	41.04	118.26	0.60	550.11	39.36	65.94	421.37	41.04	106.98	0.55	528.35	18000.00
2-6V	58.03	424.42	68.40	126.43	0.57	550.85	10.17	66.69	420.32	41.04	107.73	0.55	528.05	18000.00
3-6V	79.64	430.66	41.04	120.68	0.59	551.34	97.20	66.03	421.17	41.04	107.07	0.56	528.24	18000.00
4-6V	57.52	433.21	68.40	125.92	0.58	559.13	15.25	67.36	428.78	41.04	108.40	0.56	537.18	18000.00
5-6V	58.85	424.31	68.40	125.25	0.57	551.56	7.54	66.80	422.24	41.04	107.84	0.56	530.08	9663.27
1-9V	107.16	648.43	68.40	175.56	0.59	823.99	511.50	103.02	636.18	54.72	157.74	0.56	793.92	152.39
2-9V	109.18	648.34	68.40	177.58	0.59	825.92	125.38	103.11	635.81	54.72	157.83	0.56	793.64	242.75
3-9V	104.29	652.96	68.40	172.69	0.60	825.65	20.56	104.72	637.79	54.72	159.44	0.56	797.23	238.08
4-9V	97.38	656.60	82.08	179.46	0.59	836.06	95.77	105.02	646.43	54.72	159.74	0.56	806.17	185.05
5-9V	96.27	661.93	82.08	178.35	0.59	840.28	9.43	104.72	650.94	54.72	159.44	0.56	810.38	357.57

Table 3.9 – Costs obtained when minimizing energy and FRD costs

	Summer rates							Winter rates						
Instance	Energy (1)	Deg. (2)	FRD (3)	Total A (1)+(3)	Avg. SOC	Total B (1)+(2)+(3)	Time (s)	Energy (1)	Deg. (2)	FRD (3)	Total A (1)+(3)	Avg. SOC	Total B (1)+(2)+(3)	Time (s)
1-3V	32.38	250.46	27.36	59.74	0.76	310.20	0.06	35.83	249.22	13.68	49.51	0.74	298.73	0.06
2-3V	31.04	239.84	27.36	58.40	0.73	298.24	0.16	34.71	237.17	13.68	48.39	0.72	285.56	0.08
3-3V	35.43	241.39	27.36	62.79	0.70	304.18	0.08	36.89	252.42	13.68	50.57	0.74	302.99	0.10
4-3V	31.46	237.77	27.36	58.82	0.71	296.59	0.12	35.20	242.71	13.68	48.88	0.72	291.59	0.04
5-3V	30.43	241.53	27.36	57.79	0.71	299.32	0.55	34.81	239.81	13.68	48.49	0.70	288.30	0.11
1-6V	68.24	472.83	41.04	109.28	0.70	582.11	141.43	69.91	484.67	27.36	97.27	0.72	581.94	36.21
2-6V	69.30	478.72	41.04	110.34	0.71	589.06	119.27	70.20	495.01	27.36	97.56	0.74	592.57	189.57
3-6V	68.53	480.48	41.04	109.57	0.71	590.05	56.58	69.67	488.21	27.36	97.03	0.72	585.24	89.35
4-6V	70.17	499.46	41.04	111.21	0.74	610.67	77.03	71.41	503.71	27.36	98.77	0.75	602.48	107.36
5-6V	69.44	492.97	41.04	110.48	0.74	603.45	161.81	70.44	492.92	27.36	97.80	0.74	590.72	214.44
1-9V	97.67	711.91	68.40	166.07	0.70	877.98	271.57	105.67	753.72	41.04	146.71	0.75	900.43	257.68
2-9V	97.46	698.27	68.40	165.86	0.68	864.13	219.74	105.85	736.89	41.04	146.89	0.73	883.78	98.70
3-9V	98.95	728.59	68.40	167.35	0.72	895.94	227.92	106.79	749.34	41.04	147.83	0.74	897.17	246.34
4-9V	99.42	714.88	68.40	167.82	0.70	882.70	52.68	107.77	749.39	41.04	148.81	0.73	898.20	424.69
5-9V	100.53	726.73	68.40	168.93	0.70	895.66	7649.27	108.70	760.81	41.04	149.74	0.74	910.55	103.11

Whether degradation costs are jointly optimized or not, the FRD charge for a given instance solved with the summer rates is always at least equal to the FRD charge for the same instance solved with the winter rates. This outcome is a result of the very high peak energy costs of the summer rates. With the winter rates, peak rates are sufficiently low to charge vehicles during peak hours and thus keep FRD charges lower by spreading out charging of vehicles over larger time intervals. On the other hand, with the summer rates, vehicles are rarely charged during peak hours in order to avoid very high peak rates, thereby requiring one to charge more vehicles simultaneously or the use of faster chargers retrieving more power from the grid when energy is cheap, and thus incurring higher FRD charges.

3.4.3 The impact of facility-related demand charges

Although the FRD charge makes the problem significantly harder to solve, ignoring it may lead to undesirable solutions. To demonstrate this, we solved the test instances described in Section 3.4.1 by only optimizing energy and degradation costs. The results are presented in Table 3.10 and show how disregarding the FRD charge when optimizing the charging schedule leads to solutions in which the decrease in energy costs (achievable by being able to charge any amount of vehicles simultaneously with any type of charger without any penalty) does not compensate for the much higher FRD charge, especially for the larger fleet sizes of six and nine vehicles. Indeed, for these instances, the obtained FRD charge in Table 3.10 is often larger than the sum of the energy costs and the FRD charge in Table 3.8, while still generating similar degradation costs.

One should also carefully consider such FRD charges when determining the depot charging infrastructure if fast chargers are not required from a feasibility perspective. Indeed, while the fast chargers are heavily used in the solutions

obtained when ignoring the FRD charge (i.e., those reported in Table 3.10), they are often not used at all in the solutions obtained when jointly optimizing energy, degradation and FRD costs (i.e., those reported in Table 3.8) because of the large charging power they retrieve from the grid and the associated FRD charge. Therefore, although fast chargers certainly have their utility in certain operational contexts where they are required to allow vehicles to perform their routes (as will be shown in the next section), the notion of purchasing such fast chargers solely in order to perform the bulk of charging during specific periods of the day when energy is cheap may not be justifiable in certain contexts in the presence of FRD charges.

Table 3.10 – Costs obtained when minimizing energy and degradation costs

	Summer rates					Winter rates				
Instance	Energy	Deg.	FRD	Total	Time (s)	Energy	Deg.	FRD	Total	Time (s)
1-3V	36.32	220.37	41.04	297.73	0.04	34.03	213.31	41.04	288.38	0.03
2-3V	31.69	214.85	41.04	287.58	0.03	32.61	207.44	41.04	281.09	0.03
3-3V	38.01	223.63	41.04	302.68	0.04	34.50	217.92	41.04	293.46	0.03
4-3V	33.02	216.45	41.04	290.51	0.04	33.00	209.87	41.04	283.91	0.03
5-3V	30.22	217.48	41.04	288.74	0.03	32.63	210.64	41.04	284.31	0.03
1-6V	54.71	425.14	136.80	616.65	0.46	57.12	422.40	136.80	616.32	0.44
2-6V	57.90	422.48	109.44	589.82	0.49	57.30	422.62	109.44	589.36	0.52
3-6V	59.93	423.39	123.12	606.44	0.49	58.30	421.59	136.80	616.69	0.42
4-6V	57.97	431.39	123.12	612.48	0.58	58.44	428.72	123.12	610.28	0.51
5-6V	58.32	422.64	123.12	604.08	0.51	57.40	424.14	123.12	604.66	0.55
1-9V	85.18	640.19	177.84	903.21	0.40	86.74	637.45	177.84	902.03	0.48
2-9V	86.16	637.98	191.52	915.66	0.45	86.81	637.34	177.84	901.99	0.70
3-9V	89.08	642.09	164.16	895.33	0.41	88.27	639.32	177.84	905.43	0.73
4-9V	89.39	646.19	205.20	940.78	0.52	87.93	649.51	205.20	942.64	0.42
5-9V	89.80	652.39	205.20	947.39	0.64	88.61	651.79	205.20	945.60	0.40

3.4.4 The impact of longer routes

To determine the impact of longer routes, we modified the instances described in Section 3.4.1 to generate two alternative scenarios. In the first, the two short

routes in each 24-hour interval are merged into a single long route. While performing a single long route certainly has its logistical advantages, it also leaves much less leeway regarding the selection of SOC intervals within which to cycle the battery and thus limits cyclic aging mitigation. To generate the instances with a single long route per day, we simply merge the two routes of each vehicle into a single route, departing at the time of the earliest route, lasting the sum of the lengths of each route, and using the total SOC consumption of the two routes. Therefore, in the single long route per day scenario, all routes consume between 80% and 94% of the battery (note that 94% is the maximum feasible consumption for a route considering SOC_{min} and SOC_{max}). The results are presented in Table 3.11. The column "Base case" reports the total cost obtained for that instance under the base-case scenario (see Table 3.8). The results indicate that it is indeed preferable to split the long route into two in order to avoid cycling the battery in high SOC intervals.

Table 3.11 – Costs obtained when minimizing energy, degradation and FRD costs for the scenario with one longer route per day

	Summer rates						Winter rates					
Instance	Energy	Deg.	FRD	Total	Time (s)	Base case	Energy	Deg.	FRD	Total	Time (s)	Base case
1-3V	32.89	247.59	27.36	307.84	0.13	287.64	30.48	246.97	27.36	304.81	0.38	274.73
2-3V	32.03	239.61	27.36	299.00	0.05	277.37	29.82	239.61	27.36	296.79	0.10	267.52
3-3V	33.96	254.55	27.36	315.87	0.05	292.40	31.18	254.55	27.36	313.09	0.43	279.78
4-3V	33.25	243.26	27.36	303.87	0.06	280.24	30.12	243.04	27.36	300.52	1.56	270.23
5-3V	32.61	244.06	27.36	304.03	0.05	277.58	30.38	244.06	27.36	301.80	0.23	270.63
1-6V	64.26	488.36	54.72	607.34	37.26	550.11	65.02	490.68	41.04	596.74	37.38	528.35
2-6V	64.48	486.35	54.72	605.55	43.27	550.85	64.95	486.35	41.04	592.34	20.13	528.05
3-6V	64.22	487.48	54.72	606.42	28.61	551.34	64.97	489.09	41.04	595.10	23.32	528.24
4-6V	66.36	499.75	54.72	620.83	130.44	559.13	66.52	505.30	41.04	612.86	18000.00	537.18
5-6V	65.02	490.12	54.72	609.86	43.40	551.56	65.64	490.24	41.04	596.92	30.19	530.08
1-9V	97.57	737.86	82.08	917.51	18000.00	823.99	95.91	738.07	68.40	902.38	16394.65	793.92
2-9V	98.03	736.73	82.08	916.84	18000.00	825.92	96.02	736.73	68.40	901.15	77.52	793.64
3-9V	98.30	741.24	82.08	921.62	16498.00	825.65	95.90	741.24	68.40	905.54	462.54	797.23
4-9V	99.84	753.40	82.08	935.32	275.54	836.06	97.35	753.27	68.40	919.02	229.40	806.17
5-9V	100.29	758.74	82.08	941.11	16259.38	840.28	98.07	759.21	68.40	925.68	323.50	810.38

In the second alternative scenario with longer routes, we simply use the same

routes as in the base-case scenario in terms of when they occur, but we double the SOC consumption of each route. The vehicles thus perform two routes per day, each consuming between 80% and 94% of the battery. Under this scenario, all three-vehicle instances (in which there is no fast charger) become infeasible, showing that despite their impact on FRD charges, fast chargers can be useful in high EFV utilization contexts with long routes. Indeed, the six-vehicle and nine-vehicle instances (in which there are one and two fast chargers, respectively) are feasible under this scenario and make heavy use of the fast chargers. These results are presented in Table 3.12. The total costs obtained for the base-case scenario are also reported. Each individual cost component (i.e., energy, degradation and FRD) is more than doubled compared to the results from Table 3.8 for almost all the six- and nine-vehicle instances. Indeed, the larger charge consumption of the routes requires regularly cycling the battery in high SOC intervals (explaining the large increase in degradation costs), but also forces the model to use the fast chargers in order to allow the vehicles to perform their routes (explaining the large increase in FRD charges). This contingency in turn forces a significant amount of day-time inter-route charging to occur during peak hours due to the ratio of vehicles to fast chargers (explaining the large increase in energy costs).

Table 3.12 – Costs obtained when minimizing energy, degradation and FRD costs for the scenario with two longer routes per day

	Summer rates						Winter rates					
Instance	Energy	Deg.	FRD	Total	Time (s)	Base case	Energy	Deg.	FRD	Total	Time (s)	Base case
1-6V	246.26	1211.46	95.76	1553.48	16207.84	550.11	172.64	1211.43	82.08	1466.15	18000.00	528.35
2-6V	245.44	1211.01	95.76	1552.21	16078.18	550.85	166.82	1209.18	95.76	1471.76	18000.00	528.05
3-6V	259.97	1211.87	95.76	1567.60	473.43	551.34	168.56	1210.69	95.76	1475.01	18000.00	528.24
4-6V	254.13	1237.57	95.76	1587.46	474.61	559.13	169.54	1235.18	95.76	1500.48	18000.00	537.18
5-6V	247.53	1216.01	95.76	1559.30	16231.25	551.56	168.69	1213.96	95.76	1478.41	18000.00	530.08
1-9V	351.02	1829.45	164.16	2344.63	1103.25	823.99	244.17	1828.40	164.16	2236.73	18000.00	793.92
2-9V	362.35	1827.63	164.16	2354.14	16246.07	825.92	246.26	1827.63	164.16	2238.05	18000.00	793.64
3-9V	364.32	1836.28	164.16	2364.76	16265.76	825.65	247.96	1834.70	164.16	2246.82	18000.00	797.23
4-9V	349.52	1861.71	164.16	2375.39	16319.24	836.06	247.82	1861.71	164.16	2273.69	18000.00	806.17
5-9V	362.45	1869.12	164.16	2395.73	16243.70	840.28	249.09	1869.12	164.16	2282.37	18000.00	810.38

3.4.5 The impact of the grid restriction

We now investigate the impact of maximum allowed loads on energy and degradation costs by solving the instances described in Section 3.4.1 with another rate plan offered by Southern California Edison (2017): TOU-EV-3-B (see Table 3.13). Under this plan, the maximum power retrieved from the grid must always remain below 20 kW. In this case, the \$7.23/kW monthly FRD fee is equivalent to approximately \$0.99/kW for the three-day planning horizon, assuming once again 22 working days per month.

Table 3.13 – Rates (\$/kWh) and monthly FRD charge (\$/kW) under the TOU-EV-3-B plan

	Summer	Winter
Peak (12:00–18:00)	0.33	0.12
Mid-peak (8:00–12:00, 18:00–23:00)	0.14	0.11
Off-peak (23:00–8:00)	0.06	0.07
FRD	7.23	7.23

All three-vehicle instances use a maximum charging power under 20 kW with the plan TOU-EV-3-B, regardless of whether the restriction of 20 kW is enforced or not, and all nine-vehicle instances are infeasible under the grid restriction of 20 kW. We therefore present only the results for the six-vehicle instances under plan TOU-EV-3-B in Table 3.14, in which G indicates that the grid restriction of 20 kW was enforced during the optimization process, and NG indicates that the grid restriction was ignored. All three cost components are jointly optimized. The most notable impact of the grid restriction is on energy costs. With the summer rates, the energy costs are nearly doubled when solving the same instance without the grid restriction and with the grid restriction of 20 kW. Indeed, the grid restriction prevents the model from taking advantage of significant savings regarding energy costs since it limits the number of vehicles that can be simultaneously charged at any given moment, namely when energy is cheaper. Although the

grid restriction naturally leads to a smaller FRD charge, the increase in energy and degradation costs outweighs these savings and results in significantly higher total costs. The increase in energy costs is, however, less significant with the winter rates, since energy costs outside off-peak hours are smaller than with the summer rates. The difference in total costs obtained with and without the grid restriction is therefore quite smaller with the winter rates.

We also mention that while all the six-vehicle instances from Section 3.4.1 are feasible despite the grid restriction of 20 kW, they are no longer feasible when modified as described in the first paragraph of Section 3.4.4, i.e., when the two routes of each day are merged into one long route. This suggests that binding grid restrictions can hinder high EFV utilization in the presence of long routes, and that splitting such long routes into shorter ones spread out throughout the day and night can also be beneficial with regard to vehicle operation flexibility in the presence of such grid restrictions.

Table 3.14 – The impact of the grid restriction on costs under plan TOU-EV-3-B

	Summer rates					Winter rates				
Instance	Energy	Deg.	FRD	Total	Time (s)	Energy	Deg.	FRD	Total	Time (s)
1-6V-G	132.25	455.28	15.05	602.58	7.11	83.25	448.85	15.05	547.15	4.25
2-6V-G	133.68	459.80	15.05	608.53	3.51	83.54	454.31	15.05	552.90	3.60
3-6V-G	130.37	452.25	15.05	597.67	3.73	82.97	445.84	15.05	543.86	3.13
4-6V-G	136.39	470.10	15.05	621.54	4.54	84.77	464.72	15.05	564.54	7.93
5-6V-G	134.83	462.33	15.05	612.21	3.37	83.79	456.58	15.05	555.42	4.10
1-6V-NG	68.02	425.22	37.62	530.86	1.32	77.21	421.78	22.57	521.56	38.16
2-6V-NG	67.98	424.83	37.62	530.43	2.27	78.97	420.68	22.57	522.22	46.47
3-6V-NG	69.77	425.54	37.62	532.93	1.37	77.50	421.25	22.57	521.32	44.54
4-6V-NG	68.17	433.27	37.62	539.06	2.56	78.99	428.74	22.57	530.30	7.56
5-6V-NG	70.26	424.25	37.62	532.13	0.96	78.91	423.39	22.57	524.87	70.74

3.4.6 Using the model to select an energy rate plan

A desirable feature of our model is that it can be used to choose among different rate plans offering trade-offs between energy costs, FRD charges, and fixed customer charges when the operational context is compatible with the grid restriction of each option. For example, the TOU-EV-3-B plan has higher energy costs, a lower FRD charge, and a fixed customer charge of $0.84 per day, while the TOU-EV-4 plan has lower energy costs, a higher FRD charge, and a fixed customer charge of $198.79 per month. Table 3.15 presents the costs obtained with each of the plans for the six-vehicle instances described in Section 3.4.1 when optimizing all cost components. The total cost also includes the fixed customer charge of $2.52 for the TOU-EV-3-B plan (i.e., $0.84 per day for a three day planning horizon) and of $19.88 for the TOU-EV-4 plan (based on $198.79 per month for a three day planning horizon, assuming 30 days per month). The TOU-EV-4 plan appears to be the best choice in this context.

Table 3.15 – Cost comparison of the TOU-EV plan options

	Summer rates					Winter rates				
Instance	Energy	Deg.	FRD	Cus.chg	Total	Energy	Deg.	FRD	Cus.chg	Total
1-6V-TOU-EV-3-B	132.25	455.28	15.05	2.52	605.10	83.25	448.85	15.05	2.52	549.67
2-6V-TOU-EV-3-B	133.68	459.80	15.05	2.52	611.05	83.54	454.31	15.05	2.52	555.42
3-6V-TOU-EV-3-B	130.37	452.25	15.05	2.52	600.19	82.97	445.84	15.05	2.52	546.38
4-6V-TOU-EV-3-B	136.39	470.10	15.05	2.52	624.06	84.77	464.72	15.05	2.52	567.06
5-6V-TOU-EV-3-B	134.83	462.33	15.05	2.52	614.73	83.79	456.58	15.05	2.52	557.94
1-6V-TOU-EV-4	77.22	431.85	41.04	19.88	569.99	65.94	421.37	41.04	19.88	548.23
2-6V-TOU-EV-4	58.03	424.42	68.40	19.88	570.73	66.69	420.32	41.04	19.88	547.93
3-6V-TOU-EV-4	79.64	430.66	41.04	19.88	571.22	66.03	421.17	41.04	19.88	548.12
4-6V-TOU-EV-4	57.52	433.21	68.40	19.88	579.01	67.36	428.78	41.04	19.88	557.06
5-6V-TOU-EV-4	58.85	424.31	68.40	19.88	571.44	66.80	422.24	41.04	19.88	549.96

3.4.7 The impact of battery size

A possible way to decrease EFV purchase costs may be to acquire vehicles with a smaller battery. However, a smaller battery would need to be discharged with a larger DOD more frequently, which could accelerate its deterioration. To investigate the impact of battery size, we solved the test instances described in Section 3.4.1 by assuming the battery pack now contains 300 of the considered lithium-ion cells rather than 600, so that a full charge from SOC_{min} to SOC_{max} corresponds to approximately 40 kWh instead of 80 kWh as in all previous experiments. Using the same battery costs of \$410/kWh, the battery price thus becomes \$16,400. With the cycle life data used by Han et al. (2014) as well as the new battery price and energy capacity, the wear costs from Table 3.7 remain the same. Assuming the chargers described in Section 3.4.1 would apply the same maximum charging powers to the smaller battery, the charging currents applied during the CC phase become 7 A and 35 A for the 7.6 kW and 38 kW chargers, respectively. The piecewise functions used to approximate the CC-CV processes are adjusted accordingly. Since the initial SOC in all previous experiments with the large 80 kWh battery was set to 0.9, in order to achieve a fair comparison with the small 40 kWh battery we solved the base-case scenario with the large battery again but with a different initial SOC. The initial SOC is set to 0.45 for the 80 kWh battery, and to 0.90 for the 40 kWh battery. The results are presented in Table 3.16 for both the 40 kWh battery and the 80 kWh battery.

The results show that total costs are always lower with the larger battery, mostly because of savings in degradation costs. Since performing the routes with the smaller battery size requires larger discharge cycles, the batteries must be cycled in less preferable SOC intervals with regard to cyclic aging. With the summer rates the larger battery size also allows for significant energy cost savings since more energy can be charged when it is cheap and stored for future use,

Table 3.16 – Comparison of costs obtained when minimizing energy, FRD and degradation costs with two different battery sizes

	Summer rates										Winter rates									
	80 kWh battery					40kWh battery					80kWh battery					40 kWh battery				
Instance	Energy	Deg.	FRD	Total	Time (s)	Energy	Deg.	FRD	Total	Time (s)	Energy	Deg.	FRD	Total	Time (s)	Energy	Deg.	FRD	Total	Time (s)
1-3V	55.12	274.73	27.36	357.21	0.05	76.43	307.13	27.36	410.92	0.53	43.95	267.72	27.36	339.03	768.41	44.71	306.70	27.36	378.77	2.24
2-3V	50.67	269.86	27.36	347.89	0.05	71.59	297.60	27.36	396.55	0.20	42.70	261.62	27.36	331.68	4413.24	43.10	297.48	27.36	367.94	0.64
3-3V	55.76	281.75	27.36	364.87	0.05	74.56	313.42	27.36	415.34	0.19	44.70	272.21	27.36	344.27	81.27	44.84	313.42	27.36	385.62	0.61
4-3V	52.20	272.41	27.36	351.97	0.04	69.90	301.90	27.36	399.16	0.35	42.95	264.14	27.36	334.45	156.05	42.95	301.90	27.36	372.21	1.01
5-3V	46.01	275.29	27.36	348.66	0.06	66.82	304.19	27.36	398.37	0.19	42.51	265.14	27.36	335.01	355.49	42.60	303.54	27.36	373.50	1.49
1-6V	76.94	534.92	68.40	680.26	5.18	131.82	608.20	41.04	781.06	20.95	85.42	530.09	41.04	656.55	8176.51	85.84	605.84	41.04	732.72	74.16
2-6V	78.85	534.28	68.40	681.53	15.80	134.08	604.89	41.04	780.01	107.61	85.99	529.13	41.04	656.16	277.19	86.23	604.58	41.04	731.85	21.06
3-6V	75.91	539.95	68.40	684.26	3.63	137.21	606.35	41.04	784.60	10.21	85.85	529.82	41.04	656.71	1385.55	86.54	605.46	41.04	733.04	16.72
4-6V	76.69	544.58	68.40	689.67	4.23	138.76	618.29	41.04	798.09	58.34	87.21	537.54	41.04	665.79	160.92	87.94	617.64	41.04	746.62	14.49
5-6V	77.37	534.72	68.40	680.49	3.61	134.10	608.99	41.04	784.13	102.86	86.13	530.89	41.04	658.06	33.76	86.67	607.63	41.04	735.34	18.78
1-9V	128.81	813.96	82.08	1024.85	213.78	190.04	914.45	82.08	1186.57	18000.00	133.95	800.35	54.72	989.02	1508.82	133.61	914.91	54.72	1103.24	164.15
2-9V	127.88	815.66	82.08	1025.62	307.14	196.97	915.99	68.40	1181.36	36.10	134.23	799.55	54.72	988.50	218.70	133.56	918.47	54.72	1106.75	299.38
3-9V	132.93	814.71	82.08	1029.72	7372.71	197.32	918.02	82.08	1197.42	18000.00	135.06	802.14	54.72	991.92	338.02	129.75	917.40	68.40	1115.55	18000.00
4-9V	120.66	819.85	95.76	1036.27	541.93	191.25	931.07	82.08	1204.40	18000.00	134.84	810.92	54.72	1000.48	365.15	130.32	930.92	68.40	1129.64	18000.00
5-9V	120.25	826.23	95.76	1042.24	896.74	197.34	935.12	82.08	1214.54	18000.00	135.08	813.65	54.72	1003.45	1438.20	130.96	934.75	68.40	1134.11	18000.00

whereas with the smaller battery size this is not always possible since each route requires discharging almost the entirety of the battery of the vehicle performing it. For example, as stated in Section 3.4.1, the vehicles in K_1 perform one route between 7:00 and 13:00 and another between 19:00 and 1:00 each day. With the larger battery size, these vehicles often leave for their first route with more energy than required since the peak rates between 12:00 and 18:00 are very high under the summer rates and routes only induce a SOC variation between 0.40 and 0.47. With the smaller battery, each route induces a SOC variation between 0.80 and 0.94, which makes it difficult for the vehicles in K_1 to store energy for their second route prior to leaving for their first route; more energy must thus be charged during peak hours.

Whether or not these savings justify purchasing larger and more costly batteries should ultimately be determined based on a total cost of ownership analysis that takes into account the time-value of money, the projected number of battery replacements over the course of vehicle ownership, and the specific context at hand (and all its associated costs). The type of experiment conducted in this section can, however, help perform this analysis for different battery sizes and operational contexts since 1) its results can be used to assign values to operational costs that should be included in the total cost of ownership calculation (e.g., energy and FRD costs), and 2) the obtained degradation costs can be used to estimate the

frequency of battery replacements by assuming a replacement will be required when the cumulative degradation costs of a battery reaches its purchase cost.

3.4.8 The impact of non-increasing cycling degradation costs

A significant benefit of the non-decreasing degradation costs of Table 3.7 used in all previous experiments is that cycling the battery in lower SOC intervals not only increases cycle life, but also indirectly benefits calendar life. This is, however, not the case when the battery wear function is non-increasing. Indeed, the cycle life data of some batteries may result in non-increasing cycling wear functions, suggesting that it would be preferable to avoid cycling such batteries in low SOC values, which would most likely lead to an increase in calendar aging. We illustrate this by solving the six-vehicle instances described in Section 3.4.1 with the winter rates of the TOU-EV-4 plan and the DOD cycle life data used in Hoke et al. (2011), which results in the non-increasing wear costs W_d reported in Table 3.17.

Table 3.17 – Non-increasing battery degradation costs

SOC interval	Degradation costs
0–0.25	\$0.19/kWh
0.25–0.5	\$0.17/kWh
0.5–0.75	\$0.13/kWh
0.75–1	\$0.07/kWh

The results are reported in Table 3.18. The column "Avg. P. SOC" presents the average periodic SOC of the vehicles. In the determination of the average periodic SOC, it is assumed that the SOC decreases linearly from period to period while vehicles perform routes. The results presented in Table 3.18 show that calendar life is adversely affected when optimizing the charging schedule with the non-increasing battery wear function from Table 3.17, since the average periodic SOC of the batteries is then significantly higher than the one obtained when

optimizing without the wear costs. We therefore tried to mitigate calendar life losses resulting from the non-increasing wear cost function with the methodology proposed in Section 3.3.2 by minimizing the sum of the periodic SOC variables while allowing a maximum increase in total costs of 11% compared to those in the first phase solutions. The second phase solutions in Table 3.18 show that calendar aging can indeed be mitigated (since the average periodic SOC value decreases) while still ensuring smaller cycling degradation costs than those obtained when optimizing without the degradation costs, as well as similar energy and FRD costs to those obtained when optimizing with the degradation costs.

Table 3.18 – Costs and average periodic SOC before and after mitigating calendar aging

	Solution without degradation costs				First phase solution with degradation costs					Second phase solution with degradation costs				
Instance	Energy	Deg.	FRD	Avg. P. SOC	Energy	Deg.	FRD	Avg. P. SOC	Time (s)	Energy	Deg.	FRD	Avg. P. SOC	Time (s)
1-6V	69.91	298.39	27.36	0.50	66.04	221.52	41.04	0.67	18000.00	67.09	256.63	41.04	0.55	18000.00
2-6V	70.20	289.27	27.36	0.52	65.80	220.71	41.04	0.68	18000.00	70.39	265.83	27.36	0.54	18000.00
3-6V	69.67	295.41	27.36	0.50	66.56	221.46	41.04	0.68	18000.00	68.25	255.97	41.04	0.55	18000.00
4-6V	71.41	293.65	27.36	0.51	66.98	223.26	41.04	0.68	18000.00	67.66	259.02	41.04	0.55	18000.00
5-6V	70.44	291.80	27.36	0.52	66.39	221.28	41.04	0.67	18000.00	70.60	266.90	27.36	0.54	18000.00

Moreover, Keil et al. (2016) have recently shown that the increase of calendar aging with SOC is not continuous but rather varies between a few SOC intervals (depending on the battery chemistry) within which calendar aging is similar. Figure 3.5 illustrates this by presenting the results of the accelerated calendar aging experiments conducted by Keil et al. (2016). As can be seen, even small reductions in the storage SOC can go a long way if it allows moving from a higher capacity fade plateau to a lower one, considering that the end of life of an electric vehicle battery is usually assumed to occur when its capacity has decreased to 80% of its initial value. Thus, assuming that the calendar aging incurred while a battery's SOC varies around an average SOC is similar to the calendar aging that would be incurred if the battery was only stored at that average SOC, the second phase solutions reported in Table 3.18 would significantly mitigate calendar aging for

two of the three lithium-ion battery types presented in Figure 3.5 (i.e., NCA and NMC).

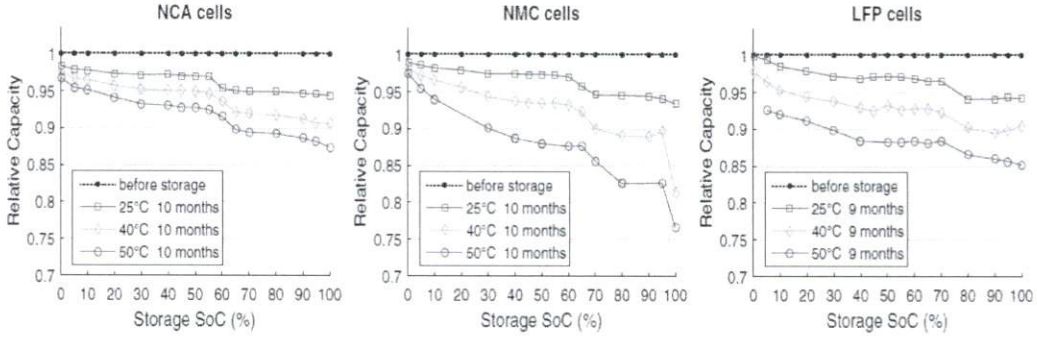

Figure 3.5 – Results of accelerated calendar aging tests at various SOCs and temperatures (Source: Keil et al., 2016)

Finally, we mention that when optimizing energy, degradation and FRD costs with the non-decreasing wear costs (i.e., those in Table 3.7) used in all previous experiments, the average periodic SOC value obtained for the five instances of Table 3.18 is approximately 0.34. Jointly optimizing those degradation costs with the energy and FRD costs is therefore beneficial to both cycle life (as demonstrated in our previous experiments through the reduction of degradation costs) and calendar life, since the average periodic SOC value decreases compared to the solutions obtained without degradation costs in Table 3.18.

3.5. Conclusions

The goal of this study was to develop and solve a comprehensive and practical mathematical model for depot charge scheduling that would integrate several useful considerations, as well as to derive managerial insights through computational experiments. The model can handle realistic charging functions, time-dependent energy costs, grid restrictions and FRD charges. We have also pro-

vided tractable methods for integrating an existing battery degradation function into the model. The tool can therefore be used to help the business case of EFVs operated in high use rate contexts by mitigating battery degradation occurring at a faster rate as a result of higher vehicle utilization, and by achieving the appropriate balance between energy and FRD costs.

Our numerical experiments suggest that degradation costs can indeed be mitigated by incurring slightly higher energy and FRD costs. We have also shown that when degradation costs are taken into account, the total costs can be decreased by splitting long routes into shorter ones with respect to SOC consumption. This modification allows more leeway regarding the selection of SOC intervals in which the battery is cycled. This may be of interest in operational contexts for which delivery routes stay relatively close to the depot so that vehicles can return to the depot more frequently, and where vehicles may be allowed perform evening or night-time deliveries so as to leave sufficient time for inter-route charging. Both of these operational characteristics are more likely to arise in the context where electric vehicles are used for city logistics due to their limited range and silent operation.

We have shown that fees based on maximum charging powers can render the purchase of fast chargers solely for reducing energy costs unjustifiable in some contexts. However, such fast chargers may be required for vehicle operation flexibility when longer routes are performed. Moreover, we have demonstrated how the model may be used to compare different plans offering tradeoffs between grid restrictions, energy costs, FRD charges, and fixed customer charges. In the same vein, the model can help compare achievable costs with different battery sizes. We have also concluded that depending on the nature of the cycling wear function (i.e., depending on the battery), the integration of calendar aging considerations becomes less critical. If the cycling wear cost function increases with the SOC, then even without calendar aging mitigation, the joint optimization of

energy, FRD and degradation costs is beneficial to both the cycle and calendar lifetime of the batteries. However, if the cycling wear cost function decreases with the SOC, our results suggest that additional steps may be required to mitigate calendar aging in order to avoid spending lengthy periods of time at high SOC values. We have therefore provided a simple methodology to this end.

Finally, we believe that interesting research avenues lie in the integration of some of the methods discussed in this paper into other problem settings. These may include simultaneously optimizing the charging schedule and assigning vehicles to routes, or even simultaneously routing the vehicles, both of which would require the development of heuristics. Moreover, the proposed methodology for incorporating cycling wear costs is applicable to any electric vehicle routing problem with en route partial recharging, and could thus be used to investigate the impact of such wear costs on solutions of these problems, e.g., it may induce more frequent stops at charging stations in order to cycle the batteries in the SOC intervals with the lowest wear costs.

Acknowledgements

This research was partly supported by the Canadian Natural Sciences and Engineering Research Council under grants 463834-2014, 436014-2013 and 2015-06189. This support is gratefully acknowledged. Thanks are due to the reviewers for their valuable comments

3.6. Appendix A – Glossary of abbreviations

A: Ampere.

Ah: Ampere-hour.

ACC-DOD: Achievable cycle count as a function of DOD.

CC-CV: Constant current-constant voltage.

DOD: Depth of discharge.

EFV: Electric freight vehicle.

FRD charges: Facility-related demand charges.

kW: Kilowatt.

kWh: Kilowatt-hour.

SOC: State of charge.

V: Volt.

3.7. Appendix B – Incorporating general wear cost functions into the EFV-CSP

Since the wear cost is constant in a given SOC interval, a cumulative wear cost function can be represented as a piecewise linear function of SOC regardless of the shape of the wear cost function. A point at a given SOC in this cumulative wear cost function would indicate the total wear costs incurred for charging the battery from 0 to that SOC. The idea is essentially to determine initial and final positions on a piecewise linear function by constructing convex combinations of the function's breakpoints. As for non-increasing wear cost functions with respect to SOC, with a general wear cost function, some energy could be charged

that will never be discharged in an EFV-CSP optimal solution. We must therefore monitor the amount of energy charged and discharged in each SOC interval of the degradation model separately in order to incorporate both charging and discharging cyclic degradation. For the sake of brevity, we only provide a formulation to incorporate the cyclic aging incurred during charging for general wear cost functions, however the cyclic aging incurred during discharging can be incorporated in a very similar fashion.

Let ζ_{dr} be a binary variable equal to 1 if and only if the SOC of vehicle v_r lies between $\overline{S}_{d-1}$ and $\overline{S}_d$ upon arriving from route η_r or at the start of the horizon if $r = f_{v_r}$, with $\overline{S}_0 = \underline{S}_1$. Similarly, let ψ_{dr} be a binary variable equal to 1 if and only if the SOC of vehicle v_r lies between $\overline{S}_{d-1}$ and $\overline{S}_d$ upon leaving for route r. Let ϵ_{dr} and w_{dr} be the coefficients of breakpoint $\overline{S}_d$ used in the convex combinations to determine the position of vehicle v_r on the cumulative wear function when arriving from η_r (or the start of the horizon if $r = f_{v_r}$) and leaving for r respectively. Let cs_r and ce_r be the starting and ending cost positions of vehicle v_r on the cumulative wear function when arriving from η_r (or the start of the horizon if $r = f_{v_r}$) and leaving for r respectively. Let C_d be the cumulative wear cost in the piecewise linear function at breakpoint $\overline{S}_d$, for all $d \in D \cup \{0\}$. Then any discrete wear cost function can be incorporated into the EFV-CSP by means of the following constraints:

$$\sum_{d \in D \cup \{0\}} \epsilon_{dr} = \sum_{d \in D} \zeta_{dr} = 1 \quad r \in R \tag{3.31}$$

$$\sum_{d \in D \cup \{0\}} w_{dr} = \sum_{d \in D} \psi_{dr} = 1 \quad r \in R \tag{3.32}$$

$$soc_{\alpha_{\eta_r}, v_r} = \sum_{d \in D \cup \{0\}} \epsilon_{dr} \cdot \overline{S}_d \quad r \in R \tag{3.33}$$

$$soc_{\beta_r, v_r} = \sum_{d \in D \cup \{0\}} w_{dr} \cdot \overline{S}_d \quad r \in R \tag{3.34}$$

$$cs_r = \sum_{d \in D \cup \{0\}} \epsilon_{dr} \cdot C_d \quad r \in R \tag{3.35}$$

$$ce_r = \sum_{d \in D \cup \{0\}} w_{dr} \cdot C_d \quad r \in R \tag{3.36}$$

$$\epsilon_{0r} \leq \zeta_{1r} \quad r \in R \tag{3.37}$$

$$\epsilon_{dr} \leq \zeta_{dr} + \zeta_{d+1,r} \quad d \in D \backslash \{n_d\}, r \in R \tag{3.38}$$

$$\epsilon_{n_d,r} \leq \zeta_{n_d,r} \quad r \in R \tag{3.39}$$

$$w_{0r} \leq \psi_{1r} \quad r \in R \tag{3.40}$$

$$w_{dr} \leq \psi_{dr} + \psi_{d+1,r} \quad d \in D \backslash \{n_d\}, r \in R \tag{3.41}$$

$$w_{n_d,r} \leq \psi_{n_d,r} \quad r \in R \tag{3.42}$$

$$\zeta_{dr}, \psi_{dr} \in \{0,1\} \quad d \in D, r \in R \tag{3.43}$$

$$\epsilon_{dr}, w_{dr} \geq 0 \quad d \in D \cup \{0\}, r \in R. \tag{3.44}$$

Constraints (3.31)–(3.32) ensure that the SOC values upon arriving from a route (or at the start of the horizon) and leaving for the next route to be between two of the SOC breakpoints of the cumulative wear function, and force the sum of the breakpoint coefficients to be equal to 1. Constraints (3.31)–(3.34) and (3.44) together force the SOC values upon arriving from a route (or at the start of the horizon) and leaving for the next route to be convex combinations of the SOC breakpoints of the cumulative wear cost function. Constraints (3.35)–(3.36) determine the costs on the cumulative wear function corresponding to these convex combinations. Constraints (3.37)–(3.42) force these convex combinations to only use two consecutive breakpoints of the cumulative wear cost function. Constraints (3.43)–(3.44) define the domains of the new variables. Finally, in this case,

the objective function (3.2) should be replaced with

$$\text{minimize} \quad \sum_{k \in K} \sum_{p \in P} c_p \cdot E \cdot \frac{\delta \cdot i_{pk}}{Q} + F \cdot y + \sum_{r \in R} (ce_r - cs_r). \tag{3.45}$$

References

Afroditi, A., M. Boile, S. Theofanis, E. Sdoukopoulos, D. Margaritis. 2014. Electric vehicle routing problem with industry constraints: Trends and insights for future research. *Transportation Research Procedia* **3** 452–459.

Barré, A., B. Deguilhem, S. Grolleau, M. Gérard, F. Suard, D. Riu. 2013. A review on lithium-ion battery ageing mechanisms and estimations for automotive applications. *Journal of Power Sources* **241** 680–689.

Bashash, S., S.J. Moura, J.C. Forman, H.K. Fathy. 2011. Plug-in hybrid electric vehicle charge pattern optimization for energy cost and battery longevity. *Journal of Power Sources* **196** 541–549.

Bruglieri, M., F. Pezzella, O. Pisacane, S. Suraci. 2015. A variable neighborhood search branching for the electric vehicle routing problem with time windows. *Electronic Notes in Discrete Mathematics* **47** 221–228.

Conrad, R.G., M.A. Figliozzi. 2011. The recharging vehicle routing problem. T. Doolen, E. Van Aken, eds., *Proceedings of the 2011 Industrial Engineering Research Conference* (Institute of Industrial Engineers, Norcross, GA), 2785–2792.

Davis, B.A., M.A. Figliozzi. 2013. A methodology to evaluate the competitiveness of electric delivery trucks. *Transportation Research Part E: Logistics and Transportation Review* **49**(1) 8–23.

E-Mobility NSR. 2013. Comparative analysis of European examples of schemes for freight electric vehicles – Compilation report. URL

http://e-mobility-nsr.eu/fileadmin/user_upload/downloads/info-pool/E-Mobility_-_Final_report_7.3.pdf. Last accessed January 2019.

eMotorWerks. 2017. JuiceBox EV Charging Stations. URL https://emotorwerks.com/products/juicebox. Last accessed June 2017.

Felipe, Á., M.T. Ortuño, G. Righini, G. Tirado. 2014. A heuristic approach for the green vehicle routing problem with multiple technologies and partial recharges. *Transportation Research Part E: Logistics and Transportation Review* **71** 111–128.

Feng, W., M. Figliozzi. 2013. An economic and technological analysis of the key factors affecting the competitiveness of electric commercial vehicles: A case study from the USA market. *Transportation Research Part C: Emerging Technologies* **26** 135–145.

Franceschetti, A.,D. Honhon, G. Laporte, T. Van Woensel, J.C. Fransoo. 2017. Strategic fleet planning for city logistics. *Transportation Research Part B: Methodological* **95** 19–40.

Goeke, D., M. Schneider. 2015. Routing a mixed fleet of electric and conventional vehicles. *European Journal of Operational Research* **245**(1) 81–99.

Han, S., S. Han, H. Aki. 2014. A practical battery wear model for electric vehicle charging applications. *Applied Energy* **113** 1100–1108.

Hiermann, G., J. Puchinger, S. Ropke, R.F. Hartl. 2016. The electric fleet size and mix vehicle routing problem with time windows and recharging stations. *European Journal of Operational Research* **252**(3) 995–1018.

Hoke, A., A. Brissette, D. Maksimović, A. Pratt, I. Labs, K. Smith. 2011. Electric vehicle charge optimization including effects of lithium-ion battery degradation. *2011 IEEE Vehicle Power and Propulsion Conference (VPPC)* (IEEE, Piscataway, NJ), 1–8.

Keil, P., S.F. Schuster, J. Wilhelm, J. Travi, A. Hauser, R.C. Karl, A. Jossen. 2016. Calendar aging of lithium-ion batteries – I. Impact of the graphite anode on capacity fade. *Journal of The Electrochemical Society* **163**(9) A1872–A1880.

Kovacs, A.A., B.L. Golden, R.F. Hartl, S.N. Parragh. 2014. Vehicle routing problems in which consistency considerations are important: A survey. *Networks* **64**(3) 192–213.

Lam, L. 2011. A practical circuit-based model for state of health estimation of li-on battery cells in electric vehicles. Master's thesis, Delft University of Technology, The Netherlands.

Lebeau, P., C. De Cauwer, J. Van Mierlo, C. Macharis, W. Verbeke, T. Coosemans. 2015. Conventional, hybrid, or electric vehicles: Which technology for an urban distribution centre? *The Scientific World Journal*, Article ID 302867.

Lee, D.Y., V.M. Thomas, M.A. Brown. 2013. Electric urban delivery trucks: Energy use, greenhouse gas emissions, and cost-effectiveness. *Environmental science & technology* **47**(14) 8022–8030.

Lunz, B., Z. Yan, J.B. Gerschler, D.U. Sauer. 2012. Influence of plug-in hybrid electric vehicle charging strategies on charging and battery degradation costs. *Energy Policy* **46** 511–519.

Marra, F., G.Y. Yang, C. Traholt, E. Larsen, C.N. Rasmussen, S. You. 2012. Demand profile study of battery electric vehicle under different charging options. *2012 IEEE Power and Energy Society General Meeting* (IEEE, Piscataway, NJ), 3428–3434.

Montoya, A., C. Guéret, J.E. Mendoza, J.G. Villegas. 2017. The electric vehicle routing problem with nonlinear charging function. *Transportation Research Part B: Methodological* **103** 87–110.

Morganti, E., M. Browne. 2018. Technical and operational obstacles to the adoption of electric vans in France and the UK: An operator perspective. *Transport Policy* **63** 90–97.

Naberezhnykh, D., J. Wardle, J. Lowes, C. Herron, T. Brightman, T. Parker. 2012. Electric vehicle charging points for freight vehicles in central London (Version – Final 1.0). Prepared for Central London FQP by Transport & Travel Research Ltd, in partnership with TRL and Zero Carbon Futures. URL `http://www.centrallondonfqp.org/app/download/12240926/CLFQP_EVCP_strategy+report_Final+v1+0.pdf`. Last accessed January 2019.

Nesterova, N., H. Quak, S. Balm, I. Roche-Cerasi, T. Tretvik. 2013. Project FREVUE deliverable D1.3: State of the art of the electric freight vehicles implementation in city logistics. TNO and SINTEF. European Commission Seventh framework programme.

Nykvist, B., M. Nilsson. 2015. Rapidly falling costs of battery packs for electric vehicles. *Nature Climate Change* **5** 329–332.

Pelletier, S., O. Jabali, G. Laporte. 2016. 50th anniversary invited article – Goods distribution with electric vehicles: Review and research perspectives. *Transportation Science* **50**(1) 3–22.

Pelletier, S., O. Jabali, G. Laporte, M. Veneroni. 2017. Battery degradation and behaviour for electric vehicles: Review and numerical analyses of several models. *Transportation Research Part B: Methodological* **103** 158–187.

Preis, H., S. Frank, K. Nachtigall. 2014. Energy-optimized routing of electric vehicles in urban delivery systems. S. Helber, M. Breitner, D. Rösch, C. Schön, J-M. Graf von der Schulenburg, P. Sibbertsen, M. Steinbach, S. Weber, A. Wolter, eds., *Operations Research Proceedings 2012* (Springer International Publishing, Switzerland), 583–588.

Quak, H., N. Nesterova, T. van Rooijen. 2016. Possibilities and barriers for using electric-powered vehicles in city logistics practice. *Transportation Research Procedia* **12** 157–169.

Sassi, O., A. Oulamara. 2014a. Joint scheduling and optimal charging of electric vehicles problem. B. Murgante, S. Misra, A.M.A.C. Rocha, C. Torre, J.G. Rocha, M.I. Falcão, D. Taniar, B.O. Apduhan, O. Gervasi, eds., *ICCSA 2014 Proceedings, Part II*. Lecture Notes in Computer Science, vol. 8580 (Springer International Publishing, Switzerland), 76–-91.

Sassi, O., A. Oulamara. 2014b. Simultaneous electric vehicles scheduling and optimal charging in the business context: Case study. *5th IET Hybrid and Electric Vehicles Conference* (IET, Stevenage, UK), 105–110.

Schiffer, M., M. Schneider, G. Laporte. 2018. Designing sustainable mid-haul logistics networks with intra-route multi-resource facilities. *European Journal of Operational Research* **265**(2) 517–532.

Schiffer, M., G. Walther. 2017a. An adaptive large neighborhood search for the location routing problem with intraroute facilities. *Transportation Science* **52**(2) 331–352.

Schiffer, M., G. Walther. 2017b. The electric location routing problem with time windows and partial recharging. *European Journal of Operational Research* **260**(3) 995–1013.

Schiffer, M., G. Walther. 2018. Strategic planning of electric logistics networks: A robust location-routing approach. *Omega* **80** 31–42.

Schneider, M., A. Stenger, D. Goeke. 2014. The electric vehicle-routing problem with time windows and recharging stations. *Transportation Science* **48**(4) 500–520.

Shareef, H., M.M. Islam, A. Mohamed. 2016. A review of the state-of-the-art charging technologies, placement methodologies, and impacts of electric vehicles. *Renewable and Sustainable Energy Reviews* **64** 403–420.

Southern California Edison. 2017. Electric car rate options. URL `sce.com/wps/portal/home/business/rates/electric-car-business-rates`. Last accessed June 2017.

Taefi, T.T. 2016. Viability of electric vehicles in combined day and night delivery: A total cost of ownership example in Germany. *European Journal of Transport and Infrastructure Research* **16**(4) 600–618.

Taefi, T.T., S. Stütz, A. Fink. 2016. Increasing the mileage of battery electric medium duty vehicles: A recipe for competitiveness? Helmut-Schmidt University Hamburg, Institute of Computer Science Research Paper Series, Research Paper 16–01.

Tremblay, O., L.-A. Dessaint, A.-I. Dekkiche. 2007. A generic battery model for the dynamic simulation of hybrid electric vehicles. *2007 Vehicle Power and Propulsion Conference* (IEEE, Piscataway, NJ), 284–289.

Yang, J., H. Sun. 2015. Battery swap station location-routing problem with capacitated electric vehicles. *Computers & Operations Research* **28** 217–232.

Chapter 4

The electric vehicle routing problem with energy consumption uncertainty

Chapter information

This article is the result of a collaboration with my thesis advisors. It was published in *Transportation Research Part B: Methodological*: S. Pelletier, O. Jabali, G. Laporte. 2019. The electric vehicle routing problem with energy consumption uncertainty. *Transportation Research Part B: Methodological* **126** 225–255.

Abstract

Compared with conventional freight vehicles, electric freight vehicles create less local pollution and are thus generally perceived as a more sustainable means of goods distribution. In urban areas, such vehicles must often perform the entirety of their delivery routes without recharging. However, their energy consumption is subject to a fair amount of uncertainty, which is due to exogenous factors such as the weather and road conditions, endogenous factors such as driver be-

haviour, and several energy consumption parameters that are difficult to measure precisely. Hence we propose a robust optimization framework to take into account these energy consumption uncertainties in the context of an electric vehicle routing problem. The objective is to determine minimum cost delivery routes capable of providing strong guarantees that a given vehicle will not run out of charge during its route. We formulate the problem as a robust mixed integer linear program and solve small instances to optimality using robust optimization techniques. Furthermore, we develop a two-phase heuristic method based on large neighbourhood search to solve larger instances of the problem, and we conduct several numerical tests to assess the quality of the methodology. The computational experiments illustrate the trade-off between cost and risk, and demonstrate the influence of several parameters on best found solutions. Furthermore, our heuristic identifies 42 new best solutions when tested on instances of the closely related robust capacitated vehicle routing problem.

Keywords: electric vehicle routing; robust optimization; city logistics; metaheuristics.

4.1. Introduction

There currently exists a strong interest on the part of the transportation science community in the design of distribution schemes that may reduce the environmental impact of goods distribution, namely in the context of city logistics. Whereas some researchers have focused on taking emission costs into account when routing conventional vehicles (e.g., Jabali et al., 2012; Bektaş and Laporte, 2011), others have dealt with the challenges arising from the use of cleaner alternatives such as electric freight vehicles (EFVs) (Pelletier et al., 2016). Indeed, EFVs create less local air pollution and less noise than conventional vehicles, and are there-

fore considered to be a more sustainable means of goods distribution. Despite the environmental benefits of EFVs, there exist significant issues associated with their integration into goods distribution schemes, most notably their high initial investments, limited range and payload, long recharging times, and the scarcity of public charging stations. In an urban environment, however, delivery routes tend to be shorter than the range of currently available EFVs (Feng and Figliozzi, 2013), which means that some of the aforementioned issues, namely those concerning recharging times and public charging infrastructures, can be averted by recharging the batteries at a central depot. Indeed, companies that use EFVs for goods distribution will usually charge them on company grounds overnight and will rarely use public charging stations (Naberezhnykh et al., 2012; E-Mobility NSR, 2013; Quak et al., 2017; Morganti and Browne, 2018). This practice also mitigates cargo security concerns and avoids inefficient use of drivers' time during en route charging. Furthermore, depot charging offers the possibility of benefiting from lower energy costs through commercial off-peak electricity rates at the depot (Pelletier et al., 2018).

In the case of exclusive charging EFVs at the depot, vehicle routes must be planned carefully as a result of the limited range of the vehicles, and in a way that ensures that the vehicles will be able to perform their full route with their departing battery charge. This is particularly important in the presence of strong uncertainties surrounding the energy consumption of the vehicles along the planned routes. Indeed, Asamer et al. (2016) show that several parameters of the comprehensive emissions model of Barth et al. (2005) commonly used to estimate energy consumption in electric vehicle routing problems (EVRPs) are difficult to measure or depend on uncontrolable exogenous factors, and it is therefore wiser to think of their value as lying within an uncertainty range. Yi and Bauer (2017) also demonstrate how environmental factors such as wind speed, weather, road surface conditions, and temperature can significantly alter the achievable range of

electric vehicles. Bingham et al. (2012) reach similar conclusions concerning the influence of driver behaviour, and note that driving less aggressively (e.g., with fewer acceleration phases) can yield substantial energy consumption savings.

The scientific aim of this paper is to introduce, model and solve a practical transportation problem in which EFVs must be optimally routed with strong guarantees that they never get stranded along their routes regardless of the realization of energy consumption uncertainties. We refer to this problem as the electric vehicle routing problem with energy consumption uncertainty (EVRP-ECU) and solve it by means of a robust optimization framework. With this goal in mind, Section 4.2 provides a short review of the literature related to goods distribution with electric vehicles and robust vehicle routing problems. Section 4.3 describes the EVRP-ECU and presents its mathematical formulation. Section 4.4 details two robust optimization approaches that can be used to solve small instances of the problem to optimality. Section 4.5 presents a two-phase heuristic method for larger instances in which candidate routes are generated via a first phase based on large neighbourhood search (LNS) and are then assembled via a set partitioning (SP) formulation in the second phase. Section 4.6 provides the results of extensive computational experiments. Finally, conclusions are drawn in Section 4.7.

4.2. Related literature

Several new routing problems associated with the use of EFVs have been studied since 2010 in order to ease their integration into distribution operations (e.g., Conrad and Figliozzi, 2011; Preis et al., 2014; Schneider et al., 2014; Felipe et al., 2014; Goeke and Schneider, 2015; Montoya et al., 2017; Schiffer and Walther, 2017; Hiermann et al., 2016, 2019). The generic objective in these problems is to use a

fleet of EFVs to deliver goods to a set of customers at minimal cost. A recurring feature of the proposed models is that the vehicles can stop at charging stations along their delivery routes to recharge their batteries if needed, thus distinguishing these problems from conventional vehicle routing problems (VRPs) for which the planning of intraroute refueling stops is rarely required. Indeed, many fuel stations are available for conventional vehicles and refueling times are negligible regardless of the fuel station, whereas for EFVs the recharging infrastructure is scarce and recharging times are longer and can vary significantly depending on the type of recharging station. Although en route recharging is rarely needed in urban delivery routes, such studies remain relevant since they could facilitate the use of EFVs outside urban environments (e.g., for mid- and long-haul goods distribution).

In addition, because of the limited battery capacity and the resulting shorter achievable range of EFVs, such routing problems require solution methods that can accurately monitor the vehicles' energy consumption in order to ensure they never get stranded. Some studies assume that the battery discharges itself at a linear rate with respect to distance (e.g., Felipe et al., 2014; Schneider et al., 2014; Hiermann et al., 2016). Others have considered a more detailed energy consumption model based on the comprehensive emissions model of Barth et al. (2005) which computes the required energy to traverse any given arc based on certain vehicle and arc characteristics (e.g., speed, acceleration, mass, elevation, frontal area, rolling friction, air drag). This energy consumption model was first applied in a VRP setting for the pollution-routing problem to estimate fuel consumption and emissions (Bektaş and Laporte, 2011), and subsequently in many EVRP studies to track the state of charge of the vehicles' batteries (e.g., Preis et al., 2014; Goeke and Schneider, 2015; Lebeau et al., 2015).

Many existing studies have also considered stochastic variants of the VRP in which the objective is to minimize the total expected cost. The problem inputs

that are assumed to be uncertain in such problems are usually customer demands, travel and service times, or customer presence, and these uncertainties are generally handled via a priori optimization or through the reoptimization modeling paradigm (Gendreau et al., 2016). The issue of uncertain energy consumption has not yet been studied in VRP settings due to the ease with which intraroute refueling stops for conventional vehicles can be incorporated in a solution.

Robust optimization is a methodology that has increased in popularity in the last two decades, as witnessed by the growing number of publications on this topic. The main benefit of robust optimization lies in its ability to incorporate uncertainty into a problem in a relatively tractable way. This is typically achieved by defining uncertainty sets containing realizations of the uncertain parameters. Moreover, strong probabilistic guarantees can often be attained with very limited information regarding the underlying distribution of the uncertain parameters, while still achieving less conservative solutions than by working with worst-case values (Ben-Tal et al., 2009).

To the best of our knowledge, only Fontana (2013) has considered the uncertainty surrounding the energy consumption of electric vehicles and has modeled the problem within a robust optimization framework. However, this author considers the idea of uncertainty surrounding the energy consumption of electric vehicles in an optimal path problem setting, while we extend it to a VRP setting in which the vehicle loads influence energy consumption. Schiffer and Walther (2018) have also used a robust optimization framework in an EVRP context, but their work considers the problem of simultaneously routing EFVs and locating charging stations to be used en route in the presence of uncertain customer locations, demand, and service time windows. Examples of other studies on robust VRPs include the work of Sungur et al. (2008), Gounaris et al. (2013) and Gounaris et al. (2016) on the capacitated VRP with demand uncertainty; the work of Agra et al. (2012) and Braaten et al. (2017) on the VRP with time windows and travel

time uncertainty; the work of Hu et al. (2018) on the VRP with time windows and both demand and travel time uncertainties; and the work of Lee et al. (2012) on the VRP with deadlines, as well as demand and travel time uncertainties.

In summary, the main contributions of this study are to model and solve a practical problem resulting from the fact that EFVs must be able to perform their full delivery routes in urban areas with their departing battery charge, despite uncertainties surrounding their energy consumption. We believe that this paper constitutes a valuable complement to the existing EVRP studies on the design of routes that incorporate en route recharging. We note that such studies relate to the use of EFVs for mid- and long-haul goods distribution, while our objective is to support the use of EFVs for urban operations specifically. This paper is indeed the first to consider the important issue of uncertain energy consumption in an EVRP setting without en route recharging. We use a robust optimization approach to take into account such energy consumption uncertainties (both exact and heuristic solution methods are proposed), and we conduct extensive numerical tests to demonstrate the quality of our methodology. We therefore believe that this study successfully deals with a key challenge arising from the use of EFVs as a more sustainable means of goods distribution, which should be of interest to both transportation scientists and fleet managers.

4.3. The electric vehicle routing problem with energy consumption uncertainty

The objective of this section is to formally introduce the EVRP-ECU. The section is organized as follows. We first provide a general description of the EVRP-ECU in Section 4.3.1. In Section 4.3.2 we elaborate on how the expected values for the arcs' uncertain energy consumption parameters can be approximated. Sec-

tion 4.3.3 provides comments on the incorporation of the uncertainty surrounding those energy consumption parameters. The mathematical formulation of the EVRP-ECU is then given in Section 4.3.4, and finally we present in Section 4.3.5 the uncertainty sets that we use in our computational experiments.

4.3.1 Problem description

The EVRP-ECU is defined on a complete directed graph $G = (N, A)$. The node set N is partitioned into $\{N_0, \{0\}\}$, where N_0 is the set of n customers, and node 0 is the depot. The set of arcs is denoted by A. We denote by K the set of homogeneous EFVs that must be used to visit the customers. Each vehicle has a load capacity L (kg) and a battery capacity Q (kWh). Each node i has a demand q_i (kg), with $q_i > 0$ for $i \in N_0$ and $q_0 = 0$.

Each arc (i, j) is assigned a length d_{ij} (m), an expected empty-vehicle energy consumption a_{ij} (kWh), and an expected load-dependent energy consumption b_{ij} (kWh/kg). We assume that the realized empty-vehicle and load-dependent energy consumption values along the arcs will deviate from the expected ones due to the uncertainty surrounding several parameters in the underlying energy consumption model used to estimate a_{ij} and b_{ij}. This will be explained in more detail in Section 4.3.3. A fixed cost of c_F is incurred for dispatching a vehicle, representing the daily salary of a driver. Parameters c_E and c_M represent energy (\$/kWh) and maintenance (\$/m) costs, respectively.

The following decision variables are required for the formulation of the EVRP-ECU. Binary variables x_{ijk} take value 1 if and only if vehicle k travels on arc (i, j). Variables f_{ijk} refer to the load (kg) carried on arc (i, j) by vehicle k. Variables w_k refer to the worst-case energy consumption (kWh) that could occur for vehicle k out of all energy consumption realizations in the uncertainty set U_k (which will

be formally defined in Section 4.3.3). We assume that the uncertainty sets U_k are calibrated so as to ensure a probability of at most β that the realized energy consumption of vehicle k will be larger than w_k (with β chosen by the decision maker). For example, if parameter β is set to 0.01 and variable w_k is assigned a value of 40 kWh in an optimal solution to the EVRP-ECU for some vehicle k, then the probability that the delivery route of vehicle k will consume more than 40 kWh will be at most 1%. The objective of the EVRP-ECU is to determine a set of routes that minimizes the sum of fixed, maintenance and worst-case energy costs. Furthermore, each customer demand is satisfied by exactly one vehicle, routes start and end at the depot, and total route loads are at most L. Finally, the worst-case energy consumption w_k of each vehicle is at most Q (i.e., the probability that vehicle k can complete its route without getting stranded is at least $1 - \beta$).

4.3.2 Estimating the expected values of the arcs' uncertain energy consumption parameters

The expected values a_{ij} and b_{ij} for the arcs' energy consumption parameters can be approximated using a two-phase approach similar to those discussed by Goeke and Schneider (2015) and Basso et al. (2019). Acknowledging that an arc (i, j) in a VRP graph typically represents a precomputed shortest path between nodes i and j on a more detailed road graph, the idea is to first compute such shortest paths in the road graph, and then determine values representing the expected empty-vehicle and load-dependent energy consumption of a vehicle traveling that path. First assume that each vehicle in K has a curb mass w (kg), a frontal area A (m^2), an air drag coefficient C_d, and an auxiliary power demand P (W). Let $R = (N_R, A_R)$ be a directed graph representing the underlying road graph in which the shortest paths representing the arcs in G are computed. The nodes in set N_R can be assumed to be road intersections, and the arcs in set A_R can be

assumed to be road segments. Then if a road segment $(l,m) \in A_R$ (i.e., a road section between intersections $l \in N_R$ and $m \in N_R$) is traveled at constant speed v_{lm} (m/s) by a vehicle in K, then the amount of mechanical energy e_{lm} (kWh) required for that vehicle to travel that road segment with a load f is computed with the longitudinal dynamics model from Asamer et al. (2016), which estimates energy consumption in a similar way to the comprehensive emissions model of Barth et al. (2005):

$$e_{lm} = \frac{1}{3.6 \cdot 10^6}\Big((w+f)(g d_{lm} \sin\theta_{lm} + g C_r d_{lm} \cos\theta_{lm}) + 0.5 A C_d \rho v_{lm}^2 d_{lm}\Big), \tag{4.1}$$

where g is the gravitational constant, ρ is the air density (kg/m^3), C_r is the rolling friction coefficient, and d_{lm} and θ_{lm} are the length (m) and road angle (rad) of the road segment (l,m). With a travel time of $t_{lm} = d_{lm}/v_{lm}$ associated with road segment (l,m) and assuming the vehicles have a total drivetrain efficiency of ϕ, the amount of energy B_{lm} (kWh) required from the battery on road segment (l,m) is then

$$B_{lm} = \begin{cases} \phi \cdot e_{lm} + \frac{1}{3.6 \cdot 10^6} \cdot P \cdot t_{lm}, & \text{if } e_{lm} \geq 0 \\ \frac{1}{3.6 \cdot 10^6} \cdot P \cdot t_{lm} & \text{if } e_{lm} < 0. \end{cases} \tag{4.2}$$

Although electric vehicles can sometimes recharge their battery when braking and driving downhill by using the electric motor as a generator, for sake of simplicity we do not consider energy recuperation in this study. This also makes the EVRP-ECU solution even more protected against energy consumption uncertainties (i.e., if the vehicle ends up occasionally recuperating some energy while performing its route, the solution becomes even more robust).

Note that acceleration can also be incorporated into the estimation of e_{lm} if necessary. We first show how this can be done for the simple case of constant acceleration throughout an entire road segment, and we then illustrate how this simple case can be used to establish more involved structures of e_{lm}. If road segment (l,m) is traveled by starting at time $t = 0$ at an initial speed of v_I and

accelerating or decelerating at a constant acceleration a during the entire road segment, then a speed of

$$v_{lm} = \sqrt{v_I^2 + 2ad_{lm}} \tag{4.3}$$

will be reached at the end of the road segment at time

$$t_{lm} = \frac{2d_{lm}}{v_I + v_{lm}}. \tag{4.4}$$

In this case, the amount of mechanical energy e_{lm} (kWh) required for vehicle $k \in K$ to travel that road segment with a load of f becomes

$$e_{lm} = \frac{1}{3.6 \cdot 10^6}\left((w+f)(\alpha a d_{lm} + g d_{lm} \sin\theta_{lm} + g C_r d_{lm} \cos\theta_{lm}) + \int_0^{t_{lm}} 0.5 A C_d \rho (v_I + at)^3 dt\right), \tag{4.5}$$

where α is a mass factor greater than one to account for the rotational inertia of the vehicle's moving parts (Asamer et al., 2016). The integral in the last term can be developed to yield

$$e_{lm} = \frac{1}{3.6 \cdot 10^6}\left((w+f)(\alpha a d_{lm} + g d_{lm} \sin\theta_{lm} + g C_r d_{lm} \cos\theta_{lm}) + 0.5 A C_d \rho d_{lm} (v_I^2 + \frac{v_{lm}^2 - v_I^2}{2})\right). \tag{4.6}$$

Equations (4.4)–(4.6) can then be used in (4.2) to compute B_{lm}. Finally, if road segment (l, m) is traveled by starting at an initial speed v_I at time $t = 0$, accelerating at a constant rate a^+ until reaching a speed of v_{lm}, traveling at a constant speed v_{lm} for a certain period of time and then decelerating at a constant rate a^- to reach a speed v_F at time $t = t_{lm}$, then the distance and time traveled in each phase (i.e., acceleration, constant speed, and deceleration) can be computed through Equations (4.3) and (4.4), respectively. Equations (4.1) and (4.6) can then be used to determine the required mechanical energy during each phase. Each of these values can subsequently be used in (4.2) to compute the amount of energy required by the battery during each phase.

Regardless of the case, the final equation for B_{lm} will always be linear in f. We derive a_{lm} and b_{lm} so that $B_{lm} = a_{lm} + b_{lm} \cdot f$. Thus, once a shortest path S_{ij}

has been found for each arc $(i,j) \in A$, we can aggregate the road segment energy consumption parameters of each path to determine the net expected values for the empty-vehicle and load-dependent energy consumption of the fleet vehicles when traveling arc (i,j):

$$a_{ij} = \sum_{(l,m)\in S_{ij}} a_{lm} \quad \forall (i,j) \in A \tag{4.7}$$

$$b_{ij} = \sum_{(l,m)\in S_{ij}} b_{lm} \quad \forall (i,j) \in A. \tag{4.8}$$

4.3.3 Incorporating uncertainty

An issue associated with the values a_{ij} and b_{ij} describing the expected energy consumption on arc (i,j) is of course that several uncertain parameters are needed to estimate them. As discussed by Asamer et al. (2016) and Yi and Bauer (2017), many parameters in the energy consumption model used in the previous section may vary according to some operating conditions, or are difficult to measure precisely. For example, the rolling friction coefficient C_r is difficult to measure and depends on the road surface, the tires, the travel speed, and even the temperature. The air drag coefficient C_d may vary depending on vehicle shape, opened windows, wind speed, and the vehicle's angle of attack. The air density ρ depends on factors such as temperature, atmospheric pressure, and humidity. The drivetrain efficiency ϕ can vary with speed and power. The auxiliary power P depends on driver behaviour and environmental conditions (air conditioning, heating, light, radio). Moreover, driver behaviour and external factors such as traffic conditions may influence the vehicle's travel speed and acceleration cycle. Therefore, even if we compute a_{ij} and b_{ij} with expected values for all these uncertain parameters, it is likely that the realized empty-vehicle and load-dependent energy consumption along some arcs will deviate from a_{ij} and b_{ij} for each vehicle.

To deal with these uncertainties, we derive a robust optimization model by integrating uncertainty on how much the realized energy consumption of a given vehicle k on each arc in A will deviate from its expected value through uncertainty set U_k. Hence we assume that the maximum deviations $\hat{a}_{ij} \geq 0$ and $\hat{b}_{ij} \geq 0$ from a_{ij} and b_{ij}, respectively, are known. For example, the methodology described in Section 4.3.2 could be applied with worst-case values for the uncertain parameters mentioned in the previous paragraph to estimate $\hat{a}_{ij}$ and $\hat{b}_{ij}$. Asamer et al. (2016) report worst-case values for some of the uncertain parameters in the energy consumption model (e.g., C_r, C_d, ρ, ϕ, P), based on the literature and on measurements from an electric vehicle. Uncertainty ranges for speed and acceleration can then be estimated on the basis of the road graph and of the driver's behaviour, which can further be used with worst-case values of C_r, C_d, ρ, ϕ, and P to determine $\hat{a}_{ij}$ and $\hat{b}_{ij}$. Of course, historical data can also be used to determine $\hat{a}_{ij}$ and $\hat{b}_{ij}$ when available.

Let $Z_k \in \mathbb{R}^{|A|}$ be a random vector with known support $[-1, 1]$ representing the deviation of vehicle k's empty-vehicle and load-dependent energy consumption along each arc from their expected values. Once we pick a solution to the EVRP-ECU (i.e., in terms of the variables x_{ijk}, f_{ijk} and w_k), we assume an adversary can select any $\zeta_k \in U_k$ to make vehicle k's route energy-infeasible, where ζ_k is a realization of Z_k. A given element $\zeta_k \in U_k$ thus provides a ζ_{ijk} value that sets the realized empty-vehicle and load-dependent energy consumption parameters for vehicle k along arc (i, j) as $a_{ij} + \hat{a}_{ij} \cdot \zeta_{ijk}$ and $b_{ij} + \hat{b}_{ij} \cdot \zeta_{ijk}$, respectively. The idea is to choose and calibrate sets U_k so as to achieve the desired protection level β by covering enough realizations of the random vectors Z_k. We will use sets U_k to approximate the following chance constraint for each vehicle in the mathematical formulation of Section 4.3.4:

$$P\left(\sum_{(i,j)\in A}\left(a_{ij} \cdot x_{ijk} + b_{ij} \cdot f_{ijk} + (\hat{a}_{ij} \cdot x_{ijk} + \hat{b}_{ij} \cdot f_{ijk}) \cdot Z_{ijk}\right) \leq w_k\right) \geq 1 - \beta. \quad (4.9)$$

We assume that the expected values a_{ij} and b_{ij} as well as the maximum deviations $\hat{a}_{ij}$ and $\hat{b}_{ij}$ are the same for each vehicle for a given arc (i,j), and hence we do not index them by vehicle.

4.3.4 Mathematical formulation

The EVRP-ECU is formulated as the following robust mixed integer optimization model:

$$\text{minimize} \quad \sum_{k\in K}\sum_{j\in N_0} c_F \cdot x_{0jk} + \sum_{k\in K}\sum_{(i,j)\in A} c_M \cdot d_{ij} \cdot x_{ijk} + \sum_{k\in K} c_E \cdot w_k \tag{4.10}$$

subject to

$$\sum_{j\in N_0} x_{0jk} \leq 1 \quad k \in K \tag{4.11}$$

$$\sum_{k\in K}\sum_{j\in N\setminus\{i\}} x_{ijk} = 1 \quad i \in N_0 \tag{4.12}$$

$$\sum_{j\in N\setminus\{i\}} x_{jik} = \sum_{j\in N\setminus\{i\}} x_{ijk} \quad i \in N, k \in K \tag{4.13}$$

$$q_j \cdot x_{ijk} \leq f_{ijk} \leq (L - q_i) \cdot x_{ijk} \quad (i,j) \in A, k \in K \tag{4.14}$$

$$\sum_{k\in K}\sum_{j\in N\setminus\{i\}} f_{jik} - \sum_{k\in K}\sum_{j\in N\setminus\{i\}} f_{ijk} = q_i \quad i \in N_0 \tag{4.15}$$

$$\sum_{(i,j)\in A} \left((a_{ij} + \hat{a}_{ij} \cdot \zeta_{ijk}) \cdot x_{ijk} + (b_{ij} + \hat{b}_{ij} \cdot \zeta_{ijk}) \cdot f_{ijk}\right) \leq w_k \quad k \in K, \zeta_k \in U_k \tag{4.16}$$

$$0 \leq w_k \leq Q \quad k \in K \tag{4.17}$$

$$x_{ijk} \in \{0,1\} \quad (i,j) \in A, k \in K. \tag{4.18}$$

The objective function (4.10) minimizes total fixed, maintenance and worst-case energy costs. Constraints (4.11) ensure that each vehicle is dispatched at

most once. Constraints (4.12) force each customer node to be visited exactly once. Constraints (4.13) are flow conservation equations. Constraints (4.14) ensure that the load capacity is respected, that a load can only be carried along an arc if a vehicle travels that arc, and bound that load appropriately for each arc. Constraints (4.15) state that the incoming load minus the outgoing load for each customer node must be equal to its demand. These constraints also serve as subtour elimination constraints. Constraints (4.16) are used to determine the worst-case total energy consumption w_k that could occur for vehicle k out of all possible scenarios in the uncertainty set U_k, which is assumed to have been calibrated to approximate the chance constraint (4.9). Constraints (4.17) ensure that the worst-case energy consumption of each vehicle is at most the battery capacity Q. Finally, constraints (4.18) define the domain of the x_{ijk} variables.

Note that once the problem is solved, even if the optimal values for the w_k variables are much smaller than Q, the information they provide can still be useful from both a depot scheduling and a battery degradation perspective. Indeed, frequently charging a battery to a high level (and keeping it at this level for a lenghty period) can shorten its expected lifespan (see, e.g., Lunz et al., 2012). Hence companies using EFVs should ideally try to charge the minimum required for their operations, and do this as closely as possible to the vehicles' departure times (Pelletier et al., 2017). This is especially true considering that having to replace the battery of EFVs over the course of their lifetime has been shown to significantly impact their business case (Davis and Figliozzi, 2013; Feng and Figliozzi, 2013; Lee et al., 2013). The EVRP-ECU can thus provide valuable information regarding the smallest "safe" amount of energy to recharge in each vehicle. Moreover, when charging is only performed at the depot, full charges may not be possible nor optimal because of time-dependent energy costs, demand charges, battery degradation, depot charging infrastructures or multi-shift operational contexts (Pelletier et al., 2018). The information given by the solu-

tion to the EVRP-ECU can thus also help plan the depot charging activities by knowing the smallest departing battery level w_k required for each vehicle.

4.3.5 Uncertainty sets

As mentioned in Section 4.3.3, the uncertainty sets U_k used in constraints (4.16) are assumed to be designed so as to ensure a probability at most equal to β that the real energy consumption of vehicle k be larger than w_k, i.e., we want to approximate chance constraint (4.9) for each vehicle through constraints (4.16). It is ultimately up to the decision maker to choose and calibrate the uncertainty sets based on what is known about the random vectors Z_k so as to reach the desired trade-off between cost and risk. In what follows we present five uncertainty sets to illustrate how different alternatives can be considered depending on the desired protection level and on the assumptions made about the distribution of the uncertain parameters. For example, in order to have a zero probability that the real energy consumption of vehicle k will be larger than w_k, one could use the entire support of random vector Z_k through the following box uncertainty set (Ben-Tal et al., 2009):

$$U_k^1 = \{\zeta_k \in \mathbb{R}^{|A|} \mid -1 \leq \zeta_{ijk} \leq 1 \; \forall (i,j) \in A\}, \tag{4.19}$$

which is equivalent to solving the problem with the worst-case energy parameter values $(a_{ij} + \hat{a}_{ij})$ and $(b_{ij} + \hat{b}_{ij})$ for each arc. However, one does not expect the worst-case value to occur on every arc simultaneously, and cost savings may be achievable by being less conservative but still ensuring that the real energy consumption of vehicle k is almost never larger than w_k. Budgeted uncertainty sets calibrated through parameter Γ could therefore be used (Ben-Tal et al., 2009):

$$U_k^2 = \{\zeta_k \in \mathbb{R}^{|A|} \mid -1 \leq \zeta_{ijk} \leq 1 \; \forall (i,j) \in A, \sum_{(i,j)\in A} |\zeta_{ijk}| \leq \Gamma\}, \tag{4.20}$$

thereby only allowing up to Γ arcs to deviate from their expected energy consumption values on each route in order to render that route energy-infeasible. There also exist studies (e.g., Poss, 2013) that show how allowing the size of the uncertainty set to depend on the number of non-zero decisions in combinatorial problems can often yield less conservative solutions while providing the same probabilistic guarantees. Hence one may consider route-dependent budgeted uncertainty sets calibrated with parameters θ_0 and θ:

$$U_k^3 = \{\zeta_k \in \mathbb{R}^{|A|} \mid -1 \leq \zeta_{ijk} \leq 1 \; \forall (i,j) \in A, \sum_{(i,j)\in A} |\zeta_{ijk}| \leq \theta_0 + \theta \sum_{(i,j)\in A} x_{ijk}\} \quad \forall k \in K, \tag{4.21}$$

where the budget of uncertainty that can affect vehicle k now depends on the length of the route. Hu et al. (2018) have proposed similar route-dependent uncertainty sets. Another option to prevent all parameters from taking their worst-case value simultaneously may be to use the known support of Z_k intersected with a ball of radius γ centered at the origin (Ben-Tal et al., 2009):

$$U_k^4 = \{\zeta_k \in \mathbb{R}^{|A|} \mid -1 \leq \zeta_{ijk} \leq 1 \; \forall (i,j) \in A, ||\zeta_k||_2 \leq \gamma\}. \tag{4.22}$$

If all that is known about Z_k is that it is symmetrically distributed on the interval $[-1, 1]$ and that its components are independent, then any of the sets U_k^2, U_k^3 or U_k^4 can be calibrated to approximate (4.9) (see, e.g., Ben-Tal et al., 2009; Poss, 2013). There also exist some uncertainty sets that can be used to account for the correlation between the components of Z_k, which may be relevant for the EVRP-ECU considering that driver behaviour and external conditions like the weather and road conditions should not differ too much along a given route. For example, ellipsoidal uncertainty sets defined by the following can be useful if all that is known about Z_k is that it is distributed with a mean of zero and a covariance matrix $\sum \in \mathbb{R}^{|A|\times|A|}$:

$$U_k^5 = \{\zeta_k \in \mathbb{R}^{|A|} \mid \sqrt{\zeta_k^T \sum^{-1} \zeta_k} \leq r\}, \tag{4.23}$$

where the parameter r determines the cardinality of the set and can hence be chosen according to the desired level of protection and any additional assumptions on the distribution of Z_k, e.g., normal or arbitrary (El Ghaoui et al., 2003). A few other uncertainty sets that can be used to deal with the correlation among the components of Z_k can be found in Bandi and Bertsimas (2012), Yuan et al. (2016), Jalilvand-Nejad et al. (2016) and Gounaris et al. (2013, 2016). Some ideas on how to construct uncertainty sets in the presence of historical data are also discussed in Bertsimas et al. (2018). In Section 4.6, we conduct numerical tests with each of the above uncertainty sets except U_k^2, since it can be viewed as a special case of U_k^3 with $\theta = 0$.

4.4. Exact methods

Non-discrete uncertainty sets such as those presented in Section 4.3.5 amount to having an infinite number of constraints (4.16) in the robust optimization model, thus rendering the model intractable for commercial solvers, even for small instances. We have therefore implemented robust optimization techniques in order to solve small instances of the problem to optimality. These include 1) reformulating the model of Section 4.3.4 so as to obtain a tractable deterministic mixed integer linear program in the case of polyhedral uncertainty sets, and 2) using a cutting-plane method. In what follows we briefly present these methods. Their results will be used to evaluate the performance of the metaheuristic presented in Section 4.5.

4.4.1 Reformulation

If the uncertainty set is polyhedral, then the model of Section 4.3.4 can be reformulated to yield a tractable deterministic mixed integer linear program. We illustrate this with the budgeted uncertainty sets U_k^2 and U_k^3. First, because we assume that $\hat{a}_{ij}, \hat{b}_{ij} \geq 0 \ \ \forall (i,j) \in A$, it is never beneficial for the adversary to set $\zeta_{ijk} < 0$ for an arc. Hence we can reformulate sets U_k^2 and U_k^3 by setting $0 \leq \zeta_{ijk} \leq 1$ instead of $-1 \leq \zeta_{ijk} \leq 1$, and by dropping the absolute value in the sums.

In the case of the route-independent budgeted sets U_k^2, for a given solution of the EVRP-ECU (i.e., for fixed variables) we can check whether constraints (4.16) are satisfied for vehicle k by verifying whether the optimal solution value of the following linear program is at most $w_k - \sum_{(i,j)\in A} \left(a_{ij} \cdot x_{ijk} + b_{ij} \cdot f_{ijk}\right)$:

$$\text{maximize} \quad \sum_{(i,j)\in A} \left(\hat{a}_{ij} \cdot x_{ijk} + \hat{b}_{ij} \cdot f_{ijk}\right) \cdot \zeta_{ijk} \tag{4.24}$$

subject to

$$\sum_{(i,j)\in A} \zeta_{ijk} \leq \Gamma \tag{4.25}$$

$$0 \leq \zeta_{ijk} \leq 1 \quad (i,j) \in A. \tag{4.26}$$

The dual of the above linear program can be written with variables λ_k and σ_{ijk} as

$$\text{minimize} \quad \Gamma \cdot \lambda_k + \sum_{(i,j)\in A} \sigma_{ijk} \tag{4.27}$$

subject to

$$\lambda_k + \sigma_{ijk} \geq \hat{a}_{ij} \cdot x_{ijk} + \hat{b}_{ij} \cdot f_{ijk} \quad (i,j) \in A \tag{4.28}$$

$$\lambda_k \geq 0 \tag{4.29}$$

$$\sigma_{ijk} \geq 0 \quad (i,j) \in A. \tag{4.30}$$

Hence we obtain a tractable deterministic mixed integer linear programming

formulation of the EVRP-ECU by replacing constraints (4.16) in the model of Section 4.3.4 with

$$\sum_{(i,j)\in A} \left(a_{ij} \cdot x_{ijk} + b_{ij} \cdot f_{ijk} + \sigma_{ijk}\right) + \Gamma \cdot \lambda_k \leq w_k \quad k \in K, \tag{4.31}$$

and by adding constraints (4.28)–(4.30) for each vehicle $k \in K$, since duality theory ensures that $\Gamma \cdot \lambda_k + \sum_{(i,j)\in A} \sigma_{ijk} \geq \max_{\zeta_k \in U_k} \left\{ \sum_{(i,j)\in A} \left(\hat{a}_{ij} \cdot x_{ijk} + \hat{b}_{ij} \cdot f_{ijk}\right) \cdot \zeta_{ijk} \right\}$ for vehicle k as long as constraints (4.28)–(4.30) are satisfied. Note that λ_k and σ_{ijk} are variables in the reformulation.

In the case of the route-dependent budgeted uncertainty sets U_k^3, we would instead need to solve the following to check if constraints (4.16) are satisfied for k in a given solution:

$$\text{maximize} \quad \sum_{(i,j)\in A} \left(\hat{a}_{ij} \cdot x_{ijk} + \hat{b}_{ij} \cdot f_{ijk}\right) \cdot \zeta_{ijk} \tag{4.32}$$

subject to

$$\sum_{(i,j)\in A} \zeta_{ijk} \leq \theta_0 + \theta \sum_{(i,j)\in A} x_{ijk} \tag{4.33}$$

$$0 \leq \zeta_{ijk} \leq 1 \quad (i,j) \in A. \tag{4.34}$$

The dual of the above linear program can once again be written with variables λ_k and σ_{ijk}:

$$\text{minimize} \quad \theta_0 \cdot \lambda_k + \sum_{(i,j)\in A} \left(\theta \cdot x_{ijk} \cdot \lambda_k + \sigma_{ijk}\right)$$

subject to (4.28)–(4.30).

Constraints (4.16) are therefore equivalent to

$$\sum_{(i,j)\in A}\Big((a_{ij}+\theta\cdot\lambda_k)\cdot x_{ijk}+b_{ij}\cdot f_{ijk}+\sigma_{ijk}\Big)+\theta_0\cdot\lambda_k\leq w_k\quad k\in K \tag{4.35}$$

$$\lambda_k+\sigma_{ijk}\geq\hat{a}_{ij}\cdot x_{ijk}+\hat{b}_{ij}\cdot f_{ijk}\quad k\in K,(i,j)\in A \tag{4.36}$$

$$\lambda_k\geq 0\quad k\in K \tag{4.37}$$

$$\sigma_{ijk}\geq 0\quad k\in K,(i,j)\in A. \tag{4.38}$$

Since the x_{ijk} variables are binary, as in Poss (2013) we linearize constraints (4.35) by introducing real variables u_{ijk} to represent the product of variables x_{ijk} and λ_k. Constraints (4.35) can thus be replaced with

$$\sum_{(i,j)\in A}\Big(a_{ij}\cdot x_{ijk}+\theta\cdot u_{ijk}+b_{ij}\cdot f_{ijk}+\sigma_{ijk}\Big)+\theta_0\cdot\lambda_k\leq w_k\quad k\in K \tag{4.39}$$

$$u_{ijk}\geq\lambda_k-M(1-x_{ijk})\quad k\in K,(i,j)\in A \tag{4.40}$$

$$u_{ijk}\geq 0\quad k\in K,(i,j)\in A, \tag{4.41}$$

where M is a large constant. We can therefore obtain a tractable deterministic mixed integer linear programming formulation of the EVRP-ECU with route-dependent budgeted uncertainty sets as well. The robust problem can also be reformulated through duality theory as a deterministic problem in the presence of non-polyhedral uncertainty sets like those defined by U_k^4 and U_k^5, but in this case the reformulation gives rise to a second-order cone problem. We therefore present a cutting plane method for these cases in the next section.

4.4.2 Cutting-plane method

An alternative to reformulating the robust optimization model is to initiate a branch-and-cut procedure on the nominal version of the problem (i.e., without uncertainty), and whenever an integer feasible solution is found, to verify the

worst-case energy consumption of each route and add cuts accordingly (Bertsimas et al., 2016). To this end, we need to solve the following problem for each route k in the current integer feasible solution of the search tree:

$$\text{maximize} \sum_{(i,j)\in A} \left(a_{ij} \cdot x_{ijk} + b_{ij} \cdot f_{ijk} + \left(\hat{a}_{ij} \cdot x_{ijk} + \hat{b}_{ij} \cdot f_{ijk} \right) \cdot \zeta_{ijk} \right) \quad (4.42)$$

subject to

$$\zeta_k \in U_k, \quad (4.43)$$

where U_k is the considered uncertainty set. Let H_k be the value of the optimal solution of (4.42)–(4.43) for the route of vehicle k, achieved with scenario $\overline{\zeta}_k \in U_k$. If 1) the uncertainty sets used are not route-dependent, 2) H_k is larger than the value of variable w_k in the current solution, and 3) the uncertainty sets are the same for all vehicles, then we add the following cuts:

$$\sum_{(i,j)\in A} \left((a_{ij} + \hat{a}_{ij} \cdot \overline{\zeta}_{ijk}) \cdot x_{ijl} + (b_{ij} + \hat{b}_{ij} \cdot \overline{\zeta}_{ijk}) \cdot f_{ijl} \right) \leq w_l \quad l \in K, \quad (4.44)$$

since the realization $\overline{\zeta}_k$ is valid for any other route that could be assigned to any vehicle. Constraints (4.44) force a sufficient worst-case energy consumption of H_k whenever a vehicle performs the route that vehicle k was performing in the current solution, thereby simultaneously forbidding the route whenever $H_k > Q$, due to constraints (4.17). If the branch-and-cut procedure eventually finds an optimal solution in which all routes are robust, only a subset of constraints (4.16) would have been added. The solution is therefore also optimal for the entire problem.

However, if the uncertainty set is route-dependent, we cannot add constraints (4.44) since realization $\overline{\zeta}_k$ it is not necessarily valid for other route lengths. Alternatively, we can add cuts similar to those proposed by Laporte and Louveaux (1993) for the integer L-shaped method. Letting R_k be the set containing the arcs in the route of vehicle k and assuming once again that the uncertainty sets are the

same for each vehicle, the following cuts are added if H_k is larger than the value of variable w_k in the current solution, and the uncertainty sets are route-dependent:

$$H_k \cdot \left(\sum_{(i,j) \in R_k} x_{ijl} - \sum_{(i,j) \notin R_k} x_{ijl} \right) - H_k \cdot (|R_k| - 1) \leq w_l \quad l \in K. \tag{4.45}$$

If $H_k \leq Q$, then constraints (4.45) will ensure that the worst-case energy consumption of the vehicle performing route R_k be at least H_k. If $H_k > Q$, then constraints (4.45) will ensure that no vehicle performs route R_k due to constraints (4.17). Note that although this is not optimal, some feasible solutions encountered during the branch-and-cut procedure could have vehicles returning to the depot carrying loads. Therefore, one should update the load carried along the route so as to have no returning loads before solving (4.42)–(4.43) to obtain H_k and subsequently adding constraints (4.45). If not, constraints (4.45) could forbid a route that would otherwise be feasible by making this correction. Finally, we mention that the method discussed here for route-dependent uncertainty sets is also valid for those sets that are not, and that if the uncertainty sets are the same for each vehicle, then (4.42)–(4.43) only needs to be solved the first time a specific route is encountered in the search tree.

4.5. Two-phase metaheuristic

In order to solve large instances of the EVRP-ECU, we propose a two-phase heuristic in which a pool of candidate routes is generated in a first phase, and then combined via an SP formulation in the second phase. Similar two-phase methods have been shown to be quite successful in both deterministic and stochastic routing problem settings (see, e.g., Mendoza and Villegas, 2013; Montoya et al., 2016; Mendoza et al., 2016; Montoya et al., 2017). The first phase uses the LNS framework first proposed by Shaw (1998) to construct a pool of routes, thereby

destroying and repairing large portions of the solution at each iteration to move from one area of the search space to another. Rather than forcing solutions to remain energy-feasible during the first phase of the procedure with respect to their routes' worst-case energy consumption, we only ensure energy feasibility with respect to their routes' expected energy consumption. However, after destroying and repairing the current solution at each iteration of the LNS in the first phase of the method (and occasionally during and after an additional local search phase), we check whether the resulting solution contains any new robust routes, i.e., routes with a worst-case energy consumption that is less than the battery capacity. If so, we add them to the pool of robust routes. In the second phase, after a number of iterations of the LNS, we solve a set partitioning problem over this pool to generate a complete robust solution. This allows 1) to only have to evaluate the robustness of routes once moves have been implemented, rather then when evaluating a potential move (which could significantly increase the solution times), 2) to generate infeasible solutions during the search in terms of energy, which can act as a diversification mechanism, and 3) to easily adapt the implementation of the algorithm when solving the problem with new uncertainty sets.

In contrast to earlier LNS methods that used only one operator to remove customers and one operator to insert them, we apply several removal and insertion operators, as in the adaptive LNS (ALNS) introduced by Ropke and Pisinger (2006). ALNS is an extension of the LNS framework in which several destroy and repair operators compete against each other to modify the current solution. The probabilities of selecting the different operators are dynamically updated through an adaptive mechanism, thereby allowing operators that perform well on a given instance to be used more frequently. The LNS heuristic we have implemented in the first phase of our heuristic contains all the ingredients of an ALNS procedure besides the adaptive layer. We initially implemented our method within

the ALNS framework, but we observed that the adaptive component did not improve solution quality significantly. We therefore opted to keep the probability of selecting each operator fixed throughout the search in order to reduce the number of parameters of the algorithm.

The main steps of our solution method are as follows. We first build an initial solution with a simple constructive heuristic (Section 4.5.1). Then, at each iteration, random numbers are drawn to determine which removal and insertion operators to apply. Most of our operators are inspired by those used in Ropke and Pisinger (2006), Demir et al. (2012), and Goeke and Schneider (2015). The selected removal operator is then applied to remove a random number of customers n_r between $\underline{n}_c$ and $\overline{n}_c$, or to eliminate an entire route (Section 4.5.2). The removed customers are then placed in a removal list until they are reinserted in the solution (Section 4.5.3). A local search (LS) phase is then performed when the repaired solution seems promising (Section 4.5.4), and the resulting solution is then accepted or rejected according to the simulated annealing mechanism (Section 4.5.5). Solutions are checked for new robust routes before, after, and occasionally during the LS phase. It is therefore important to efficiently compute the worst-case energy consumption of new routes (Section 4.5.6). We also update the best found (if any) robust solution during the LNS phase when a solution only contains robust routes. Finally, a robust LS is performed on the best found nominal solution (which is not necessarily robust) throughout the procedure prior to the set partitioning phase, and on the robust solution obtained after solving the set partitioning problem (Section 4.5.7). The best candidate between the resulting solution and the best found robust solution over the course of the LNS phase is then chosen as the final solution. An outline of the method is provided in Algorithm 1.

Algorithm 1 Two-phase heuristic method

Input: parameters ω, δ, τ, r, and κ
Output: a robust solution X_{Final}

Generate an initial solution $X_{Initial}$ with the savings algorithm
Initiate temperature T according to $X_{Initial}$ and ω
Check robustness of routes in $X_{Initial}$ and add all robust routes to Ω_R
if All routes in $X_{Initial}$ are robust **then**
    $X_{BestRobust} \leftarrow X_{Initial}$
$X_{Cur} \leftarrow X_{Initial}$, $X_{BestNominal} \leftarrow X_{Initial}$
repeat
    Select a removal operator and an insertion operator and apply them on X_{Cur} to get X_{Temp}
    Check robustness of any new routes in X_{Temp} and add all new robust routes to Ω_R
    if All routes in X_{Temp} are robust and $C^R(X_{temp}) < C^R(X_{BestRobust})$ **then**
        $X_{BestRobust} \leftarrow X_{Temp}$
    if $C(X_{Temp}) \leq \delta \cdot C(X_{BestNominal})$ **then**
        if $C(X_{Temp}) \leq \tau \cdot C(X_{BestNominal})$ **then**
            Perform local search on X_{Temp} to get X_{New}, add all new robust routes encountered during the search to Ω_R, and update $X_{BestRobust}$ during the search
        else
            Perform local search on X_{Temp} to get X_{New} and add all new robust routes in X_{New} to Ω_R
            if All routes in X_{New} are robust and $C^R(X_{New}) < C^R(X_{BestRobust})$ **then**
                $X_{BestRobust} \leftarrow X_{New}$
    else
        $X_{New} \leftarrow X_{Temp}$
    if $C(X_{New}) < C(X_{BestNominal})$ **then**
        $X_{Cur} \leftarrow X_{New}$
        $X_{BestNominal} \leftarrow X_{New}$
    else
        if $C(X_{New}) < C(X_{Cur})$ or the *Random insertion* was applied **then**
            $X_{Cur} \leftarrow X_{New}$
        else
            Generate a random number $p \in [0, 1]$
            if $p \leq \exp[-(C(X_{New}) - C(X_{Cur}))/T]$ **then**
                $X_{Cur} \leftarrow X_{New}$
    $T \leftarrow r \cdot T$
until κ iterations have been performed
Perform robust local search on $X_{BestNominal}$ to get $X_{LNS/RLS}$ and add any new robust routes encountered during the search to Ω_R
if All routes in $X_{LNS/RLS}$ are robust and $C^R(X_{X_{LNS/RLS}}) < C^R(X_{BestRobust})$ **then**
    $X_{BestRobust} \leftarrow X_{X_{LNS/RLS}}$
Solve set partioning problem to find a robust solution X_{SP}
Perform robust local search on X_{SP} to get the robust solution $X_{SP/RLS}$
if $X_{BestRobust} \neq \emptyset$ and $C^R(X_{BestRobust}) < C^R(X_{SP/RLS})$ **then**
    $X_{Final} \leftarrow X_{BestRobust}$
else
    $X_{Final} \leftarrow X_{SP/RLS}$

4.5.1 Initial solution construction

In order to construct an initial solution $X_{Initial}$, we apply the Clarke and Wright savings algorithm (1964). An initial solution is constructed by creating n back-and-forth routes, followed by merging, at each iteration, a route ending at customer i with a route starting at customer j so as to maximize the distance saving $s_{ij} = d_{i0} + d_{0j} - d_{ij}$. We only merge routes when feasibility can be maintained with respect to capacity and expected energy consumption. The initial back-and-forth routes are checked for robustness and added to the pool of robust routes accordingly.

4.5.2 Removal operators

We now briefly describe the operators that we use in the LNS phase of our method. At the start of each iteration, one of the following removal operators is randomly chosen to remove a certain number of customers from the current solution X_{Cur}.

Random removal randomly selects n_r customers and removes them from the current solution.

Worst removal assigns a value to each customer indicating the difference between the solution value with the customer and without it. These are then stored in an ordered set S and the customer with the $\lfloor |S| \cdot \epsilon^{\lambda_{WR}} \rfloor^{th}$ largest value is removed from the solution (with the 0th referring to the highest value). The parameter ϵ is randomly drawn in $[0, 1)$ according to a continuous uniform distribution and the parameter λ_{WR} is used to randomize the removal. The procedure is reiterated until n_r customers have been removed. Note that when evaluating the difference between the solution value with a customer and without it, the energy costs are computed with the vehicles' expected energy consumption.

Worst energy removal is similar to *Worst removal*, but the cost assigned to a customer j is given by $(a_{ij} + b_{ij} \cdot f_{ijk}) + (a_{jl} + b_{jl} \cdot f_{jlk})$, where i and l are the nodes immediately preceding and following j in its route in the current solution. As with *Worst removal*, a parameter λ_{WE} is introduced to randomize the removal.

Worst distance removal is the same as *Worst energy removal*, but the cost assigned to a customer j is given by $d_{ij} + d_{jl}$, where i and l are the nodes directly preceding and following j in its route in the current solution. The parameter λ_{WD} is introduced to randomize the removal as with the previous two removal operators.

Shaw removal is intended to remove customers that are similar, based on predetermined criteria. First, a customer i is randomly selected and removed from the solution. The relatedness $R(i, j)$ between customer i and a customer j in our implementation is defined as

$$R(i,j) = \mu_1 \cdot \frac{d_{ij}}{\max\limits_{(l,m)\in A}(d_{lm})} + \mu_2 \cdot s_{ij} + \mu_3 \cdot \frac{|q_i - q_j|}{\max\limits_{l\in N_0}(q_l) - \min\limits_{m\in N_0}(q_m)} + \mu_4 \cdot \frac{a_{ij}}{\max\limits_{(l,m)\in A}(a_{lm})},$$

where $s_{ij} = -1$ if i and j are on the same route, and $s_{ij} = 1$ otherwise. The customers in the solution are then stored in S and the customer with the $\lfloor |S| \cdot \epsilon^{\lambda_{Shaw}} \rfloor^{th}$ smallest relatedness value is removed (with the 0th referring to the smallest value). As with the previous three operators, ϵ is randomly selected in $[0, 1)$, and λ_{Shaw} is a parameter used to introduce some randomness in the search process. The procedure is then repeated by setting i as the last removed customer until n_r customers have been removed. The parameters μ_1, μ_2, μ_3, and μ_4 are used to attribute weights to similarities regarding different (normalized) criteria. Our implementation defines the relatedness $R(i, j)$ between customers i and j based on the distance separating them (weight μ_1), on whether they are in the same route or not (weight μ_2), on the difference between their demands (weight μ_3), and on the expected energy consumption required for an empty vehicle to travel from i to j (weight μ_4).

Node neighbourhood removal first selects a customer i randomly and removes it from the solution. It then removes the $n_r - 1$ nodes closest to i.

Random route removal randomly selects a route in the solution and removes all its customers.

Distance-based route removal removes the longest route from the current solution.

Energy-based route removal removes the route with the largest expected energy consumption from the current solution.

4.5.3 Insertion operators

Once the removal phase is completed, one of the following insertion operators is randomly chosen to insert the removed customers back into the partially destroyed solution. The insertion operators only ensure energy feasibility with respect to the vehicles' expected energy consumption, and evaluate energy costs with the vehicles' expected energy consumption when comparing solution values.

Greedy insertion determines the best position where each removed customer can be inserted in the solution, and inserts the customer whose best insertion position yields the smallest increase in the solution value. This process is then reiterated until all removed customers have been inserted. A removed customer i can be inserted in any feasible position in an existing route, or a new route containing only i can be created.

Regret insertion seeks to avoid delaying the insertion of customers that could deteriorate the solution if they are not inserted with a higher priority. A *Regret-k insertion* in our implementation will determine the k best insertion positions of each removed node. Letting c_{ik} refer to the cost of the partial solution resulting

from inserting i in its kth best position, *Regret-k insertion* will insert the removed node i yielding the largest value of $\sum_{j=2}^{k}(c_{ij} - c_{i1})$. The LNS phase of our method uses *Regret-2 insertion* and *Regret-3 insertion*.

Randomized greedy insertion is similar to *Greedy insertion*, but the insertion costs associated with the best insertion position of each removed customer are stored in S, and the customer with the $\lfloor |S| \cdot \epsilon^{\lambda_{RG}} \rfloor^{th}$ smallest value is inserted into its best position. As with several of the removal operators, ϵ is randomly selected from $[0, 1)$ and the parameter λ_{RG} is used to randomize the heuristic. The procedure is repeated until all removed customers have been inserted.

Randomized regret-2 insertion is similar to *Regret-2 insertion*, but instead of always inserting the removed customer i with the largest $(c_{i2} - c_{i1})$ value, the selection is randomized as in *Randomized Greedy insertion*, using the parameter λ_{RR} to control the degree of randomization.

Energy-based insertion calculates the cost of inserting a removed customer i along a route, based on the expected energy consumption of the route prior to and after inserting i in it. The operator thus determines the best possible position where each removed node can be inserted in the partial solution based on such energy-based insertion costs, and inserts the customer whose best insertion position results in the smallest increase of the associated route's expected energy consumption.

4.5.4 Local search

If the solution X_{Temp} resulting from the destroy and repair phase has a nominal cost (i.e., with energy costs computed with the expected energy consumption of vehicles) at most equal to δ times the nominal cost of the best known nominal solution $X_{BestNominal}$, where $\delta > 1$, an LS phase is performed following a first-

improvement strategy with respect to nominal costs. We refer to solutions in which energy feasibility and energy costs are evaluated with respect to the vehicles' expected energy consumption as nominal solutions. The LS uses a composite neighbourhood of *2-Opt* (intra-route moves), *2-Opt** (inter-route moves), *Relocate* (intra- and inter-route moves), and *Exchange* (intra- and inter-route moves). Energy feasibility is only ensured with respect to the vehicles' expected energy consumption during the LS.

2-Opt removes two arcs from a route and inserts two other arcs to reconnect the remaining paths, thereby inverting the order in which the nodes between the two removed arcs are visited. We only consider *2-Opt* moves involving at most three nodes between the two removed arcs. *2-Opt** selects two routes and removes an arc from each of them. It then merges the first sequence of each route with the second sequence of the other (Potvin and Rousseau, 1995). *Exchange* swaps the positions of two nodes, and *Relocate* shifts one node from its current position to another position.

The neighbourhoods are searched in a way that is similar to that of the LS procedure of Hiermann et al. (2016). The four neighbourhoods are stored in a list that is randomly shuffled prior to each LS phase to determine in which order they will be searched. The first neighbourhood in the list is then searched until the solution cannot be further improved. Once this occurs, the following neighbourhood is explored, and so on. The search restarts with the first neighbourhood in the list once the end of the list is reached. When none of the neighbourhoods can further improve the current solution, the LS phase terminates. The ordering of the potential moves when searching a neighbourhood is also randomly shuffled each time a move is implemented.

4.5.5 Acceptance criterion

A simulated annealing mechanism is used to determine whether the solution generated at an iteration should be accepted or not. The term $C(X)$ refers to the nominal cost of a solution X, and X_{Cur} and X_{New} refer to the current and new solution at a given iteration, respectively. If $C(X_{New}) < C(X_{Cur})$, then X_{New} is always accepted. If $C(X_{New}) > C(X_{Cur})$, then the solution X_{New} is accepted with probability $\exp[-(C(X_{New}) - C(X_{Cur}))/T]$, where T is the current temperature. We initialize the temperature to a value of T_{init} and multiply it at each iteration by a cooling rate $r \in (0,1)$. With $X_{Initial}$ referring to the initial solution of the algorithm, T_{Init} is set according to parameter ω, itself determined so that a solution X of value $C(X) = \omega \cdot C(X_{Initial})$ is accepted with probability 0.5. The cooling rate r is set so that the temperature is below 0.001 for the last 20% of the iterations. In Algorithm 1, $C^R(X)$ refers to the robust cost (i.e., with energy costs computed with the worst-case energy consumption of vehicles) of solution X.

Finally, to further diversify the search, when the solution X_{New} is not a new solution for D consecutive iterations of the LNS phase, the nodes that are removed during the following iteration are subsequently inserted back into the solution with a *Random insertion* operator, and the resulting solution is always accepted. The *Random insertion* operator first shuffles the list containing the removed nodes to determine the order in which they will be inserted back into the solution. For each node in the list, a random insertion position is computed iteratively until a feasible insertion position has been found. The less costly option between inserting the node in that position or creating a new route is then implemented.

4.5.6 Checking robustness

In order to generate a sufficient number of energy-robust routes for the SP phase, we always check whether any new robust routes are in the solution X_{Temp} obtained immediately after applying a removal operator and an insertion operator on X_{Cur}. However, in order to avoid making the set partitioning problem too large and slowing down the LS, we do not always check for new robust routes during the LS when it is performed. When the LS is performed starting from solution X_{Temp}, if the nominal cost of X_{Temp} is less than a given threshold, we check the robustness of any new routes encountered during the LS phase (i.e., whenever we move from the current solution to a neighbour solution during the LS, any new routes in the chosen neighbour solution are checked for robustness and added to the pool of robust routes accordingly). The threshold is set as τ times the nominal cost of the best known nominal solution $X_{BestNominal}$, with τ being a parameter of the algorithm. If the LS is performed starting from solution X_{Temp} but the nominal cost of X_{Temp} is more than this threshold, then new routes encountered during the LS are not checked for robustness. However, we check the robustness of any new routes in the final solution returned by the LS. Moreover, whenever any solution X is checked for new robust routes during the LNS phase, we also verify whether all its routes happen to be robust. If this is the case, we update the best known robust solution $X_{BestRobust}$ found during the first phase of the heuristic according to whether $C^R(X) < C^R(X_{BestRobust})$ or not. Note that $X_{BestRobust}$ could be empty at the end of the first phase. If it is not, after the SP phase we choose the best alternative between $X_{BestRobust}$ and the solution to the SP problem (see next section) as the final solution.

Efficiently computing the worst-case energy consumption of a route in the current solution is critical to the two-phase heuristic. Checking whether the worst-case energy consumption of vehicle k is feasible (i.e., if $w_k \leq Q$) is equiv-

alent to checking whether the optimal value of (4.42)–(4.43) is at most Q. With the budgeted uncertainty sets U_k^2 and U_k^3, this can be done efficiently by sorting the values of $\left(\hat{a}_{ij} + \hat{b}_{ij} \cdot f_{ijk}\right)$ for the arcs in the route of vehicle k and setting the ζ_{ijk} variables in problem (4.42)–(4.43) accordingly. For example, with route-dependent uncertainty sets U_k^3, because $\hat{a}_{ij}, \hat{b}_{ij} \geq 0 \ \ \forall (i,j) \in A$, the optimal solution of problem (4.42)–(4.43) is

- $\zeta_{ijk} = 1$ for the $\lfloor \theta_0 + \theta \sum\limits_{(i,j) \in A} x_{ijk} \rfloor$ arcs with the largest $\left(\hat{a}_{ij} + \hat{b}_{ij} \cdot f_{ijk}\right)$ values in the route of vehicle k,
- $\zeta_{ijk} = \theta_0 + \theta \sum\limits_{(i,j) \in A} x_{ijk} - \lfloor \theta_0 + \theta \sum\limits_{(i,j) \in A} x_{ijk} \rfloor$ for the arc with the $\lfloor \theta_0 + \theta \sum\limits_{(i,j) \in A} x_{ijk} \rfloor + 1^{th}$ largest $\left(\hat{a}_{ij} + \hat{b}_{ij} \cdot f_{ijk}\right)$ value in the route of vehicle k,
- $\zeta_{ijk} = 0$ otherwise.

With the ellipsoidal uncertainty sets U_k^5, solving (4.42)–(4.43) can also be done efficiently since the Karush-Kuhn-Tucker optimality conditions yield the following closed formula for its optimal solution (Ilyina, 2017):

$$\zeta_{ijk} = \frac{r \cdot \sum\limits_{(l,m) \in A} \sigma_{(i,j),(l,m)} \cdot \left(\hat{a}_{lm} \cdot x_{lmk} + \hat{b}_{lm} \cdot f_{lmk}\right)}{\sqrt{\sum\limits_{(p,q) \in A} \left(\hat{a}_{pq} \cdot x_{pqk} + \hat{b}_{pq} \cdot f_{pqk}\right) \cdot \left(\sum\limits_{(l,m) \in A} \sigma_{(p,q),(l,m)} \cdot \left(\hat{a}_{lm} \cdot x_{lmk} + \hat{b}_{lm} \cdot f_{lmk}\right)\right)}} \quad \forall (i,j) \in A,$$

where $\sigma_{(i,j),(l,m)}$ is the covariance between arcs (i,j) and (l,m), or the variance in the case that $(i,j) = (l,m)$. The optimal value of (4.42)–(4.43) is then

$$\sum_{(i,j) \in A} \left(a_{ij} \cdot x_{ijk} + b_{ij} \cdot f_{ijk}\right) + r \cdot \sqrt{\sum_{(i,j) \in A} \left(\hat{a}_{ij} \cdot x_{ijk} + \hat{b}_{ij} \cdot f_{ijk}\right) \cdot \left(\sum_{(l,m) \in A} \sigma_{(i,j),(l,m)} \cdot \left(\hat{a}_{lm} \cdot x_{lmk} + \hat{b}_{lm} \cdot f_{lmk}\right)\right)}.$$

Note that the correlation between components of Z_k that are associated with arcs in the route of vehicle k and components of Z_k that are associated with arcs that

are not in the route of vehicle k does not influence the above optimal value of (4.42)–(4.43).

With the uncertainty sets U_k^4 formed by the intersection of the box uncertainty set with the ball of radius γ centered at the origin, problem (4.42)–(4.43) becomes a quadratically constrained program. We therefore use a commercial solver within the LNS phase itself to check the robustness of new routes when solving the problem with sets U_k^4. Since this renders the evaluation of the worst-case energy consumption of a route more difficult, the benefit of not forcing robustness throughout the LNS phase becomes self-evident.

Finally, we mention that we store the information regarding the robustness of new routes (i.e., their worst-case energy consumption) for future use so that the above computations only need to be performed the first time a route is encountered. The robustness of previously encountered routes can thus be checked quickly when updating $X_{BestRobust}$.

4.5.7 Set partitioning phase

Once the LNS phase has run for κ iterations, an SP problem is solved over the pool of routes Ω_R to find a robust solution X_{SP}. Recall that all routes in Ω_R are robust, i.e., their worst-case energy consumption is less than the battery capacity. Before solving the SP problem, a robust local search (RLS) is performed on the best known nominal solution $X_{BestNominal}$ to get solution $X_{LNS/RLS}$. The RLS is the same as the LS described in Section 4.5.4, except that only those moves leading to robust routes are performed, and the neighbourhoods are always searched in the same order. The RLS uses the same neighbourhoods as the LS (i.e., *2-Opt*, *2-Opt**, *Relocate*, and *Exchange*), but evaluates energy feasibility and costs with the worst-case energy consumption of routes rather than with the expected one. All

new routes encountered during the RLS are then added to Ω_R, and $X_{BestRobust}$ is updated according to $X_{LNS/RLS}$.

Let binary variable y_r take value 1 if and only if energy-robust route $r \in \Omega_R$ is chosen. Let c_r be the total robust cost of route r (i.e., with energy costs computed with the route's worst-case energy consumption), and p_{ir} be a binary parameter equal to 1 if and only if customer $i \in N_0$ is in route r. The SP problem is to

$$\text{minimize} \quad \sum_{r \in \Omega_r} c_r \cdot y_r \tag{4.46}$$

subject to

$$\sum_{r \in \Omega_R} p_{ir} \cdot y_r = 1 \quad i \in N_0 \tag{4.47}$$

$$\sum_{r \in \Omega_R} y_r \leq |K| \tag{4.48}$$

$$y_r \in \{0,1\} \quad r \in \Omega_R. \tag{4.49}$$

Since the maximum fleet size is ensured via constraint (4.48) in the SP formulation, we allow solutions to contain more routes than the fleet size during the LNS phase. However, we do not consider such solutions as potential incumbents to replace $X_{BestRobust}$, i.e., we assume that $C^R(X) = \infty$ if the number of routes in solution X is larger than $|K|$. Finally, the RLS is performed once again on the best found solution X_{SP} to the SP problem. The less costly alternative between the resulting solution $X_{SP/RLS}$ and the best found robust solution $X_{BestRobust}$ over the course of the LNS phase is then chosen as the final solution.

Preliminary experiments have indicated that solving the SP problem in two phases can accelerate its resolution. Therefore, we first minimize the number of vehicles by replacing the objective (4.46) with $\sum_{r \in \Omega_r} y_r$. Letting m refer to the best found number of vehicles, we then solve (4.46)–(4.49) but replace the maximum fleet size $|K|$ with $\min\{m, |K|\}$.

4.6. Computational experiments

We have performed extensive computational experiments in order to assess the quality of our heuristic, to compare nominal solutions with robust solutions, to illustrate the trade-off between cost and risk among different robust solutions, and to investigate the influence of different parameters in the energy consumption model and in the uncertainty sets on robust solutions. To this end, we have generated test instances and solved them with the algorithms presented in the previous two sections. We have also tested our heuristic on existing benchmark instances of related problems. All algorithms were implemented in C++ and all experiments were conducted on a cluster of 27 machines, each having two Intel(R) Xeon(R) X5675 3.07 GHz processors with 96 GB of RAM running on Linux. Each machine has 12 cores, and each instance was run using a single thread. All test instances using the reformulation and the cutting plane method described in Sections 4.4.1 and 4.4.2 were solved using CPLEX 12.8 with a time limit of three hours. The SP problem within the two-phase heuristic was also solved using CPLEX 12.8. We set a time limit of T_{SP1} seconds for the vehicle minimization phase of the SP problem, and of T_{SP2} for the cost minimization phase.

The remainder of this section is organized as follows. We first provide a description of the EVRP-ECU test instances and report the values used in the experiments for the parameters of our two-phase heuristic in Section 4.6.1. In Sections 4.6.2 and 4.6.3 we evaluate the performance of the heuristic on small and large EVRP-ECU instances, respectively. The quality of the two-phase method is further assessed in Section 4.6.4 by testing it on the related capacitated vehicle routing problem (CVRP) and robust capacitated vehicle routing problem (RCVRP). In Section 4.6.5, we illustrate how the robust optimization methodology can be used to achieve the right balance between cost and risk. We then investigate the impact of correlation between arcs in a given route with respect to energy consumption

uncertainties in Section 4.6.6. Finally, in Section 4.6.7 we analyze the impact of specific uncertain parameters in the energy consumption model described in Section 4.3.2 on robust solutions.

4.6.1 Test instances and parameter tuning

We have generated test instances by using the customer configurations from the EVRP with non-linear charging function instances presented in Montoya et al. (2017). These instances were designed to represent a geographic space of 120 $\times$ 120 kilometers, which is a reasonable area to cover without en route recharging, considering the average range of modern EFVs is approximately 125 kilometers (Tretvik et al., 2017). There are five instances for each of the following number n of customers: 10, 20, 40, 80, 160, and 320. The node locations are determined according to a continuous uniform distribution, a random clustered distribution, or a mixture of both. The maximum fleet size is set to $1 + n/5$. Customer demands are randomly generated between 50 and 450 kg.

The fleet vehicles are assumed to be medium-duty electric trucks equipped with 100 kWh batteries. We have used some vehicle and expected values for the energy consumption model parameters similar to those used by Goeke and Schneider (2015) and Demir et al. (2012). However, these studies do not consider auxiliary power nor dispatching costs. Asamer et al. (2016) found that an auxiliary power of approximately 450 W is most frequently consumed by a passenger electric vehicle that is roughly seven times lighter than the electric trucks we consider in terms of gross vehicle weight. To err on the side of caution, we used half of this ratio, i.e., we assume an expected auxiliary power of $P = 3.5 \cdot 450 = 1575$ W when computing the expected energy consumption parameter values a_{ij} and b_{ij}. The energy and maintenance costs are based on those used by Davis and Figliozzi (2013). To determine the fixed dispatching cost c_F, we assume the same

hourly salary of the drivers as in Goeke and Schneider (2015) and a nine-hour shift; c_F is thus set to \$118. The values of the cost, vehicle, and energy consumption model-related parameters are reported in Table 4.1.

Table 4.1 – Vehicle, cost and expected energy consumption model parameter values

Parameter	Value used
Battery capacity Q	100 kWh
Curb mass w	6,350 kg
Load capacity L	3,650 kg
Frontal area A	3.912 m^2
Expected air drag coefficient C_d	0.7
Expected rolling friction coefficient C_r	0.01
Expected auxiliary power demand P	1,575 W
Gravitational constant g	9.81 m/s^2
Expected air density ρ	1.2041 kg/m^3
Expected drivetrain efficiency ϕ	1.3175
Maintenance costs c_M	\$0.00016/m
Energy cost c_E	\$0.11/kWh
Fixed cost c_F	\$118

Since we do not have a detailed road graph associated with the arcs in the VRP graphs of our instances, we estimate the arcs' expected energy consumption parameter values a_{ij} and b_{ij} by assuming that all arcs are traveled at an expected constant speed of 45 km/h, and that the road grade θ_{ij} is zero along all arcs. We initially set the maximum deviations $\hat{a}_{ij}$ and $\hat{b}_{ij}$ to 20% of the expected values a_{ij} and b_{ij}. In Section 4.6.7, however, we investigate the impact of using the worst-case values from Asamer et al. (2016) for certain parameters individually.

Regarding the uncertainty sets, we have conducted experiments with several of those presented in Section 4.3.5, while assuming they are the same for all vehicles. The route-dependent budgeted sets U_k^3 and the uncertainty sets U_k^4 formed by the intersection of the box uncertainty set with the ball of radius γ centered at the origin are used to represent the case of independent components in the random vectors Z_k, with each Z_{ijk} symmetrically distributed within the interval

$[-1,1]$. The ellipsoidal uncertainty sets U_k^5 are used to represent normally distributed random vectors Z_k, each of mean zero and with covariance matrix $\sum$. Since the support of Z_k is assumed to be $[-1,1]$, we set standard deviations to 0.333 for each Z_{ijk}, and assume a correlation of 0.9 between the arcs. The values used for θ_0, θ, γ and r in U_k^3, U_k^4 and U_k^5 are initially set so that there is a probability of at most $\beta = 0.05$ that the real energy consumption of vehicle k be larger than w_k. These values are given in Table 4.2. We refer the reader to Ben-Tal et al. (2009), Poss (2013) and Ilyina (2017) for more details concerning the calibration methodology, which is too extensive to discuss here.

Finally, we conducted some preliminary experiments on a small number of instances to fine-tune the parameters of the LNS-based algorithm. More specifically, we used one instance for each possible number of customers n with uncertainty sets U_k^3, and we tested a number of predetermined combinations of parameter values using our best judgment. We then chose the combination that performed best on the subset of six instances. The values corresponding to this combination are reported in Table 4.3 and were used in all experiments of the following sections.

Table 4.2 – Uncertainty set parameter values

Uncertainty set parameter	Value used
θ_0	4.22
θ	0.22
γ	2.45
r	1.65

Table 4.3 – Two-phase heuristic parameter values

Parameter	Value used
Bounds $(\underline{n}_c, \overline{n}_c)$ on number of customers to remove	$(0.1 \cdot n, 0.4 \cdot n)$
Parameters used for randomization $(\lambda_{WR}, \lambda_{WE}, \lambda_{WD}, \lambda_{Shaw}, \lambda_{RG}, \lambda_{RR})$	(3, 6, 3, 6, 1.5, 1.5)
Shaw parameters $(\mu_1, \mu_2, \mu_3, \mu_4)$	(0.4, 0.3, 0.15, 0.1)
Threshold δ to perform LS	1.04 if $n = 320$ 1.09 if $n = 160$ 1.18 if $n = 80$ ∞ otherwise
Threshold τ to check for new robust routes during LS	0.95 if $n = 320$ 1.05 if $n = 160$ ∞ otherwise
Factor ω used to set initial temperature	1.02
Number of LNS iterations κ before SP phase	12,500
Time limit T_{SP1} for vehicle minimization phase of the SP problem	60 seconds
Time limit T_{SP2} for cost minimization phase of the SP problem	1,200 seconds if $n = 320$ 900 seconds if $n = 160$ 600 seconds if $n = 80$ 300 seconds otherwise
Maximum number D of LNS iterations without encountering a new solution before using the *Random insertion* operator	10 if $n = 320$ 20 if $n = 160$ 90 if $n = 80$ 200 if $n = 40$ 1,000 if $n = 20$ 4,000 if $n = 10$

4.6.2 Performance of the two-phase method on small EVRP-ECU instances

In order to get an idea of the performance of our solution method, we have used the reformulation and cutting plane methods described in Sections 4.4.1 and 4.4.2 on small instances of the EVRP-ECU with up to 20 customers. The results are reported in Tables 4.4, 4.5 and 4.6 for $\beta = 0.05$ and the uncertainty sets U_k^3, U_k^4 and U_k^5, respectively. Results are given for both the nominal and the robust versions of the problem for each instance. Recall that in the nominal version, it is assumed

that the energy consumption parameters never deviate from their expected values. We still conduct the SP phase (and the subsequent LS) in this case since it can only improve the final solution X_{Final} returned by the procedure. However, the parameter τ is set to zero for all runs on the nominal version of the problem.

Since the route-dependent uncertainty sets are polyhedral, we apply both the reformulation approach and the cutting plane method (with cuts (4.45)) for the robust version of the problem when it is solved with CPLEX and those sets. Only the cutting plane method (with cuts (4.44)) is applied when solving the robust version with CPLEX and the other uncertainty sets. Whenever the robust version of the problem is solved with CPLEX, we report the best found solution value, the solution time, and the method that achieved it (i.e., "R" for the reformulation or "C" for the cutting plane method; ties are broken based on solution times). When the nominal version is solved with CPLEX, we only report the best found solution value and the solution time. In this case, we simply use CPLEX to solve the mixed integer linear program (MILP) resulting from having empty uncertainty sets in the model of Section 4.3.4. Symmetry breaking inequalities are also added to the formulation for both the robust and nominal cases. Specifically, these inequalities force vehicles with a smaller index k to be used before those with a larger one, and to leave the depot with a larger load. For the two-phase heuristic method, in both the nominal and robust cases, we report the cost of the best found solution over 10 runs, the number of vehicles m in the best found solution, as well as the average cost and average solution time in seconds over the 10 runs.

The results show that the two-phase method clearly outperforms the reformulation and the cutting plane method on each instance when the robust version of the problem is solved. When CPLEX finds an optimal solution within the three-hour time limit, our heuristic consistently finds it in much less time. When CPLEX cannot guarantee the optimality of its best found solution, our heuristic always quickly finds a solution at least as good as the one reported by CPLEX,

and usually better. The same holds for the results on the nominal version of the problem when comparing the heuristic to using CPLEX on the MILP representing the nominal case.

4.6.3 Performance of the two-phase method on large EVRP-ECU instances

For those instances with more than 20 customers, none of the exact methods is able to find a feasible solution within the time limit for both the robust and the nominal cases. Therefore, we only report the performance of the metaheuristic for these instances. The results are presented in Table 4.7 for the nominal version of the problem and for the robust version with the three types of uncertainty sets used. We once again report the cost of the best found solution over 10 runs, the number of vehicles in the best found solution, as well as the average cost and time over the 10 runs for each instance and variation. When no value is reported, this means that the algorithm was unable to find a feasible robust solution (the SP problem is infeasible and no robust solution was found during the LNS phase). It is conceivable that such instances are infeasible, i.e., there is a customer i for which there exists no route k visiting i so that $w_k \leq Q$, or routes require to be very short in order to be energy-robust, thereby requiring too many vehicles.

Despite the fact that we do not have benchmark solutions for these larger EVRP-ECU instances to evaluate the performance of the metaheuristic, the algorithm seems relatively stable when comparing the average cost over ten runs with the best run for most instances. The solution times could be considered high for some instances with 80 customers or more, but this is partly due to the fact that the set partitioning problem is sometimes not solved to optimality and therefore uses the entire time allotted to it. We mention, however, that when this

Table 4.4 – Results for the small instances with uncertainty sets U_k^3 and $\beta = 0.05$

	Nominal						Robust						
	CPLEX		LNS+SP				CPLEX			LNS+SP			
Instance	Best	t (s)	Best	m	Avg.	t (s)	Best	Method	t (s)	Best	m	Avg.	t (s)
1-10C	294.62	2445.86	294.62	2	294.62	2.02	321.23	R	2386.77	321.23	2	321.23	2.58
2-10C	316.45	2188.09	316.45	2	316.45	1.74	319.69	C	2996.37	319.69	2	319.69	2.27
3-10C	292.62	1584.54	292.62	2	292.62	3.99	321.95	R	1737.46	321.95	2	321.95	5.32
4-10C	324.55	248.64	324.55	2	324.55	2.75	328.08	C	374.06	328.08	2	328.08	3.65
5-10C	326.88	398.02	326.88	2	326.88	2.41	454.70	R	1634.42	454.70	3	454.70	3.23
1-20C	471.45	10800	470.64	3	470.64	8.14	–	C+R	10800	810.56	5	810.56	9.34
2-20C	326.09	6652.50	326.09	2	326.09	8.49	464.55	C	10800	459.95	3	460.74	9.57
3-20C	334.82	10800	334.79	2	334.79	9.68	610.04	R	10800	486.79	3	486.81	11.05
4-20C	324.75	548.67	324.75	2	324.75	10.38	450.64	R	10800	450.64	3	450.64	11.81
5-20C	463.41	10800	462.92	3	462.92	10.56	468.37	C	10800	468.37	3	468.37	12.65

Table 4.5 – Results for the small instances with uncertainty sets U_k^4 and $\beta = 0.05$

	Nominal						Robust						
	CPLEX		LNS+SP				CPLEX			LNS+SP			
Instance	Best	t (s)	Best	m	Avg.	t (s)	Best	Method	t (s)	Best	m	Avg.	t (s)
1-10C	294.62	2445.86	294.62	2	294.62	2.02	321.24	C	3354.75	321.24	2	321.24	4.28
2-10C	316.45	2188.09	316.45	2	316.45	1.74	319.75	C	2035.69	319.75	2	319.75	3.32
3-10C	292.62	1584.54	292.62	2	292.62	3.99	321.96	C	5108.32	321.96	2	321.96	15.47
4-10C	324.55	248.64	324.55	2	324.55	2.75	328.10	C	204.48	328.10	2	328.10	6.96
5-10C	326.88	398.02	326.88	2	326.88	2.41	454.72	C	2920.70	454.72	3	454.72	4.93
1-20C	471.45	10800	470.64	3	470.64	8.14	–	C	10800	810.58	5	810.58	16.65
2-20C	326.09	6652.50	326.09	2	326.09	8.49	464.64	C	10800	459.93	3	462.72	16.61
3-20C	334.82	10800	334.79	2	334.79	9.68	609.45	C	10800	486.88	3	486.92	18.49
4-20C	324.75	548.67	324.75	2	324.75	10.38	451.14	C	10800	450.65	3	450.65	17.77
5-20C	463.41	10800	462.92	3	462.92	10.56	472.22	C	10800	468.45	3	468.45	22.02

Table 4.6 – Results for the small instances with uncertainty sets U_k^5 and $\beta = 0.05$

	Nominal						Robust						
	CPLEX		LNS+SP				CPLEX			LNS+SP			
Instance	Best	t (s)	Best	m	Avg.	t (s)	Best	Method	t (s)	Best	m	Avg.	t (s)
1-10C	294.62	2445.86	294.62	2	294.62	2.02	295.93	C	640.76	295.93	2	295.93	2.53
2-10C	316.45	2188.09	316.45	2	316.45	1.74	318.19	C	1379.18	318.19	2	318.19	2.30
3-10C	292.62	1584.54	292.62	2	292.62	3.99	308.45	C	1210.09	308.45	2	308.45	5.36
4-10C	324.55	248.64	324.55	2	324.55	2.75	326.47	C	605.05	326.47	2	326.47	3.62
5-10C	326.88	398.02	326.88	2	326.88	2.41	333.65	C	207.45	333.65	2	333.65	3.16
1-20C	471.45	10800	470.64	3	470.64	8.14	643.58	C	10800	643.14	4	643.14	9.66
2-20C	326.09	6652.50	326.09	2	326.09	8.49	455.59	C	10800	328.13	2	328.13	9.62
3-20C	334.82	10800	334.79	2	334.79	9.68	481.60	C	10800	480.96	3	480.96	10.92
4-20C	324.75	548.67	324.75	2	324.75	10.38	449.90	C	10800	330.65	2	330.65	11.60
5-20C	463.41	10800	462.92	3	462.92	10.56	466.05	C	10800	465.28	3	465.28	12.51

occurs the optimality gap of the best found solution for the SP problem is usually relatively small (except for the 320-customer instances), and the solution is also subsequently improved through the final robust local search phase. The results with the uncertainty sets U_k^4 formed by the intersection of the box uncertainty set with the ball of radius γ centered at the origin show the importance of using sets allowing to efficiently check the robustness of routes. Recall from Section 4.5.6 that with uncertainty sets U_k^4, we solve a quadratically constrained program (with CPLEX) to check whether a new route is robust. This results in much larger solution times for the 320-customer instances.

It is also interesting to observe the difference between the best found solutions in nominal and robust versions of the problem. Indeed, for both the small instances results in Tables 4.4, 4.5 and 4.6, and the large instances results in Table 4.7, there are often significant differences between the values of the best found nominal and the best found robust solutions. Taking into account the energy consumption uncertainty sometimes results in using the same number of vehicles but routing them differently in order to be robust, or in using more vehicles than in the nominal case. The uncertainty sets U_k^3 and U_k^4 make the same assumptions regarding the random vectors Z_k and hence return similar solutions. The sets U_k^5, on the other hand, assume that we have much more information regarding the distribution of Z_k, and the robust solutions become less conservative than with the other two sets. There are even instances that appear to be infeasible with the other two uncertainty sets but not with sets U_k^5.

We further demonstrate the difference between nominal and robust solutions through Table 4.8, in which we report two measures pertaining to the best found nominal solutions. First, for each instance we report the number of routes in the best found nominal solution (out of the total in the solution) that violate constraints (4.17) under each uncertainty set. This indicates how often the nominal solution fails with each of the uncertainty sets. Second, for each instance we re-

port the cost increase or decrease (in %) of the best found robust solution under each uncertainty set with respect to the best found nominal solution, when the energy costs in the nominal solution are computed with a worst-case energy consumption under the uncertainty set in question. When no value is reported for this second measure, no feasible robust solution was found for that instance and uncertainty set. As the entries show, the majority of best found nominal solutions contain one or several routes that would be infeasible in the robust version of the problem. The degree of the cost increase in the best found robust solution depends on whether more vehicles are required to ensure energy feasibility compared to the number of vehicles in the best found nominal solution. When this is the case, the robust solution is of course significantly more costly than the nominal one. On the other hand, when no additional vehicles are required to ensure energy robustness (i.e., this can be done by rearranging the same number of routes), the cost difference between the best found robust and nominal solutions can be quite small.

Table 4.7 – Results for the large instances with sets U_k^3, U_k^4 and U_k^5, and with $\beta = 0.05$

	Nominal				Uncertainty sets U_k^3				Uncertainty sets U_k^4				Uncertainty sets U_k^5			
Instance	Best	m	Avg.	t (s)	Best	m	Avg.	t (s)	Best	m	Avg.	t (s)	Best	m	Avg.	t (s)
1-40C	632.40	4	632.40	34.65	646.45	4	646.45	39.86	646.64	4	646.64	55.69	636.25	4	636.25	39.50
2-40C	999.64	6	999.64	34.56	–	–	–	–	–	–	–	–	–	–	–	–
3-40C	632.39	4	632.39	36.13	789.92	5	789.92	41.39	789.95	5	789.95	63.40	636.42	4	636.42	41.10
4-40C	473.03	3	473.03	40.75	601.91	4	601.91	45.91	601.92	4	601.92	71.35	481.63	3	481.63	48.24
5-40C	639.31	4	639.31	46.73	801.60	5	801.61	55.57	801.81	5	801.81	97.38	787.37	5	787.66	69.04
1-80C	931.18	6	931.18	219.11	941.35	6	941.35	285.57	941.28	6	941.28	399.75	938.90	6	938.90	301.20
2-80C	950.52	6	950.68	203.23	1109.76	7	1109.76	248.97	1109.80	7	1109.80	356.81	970.96	6	1052.91	261.02
3-80C	903.02	6	903.02	251.74	922.98	6	925.07	754.40	922.43	6	923.70	970.16	911.70	6	911.76	454.58
4-80C	896.95	6	896.95	233.43	904.13	6	904.13	351.53	904.01	6	904.01	587.69	901.32	6	901.32	293.16
5-80C	943.82	6	943.82	224.74	1111.80	7	1113.62	232.13	1111.71	7	1113.25	377.38	971.58	6	1008.63	403.03
1-160C	1862.32	12	1863.63	1814.32	–	–	–	–	–	–	–	–	2068.06	13	2165.07	1933.53
2-160C	1777.43	12	1778.91	2224.54	1794.86	12	1795.35	2360.19	1794.59	12	1795.07	3349.30	1786.01	12	1788.18	2264.71
3-160C	1670.80	11	1672.70	1571.13	1683.89	11	1686.06	1609.33	1683.70	11	1686.30	2504.15	1680.14	11	1683.09	1776.55
4-160C	1684.96	11	1687.88	1470.01	1872.68	12	1929.74	1431.21	1869.79	12	1890.05	2490.75	1711.48	11	1714.93	1293.94
5-160C	1729.75	11	1731.91	1267.17	–	–	–	–	–	–	–	–	1938.09	12	2064.32	1099.00
1-320C	3780.68	24	3788.77	3034.93	–	–	–	–	–	–	–	–	–	–	–	–
2-320C	3217.63	22	3221.16	5435.32	3238.64	22	3244.47	6745.20	3241.45	22	3245.28	15972.70	3229.04	22	3235.80	6093.11
3-320C	3379.40	22	3393.95	2078.88	–	–	–	–	–	–	–	–	3769.91	24	3913.29	2485.39
4-320C	3341.18	22	3384.28	6554.97	3625.48	24	3684.60	7231.61	3626.51	24	3679.36	20420.30	3458.93	23	3489.00	7813.37
5-320C	3294.02	22	3297.16	6837.66	3366.80	22	3481.77	7478.53	3363.10	22	3460.38	18871.70	3334.11	22	3354.32	7427.62

Table 4.8 – Feasibility of best found nominal solutions and the price of robustness

Instance	Uncertainty sets U_k^3		Uncertainty sets U_k^4		Uncertainty sets U_k^5	
	Number of inf. routes	Cost diff. of rob. solution (%)	Number of inf. routes	Cost diff. of rob. solution (%)	Number of inf. routes	Cost diff. of rob. solution (%)
1-10C	1/2	8.15	1/2	8.15	0/2	0.00
2-10C	0/2	0.00	0/2	0.00	0/2	0.00
3-10C	1/2	9.16	1/2	9.16	1/2	4.96
4-10C	0/2	0.00	0/2	0.00	0/2	0.00
5-10C	1/2	37.55	1/2	37.56	1/2	1.45
1-20C	2/3	70.52	2/3	70.52	2/3	35.90
2-20C	2/2	39.61	2/2	39.61	0/2	0.00
3-20C	2/2	43.82	2/2	43.85	2/2	42.72
4-20C	1/2	37.34	1/2	37.36	1/2	1.20
5-20C	1/3	0.27	1/3	0.28	0/3	0.00
1-40C	2/4	1.31	2/4	1.32	2/4	0.03
2-40C	5/6	–	4/6	–	4/6	–
3-40C	3/4	23.65	3/4	23.66	1/4	0.06
4-40C	1/3	25.97	1/3	25.97	1/3	1.22
5-40C	2/4	24.16	2/4	24.20	2/4	22.43
1-80C	1/6	0.29	1/6	0.29	1/6	0.28
2-80C	3/6	15.79	3/6	15.80	2/6	1.55
3-80C	2/6	1.41	2/6	1.36	2/6	0.46
4-80C	0/6	0.00	0/6	0.00	0/6	0.00
5-80C	2/6	16.68	2/6	16.70	1/6	2.35
1-160C	5/12	–	5/12	–	4/12	10.43
2-160C	1/12	0.18	1/12	0.18	0/12	0.01
3-160C	1/11	0.03	1/11	0.03	1/11	0.04
4-160C	4/11	10.23	4/11	10.08	4/11	1.03
5-160C	5/11	–	5/11	–	4/11	11.40
1-320C	12/24	–	12/24	–	12/24	–
2-320C	1/22	−0.07	1/22	0.03	0/22	−0.10
3-320C	8/22	–	8/22	–	8/22	10.95
4-320C	4/22	4.17	4/22	4.26	3/22	2.98
5-320C	4/22	1.43	4/22	1.34	2/22	0.72

4.6.4 Performance of the two-phase method on CVRP and RCVRP instances

In order to further validate the performance of the two-phase solution method, we have conducted a few experiments on available benchmark instances for the related CVRP and the RCVRP. The EVRP-ECU can indeed be reduced to a CVRP when the battery capacity is infinite and there are no fixed dispatching costs nor

energy costs. We have therefore tested our heuristic on the well-known 14 instances (C1, ..., C14) of Christofides et al. (1979), the 20 instances (G1, ..., G20) of Golden et al. (1998), the instances of the sets A, B, and P of Augerat (1995), as well as the instances of the sets E, F, and M proposed by Christofides and Eilon (1969), Fisher (1994) and Christofides et al. (1979), respectively. The first group contains a number of customers n ranging from 50 to 199. The second represents large-scale instances and contains between 200 and 483 customers. The number of customers in the sets A, B, P, E, F, and M varies from 12 to 199, and the number of required routes is fixed, which is handled through the SP phase and the subsequent final local search (in this case we disregard the best found number of vehicles m in the SP vehicle minimization phase, and in Algorithm 1 we assume that $C^R(X) = \infty$ if the number of routes in solution X is not equal to the required number of routes). Some instances also have maximum route durations and customer service times. We therefore adapted our heuristic to handle these extra features (feasibility with respect to route durations is enforced throughout the procedure).

The RCVRP additionally considers that the customer demands q_i are uncertain parameters. In the RCVRP, it is therefore assumed that each customer i has a certain nominal demand q_i^0 from which we expect the realized customer demand q_i to deviate according to some uncertainty set. We have tested our heuristic on the RCVRP variants of the above instances, which were introduced by Gounaris et al. (2013) and Gounaris et al. (2016). We solve these instances with the following two uncertainty sets for the customer demands (which are those used by Gounaris et al., 2013 and Gounaris et al., 2016 in their experiments):

$$U_Q^1 = \{q \in \mathbb{R}_+^n \mid \underline{q}_i \leq q_i \leq \bar{q}_i \; \forall i \in N_0, \sum_{i \in B_j} q_i \leq b_j \text{ for } j = 1, ..., J\}, \tag{4.50}$$

$$U_Q^2 = \{q \in \mathbb{R}_+^n \mid q = q^0 + \Gamma\xi \text{ for some } \xi \in \Xi\}, \tag{4.51}$$

where $\Xi = \{\xi \in \mathbb{R}^F \mid \xi \in [-e, +e], e^T\xi \in [-\beta F, +\beta F]\}, q^0 \in \mathbb{R}_+^n, \Gamma \in \mathbb{R}^{n \times F}, F \in \mathbb{N}, \beta \in [0, 1]$, and $e \in \mathbb{R}^F$ is a vector with only ones. The uncertainty set U_Q^1

states that each customer demand q_i must lie within a given interval $[\underline{q}_i, \overline{q}_i]$, and that the sum of the demands of the customers in each subset $B_j \subseteq N_0$ must be at most b_j. The uncertainty set U_Q^2 states that the demand vector q is the sum of a nominal demand vector q^0 and a disturbance $\Gamma\xi$ that depends on F independent factors, thereby allowing correlations between customer demands to be taken into account. We modified our two-phase heuristic so that routes are added to the pool of robust routes Ω_R when their worst-case total demand is at most the vehicle's load capacity L. We use propositions from Gounaris et al. (2013) to efficiently compute a route's worst-case total demand with uncertainty sets U_Q^1 and U_Q^2. We also mention that the number of required routes is fixed in all RCVRP instances (even those based on the Christofides et al., 1979 and the Golden et al., 1998 CVRP instances), and that the vehicle capacity from the associated CVRP instance is always increased by 20%. We refer the reader to Gounaris et al. (2016) for more information on the generation of the RCVRP instances.

For all parameters of the two-phase heuristic that depend on the number of customers n in Table 4.3, if $n \geq 320$, we use the same values as for $n = 320$; if $160 \leq n < 320$, we use the same values as for $n = 160$; etc. We set parameter τ to zero in the two-phase heuristic when solving the CVRP, as for the experiments on the nominal version of the EVRP-ECU. The detailed results are reported in Tables 4.14–4.18 of Appendix A for the CVRP and RCVRP instances. We limit our presentation to instances for which benchmark solutions are available for both the CVRP and RCVRP (there are a few CVRP instances of sets A, E and M for which no corresponding RCVRP instances were generated by Gounaris et al., 2013). In Tables 4.14–4.18, we report the best found solution (BFS) value by our heuristic over 10 runs, the average cost and average solution time, the best known solution (BKS) value from the literature, as well as the gap (%) of the BFS by our heuristic with respect to the BKS. Solutions that are known to be optimal are marked by an asterisk in Tables 4.14–4.18.

We provide a summary of the detailed results of Appendix A in Table 4.9, where we distinguish between BKSs that are provenly optimal and those that are not. For each set of instances, we report the number of instances for which we identified new best solutions, the number of instances for which the BFS by our heuristic matches the non-proven optimal BKS (NPO-BKS), the number of instances for which our BFS matches the proven optimal solution (PO-BKS), and the average gap for the instances for which our BFS is worse than the BKS (whether the BKS is proven optimal or not).

Table 4.9 – Summarized results for the CVRP and RCVRP benchmark instances

Instance set	Num. of instances	CVRP		RCVRP-$U_{\square}^{1}$		RCVRP-$U_{\square}^{2}$	
Instances of the set A (Augerat, 1995)	26	Num. of new best solutions:	0	Num. of new best solutions:	1	Num. of new best solutions:	1
		Num. of matched NPO-BKSs:	0	Num. of matched NPO-BKSs:	13	Num. of matched NPO-BKSs:	9
		Num. of matched PO-BKSs:	26	Num. of matched PO-BKSs:	12	Num. of matched PO-BKSs:	16
		Avg. gap (%) when BFS>BKS:	–	Avg. gap (%) when BFS>BKS:	0.41	Avg. gap (%) when BFS>BKS:	–
Instances of the set B (Augerat, 1995)	23	Num. of new best solutions:	0	Num. of new best solutions:	1	Num. of new best solutions:	0
		Num. of matched NPO-BKSs:	0	Num. of matched NPO-BKSs:	8	Num. of matched NPO-BKSs:	8
		Num. of matched PO-BKSs:	23	Num. of matched PO-BKSs:	12	Num. of matched PO-BKSs:	15
		Avg. gap (%) when BFS>BKS:	–	Avg. gap (%) when BFS>BKS:	0.53	Avg. gap (%) when BFS>BKS:	–
Instances of the set P (Augerat, 1995)	24	Num. of new best solutions:	0	Num. of new best solutions:	0	Num. of new best solutions:	0
		Num. of matched NPO-BKSs:	0	Num. of matched NPO-BKSs:	14	Num. of matched NPO-BKSs:	13
		Num. of matched PO-BKSs:	24	Num. of matched PO-BKSs:	10	Num. of matched PO-BKSs:	11
		Avg. gap (%) when BFS>BKS:	–	Avg. gap (%) when BFS>BKS:	–	Avg. gap (%) when BFS>BKS:	–
Instances of the sets E, M and F (Christofides and Eilon, 1969; Fisher, 1994; Christofides et al., 1979)	17	Num. of new best solutions:	0	Num. of new best solutions:	1	Num. of new best solutions:	1
		Num. of matched NPO-BKSs:	0	Num. of matched NPO-BKSs:	6	Num. of matched NPO-BKSs:	8
		Num. of matched PO-BKSs:	17	Num. of matched PO-BKSs:	8	Num. of matched PO-BKSs:	7
		Avg. gap (%) when BFS>BKS:	–	Avg. gap (%) when BFS>BKS:	0.66	Avg. gap (%) when BFS>BKS:	0.81
Instances of Christofides et al. (1979)	14	Num. of new best solutions:	0	Num. of new best solutions:	7	Num. of new best solutions:	6
		Num. of matched NPO-BKSs:	4	Num. of matched NPO-BKSs:	6	Num. of matched NPO-BKSs:	7
		Num. of matched PO-BKSs:	5	Num. of matched PO-BKSs:	0	Num. of matched PO-BKSs:	0
		Avg. gap (%) when BFS>BKS:	0.39	Avg. gap (%) when BFS>BKS:	0.08	Avg. gap (%) when BFS>BKS:	0.57
Instances of Golden et al. (1998)	20	Num. of new best solutions:	0	Num. of new best solutions:	11	Num. of new best solutions:	13
		Num. of matched NPO-BKSs:	2	Num. of matched NPO-BKSs:	0	Num. of matched NPO-BKSs:	1
		Num. of matched PO-BKSs:	0	Num. of matched PO-BKSs:	0	Num. of matched PO-BKSs:	0
		Avg. gap (%) when BFS>BKS:	1.49	Num. of instances with no FS:	7	Num. of instances with no FS:	6
				Avg. gap (%) when BFS>BKS:	0.36	Avg. gap (%) when BFS>BKS:	–

Our heuristic finds the BKS for all the tested CVRP instances from sets A, B, P, E, M, and F. It also performs fairly well on the CVRP instances of Christofides et al. (1979); the BKS is found for several of these instances, and the gap is quite small when it is not. The performance of the heuristic deteriorates, however, on the larger instances of Golden et al. (1998), with a worst-case gap of 3.72% on these instances (obtained for an instance with 480 customers). Finally, the method matches or improves the BKS reported by Gounaris et al. (2016) for most RCVRP instances. The 42 new best solutions found by the heuristic are reported in bold-

face in Tables 4.14–4.18. There are, however, a few large-scaled RCVRP instances based on the Golden et al. (1998) CVRP instances for which the current configuration of the two-phase heuristic was unable to find a feasible robust solution over the 10 runs (i.e., no solution with only robust routes is encountered during the LNS phase, and CPLEX fails to find a feasible solution to the SP problem). These are reported in Table 4.9 as "Num. of instances with no FS". It is conceivable that this could be addressed (and that the method's performance as a whole on the CVRP and RCVRP instances could be further improved) by recalibrating the parameters of the algorithm. It is also possible that an adaptive layer, although not particularly useful on the EVRP-ECU instances, could also increase the heuristic's competitiveness for these problem variants. For sake of brevity we do not investigate this any further. Nonetheless, we find new best solutions for 24 of the large-scaled RCVRP instances.

4.6.5 The trade-off between cost and risk

A nice feature of the robust optimization methodology is that it can be used to present different alternatives to the decision maker who can then determine when and whether cost savings justify incurring extra risks. We illustrate this by solving the EVRP-ECU instances with the ellipsoidal uncertainty sets U_k^5 representing normally distributed random vectors Z_k, but we now calibrate them so that $\beta = 0.01$ instead of 0.05 as in the experiments of the previous sections. The parameter r is thus increased to 2.33. Moreover, we solve the instances using the box uncertainty sets U_k^1 as well, which is equivalent to setting $\beta = 0$ and solving a nominal version of the problem in which the expected values of the energy consumption parameters are all set to their worst-case values. The results are reported in Table 4.10, with the best of 10 runs presented for the new experiments. The previous best found solutions with sets U_k^5 and $\beta = 0.05$ are also reported.

As the results show, in some cases, the difference in cost between the three protection levels is rather insignificant, and one would therefore benefit from simply using the safest solution, i.e., the routing plan obtained with the box uncertainty set. However, in other cases, there is a case to be made for incurring a small risk. Indeed, for some instances, the best found solution with $\beta = 0.01$ allows interesting cost savings compared to the no-risk case of $\beta = 0$, sometimes even using fewer vehicles. The same holds when going from $\beta = 0.01$ to $\beta = 0.05$. In addition, some instances that appear to be infeasible for a smaller β become feasible by increasing the level of risk. Nevertheless, it is ultimately up to the decision maker to choose the right balance between cost and risk in the presence of uncertain parameters.

4.6.6 The impact of correlation in routes

In this section we take a quick look at the sensitivity of solutions to the correlation between the arcs in a given route, with respect to the deviation of their realized energy consumption parameter values from their expected ones, i.e., correlation between the components of Z_k. As briefly mentioned in Section 4.3.5, it is reasonable to expect driver behaviour and external conditions like the weather and road conditions to be fairly similar along the same route. We therefore investigate the impact of such dependencies on robust solutions by solving the EVRP-ECU instances with uncertainty sets U_k^5 and a protection level of $\beta = 0.01$, but by using three new correlation levels in the covariance matrix $\sum$: 0.0, 0.3 and 0.6. We report the best of 10 runs for each case in Table 4.11. The values in the column associated with the previously used correlation of 0.9 between the arcs are taken from Table 4.10. The entries suggest that the cost and number of vehicles in the best found solutions tend to increase with the degree of correlation between the components of random vectors Z_k. There is even an instance with 160 customers

Table 4.10 – Best found solutions with different uncertainty sets and different protection levels

	Sets $U_k^5/\beta = 0.05$		Sets $U_k^5/\beta = 0.01$		Sets $U_k^1/\beta = 0$	
Instance	Value	m	Value	m	Value	m
1-10C	295.93	2	296.47	2	321.25	2
2-10C	318.19	2	318.91	2	319.75	2
3-10C	308.45	2	315.78	2	321.97	2
4-10C	326.47	2	327.26	2	328.17	2
5-10C	333.65	2	453.75	3	454.74	3
1-20C	643.14	4	644.65	4	810.66	5
2-20C	328.13	2	456.29	3	464.25	3
3-20C	480.96	3	482.53	3	487.11	3
4-20C	330.65	2	449.96	3	450.95	3
5-20C	465.28	3	466.25	3	468.57	3
1-40C	636.25	4	637.76	4	776.44	5
2-40C	–	–	–	–	–	–
3-40C	636.42	4	646.41	4	790.29	5
4-40C	481.63	3	600.90	4	602.26	4
5-40C	787.37	5	794.31	5	805.45	5
1-80C	938.90	6	941.25	6	944.26	6
2-80C	970.96	6	1102.50	7	1112.45	7
3-80C	911.70	6	919.47	6	930.79	6
4-80C	901.32	6	903.12	6	905.27	6
5-80C	971.58	6	1101.59	7	1115.56	7
1-160C	2068.06	13	–	–	–	–
2-160C	1786.01	12	1792.05	12	1797.04	12
3-160C	1680.14	11	1683.14	11	1687.87	11
4-160C	1711.48	11	1852.28	12	1880.51	12
5-160C	1938.09	12	2374.66	15	–	–
1-320C	–	–	–	–	–	–
2-320C	3229.04	22	3239.65	22	3244.09	22
3-320C	3769.91	24	4410.57	28	–	–
4-320C	3458.93	23	3492.74	23	3626.51	24
5-320C	3334.11	22	3347.02	22	3378.22	22

that appears to become infeasible when going from correlations of 0.3 to 0.6.

4.6.7 The impact of specific parameters in the energy consumption model

Our last computational study concerns the impact of specific parameters in the energy consumption model described in Section 4.3.2 on robust solutions. To this end, we modify the instances by computing the maximum deviations $\hat{a}_{ij}$ and $\hat{b}_{ij}$

Table 4.11 – Best found solutions with sets U_k^5, $\beta = 0.01$, and different correlation levels

	No correlation		Correlation of 0.3		Correlation of 0.6		Correlation of 0.9	
Instance	Value	m	Value	m	Value	m	Value	m
1-10C	295.73	2	296.02	2	296.26	2	296.47	2
2-10C	317.61	2	318.16	2	318.56	2	318.91	2
3-10C	308.09	2	308.50	2	308.82	2	315.78	2
4-10C	326.17	2	326.61	2	326.96	2	327.26	2
5-10C	331.20	2	333.64	2	453.40	3	453.75	3
1-20C	486.00	3	643.53	4	644.12	4	644.65	4
2-20C	327.17	2	327.97	2	451.22	3	456.29	3
3-20C	475.05	3	480.93	3	481.72	3	482.53	3
4-20C	325.92	2	328.76	2	449.56	3	449.96	3
5-20C	464.51	3	465.25	3	465.80	3	466.25	3
1-40C	634.46	4	635.94	4	636.95	4	637.76	4
2-40C	–	–	–	–	–	–	–	–
3-40C	635.31	4	636.41	4	637.24	4	646.41	4
4-40C	480.36	3	481.60	3	600.39	4	600.90	4
5-40C	652.91	4	785.75	5	788.86	5	794.31	5
1-80C	936.09	6	938.36	6	939.84	6	941.25	6
2-80C	956.74	6	968.79	6	1094.47	7	1102.50	7
3-80C	908.85	6	911.39	6	913.53	6	919.47	6
4-80C	899.37	6	901.03	6	902.18	6	903.12	6
5-80C	951.67	6	971.30	6	1095.40	7	1101.59	7
1-160C	1927.93	12	2069.12	13	–	–	–	–
2-160C	1782.77	12	1785.76	12	1790.07	12	1792.05	12
3-160C	1674.56	11	1679.22	11	1681.18	11	1683.14	11
4-160C	1691.98	11	1707.40	11	1722.58	11	1852.28	12
5-160C	1880.24	12	2040.34	13	2210.65	14	2374.66	15
1-320C	–	–	–	–	–	–	–	–
2-320C	3225.95	22	3232.31	22	3233.93	22	3239.65	22
3-320C	3563.99	23	3877.77	25	4223.12	27	4410.57	28
4-320C	3423.48	23	3459.52	23	3476.16	23	3492.74	23
5-320C	3303.41	22	3323.69	22	3336.18	22	3347.02	22

from the expected values of the arcs' energy parameters with worst-case values inspired from those from Asamer et al. (2016) for the rolling friction coefficient C_r, the drivetrain efficiency ϕ, the auxiliary power P, and the product $C_d \cdot \rho$ of the air drag coefficient and air density. Since the expected auxiliary power and air drag coefficient are expected to be larger for a truck than for a small passenger vehicle as the one considered by Asamer et al. (2016), we simply use the same ratio as these authors between the worst-case and expected values to determine the worst-case associated with the expected values that we used for these parameters. Finally, we assume that speed can be up to 20% larger or smaller than the expected value of 45 km/h. Taking negative deviations from the expected value into account is only relevant for speed, since a lower speed can increase the energy consumed by auxiliaries. All worst-case and expected values are reported in Table 4.12.

Table 4.12 – Nominal and worst-case energy consumption model parameter values used to assess the impact of specific parameters

Energy consumption model parameter	Expected value	Worst-case value
Air drag coefficient C_d	0.7	0.735
Rolling friction coefficient C_r	0.01	0.014
Auxiliary power demand P	1,575 W	4,431 W
Air density ρ	1.2041 kg/m^3	1.296 kg/m^3
Drivetrain efficiency ϕ	1.3175	1.4706
Speed	45 km/h	36 km/h or 54 km/h

We either change the instances by determining $\hat{a}_{ij}$ and $\hat{b}_{ij}$ with the worst-case value of only one parameter in the energy consumption model (two in the case of the product $C_d \cdot \rho$) and with the expected values of the rest, or with the worst-case values of all parameters simultaneously. All experiments were run using the ellipsoidal uncertainty sets U_k^5 with the initial correlation level of 0.9 between the components of Z_k and with a protection level of $\beta = 0.01$. The best found solutions over 10 runs are reported in Table 4.13 for each case, as well as for the previously solved nominal scenario with no uncertainty. For example, column

"Rolling friction" reports best found solutions when $\hat{a}_{ij}$ and $\hat{b}_{ij}$ are computed with the worst-case value of C_r, and with expected values for C_d, P, ρ, ϕ and speed. Note that when traveling at constant speeds (as is the case in our EVRP-ECU instances), the worst-case energy consumption of an arc will always be attained with the smallest or largest possible speed. For an arc (i, j) of length d_{ij} traveled entirely at a constant speed of v_{ij}, let $B_{ij}(v_{ij})$ refer to the portion of the energy consumption when traveling (i, j) that is dependent on v_{ij}. Equations (4.1) and (4.2) allow expressing $B_{ij}(v_{ij})$ as

$$\begin{aligned} B_{ij}(v_{ij}) &= \frac{1}{3.6 \cdot 10^6}\left(0.5\phi A C_d \rho v_{ij}^2 d_{ij} + P \cdot t_{ij}\right) \\ &= \frac{1}{3.6 \cdot 10^6}\left(0.5\phi A C_d \rho v_{ij}^2 d_{ij} + P \cdot \frac{d_{ij}}{v_{ij}}\right), \end{aligned}$$

which is a convex function of v_{ij} for $v_{ij} > 0$ when all other parameters are fixed. Therefore, for the cases of 1) taking the worst-case value of speed and the expected values of the other uncertain parameters, and 2) taking the worst-case values of all parameters simultaneously, we either use the minimal or maximal speed for each arc to determine $\hat{a}_{ij}$ and $\hat{b}_{ij}$ (i.e., the one that maximizes $B_{ij}(v_{ij})$ for that arc).

Taking all worst-case values simultaneously to compute $\hat{a}_{ij}$ and $\hat{b}_{ij}$ appears to render most instances infeasible (see column "All"). When this is not the case, the best found solution cost is significantly deteriorated compared to that of the nominal case. However, taking worst-case values of the parameters one at a time to compute $\hat{a}_{ij}$ and $\hat{b}_{ij}$ shows that the uncertainty of the rolling friction coefficient seems to have the largest impact on solutions, which is line with the findings of Asamer et al. (2016) in their sensitivity analysis of the energy consumption model parameters. The uncertainty surrounding the auxiliary power, the drivetrain efficiency and the travel speed also seems to have a considerable impact for a few instances, while the uncertainty of the air drag coefficient and of the air density seems to be less influential.

Table 4.13 – Best found solutions with uncertainty sets U_k^5, $\beta = 0.01$, and different energy consumption model parameters' worst-case values used to compute $\hat{a}_{ij}$ and $\hat{b}_{ij}$

	Nominal		Rolling friction		Efficiency		Air drag + density		Aux. power		Speed		All	
Instance	Value	m	Value	m	Value	m	Value	m	Value	m	Value	m	Value	m
1-10C	294.62	2	321.22	2	295.60	2	294.92	2	296.14	2	295.47	2	–	–
2-10C	316.45	2	319.67	2	317.74	2	316.85	2	318.52	2	317.61	2	–	–
3-10C	292.62	2	321.92	2	308.05	2	292.90	2	308.71	2	307.91	2	–	–
4-10C	324.55	2	328.10	2	325.98	2	325.00	2	326.86	2	325.85	2	–	–
5-10C	326.88	2	454.66	3	331.26	2	327.34	2	453.30	3	331.09	2	–	–
1-20C	470.64	3	810.50	5	485.70	3	471.94	3	643.86	4	485.46	3	–	–
2-20C	326.09	2	464.75	3	327.61	2	326.53	2	328.37	2	327.37	2	618.72	4
3-20C	334.79	2	487.02	3	478.85	3	335.27	2	481.45	3	474.97	3	–	–
4-20C	324.75	2	450.92	3	326.22	2	325.19	2	330.98	2	326.03	2	740.71	5
5-20C	462.92	3	468.46	3	464.68	3	463.47	3	465.74	3	464.50	3	–	–
1-40C	632.40	4	776.43	5	635.33	4	633.38	4	636.66	4	634.88	4	1067.69	7
2-40C	999.64	6	–	–	–	–	–	–	–	–	–	–	–	–
3-40C	632.39	4	797.54	5	635.50	4	633.18	4	636.83	4	635.04	4	–	–
4-40C	473.03	3	602.32	4	480.53	3	473.62	3	600.08	4	480.14	3	754.02	5
5-40C	639.31	4	805.68	5	657.43	4	648.99	4	788.59	5	654.53	4	–	–
1-80C	931.18	6	944.38	6	937.60	6	932.37	6	939.41	6	936.92	6	1368.92	9
2-80C	950.52	6	1112.50	7	962.75	6	954.08	6	1092.83	7	958.56	6	–	–
3-80C	903.02	6	930.12	6	909.92	6	903.97	6	913.13	6	909.33	6	–	–
4-80C	896.95	6	905.40	6	900.23	6	897.87	6	901.72	6	899.63	6	1063.97	7
5-80C	943.82	6	1115.53	7	957.66	6	945.47	6	1093.24	7	952.12	6	–	–
1-160C	1862.32	12	–	–	2044.35	13	1882.35	12	2212.61	14	1925.58	12	–	–
2-160C	1777.43	12	1797.75	12	1783.85	12	1779.29	12	1786.55	12	1783.43	12	–	–
3-160C	1670.80	11	1688.33	11	1677.96	11	1673.31	11	1680.70	11	1676.43	11	–	–
4-160C	1684.96	11	2008.80	13	1695.96	11	1688.70	11	1715.66	11	1695.12	11	–	–
5-160C	1729.75	11	–	–	1891.51	12	1738.36	11	2082.22	13	1884.05	12	–	–
1-320C	3780.68	24	–	–	–	–	4013.81	25	–	–	–	–	–	–
2-320C	3217.63	22	3246.29	22	3225.12	22	3219.12	22	3232.37	22	3226.28	22	–	–
3-320C	3379.40	22	–	–	3600.21	23	3413.40	22	4054.46	26	3567.40	23	–	–
4-320C	3341.18	22	3633.12	24	3436.38	23	3357.65	22	3481.36	23	3425.16	23	–	–
5-320C	3294.02	22	3520.89	23	3317.11	22	3297.40	22	3335.57	22	3308.58	22	–	–

4.7. Conclusions

The goal of this study was to introduce and solve the EVRP-ECU, a practical transportation problem that can deal with the presence of uncertainties surrounding the energy consumption of EFVs without being overly conservative. We have modeled the problem within a robust optimization framework, and we have developed a two-phase metaheuristic to solve it. We have also implemented two exact robust optimization methods that can be used to solve small instances of the problem to optimality. We have adapted existing instances to generate new

instances for the EVRP-ECU and we have run several numerical experiments on them with different types of uncertainty sets. We have shown that the solution method performs extremely well on small instances of the EVRP-ECU by comparing it to solutions obtained with the exact methods. Moreover, we have tested our heuristic on existing instances of the related RCVRP, and found 42 new best solutions in the process. Our computational study has also illustrated how the EVRP-ECU can help reach the right balance between cost and risk, and has shown the influence of different uncertain parameters and of their correlation with each other on robust solutions. We have also demonstrated the importance of taking energy consumption uncertainties into account by comparing nominal to robust solutions.

We believe that promising research avenues lie in the integration of additional features in the problem. These may include, for example, the use of other types of uncertainty sets. One natural extension could be to incorporate en route recharging into the problem to render it applicable to EVRPs in mid- and long-haul contexts. Finally, the development of new solution methods for the EVRP-ECU would be welcome in order to have more available benchmark solutions for the larger instances.

Acknowledgements

This research was partly supported by the Canadian Natural Sciences and Engineering Research Council under grants 463834-2014, 436014-2013 and 2015-06189. This support is gratefully acknowledged. Thanks are also due to Erick Delage and Fan E for their valuable feedback in the early stages of this work.

4.8. Appendix A – Detailed results for the CVRP and RCVRP benchmark instances

Table 4.14 – Results for the set A of CVRP instances from Augerat (1995) and the associated RCVRP instances from Gounaris et al. (2013)

	CVRP					RCVRP-UI_Q^1					RCVRP-UI_Q^2				
Instance	BFS	Avg.	Time (s)	BKS	G (%)	BFS	Avg.	Time (s)	BKS	G (%)	BFS	Avg.	Time (s)	BKS	G (%)
A-n32-k05	784	784.00	18.13	784*	0.00	748	748.00	24.39	748*	0.00	748	748.00	29.25	748*	0.00
A-n33-k05	661	661.00	16.42	661*	0.00	642	642.00	19.57	642*	0.00	631	631.00	20.46	631*	0.00
A-n33-k06	742	742.00	15.30	742*	0.00	717	717.00	17.84	717*	0.00	710	710.00	18.71	710*	0.00
A-n34-k05	778	778.00	17.81	778*	0.00	715	716.50	18.87	715*	0.00	702	702.00	20.43	702*	0.00
A-n36-k05	799	799.00	26.97	799*	0.00	755	755.00	29.99	755*	0.00	766	767.80	38.75	766*	0.00
A-n37-k05	669	669.00	24.15	669*	0.00	650	650.00	31.69	650*	0.00	648	648.00	42.71	648*	0.00
A-n37-k06	949	949.00	23.50	949*	0.00	892	892.00	25.86	892*	0.00	892	892.00	28.72	892*	0.00
A-n38-k05	730	730.00	23.20	730*	0.00	704	705.60	29.54	704*	0.00	693	693.00	31.37	693*	0.00
A-n39-k05	822	822.00	27.43	822*	0.00	777	789.50	35.87	777*	0.00	772	778.50	36.31	772*	0.00
A-n39-k06	831	831.20	27.32	831*	0.00	787	787.00	34.01	787*	0.00	786	786.00	39.42	786*	0.00
A-n44-k06	937	937.00	36.45	937*	0.00	909	910.60	45.08	909	0.00	892	892.00	51.34	892*	0.00
A-n45-k06	944	945.70	36.13	944*	0.00	896	897.00	42.29	896*	0.00	891	892.20	47.15	891*	0.00
A-n46-k07	914	914.00	40.56	914*	0.00	888	888.60	50.64	888*	0.00	883	883.00	57.11	883*	0.00
A-n48-k07	1073	1073.00	49.59	1073*	0.00	1033	1033.00	93.00	1033	0.00	1033	1033.00	115.74	1033	0.00
A-n53-k07	1010	1010.00	57.52	1010*	0.00	974	974.00	100.70	974	0.00	967	967.00	147.82	967*	0.00
A-n54-k07	1167	1167.00	60.73	1167*	0.00	1106	1106.50	98.77	1106	0.00	1097	1099.80	138.11	1097	0.00
A-n55-k09	1073	1073.00	60.12	1073*	0.00	1030	1030.30	74.22	1030	0.00	1007	1007.00	74.63	1007*	0.00
A-n60-k09	1354	1354.00	107.61	1354*	0.00	1280	1280.00	105.61	1280	0.00	1264	1264.20	115.34	1264	0.00
A-n61-k09	1034	1034.00	76.40	1034*	0.00	983	983.00	113.32	983	0.00	974	974.00	105.62	974	0.00
A-n62-k08	1288	1288.20	222.46	1288*	0.00	1219	1221.00	236.04	1214	0.41	1201	1202.40	275.79	1201	0.00
A-n63-k09	1616	1616.00	103.07	1616*	0.00	1505	1505.00	163.48	1505	0.00	1498	1501.40	237.72	1498	0.00
A-n63-k10	1314	1315.50	112.22	1314*	0.00	**1236**	1237.60	94.07	1240	0.00	1222	1222.20	95.33	1222	0.00
A-n64-k09	1401	1401.50	135.76	1401*	0.00	1325	1326.00	137.09	1325	0.00	1314	1314.00	153.51	1314	0.00
A-n65-k09	1174	1175.50	77.02	1174*	0.00	1106	1106.00	111.98	1106	0.00	1094	1094.00	108.32	1094*	0.00
A-n69-k09	1159	1159.00	120.38	1159*	0.00	1109	1109.50	143.05	1109	0.00	1096	1096.00	139.88	1096	0.00
A-n80-k10	1763	1764.10	299.82	1763*	0.00	1662	1669.10	194.22	1662	0.00	**1644**	1650.90	222.99	1645	0.00

Table 4.15 – Results for the set B of CVRP instances from Augerat (1995) and the associated RCVRP instances from Gounaris et al. (2013)

	CVRP					RCVRP-U_Q^1					RCVRP-U_Q^2				
Instance	BFS	Avg.	Time (s)	BKS	G (%)	BFS	Avg.	Time (s)	BKS	G (%)	BFS	Avg.	Time (s)	BKS	G (%)
B-n31-k05	672	672.00	15.63	672*	0.00	651	651.00	20.25	651*	0.00	651	651.00	22.71	651*	0.00
B-n34-k05	788	788.00	19.34	788*	0.00	768	768.00	20.41	768	0.00	748*	752.90	21.68	748	0.00
B-n35-k05	955	955.00	18.86	955*	0.00	883	883.00	20.81	883*	0.00	883	883.10	22.51	883*	0.00
B-n38-k06	805	805.00	33.08	805*	0.00	729	729.00	26.62	729*	0.00	729	729.00	28.86	729*	0.00
B-n39-k05	549	549.00	29.04	549*	0.00	532	535.60	51.36	532*	0.00	529	532.00	57.80	529*	0.00
B-n41-k06	829	829.00	32.76	829*	0.00	796	796.20	59.78	796*	0.00	791	791.00	72.95	791*	0.00
B-n43-k06	742	742.00	55.94	742*	0.00	681	681.00	51.22	681*	0.00	680	680.00	63.62	680*	0.00
B-n44-k07	909	909.00	48.35	909*	0.00	835	835.00	49.19	835*	0.00	835	835.00	61.49	835*	0.00
B-n45-k05	751	751.00	37.07	751*	0.00	701	701.00	66.95	701	0.00	680	682.90	67.75	680*	0.00
B-n45-k06	678	678.00	38.78	678*	0.00	660	660.00	294.60	660*	0.00	657	657.40	344.46	657*	0.00
B-n50-k07	741	741.00	48.82	741*	0.00	679	679.00	54.88	679*	0.00	699	699.00	64.72	699*	0.00
B-n50-k08	1312	1312.50	138.91	1312*	0.00	1224	1224.80	142.06	1224	0.00	1217	1217.50	312.81	1217	0.00
B-n51-k07	1032	1032.00	63.58	1032*	0.00	962	964.00	47.99	961	0.10	928	928.00	48.62	928*	0.00
B-n52-k07	747	747.00	176.35	747*	0.00	675	675.00	60.89	675*	0.00	670	670.00	65.35	670*	0.00
B-n56-k07	707	708.50	372.55	707*	0.00	623	623.00	88.31	623*	0.00	623	623.00	105.00	623*	0.00
B-n57-k07	1153	1156.50	64.56	1153*	0.00	1055	1055.00	77.57	1055	0.00	1052	1053.10	80.85	1052	0.00
B-n57-k09	1598	1598.00	82.23	1598*	0.00	1555	1557.20	179.84	1540*	0.96	1539	1540.00	101.63	1539*	0.00
B-n63-k10	1496	1496.00	91.53	1496*	0.00	1407	1407.00	95.74	1407	0.00	1405	1405.00	119.60	1405	0.00
B-n64-k09	861	861.00	83.43	861*	0.00	803	803.00	94.89	803*	0.00	803	803.00	115.02	803*	0.00
B-n66-k09	1316	1316.80	376.44	1316*	0.00	1251	1256.50	430.13	1251	0.00	1210*	1210.00	201.57	1210	0.00
B-n67-k10	1032	1032.00	119.55	1032*	0.00	1007	1007.40	137.82	1007	0.00	1001	1001.90	169.39	1001	0.00
B-n68-k09	1272	1273.20	407.20	1272*	0.00	**1205**	1214.80	428.27	1213	0.00	1191	1195.20	398.65	1191	0.00
B-n78-k10	1221	1226.60	465.87	1221*	0.00	1131	1131.60	199.20	1131	0.00	1130	1130.60	241.24	1130	0.00

Table 4.16 – Results for the set P of CVRP instances from Augerat (1995) and the associated RCVRP instances from Gounaris et al. (2013)

	CVRP					RCVRP-U_Q^1					RCVRP-U_Q^2				
Instance	BFS	Avg.	Time (s)	BKS	G (%)	BFS	Avg.	Time (s)	BKS	G (%)	BFS	Avg.	Time (s)	BKS	G (%)
P-n16-k08	450	450.00	2.11	450*	0.00	439	439.00	3.05	439*	0.00	439	439.00	2.92	439*	0.00
P-n19-k02	212	212.00	3.68	212*	0.00	195	195.00	5.94	195*	0.00	195	195.00	7.00	195*	0.00
P-n20-k02	216	216.00	5.04	216*	0.00	208	208.00	7.20	208*	0.00	208	208.00	8.27	208*	0.00
P-n21-k02	211	211.00	6.38	211*	0.00	208	208.00	9.12	208*	0.00	208	208.00	10.78	208*	0.00
P-n22-k02	216	216.00	6.54	216*	0.00	213	213.00	9.66	213*	0.00	213	213.00	11.59	213*	0.00
P-n22-k08	603	603.00	5.38	603*	0.00	537	537.00	5.72	537*	0.00	557	557.00	5.48	557*	0.00
P-n23-k08	529	529.00	4.96	529*	0.00	504	504.00	7.84	504	0.00	503	503.00	7.37	503	0.00
P-n40-k05	458	458.00	23.46	458*	0.00	447	447.00	28.87	447*	0.00	447	447.00	33.41	447*	0.00
P-n45-k05	510	510.00	34.36	510*	0.00	501	501.30	35.76	501*	0.00	494	494.40	42.63	494*	0.00
P-n50-k07	554	554.00	42.62	554*	0.00	539	539.80	59.89	539	0.00	537	537.10	67.53	537	0.00
P-n50-k08	631	633.40	42.48	631*	0.00	592	592.00	45.14	592	0.00	588	588.00	45.70	588	0.00
P-n50-k10	696	696.00	38.75	696*	0.00	656	656.00	48.14	656	0.00	656	656.00	47.51	656	0.00
P-n51-k10	741	741.00	44.22	741*	0.00	707	707.00	52.59	707	0.00	698	698.00	53.04	698	0.00
P-n55-k07	568	568.00	61.94	568*	0.00	549	549.00	79.96	549	0.00	544	544.40	83.43	544*	0.00
P-n55-k08	588	588.00	59.38	588*	0.00	572	572.00	73.71	572	0.00	568	568.10	81.79	568	0.00
P-n55-k10	694	694.00	58.61	694*	0.00	670	670.00	62.56	670	0.00	657	657.00	61.14	657	0.00
P-n55-k15	989	989.00	45.24	989*	0.00	889	889.00	54.61	889	0.00	877	877.00	51.38	877	0.00
P-n60-k10	744	744.00	62.99	744*	0.00	712	712.00	71.52	712	0.00	705	705.00	73.46	705	0.00
P-n60-k15	968	968.00	58.72	968*	0.00	931	931.00	74.77	931	0.00	916	916.00	72.09	916	0.00
P-n65-k10	792	792.00	83.20	792*	0.00	765	765.20	85.78	765	0.00	761	761.50	90.67	761	0.00
P-n70-k10	827	827.00	104.02	827*	0.00	785	785.10	134.14	797	0.00	783	783.70	132.73	783	0.00
P-n76-k04	593	593.70	147.57	593*	0.00	590	590.00	248.04	590*	0.00	590	590.00	290.54	590*	0.00
P-n76-k05	627	627.30	136.09	627*	0.00	616	616.00	223.48	616	0.00	615	615.00	263.13	615	0.00
P-n101-k04	681	681.00	284.68	681*	0.00	673	673.00	240.19	673*	0.00	673	673.00	274.40	673*	0.00

Table 4.17 – Results for the sets E, M, and F of CVRP instances and the associated RCVRP instances from Gounaris et al. (2013)

	CVRP					RCVRP-U_Q^1					RCVRP-U_Q^2				
Instance	BFS	Avg.	Time (s)	BKS	G (%)	BFS	Avg.	Time (s)	BKS	G (%)	BFS	Avg.	Time (s)	BKS	G (%)
E-n22-k04	375	375.00	5.66	375*	0.00	373	373.00	8.45	373*	0.00	373	373.00	8.46	373*	0.00
E-n23-k03	569	569.00	11.42	569*	0.00	563	563.00	16.72	563*	0.00	544	544.00	16.75	544*	0.00
E-n30-k03	534	534.00	16.43	534*	0.00	475	475.00	18.79	475*	0.00	492	492.00	19.06	492*	0.00
E-n33-k04	835	835.00	22.22	835*	0.00	814	814.00	44.44	814*	0.00	814	814.00	38.15	814*	0.00
E-n51-k05	521	521.00	46.95	521*	0.00	516	516.00	70.48	516*	0.00	516	516.00	83.10	516*	0.00
E-n76-k07	682	682.00	168.33	682*	0.00	661	661.00	226.48	661	0.00	661	661.00	236.24	661	0.00
E-n76-k08	735	735.50	143.76	735*	0.00	709	709.70	173.48	709	0.00	700	700.00	185.40	700	0.00
E-n76-k10	830	830.20	137.28	830*	0.00	796	796.10	165.91	796	0.00	782	782.00	170.14	782	0.00
E-n76-k14	1021	1021.00	128.38	1021*	0.00	952	952.00	132.49	952	0.00	952	952.00	136.84	952	0.00
E-n101-k08	815	816.20	296.91	815*	0.00	789	789.30	229.77	789	0.00	783	784.50	213.22	783	0.00
E-n101-k14	1067	1068.70	385.58	1067*	0.00	1011	1011.10	246.24	1011	0.00	1009	1009.00	234.23	1009	0.00
F-n45-k04	724	724.40	58.20	724*	0.00	718	718.50	73.17	718*	0.00	714	714.80	77.75	714*	0.00
F-n72-k04	237	237.00	180.88	237*	0.00	232	232.00	205.54	232*	0.00	232	232.00	210.91	232*	0.00
F-n135-k07	1162	1162.00	464.69	1162*	0.00	1136	1144.50	696.67	1129	0.62	1086	1087.20	440.14	1086	0.00
M-n101-k10	820	820.00	113.01	820*	0.00	809	809.10	186.06	809*	0.00	804	804.80	186.25	804*	0.00
M-n121-k07	1034	1043.90	147.03	1034*	0.00	1001	1027.00	862.91	994	0.70	990	994.00	550.74	982	0.81
M-n151-k12	1015	1024.00	983.11	1015*	0.00	**989**	994.10	1077.24	993	0.00	**971**	982.90	907.54	986	0.00

Table 4.18 – Results for the Christofides et al. (1979) and Golden et al. (1998) CVRP instances and the associated RCVRP instances from Gounaris et al. (2016)

		CVRP					RCVRP-U_Q^1					RCVRP-U_Q^2				
Instance	n	BFS	Avg.	Time (s)	BKS	G (%)	BFS	Avg.	Time (s)	BKS	G (%)	BFS	Avg.	Time (s)	BKS	G (%)
C1	50	524.61	524.61	43.65	524.61*	0.00	519.43	519.43	71.87	519.43	0.00	519.43	519.43	94.84	519.43	0.00
C2	75	835.26	835.26	152.82	835.26*	0.00	**799.05**	799.42	205.03	807.15	0.00	785.86	785.86	192.69	785.86	0.00
C3	100	826.14	826.77	322.33	826.14*	0.00	**801.29**	802.35	274.89	803.33	0.00	794.52	796.23	232.52	794.52	0.00
C4	150	1030.83	1032.22	1368.24	1028.42*	0.23	**997.33**	1008.01	1291.08	1012.80	0.00	**982.36**	987.38	880.97	1006.33	0.00
C5	199	1295.99	1311.80	1575.52	1291.29*	0.36	**1251.29**	1262.35	1305.09	1254.38	0.00	**1236.42**	1243.71	1245.61	1243.27	0.00
C6	50	555.43	555.43	48.04	555.43	0.00	555.43	555.43	70.79	555.43	0.00	555.43	555.43	66.87	555.43	0.00
C7	75	909.68	909.68	126.95	909.68	0.00	902.01	902.01	167.77	902.01	0.00	**900.12**	901.02	182.46	901.40	0.00
C8	100	865.94	865.94	447.79	865.94	0.00	865.50	865.50	914.11	865.50	0.00	865.50	865.50	912.79	865.50	0.00
C9	150	1163.85	1165.81	1549.10	1162.55	0.11	**1161.85**	1164.51	1671.63	1167.06	0.00	**1163.48**	1165.74	1651.34	1163.81	0.00
C10	199	1408.23	1412.73	2728.72	1395.85	0.88	**1389.07**	1397.92	3138.75	1412.10	0.00	**1387.00**	1397.01	2853.88	1410.65	0.00
C11	120	1042.12	1047.95	188.04	1042.11*	0.00	1005.92	1007.23	852.08	1005.10	0.08	1000.35	1002.73	782.37	994.63	0.57
C12	100	819.56	819.56	124.34	819.56*	0.00	808.90	809.45	218.83	808.90	0.00	804.08	804.19	218.13	804.08	0.00
C13	120	1546.76	1555.54	1315.67	1541.14	0.36	**1545.96**	1559.92	1383.64	1547.06	0.00	**1542.86**	1556.15	1250.93	1544.90	0.00
C14	100	866.37	866.37	381.22	866.37	0.00	847.43	847.46	455.82	847.43	0.00	835.11	835.11	338.51	835.11	0.00
G1	240	5644.44	5669.78	2860.50	5623.47	0.37	**5618.59**	5634.48	3291.12	5694.68	0.00	**5636.22**	5637.04	3220.34	5698.06	0.00
G2	320	8447.92	8452.06	3315.92	8404.61	0.51	**8447.92**	8450.64	3638.16	8557.12	0.00	**8447.92**	8452.56	3779.75	8544.31	0.00
G3	400	11036.22	11051.80	5578.05	11036.22	0.00	**11036.22**	11047.30	5279.53	11362.36	0.00	**11036.22**	11072.00	5581.29	11423.06	0.00
G4	480	13624.53	13648.90	6698.06	13592.88	0.23	**13624.52**	13625.60	7729.72	14134.17	0.00	**13624.53**	13630.60	7774.88	13975.76	0.00
G5	200	6460.98	6460.98	965.03	6460.98	0.00	**6460.98**	6460.98	1083.11	6466.68	0.00	6460.98	6462.12	1311.87	6460.98	0.00
G6	280	8412.90	8412.95	2767.71	8404.26	0.10	**8412.90**	8412.99	3306.22	8414.28	0.00	**8412.67**	8412.88	3646.73	8415.21	0.00
G7	360	10195.59	10195.59	3901.31	10102.68	0.91	**10195.59**	10195.59	4202.26	10266.87	0.00	**10195.59**	10197.2	4054.57	10203.57	0.00
G8	440	11828.78	11835.70	8370.14	11635.34	1.64	**11744.95**	11840.40	7155.05	12078.23	0.00	**11727.83**	11817.9	7410.79	12074.27	0.00
G9	255	588.58	590.50	1831.82	579.71	1.51	572.63	575.79	1098.56	570.63	0.35	**557.86**	567.99	1334.58	562.65	0.00
G10	323	752.03	755.92	1875.66	736.26	2.10	–	–	–	736.41	–	–	–	–	724.61	–
G11	399	930.20	940.33	2183.79	912.84	1.87	–	–	–	925.88	–	–	–	–	912.17	–
G12	483	1138.07	1144.33	2707.28	1102.69	3.11	–	–	–	1181.15	–	–	–	–	1114.85	–
G13	252	862.26	871.62	1727.59	857.19	0.59	**830.95**	837.80	907.50	844.05	0.00	**825.21**	830.72	1038.67	838.49	0.00
G14	320	1101.57	1113.68	1638.26	1080.55*	1.91	**1079.85**	1089.67	1084.33	1080.59	0.00	**1060.31**	1074.00	638.75	1070.32	0.00
G15	396	1370.82	1380.98	1929.40	1337.92	2.40	1345.99	1362.28	1594.79	1341.21	0.36	**1312.29**	1334.07	1216.22	1331.96	0.00
G16	480	1674.86	1684.75	2253.96	1612.50	3.72	–	–	–	1641.95	–	**1600.30**	1611.8	2340.29	1629.12	0.00
G17	240	708.68	711.38	2076.74	707.76*	0.13	**705.89**	708.79	1747.90	713.68	0.00	**690.60**	692.90	1226.74	701.42	0.00
G18	300	1013.33	1017.71	3032.46	995.13*	1.80	–	–	–	1012.90	–	–	–	–	991.54	–
G19	360	1385.04	1395.61	2056.09	1365.60*	1.40	–	–	–	1389.32	–	–	–	–	1369.57	–
G20	420	1860.91	1902.05	2026.15	1818.32	2.29	–	–	–	1860.84	–	–	–	–	1827.02	–

References

Agra, A., M. Christiansen, R. Figueiredo, L.M. Hvattum, M. Poss, C. Requejo. 2013. The robust vehicle routing problem with time windows. *Computers & Operations Research* **40**(3) 856–866.

Asamer, J., A. Graser, B. Heilmann, M Ruthmair. 2016. Sensitivity analysis for energy demand estimation of electric vehicles. *Transportation Research Part D: Transport and Environment* **46** 182–199.

Augerat, P. 1995. Approche polyèdrale du problème de tournées de véhicules. Ph.D. thesis, Institut National Polytechnique de Grenoble, France.

Bandi, C., D. Bertsimas. 2012. Tractable stochastic analysis in high dimensions via robust optimization. *Mathematical Programming* **134**(1) 23–70.

Barth, M., T. Younglove, G. Scora. 2005. Development of a heavy-duty diesel modal emissions and fuel consumption model. Tech.rep. UCB-ITS-PRR-2005-1, California PATH Program, Institute of Transportation Studies, University of California at Berkeley.

Basso, R., B. Kulcsár, B. Egardt, P. Lindroth, I. Sanchez-Diaz. 2019. Energy consumption estimation integrated into the electric vehicle routing problem. *Transportation Research Part D: Transport and Environment* **69** 141–167.

Bektaş, T., G. Laporte. 2011. The pollution-routing problem. *Transportation Research Part B: Methodological* **45**(8) 1232–1250.

Ben-Tal, A., L. El Ghaoui, A. Nemirovski. 2009. *Robust Optimization*. Princeton Series in Applied Mathematics (Princeton University Press, Princeton, NJ).

Bertsimas, D., I. Dunning, M. Lubin. 2016. Reformulation versus cutting-planes for robust optimization: A computational study. *Computational Management Science* **13**(2) 195–217.

Bertsimas, D., V. Gupta, N. Kallus. 2018. Data-driven robust optimization. *Mathematical Programming* **167**(2) 235–292.

Bingham, C., C. Walsh, S. Carroll. 2012. Impact of driving characteristics on electric vehicle energy consumption and range. *IET Intelligent Transport Systems* **6**(1) 29–35.

Braaten, S., O. Gjønnes, L.M. Hvattum, G. Tirado. 2017. Heuristics for the robust vehicle routing problem with time windows. *Expert Systems with Applications* **77** 136–147.

Christofides, N., S. Eilon. 1969. An algorithm for the vehicle-dispatching problem. *Journal of the Operational Research Society* **20**(3) 309–318.

Christofides, N., A. Mingozzi, P. Toth. 1979. The vehicle routing problem. N. Christofides, A. Mingozzi, P. Toth, C. Sandi, eds., *Combinatorial Optimization* (Wiley, Chichester, UK), 315–338.

Clarke, G., J.W. Wright. 1964. Scheduling of vehicles from a central depot to a number of delivery points. *Operations Research* **12**(4) 568–581.

Conrad, R.G., M.A. Figliozzi. 2011. The recharging vehicle routing problem. T. Doolen, E. Van Aken, eds., *Proceedings of the 2011 Industrial Engineering Research Conference* (Institute of Industrial Engineers, Norcross, GA), 2785–2792.

Davis, B.A., M.A. Figliozzi. 2013. A methodology to evaluate the competitiveness of electric delivery trucks. *Transportation Research Part E: Logistics and Transportation Review* **49**(1) 8–23.

Demir, E., T. Bektaş, G. Laporte. 2012. An adaptive large neighborhood search heuristic for the pollution-routing problem. *European Journal of Operational Research* **223**(2) 346–359.

E-Mobility NSR. 2013. Comparative analysis of European examples of schemes for freight electric vehicles – Compilation report. URL `http://e-mobility-nsr.eu/fileadmin/user_upload/downloads/info-pool/E-Mobility_-_Final_report_7.3.pdf`. Last accessed January 2019.

El Ghaoui, L., M. Oks, F. Oustry. 2003. Worst-case value-at-risk and robust portfolio optimization: A conic programming approach. *Operations Research* **51**(4) 543–556.

Felipe, Á., M.T. Ortuño, G. Righini, G. Tirado. 2014. A heuristic approach for the green vehicle routing problem with multiple technologies and partial recharges. *Transportation Research Part E: Logistics and Transportation Review* **71** 111–128.

Feng, W., M. Figliozzi. 2013. An economic and technological analysis of the key factors affecting the competitiveness of electric commercial vehicles: A case study from the USA market. *Transportation Research Part C: Emerging Technologies* **26** 135–145.

Fisher, M. 1994. Optimal solution of vehicle routing problems using minimum K-trees. *Operations Research* **42**(4) 626–642.

Fontana, M.W. 2013. Optimal routes for electric vehicles facing uncertainty, congestion, and energy constraints. Ph.D. thesis, Massachusetts Institute of Technology, Massachusetts.

Gendreau, M., O. Jabali, W. Rei. 2016. 50th anniversary invited article: Future research directions in stochastic vehicle routing. *Transportation Science* **50**(4) 1163–1173.

Goeke, D., M. Schneider. 2015. Routing a mixed fleet of electric and conventional vehicles. *European Journal of Operational Research* **245**(1) 81–99.

Golden, B.L., E.A. Wasil, J.P. Kelly, I-M. Chao. 1998. The impact of metaheuristics on solving the vehicle routing problem: Algorithms, problem sets, and computational results. T.G. Crainic, G. Laporte, eds., *Fleet Management and Logistics* (Kluwer Academic Publishers, Boston, MA), 33–56.

Gounaris, C.E., W. Wiesemann, C.A. Floudas. 2013. The robust capacitated vehicle routing problem under demand uncertainty. *Operations Research* **61**(3) 677–693.

Gounaris, C.E., P.P. Repoussis, C.D. Tarantilis, W. Wiesemann, C.A. Floudas. 2016. An adaptive memory programming framework for the robust capacitated vehicle routing problem. *Transportation Science* **50**(4) 1239–1260.

Hiermann, G., R.F. Hartl, J. Puchinger, T. Vidal. 2019. Routing a mix of conventional, plug-in hybrid, and electric vehicles. *European Journal of Operational Research* **272**(1) 235–248.

Hiermann, G., J. Puchinger, S. Ropke, R.F. Hartl. 2016. The electric fleet size and mix vehicle routing problem with time windows and recharging stations. *European Journal of Operational Research* **252**(3) 995–1018.

Hu, C., J. Lu, X. Liu, G. Zhang. 2018. Robust vehicle routing problem with hard time windows under demand and travel time uncertainty. *Computers & Operations Research* **94** 139–153.

Ilyina, A. 2017. Combinatorial optimization under ellipsoidal uncertainty. Ph.D. thesis, Technical University of Dortmund, Germany.

Jabali, O., T. Van Woensel, A.G. de Kok. 2012. Analysis of travel times and CO2 emissions in time-dependent vehicle routing. *Production and Operations Management* **21**(6) 1060–1074.

Jalilvand-Nejad, A., R. Shafaei, H. Shahriar. 2016. Robust optimization under correlated polyhedral uncertainty set. *Computers & Industrial Engineering* **92** 82–94.

Laporte, G., F.V. Louveaux. 1993. The integer L-shaped method for stochastic integer programs with complete recourse. *Operations Research Letters* **13** 133–142.

Lebeau, P., C. De Cauwer, J. Van Mierlo, C. Macharis, W. Verbeke, T. Coosemans. 2015. Conventional, hybrid, or electric vehicles: Which technology for an urban distribution centre? *The Scientific World Journal*, Article ID 302867.

Lee, C., K. Lee, S. Park. 2012. Robust vehicle routing problem with deadlines and travel time/demand uncertainty. *Journal of the Operational Research Society* **63**(9) 1294–1306.

Lee, D.Y., V.M. Thomas, M.A. Brown. 2013. Electric urban delivery trucks: Energy use, greenhouse gas emissions, and cost-effectiveness. *Environmental Science & Technology* **47**(14) 8022–8030.

Lunz, B., Z. Yan, J.B. Gerschler, D.U. Sauer. 2012. Influence of plug-in hybrid electric vehicle charging strategies on charging and battery degradation costs. *Energy Policy* **46** 511–519.

Mendoza, J.E., L-M. Rousseau, J.G. Villegas. 2016. A hybrid metaheuristic for the vehicle routing problem with stochastic demand and duration constraints. *Journal of Heuristics* **22**(4) 539–566.

Mendoza, J.E., J.G. Villegas. 2013. A multi-space sampling heuristic for the vehicle routing problem with stochastic demands. *Optimization Letters* **17**(7) 1503–1516.

Montoya, A., C. Guéret, J.E. Mendoza, J.G. Villegas. 2016. A modified multi space sampling heuristic for the green vehicle routing problem. *Transportation Research Part C: Emerging Technologies* **70** 113–128.

Montoya, A., C. Guéret, J.E. Mendoza, J.G. Villegas. 2017. The electric vehicle routing problem with nonlinear charging function. *Transportation Research Part B: Methodological* **103** 87–110.

Morganti, E., M. Browne. 2018. Technical and operational obstacles to the adoption of electric vans in France and the UK: An operator perspective. *Transport Policy* **63** 90–97.

Naberezhnykh, D., J. Wardle, J. Lowes, C. Herron, T. Brightman, T. Parker. 2012. Electric vehicle charging points for freight vehicles in central London (Version – Final 1.0). Prepared for Central London FQP by Transport & Travel Research Ltd, in partnership with TRL and Zero Carbon Futures. URL `http://www.centrallondonfqp.org/app/download/12240926/CLFQP_EVCP_strategy+report_Final+v1+0.pdf`. Last accessed January 2019.

Pelletier, S., O. Jabali, G. Laporte. 2016. 50th anniversary invited article – Goods distribution with electric vehicles: Review and research perspectives. *Transportation Science* **50**(1) 3–22.

Pelletier, S., O. Jabali, G. Laporte. 2018. Charge scheduling for electric freight vehicles. *Transportation Research Part B: Methodological* **115** 246–269.

Pelletier, S., O. Jabali, G. Laporte, M. Veneroni. 2017. Battery degradation and behaviour for electric vehicles: Review and numerical analyses of several models. *Transportation Research Part B: Methodological* **103** 158–187.

Poss, M. 2013. Robust combinatorial optimization with variable budgeted uncertainty. *4OR* **11**(1) 75–92.

Potvin, J.-Y., J.-M. Rousseau. 1995. An exchange heuristic for routeing problems with time windows. *Journal of the Operational Research Society* **46**(12) 1433–1446.

Preis, H., S. Frank, K. Nachtigall. 2014. Energy-optimized routing of electric vehicles in urban delivery systems. S. Helber, M. Breitner, D. Rösch, C. Schön, J-M.

Graf von der Schulenburg, P. Sibbertsen, M. Steinbach, S. Weber, A. Wolter, eds., *Operations Research Proceedings 2012* (Springer International Publishing, Switzerland), 583–588.

Quak, H., R. Koffrie, T. van Rooijen, N. Nesterova. 2017. Project FREVUE deliverable D3.2: Economics of electric vehicles for city logistics. TNO. European Commission Seventh Framework Programme.

Ropke, S., D. Pisinger. 2006 An adaptive large neighborhood search heuristic for the pickup and delivery problem with time windows. *Transportation Science* **40**(4) 455–472.

Schiffer, M., G. Walther. 2017. The electric location routing problem with time windows and partial recharging. *European Journal of Operational Research* **260**(3) 995–1013.

Schiffer, M., G. Walther. 2018. Strategic planning of electric logistics networks: A robust location routing approach. *Omega* **80** 31–42.

Schneider, M., A. Stenger, D. Goeke. 2014. The electric vehicle-routing problem with time windows and recharging stations. *Transportation Science* **48**(4) 500–520.

Shaw, P. 1998. Using constraint programming and local search methods to solve vehicle routing problems. M. Maher, J-F. Puget, eds., *Proceedings of the 4th International Conference on Principles and Practice of Constraint Programming*. Lecture Notes in Computer Science, Vol. 1520 (Springer-Verlag, Berlin Heidelberg), 417–431.

Sungur, I., F. Ordóñez, M. Dessouky. 2008. A robust optimization approach for the capacitated vehicle routing problem with demand uncertainty. *IIE Transactions* **40**(5) 509–523.

Tretvik, T., I. Roche Cerasi, E. Dahl. 2017. Project FREVUE deliverable D3.1: Technical suitability of EVs for logistics. SINTEF. European Commission Seventh Framework Programme.

Yi, Z., P.H. Bauer. 2017 Effects of environmental factors on electric vehicle energy consumption: A sensitivity analysis. *IET Electrical Systems in Transportation* **7**(1) 3–13.

Yuan, Y., Z. Li, B. Huang. 2016. Robust optimization under correlated uncertainty: Formulations and computational study. *Computers & Chemical Engineering* **85** 58–71.

Chapter 5

The electric fleet transition problem

Chapter information

This chapter is the result of a collaboration with my thesis advisors and Professor Jorge E. Mendoza. An article based on its contents was submitted to *Transportation Research Part C: Emerging Technologies* in June 2019: S. Pelletier, O. Jabali, J.E. Mendoza, G. Laporte. 2019. The electric bus fleet transition problem. Under second round review for publication in *Transportation Research Part C: Emerging Technologies*.

Abstract

The incorporation of electric vehicles in vehicle fleets has become a topical issue in recent years. Several companies and municipalities, either voluntarily or to comply with legal requirements, will transition to greener fleets in the next decades. Such transitions are often established by fleet electrification targets, which dictate the number of electric vehicles that should be in the fleet by a given time period. In this research we introduce optimization-based decision making

tools to support such transitions. More precisely, we present a fleet replacement problem which allows organizations to determine vehicle replacement plans that will respect their fleet electrification targets in a cost-effective way, namely considering purchase costs, salvage revenues, operating costs, charging infrastructure investments, and demand charges. We refer to this problem as the electric fleet transition problem, and we model its deterministic and its stochastic versions as an integer and a mixed integer linear program, respectively. We conduct several computational experiments based on real data provided by a public transit agency in order to draw insights regarding optimal transition plans.

Keywords: electric vehicles; fleet replacement; integer programming; stochastic optimization.

5.1. Introduction

In order to improve air quality in metropolitan areas, several companies and municipalities, either voluntarily or to comply with legal requirements, will need to transition to greener fleets in the upcoming years (see, e.g., The Climate Group, 2018; Bloomberg New Energy Finance, 2018; Avere-France, 2017). In the last decade, battery price reductions and performance improvements have led electric vehicles (EVs) to emerge as likely candidates to be used as a means of reducing local air and noise pollution. The latter is true in both goods distribution and public transportation contexts. Several organizations have therefore set specific fleet electrification targets that should be met in the next decade or two. For example, the cities of Paris and Los Angeles aim to operate only electric buses by 2025 and 2030, respectively (Bloomberg New Energy Finance, 2018). In France, 50% and 100% of newly purchased buses will need to be low-emission vehicles as of 2020 and 2025, respectively, for municipalities operating at least 20 buses

(Avere-France, 2017). London and Mexico City have also committed to purchasing only zero-emission buses by 2025 (Bloomberg New Energy Finance, 2018). In the province of Québec, the cities of Laval and Montreal plan to purchase only electric buses by 2023 and 2025, respectively (Montreal Gazette, 2018). Amazon, Deutsche Post DHL Group, METRO AG, and Nippon Telegraph and Telephone Corporation are all examples of companies having set ambitious electrification targets that often dictate the proportion of the fleet that should consist of EVs by a given year (The Climate Group, 2018; CNBC, 2019). However, determining how to attain such fleet electrification targets is by no means a simple task, and we believe this complexity is mainly due to two interrelated issues.

The first issue concerns the timing of EV purchases. Battery prices have been continuously falling in the last decade, while their specific energy (which directly impacts EV driving ranges) and lifetimes have been steadily improving. This could be an incentive to wait as long as possible before making significant EV purchases in order to benefit from lower EV purchase costs (which include the battery cost), and to avoid missing out on further technological improvements. On the other hand, energy and maintenance costs of EVs are already known to yield significant savings over their diesel counterparts, and such savings may well be amplified in the near future if fossil fuel prices are subject to unexpected hikes. There could therefore also be some value in immediately starting to incorporate EVs into one's fleet. Because future battery prices, technological improvements and fossil fuel prices are difficult to predict and subject to a fair amount of uncertainty, weighing these trade-offs against each other is not straightforward.

The second issue concerns the selection of the type of EVs to purchase. Consider the case of a public transit organization looking to purchase electric buses. Should the organization purchase electric buses with large batteries that do not require being recharged en route, or electric buses with smaller batteries that do? The large battery alternative avoids costly investments associated with en route

charging infrastructure, but will adversely affect the purchase cost of the vehicles and the number of passengers they can carry (and hence which lines the buses can serve). Moreover, having to charge large batteries at a depot overnight with slower charging equipment may reduce the time during which the vehicles can be operated each day. The small battery alternative of course has all the opposite pros and cons: smaller purchase costs, larger payloads and less time-related constraints due to depot charging, but a need for en route charging infrastructure investments. Furthermore, if one chooses the small battery alternative for the above advantages, one must then decide which kind of en route charging infrastructure should be installed. Typical alternatives for en route recharging of electric buses include fast plug-in stations, overhead pantograph chargers, and inductive (wireless) chargers, but each of these options has its own set of desirable and less desirable characteristics (Bloomberg New Energy Finance, 2018).

The scientific aim of this paper is to deal with the aforementioned complexities by introducing optimization-based decision making tools that offer some strategic guidance to organizations having set electrification targets in the next decades. More precisely, we model a fleet replacement problem whose resolution provides a transition plan that will respect such targets in a cost-effective way. We refer to this problem as the electric fleet transition problem (EFTP). With this goal in mind, Section 5.2 provides a short review of the literature related to fleet replacement problems associated with EVs. Sections 5.3 and 5.4 introduce the EFTP in its deterministic and stochastic forms. Section 5.5 presents extensive computational experiments based on data provided by a public transit agency, and managerial insights are derived from the results. Finally, the paper closes with conclusions in Section 5.6.

5.2. Literature review

Due to the potential societal benefits associated with EVs, several researchers have introduced and studied optimization problems involving their use in vehicle fleets. The main transportation science literature on fleet EVs concerns vehicle routing problems, fleet size and mix problems, optimal path problems, charging infrastructure design problems, depot charge scheduling problems, and fleet replacement problems (Pelletier et al., 2016, 2018; Bektaş et al., 2018). The latter involve decisions regarding purchasing (and potentially salvaging) or leasing of fleet vehicles that must be made over the course of a planning horizon. Such fleet replacement problems are closely related to classical equipment replacement problems, in which a sequence of replacement decisions must be made regarding a machine or an asset based on trade-offs between operating costs, maintenance costs, salvage revenues, purchase costs and rewards generated by the equipment (Aronson and Aronofsky, 1983). Evaluating such trade-offs is particularly complex in the case of parallel replacement problems (as is the case for the EFTP). In these problems, replacement decisions must be simultaneously made for several assets that possess some kind of economic interdependence, prohibiting one from making such decisions for each asset separately, e.g., a joint demand to satisfy, a fixed cost incurred whenever a purchase is made (regardless of how many assets are involved), or a total purchasing budget to respect (Karabakal et al., 1994). The remainder of this section focuses on the existing fleet replacement studies that are most related to the problem studied in this paper, i.e., those involving EVs or low-emission vehicles.

Feng and Figliozzi (2013) developed a deterministic fleet replacement model for fleets with electric and diesel trucks in which vehicles can be purchased and resold on a yearly basis. The objective is to minimize the discounted sum of all costs over a planning horizon of 30 years, while satisfying each year's travel

demand in miles. The authors investigated several scenarios with varying vehicle use rates and fuel efficiencies for diesel vehicles. Optimal solutions obtained with a commercial solver showed that electric trucks were only profitable in scenarios with high vehicle use rates. Feng and Figliozzi (2014) used a similar model for a case study based on data supplied by a public transit agency that had to choose between replacing their current fleet with diesel or hybrid buses.

Ahani et al. (2016) subsequently revisited the problem introduced by Feng and Figliozzi (2013), but modified the objective so as to minimize the sum of deterministic discounted total costs and the weighted variance of total costs when purchase and energy costs are assumed to follow a geometric random walk. Due to the additional risk component, the formulation becomes a mixed integer quadratic program and is solved using the SCIP solver of MATLAB's toolbox OPTI. Computational experiments indicated that due to the volatility of diesel fuel prices, EVs become more competitive as more weight is placed on risk in the objective function,

Ansaripoor et al. (2016) formulated a fleet replacement problem with hybrid, electric and conventional vehicles as a mean-risk model. Vehicles are leased rather than purchased, thus removing salvaging decisions. The objective is to minimize a weighted sum of expected costs and what the authors call the recursive expected conditional value-at-risk. The authors generate scenarios for several uncertain parameters to formulate the deterministic equivalent of the stochastic mixed integer program, which they in turn solve with CPLEX. Numerical results indicated that EVs become more utilized in high mileage scenarios, but that diesel and petrol vehicles remain the dominant choice in general over the course of the considered planning horizon (i.e., 2016–2019).

Kleindorfer et al. (2012) studied a fleet replacement problem faced by the French national postal operator La Poste, in which electric and conventional vehicles must be leased over the course of several periods under uncertain future

fuel and battery prices. Diesel prices are modeled as a Brownian motion with drift, while battery prices are stated as an Ornstein-Uhlenbeck process. Periodic demands are given in terms of a required number of vehicles. The problem is formulated as a stochastic dynamic program with the objective of minimizing the expected total costs, and the optimal policy is derived analytically.

Bakır (2017) considered a multi-period deterministic long-haul trucking context in which alternative fuel vehicles (AFVs) must be introduced in a fleet of diesel trucks. The problem consists of determining how many vehicles of each type (i.e., AFV or diesel) to purchase, salvage and assign to each route in each period, and where to open maintenance facilities for AFVs. An AFV cannot perform a given type of route during a given period if no maintenance facility has previously been opened along that route. Moreover, a minimal proportion of operations need to be performed by AFVs in each period. The problem is solved via Benders decomposition and a variable neighbourhood search heuristic.

Stasko and Gao (2010) proposed a fleet replacement model that aims to reduce emissions of a public transit organization in a cost-effective way. Purchase, retrofit, and task assignment decisions are included in the model. Retrofits may be performed on vehicles to reduce their emissions. The model also includes a term for facility upgrades that may be required at the depot for some AFVs. A case study is performed in which conventional, hybrid and compressed natural gas (CNG) buses may be purchased over the course of the planning horizon. The model was solved with CPLEX. Results showed that the CNG buses were the most cost-effective way to reduce emissions, and highlighted the benefit of adopting a long-term perspective when making replacement decisions.

Finally, Islam (2018) introduced a fleet replacement model for transit agencies similar to that of Feng and Figliozzi (2014), with the addition of yearly emissions constraints, an electrification target that must be met by the end of the planning horizon, and the need to make charging infrastructure investments for electric

buses. They assumed that only one type of electric bus and one type of hybrid bus may be purchased to replace the initial bus fleet, and that a depot charger is required for each EV in the fleet at all times. Yearly demands are expressed as a number of vehicles.

To the best of our knowledge, the problem we introduce in this paper is the first to simultaneously take into account temporal electrification targets, vehicle purchasing and salvaging decisions, several EV types with different charging infrastructure requirements, charger type-specific investments and demand charges, and aggregated task assignment decisions within a fleet replacement optimization framework. Moreover, we provide a stochastic formulation of the EFTP.

5.3. Deterministic problem description and formulation

The objective of this section is to introduce and formulate the deterministic version of the EFTP. We first provide a general description of the problem, and then formulate it as an integer linear program. Given a set of vehicle types $K = \{1, ..., m\}$, let $K_E \subseteq K$ denote the subset of vehicle types that are EVs. We assume that $|K_E| > 1$. We consider a planning horizon $T = \{1, \ldots, t_F\}$ of t_F periods, and a target period $t_G \in T$ at which point at least a proportion P of the fleet should consist of EVs. We assume that $t_G \leq t_F$, but that all periods $t \geq t_G$ in the planning horizon should respect the target P.

We adopt an aggregated approach to task assignment decisions similar to that of Stasko and Gao (2010) – that is, we assume that the operations in each period of the planning horizon have already been partitioned into assignment runs. Each

run is required to be performed by a single vehicle during its associated period, and possesses certain operational characteristics (e.g., typical distance and duration of daily operations, typical weight of the loads to be carried, potential vehicle types to be used, etc.). We assume that during a given period, each vehicle in the fleet must be assigned to a single run. Task assignment decisions can be further simplified (if required) by clustering the runs based on similarities of operational characteristics. Our motivation for this approach first stems from a need for realistic demand forecasting and computational tractability. As discussed by Stasko and Gao (2010), predicting the general characteristics of future daily operations may be simpler than predicting specific future routes; in addition simultaneously making fleet composition decisions and traditional vehicle scheduling or routing over a long-term planning horizon quickly becomes intractable. Second, since it is assumed that there are several EV types in K with different charging infrastructure requirements and different distance-, time- and load-related capacities, we believe it is necessary to express periodic demands in a more granular manner than as a total number of vehicles or kilometers without any form of compatibility considerations between vehicle types and the operations they will be assigned to. The aggregated approach of Stasko and Gao (2010) thus seems like an appropriate compromise between tractability and granularity to express fleet demands.

We denote by R the set of types of runs to be performed over the course of the planning horizon, and by q_{tr} the number of vehicles that need to be assigned to run type r during period $t \in T$. Note that $q_{tr} \in \{0,1\}\ \forall r \in R, t \in T$ would correspond to not performing the optional clustering of individual runs mentioned above. We assume that the compatibility between assignment runs and vehicle types is encapsulated by a binary parameter h^k_{jtr} that takes a value of 1 if and only if a vehicle of type k and age j is compatible with assignment run type r during period t. The compatibility between runs and vehicle types depends on relevant features in the specific context at hand, e.g., distance, time, load, required charg-

ing infrastructure, regulations prohibiting polluting vehicles, etc.

We assume that the set $J^k = \{0, 1, \ldots, \kappa^k + 1\}$ contains all possible ages for a vehicle of type k, with $j \in J^k$ representing an age of j periods. An age of $j = 0$ corresponds to a new vehicle, and a vehicle of type k is legally operational until it reaches an age of $\kappa^k + 1$ periods, at which point it must be salvaged. At the start of the planning horizon, the fleet consists of a_j^k vehicles of type k and age j. A maximum average vehicle age of Γ periods is imposed in the final period t_F. Let o_{jtr}^k be the total periodic operating cost incurred when a vehicle of type k is of age j at the start of period t, and executes a run of type r during period t. These operating costs account for energy and maintenance costs. Let f_t^k be the purchase cost of vehicle type k at the start of period t. We assume that only new vehicles are purchased in the model of Section 5.3.1, but this can of course be modified to account for the possibility of purchasing or leasing used vehicles as well. Let s_{jt}^k be the salvage value of a vehicle of type k and age j retired at the start of period t.

In addition to cost components related to the purchase, operation, and retirement of vehicles, we also take into account that different charging infrastructure-related costs will be incurred depending on the chosen EV types. We define set $CT = \{1, \ldots, n_c\}$ as the set of possible charger types to be used to recharge EVs in the fleet. We assume that an EV of type $k \in K_E$ must be recharged using charger types given by set $C^k \subseteq CT$. Moreover, the proportion of chargers of a given type $c \in CT$ with respect to the total number of EVs of types $\{k \in K_E | c \in C^k\}$ that are in the fleet must remain above θ^c at all times. A charger of type c costs p^c to purchase and retrieves g^c kilowatts (kW) from the grid. It is assumed that e^c chargers of type c are already owned at the start of the planning horizon.

Demand charges that are present in some electricity rate plans can also have a significant impact on operational costs of electric trucks and buses (see, e.g., Pelletier et al., 2018; Gallo et al., 2014). Such monthly fees depend on the largest registered charging power over the course of each month. We assume that there

are periodic demand charges of F \$/kW in each location where EV chargers are or can be installed, and we compute demand charges assuming all chargers at a single location will be used simultaneously at some point in each month. Due to potential power and space limitations associated with depot charging (Bloomberg New Energy Finance, 2018), we assume that charger types in set $DC \subseteq CT$ refer specifically to depot chargers, and that it must be possible to simultaneously use all depot chargers without violating a total grid restriction of G kW during each period of the planning horizon, and that no more than H depot chargers may be installed in total.

A budget b_t is available for purchases (vehicles and charging infrastructure) at the start of period t, which we assume may be increased by salvage revenues earned at the start of t. Finally, let dr be the periodic discount rate used to take into account the time-value of money, and $\beta = (1 + dr)^{-1}$ be the corresponding one-period discount factor.

5.3.1 Mathematical formulation

The decision variables used in the deterministic version of the EFTP are as follows:

- x_t^k is the number of vehicles of type k purchased at the beginning of period t,
- y_{jt}^k is the number of vehicles of type k and age j salvaged at the beginning of period t,
- z_{jt}^k is the number of available vehicles of type k and age j in period t,
- w_{jtr}^k is the number of vehicles of type k and age j assigned to run type r in period t,
- u_t^c is the number of chargers of type c purchased and installed at the start of period t, and

- v_t^c is the number of available chargers of type c during period t.

The EFTP is thus stated as the following integer linear program:

$$\text{minimize } \sum_{t\in T}\beta^{t-1}\left(\sum_{k\in K}\left(f_t^k x_t^k - \sum_{j=1}^{\kappa^k+1} s_{jt}^k y_{jt}^k + \sum_{r\in R}\sum_{j=0}^{\kappa^k} o_{jtr}^k w_{jtr}^k\right) + \sum_{c\in CT}\left(p^c u_t^c + Fg^c v_t^c\right)\right) + \sum_{k\in K}\sum_{r\in R}\sum_{j=0}^{\kappa^k-1}\sum_{i=1}^{\kappa^k-j}\beta^{t_F+i-1} o_{j+i,t_F,r}^k w_{jt_Fr}^k - \sum_{k\in K}\sum_{j=0}^{\kappa^k}\beta^{t_F+\kappa^k-j} s_{\kappa^k+1,t_F}^k z_{jt_F}^k \quad (5.1)$$

subject to

$$\sum_{k\in K_E}\sum_{j=0}^{\kappa^k} z_{jt}^k \geq P\Big(\sum_{k\in K}\sum_{j=0}^{\kappa^k} z_{jt}^k\Big) \quad t\in T | t\geq t_G \quad (5.2)$$

$$\sum_{k\in K}\sum_{j=0}^{\kappa^k} w_{jtr}^k = q_{tr} \quad r\in R, t\in T \quad (5.3)$$

$$w_{jtr}^k \leq h_{jtr}^k z_{jt}^k \quad k\in K, r\in R, t\in T, j\in J^k\backslash\{\kappa^k+1\} \quad (5.4)$$

$$\sum_{r\in R} w_{jtr}^k = z_{jt}^k \quad k\in K, t\in T, j\in J^k\backslash\{\kappa^k+1\} \quad (5.5)$$

$$x_t^k = z_{0t}^k \quad k\in K, t\in T\backslash\{1\} \quad (5.6)$$

$$x_1^k + a_0^k = z_{0,1}^k \quad k\in K \quad (5.7)$$

$$z_{jt}^k = z_{j-1,t-1}^k - y_{jt}^k \quad k\in K, t\in T\backslash\{1\}, j\in J^k\backslash\{0,\kappa^k+1\} \quad (5.8)$$

$$y_{\kappa^k+1,t}^k = z_{\kappa^k,t-1}^k \quad k\in K, t\in T\backslash\{1\} \quad (5.9)$$

$$y_{\kappa^k+1,1}^k = a_{\kappa^k+1}^k \quad k\in K \quad (5.10)$$

$$z_{j1}^k = a_j^k - y_{j1}^k \quad k\in K, j\in J^k\backslash\{0,\kappa^k+1\} \quad (5.11)$$

$$\sum_{k\in K}\Big(f_t^k x_t^k - \sum_{j=1}^{\kappa^k+1} s_{jt}^k y_{jt}^k\Big) + \sum_{c\in CT} p^c u_t^c \leq b_t \quad t\in T \quad (5.12)$$

$$v_t^c \geq \theta^c \sum_{k \in K_E | c \in C^k} \sum_{j=0}^{\kappa^k} z_{jt}^k \quad c \in CT, t \in T \tag{5.13}$$

$$\sum_{c \in DC} g^c v_t^c \leq G \quad t \in T \tag{5.14}$$

$$\sum_{c \in DC} v_t^c \leq H \quad t \in T \tag{5.15}$$

$$v_1^c = e^c + u_1^c, \quad c \in CT \tag{5.16}$$

$$v_t^c = v_{t-1}^c + u_t^c \quad t \in T \backslash \{1\}, c \in CT \tag{5.17}$$

$$\sum_{k \in K} \sum_{j=0}^{\kappa^k} j z_{jt_F}^k \leq \Gamma \sum_{k \in K} \sum_{j=0}^{\kappa^k} z_{jt_F}^k \tag{5.18}$$

$$y_{jt}^k, z_{j-1,t}^k \in \mathbb{Z}^+ \quad k \in K, t \in T, j \in J^k \backslash \{0\} \tag{5.19}$$

$$x_t^k \in \mathbb{Z}^+ \quad k \in K, t \in T \tag{5.20}$$

$$u_t^c, v_t^c \in \mathbb{Z}^+ \quad c \in CT, t \in T \tag{5.21}$$

$$w_{jtr}^k \in \mathbb{Z}^+ \quad k \in K, r \in R, t \in T, j \in J^k \backslash \{\kappa^k + 1\}. \tag{5.22}$$

The objective function (5.1) minimizes the total discounted cost of the entire transition plan, which includes discounted purchase costs, salvage revenues, operating costs, charging infrastructure investments, and demand charges. We discount costs that are gradually incurred over the course of a period (i.e., operational costs and demand charges) as if they were incurred at the start of the period. Note that β^{t-1} means β raised to the power of $t-1$, i.e., β is not indexed by periods. The last two terms of the second line in the objective function are used to mitigate end-of-horizon effects that may arise as a result of decisions being made near the end of the planning horizon without appropriately weighing

vehicles' purchase costs against their operational costs and salvage revenues (see, e.g., Grinold, 1983 for a discussion of end-of-horizon effects). The end-of-horizon mitigation terms are based on the assumption that a vehicle of type k and age j performing a run of type r in period t_F will continue doing so after the end of the planning horizon until it reaches its maximum operating age, and will then be salvaged. For the sake of simplicity the end-of-horizon mitigation terms assume that salvage values s^k_{jt} and operating costs o^k_{jtr} in periods after the end of the planning horizon remain the same as those in final period t_F, but if projections are available for periods beyond t_F then these should of course be used instead.

Contraints (5.2) ensure that the electrification target will be satisfied. The formulation above assumes that the target dictates a minimum percentage of fleet vehicles that should be EVs by year t_G, but this can be easily modified to represent other types of electrification targets as well. As discussed in the introduction of this paper, for some organizations, targets may concern newly purchased vehicles instead of available vehicles, and multiple time-varying targets may need to be met over the course of the planning horizon as well. Contraints (5.3) ensure that all runs will be assigned to vehicles. Constraints (5.4) state that the run assignments must respect compatiblities with vehicle types and ages during each period. Constraints (5.5) mean that all available vehicles of a given type and age during a given period should be assigned to runs. One could argue that the equality in constraints (5.5) should be replaced by an inequality to allow for some form of overcapacity. However, organizations would probably prefer having some control over such overcapacities (e.g., to have a specific number of spare vehicles for specific types of operations). The proposed formulation allows for such control, since one can add a specific number of "empty" runs with operating costs of zero in order to have predetermined overcapacities. Moreover, the compatibility parameters h^k_{jtr} of such "empty" runs can be used to impose specific overcapacities for different types of operations. Constraints (5.6) and (5.7)

ensure that the number of available new vehicles of each type in each period is equal to the number of vehicles of that type that were purchased at the start of that period (plus any vehicles already owned that can be considered as new for the first period). Constraints (5.8) state that the number of available vehicles of a certain type and age during a given period $t > 1$ is equal to the number of available vehicles of that type that were a period younger in $t - 1$, minus the number salvaged at the start of t. Constraints (5.9) and (5.10) force vehicles of age $\kappa^k + 1$ to be salvaged. Constraints (5.11) impose that the number of available vehicles of a given type and age during the first period be equal to the number already owned minus the number salvaged at the start of the planning horizon. Constraints (5.12) state that the amount of purchasing funds available at the start of a period is the sum of the budget and salvage revenues made at the start of that period. Constraints (5.13) ensure that the ratio of EVs to chargers for each type of charger is respected. Constraints (5.14) and (5.15) guarantee that the power and space limitations at the depot(s) are respected in each period. Constraints (5.16) and (5.17) track the number of each type of EV charger. Finally, constraints (5.18) are imposed to further mitigate end-of-horizon effects by setting the maximum average vehicle age to Γ in the final period t_F. Constraints (5.19)–(5.22) define the domain of the decision variables. Variables y^k_{jt} are not defined for $j = 0$, while z^k_{jt} and w^k_{jtr} are not for $j = \kappa^k + 1$, i.e., a brand new vehicle cannot be salvaged (but it can be operated), and a vehicle of maximal age cannot be operated (but it can be salvaged).

5.4. Stochastic formulation

Because some parameters in the EFTP are subject to a fair amount of uncertainty (e.g., future energy and battery prices), in this section we formulate a stochastic version of the EFTP that minimizes an expected discounted cost. We assume that

discretely generated scenarios may be used to appropriately represent the true underlying joint distribution of the random parameters (or at least the distribution specified by the decision maker), thereby allowing the representation of the stochastic process in discrete time as a scenario tree. Each possible state of the stochastic process therefore corresponds to a specific node in the scenario tree. Although the resulting equivalent deterministic mixed integer linear programming formulation can quickly become computationally intractable, this may not be the case if certain conditions hold, e.g., if few scenarios are required to represent the stochastic process, or the instance at hand is not too large in terms of number of vehicle types, periods and run types.

We denote by $\Omega = \{1, 2, ..., |\Omega|\}$ the set of all nodes in the tree, with node 1 being the root node. Let Ω_t denote the set of nodes that could be reached at the start of period $t \in T$. A given node in Ω_t thus corresponds to a possible realization of all uncertain parameters from the start of the planning horizon up until the start of period t. The set C_n refers to the children nodes of node $n \in \Omega$, with $C_n = \emptyset$ if $n \in \Omega_{t_F}$. Note that $n_1 \in C_{n_2}$ and $n_2 \in \Omega_t$ implies that $n_1 \in \Omega_{t+1}$. Each node $n \in \Omega \backslash \{1\}$ has exactly one parent node ω_n. Finally, let η_n denote the probability of reaching node n given that the current state is the root node of the tree.

We assume that operating costs o^k_{jtr} and purchase costs f^k_t are random variables in the stochastic version of the EFTP because of the uncertainty surrounding future energy and battery prices. Therefore, in the stochastic formulation we use the notation o^k_{jnr} and f^k_n to refer to operating and purchase costs, respectively, at node n. We use the same notation as in the deterministic model from Section 5.3.1 for all other parameters. All decision variables from the deterministic formulation are also indexed by node n rather than by time period t in the stochastic formulation. The only new decision variables in the stochastic formulation are Q_n, which represent the total discounted costs incurred since the start

of the planning horizon up until the end of period t (but before the start of period $t+1$) when the state is n at the start of period t. The stochastic counterpart of the EFTP is thus stated as the following mixed integer linear program:

$$\text{minimize} \quad \sum_{n \in \Omega_{t_F}} \eta_n Q_n \tag{5.23}$$

subject to

$$\sum_{k \in K_E} \sum_{j=0}^{\kappa^k} z_{jn}^k \geq P\left(\sum_{k \in K} \sum_{j=0}^{\kappa^k} z_{jn}^k\right) \quad t \in T | t \geq t_G, n \in \Omega_t \tag{5.24}$$

$$\sum_{k \in K} \sum_{j=0}^{\kappa^k} w_{jnr}^k = q_{tr} \quad r \in R, t \in T, n \in \Omega_t \tag{5.25}$$

$$w_{jnr}^k \leq h_{jtr}^k z_{jn}^k \quad k \in K, r \in R, j \in J^k \backslash \{\kappa^k + 1\}, t \in T, n \in \Omega_t \tag{5.26}$$

$$\sum_{r \in R} w_{jnr}^k = z_{jn}^k \quad k \in K, j \in J^k \backslash \{\kappa^k + 1\}, n \in \Omega \tag{5.27}$$

$$x_n^k = z_{0n}^k \quad k \in K, n \in \Omega \backslash \{1\} \tag{5.28}$$

$$x_1^k + a_0^k = z_{0,1}^k \quad k \in K \tag{5.29}$$

$$z_{jn}^k = z_{j-1,\omega_n}^k - y_{jn}^k \quad k \in K, n \in \Omega \backslash \{1\}, j \in J^k \backslash \{0, \kappa^k + 1\} \tag{5.30}$$

$$y_{\kappa^k+1,n}^k = z_{\kappa^k,\omega_n}^k \quad k \in K, n \in \Omega \backslash \{1\} \tag{5.31}$$

$$y_{\kappa^k+1,1}^k = a_{\kappa^k+1}^k \quad k \in K \tag{5.32}$$

$$z_{j1}^k = a_j^k - y_{j1}^k \quad k \in K, j \in J^k \backslash \{0, \kappa^k + 1\} \tag{5.33}$$

$$\sum_{k \in K} \left(f_n^k x_n^k - \sum_{j=1}^{\kappa^k+1} s_{jt}^k y_{jn}^k\right) + \sum_{c \in CT} p^c u_n^c \leq b_t \quad t \in T, n \in \Omega_t \tag{5.34}$$

$$v_n^c \geq \theta^c \sum_{k \in K_E | c \in C^k} \sum_{j=0}^{\kappa^k} z_{jn}^k \quad c \in CT, n \in \Omega \tag{5.35}$$

$$\sum_{c\in DC} g^c v_n^c \le G \quad n \in \Omega \tag{5.36}$$

$$\sum_{c\in DC} v_n^c \le H \quad n \in \Omega \tag{5.37}$$

$$v_1^c = e^c + u_1^c \quad c \in CT \tag{5.38}$$

$$v_n^c = v_{\omega_n}^c + u_n^c \quad c \in CT, n \in \Omega\backslash\{1\} \tag{5.39}$$

$$\sum_{k\in K}\sum_{j=0}^{\kappa^k} j z_{jn}^k \le \Gamma \sum_{k\in K}\sum_{j=0}^{\kappa^k} z_{jn}^k \quad n \in \Omega_{t_F} \tag{5.40}$$

$$Q_1 = \sum_{k\in K}\left(f_1^k x_1^k - \sum_{j=1}^{\kappa^k+1} s_{j1}^k y_{j1}^k + \sum_{r\in R}\sum_{j=0}^{\kappa^k} o_{j1r}^k w_{j1r}^k\right) + \sum_{c\in CT}\left(p^c u_1^c + F g^c v_1^c\right) \tag{5.41}$$

$$Q_n = \beta^{t-1}\left(\sum_{k\in K}\left(f_n^k x_n^k - \sum_{j=1}^{\kappa^k+1} s_{jt}^k y_{jn}^k + \sum_{r\in R}\sum_{j=0}^{\kappa^k} o_{jnr}^k w_{jnr}^k\right) + \sum_{c\in CT}\left(p^c u_n^c + F g^c v_n^c\right)\right) + Q_{\omega_n} \quad t \in T\backslash\{1, t_F\}, n \in \Omega_t \tag{5.42}$$

$$Q_n = \beta^{t_F-1}\left(\sum_{k\in K}\left(f_n^k x_n^k - \sum_{j=1}^{\kappa^k+1} s_{jt_F}^k y_{jn}^k + \sum_{r\in R}\sum_{j=0}^{\kappa^k} o_{jnr}^k w_{jnr}^k\right) + \sum_{c\in CT}\left(p^c u_n^c + F g^c v_n^c\right)\right) + \sum_{k\in K}\sum_{r\in R}\sum_{j=0}^{\kappa^k-1}\sum_{i=1}^{\kappa^k-j} \beta^{t_F+i-1} o_{j+i,n,r}^k w_{jnr}^k - \sum_{k\in K}\sum_{j=0}^{\kappa^k} \beta^{t_F+\kappa^k-j} s_{\kappa^k+1,t_F}^k z_{jn}^k + Q_{\omega_n} \quad n \in \Omega_{t_F} \tag{5.43}$$

$$y_{jn}^k, z_{j-1,n}^k \in \mathbb{Z}^+ \quad k \in K, n \in \Omega, j \in J^k\backslash\{0\} \tag{5.44}$$

$$x_n^k \in \mathbb{Z}^+ \quad k \in K, n \in \Omega \tag{5.45}$$

$$u_n^c, v_n^c \in \mathbb{Z}^+ \quad c \in CT, n \in \Omega \tag{5.46}$$

$$w_{jnr}^k \in \mathbb{Z}^+ \quad k \in K, r \in R, n \in \Omega, j \in J^k\backslash\{\kappa^k+1\}. \tag{5.47}$$

The objective function (5.23) is now to minimize the expected total discounted cost. All constraints except (5.41), (5.42) and (5.43) are similar to those in the deterministic formulation of Section 5.3.1, but adjusted to the scenario tree representation of the stochastic process (i.e., links between consecutive periods in the deterministic formulation become links between parent and children nodes in the stochastic formulation). Constraint (5.41) simply defines the costs that are incurred in the first period (i.e., at the root node). Constraints (5.42) mean that if the state at the start of period t is node $n \in \Omega_t$ and $t \notin \{1, t_F\}$, then the total discounted cost Q_n incurred from the start of the planning horizon up until the end of period t is equal to the discounted cost incurred during period t at node n, plus the total discounted cost incurred from the start of the planning horizon up until the end of period $t-1$ when the state at the start of $t-1$ was the parent node ω_n of n. Constraints (5.43) are the same as constraints (5.42) but with the additional end-of-horizon mitigation terms, since they concern nodes in Ω_{t_F}. For the sake of simplicity the end-of-horizon terms assume that salvage values s^k_{jt} and operating costs o^k_{jnr} after the end of the planning horizon remain the same as those in the state reached in period t_F.

5.5. Computational experiments

We have performed an extensive computational study in order to validate the proposed formulations and to analyze the sensitivity of transition plans to several problem parameters. To this end, we have generated test instances based on real data obtained from a bus operator in France. All instances were solved using CPLEX 12.9. The models were implemented in C++ and all experiments were conducted on a cluster of 27 machines, each having two Intel(R) Xeon(R) X5675 3.07 GHz processors with 96 GB of RAM running on Linux. Each machine has 12 cores, and each experiment was run using a single thread. All instances were

solved to optimality in the stated solution times.

5.5.1 Description of the base-case scenario

We have assumed a planning horizon that begins in 2019 and ends in 2050, with periods corresponding to years. We first designed and solved a base-case scenario with the deterministic model from Section 5.3.1 and the most likely values for all parameters, and then modified it in subsequent sections to investigate the impact of specific problem features on optimal transition plans. We attempted to assign realistic values to as many parameters as possible in the base-case scenario.

The operations in our case study, as indicated by the set of run types R and their vehicle requirements q_{tr}, are inspired by data provided by a real transit agency. This agency has supplied us with information regarding their current fleet of vehicles and the daily runs that must currently be performed by their buses over the course of a multi-day schedule. Aside from a few daily runs for mini-buses (which were excluded from our analysis), there were 84 daily runs in the data, varying by total daily distance and the type of bus that must perform them, i.e., articulated 60 feet (hereafter ft) buses or standard 40 ft buses. In order to represent the typical day of operation of a vehicle performing a given run, we computed the average daily distance of each run over all days in the schedule. A few of the runs switched from requiring a standard bus to an articulated one or vice versa during a day or two of the schedule, so we assumed such runs to be associated with the bus size required during the majority of days. Three runs were also missing the associated bus size information, so we assumed them to be standard-bus runs. The result was that 32 daily runs must be performed by articulated 60 ft buses, and 52 daily runs must be performed by standard 40 ft buses. We then clustered the 84 runs based on similar operational characteristics by grouping them according to the size of the bus required (i.e., standard or ar-

ticulated), and the nearest multiple of five to their average daily distance, (e.g., a standard-bus run with an average daily distance of 163 km and a standard-bus run with an average daily distance of 167 km were both assumed to be a standard-bus run type associated with an approximate daily distance of 165 km). The final result was a set of 52 types of runs, each type currently required to be performed by a number of buses ranging from one to four.

In order to translate the daily runs into yearly assignment runs, we assumed that each vehicle will perform the daily run it was assigned to in a given year during 85% of the time (i.e., 310 days), with the run performed by a substitute vehicle in the remaining 15% of the time (i.e., 55 days) while the usual vehicle is pulled from operations for maintenance activities. Therefore, we have added two additional types of yearly assignment runs representing operations of vehicles designated as such substitutes to the usual vehicles. We have assumed that each of these two "substitute" run types is associated to a specific bus size (i.e., standard or articulated), and that a bus assigned to a substitute run must be able to perform any of the real daily runs for the associated bus size (i.e., it must be able to act as a substitute for any bus of the same size because it will replace several of such buses in their daily runs over the course of the year). Assuming that each vehicle performing a substitute run can cover $\frac{310}{55} = 5.64$ vehicles per year while they are pulled for maintenance, we considered requirements of $\lceil \frac{32}{5.64} \rceil = 6$ additional articulated buses performing substitute runs, and $\lceil \frac{52}{5.64} \rceil = 10$ additional standard buses performing substitute runs. The total yearly residual distances of all normal articulated and standard bus runs (i.e., associated with the 55 days during which the usual buses are pulled) were assumed to be evenly distributed among the six articulated and 10 standard buses performing the substitute runs, respectively. We have assumed that the vehicle requirements for each type of run remain the same over the course of the entire planning horizon, resulting in a total fleet size requirement of 100 vehicles in each period.

We mention here that although our approach to translate daily runs into yearly assignment runs in our case study is based on the assumption of a vehicle performing the same typical daily run throughout the year (aside from the substitute runs which are associated with several daily runs), this does not need to be the case in all instantiations of the EFTP, which is intentionally formulated so as to leave such flexibility when setting parameter values. For example, one may choose to represent a yearly assignment run as a vehicle performing a known sequence of varying daily runs over the course of a repeating multi-day schedule if such sequences are known and can be forecasted in future years.

The initial vehicles in our case study are all diesel vehicles, and their age distribution, as given by parameters a_j^k, is estimated based on data provided by the transit agency regarding the distribution of cumulative kilometers traveled by vehicles in their fleet. We assumed each vehicle to have traveled 60,000 km per year in order to translate cumulative distance traveled to an age in years, which corresponds approximately to the average daily distance of all runs multiplied by 310 days. All other parameters were assigned best found values in the literature. Due to the large number of parameters, several of which vary by vehicle type, vehicle age, and year, instead of reporting specific values of each parameter we discuss our sources and assumptions regarding each of them in the following list.

- **Types of vehicles:** The types of electric buses we have considered represent different charging configurations identified by Bloomberg New Energy Finance (2018) as the most likely charging configurations for transit operations in a medium-sized city in which buses would typically travel approximately 200 km per day. This distance corresponds to the average distance of the daily runs in the data we obtained from the French transit agency. In addition, we have considered standard 40 ft and articulated 60 ft diesel, hybrid, and CNG buses as alternatives as well. The set of vehicle types K we have considered thus contains the following elements:

- 40 ft diesel bus,
- 60 ft diesel bus,
- 40 ft hybrid bus,
- 60 ft hybrid bus,
- 40 ft CNG bus,
- 60 ft CNG bus,
- 40 ft electric bus with a 110 kWh battery using depot charging exclusively,
- 40 ft electric bus with a 250 kWh battery using depot charging exclusively,
- 40 ft electric bus with a 350 kWh battery using depot charging exclusively,
- 60 ft electric bus with a 650 kWh battery using depot charging exclusively,
- 40 ft electric bus with a 250 kWh battery using depot charging and fast plug-in charging at line terminals,
- 40 ft electric bus with a 110 kWh battery using depot charging and pantograph charging at bus stops.

A terminal refers to a location where several bus lines end and layovers occur, and a depot refers to a location where buses are kept when not in service. As in Bloomberg New Energy Finance (2018), all electric buses are assumed to use depot charging, with some requiring additional en route recharging. The lifetime of all vehicle types was assumed to be 15 years as in Bloomberg New Energy Finance (2018), with the maximum average final age of the fleet Γ set to 7.5 years.

- **Vehicle purchase costs:** We have used approximate median purchase prices of 40 ft and 60 ft diesel, CNG and hybrid buses derived from the American Public Transportation Association (APTA) purchase data by Ambrose et al.

(2017). We have used the same purchase prices as Bloomberg New Energy Finance (2018) for 40 ft electric buses with battery sizes of 350 kWh, 250 kWh and 110 kWh. The Bloomberg report does not consider 60 ft electric buses, so we have used the median purchase price derived from the APTA purchase data by Ambrose et al. (2017) for 60 ft electric buses. We have assumed that the purchase price of diesel, hybrid and CNG buses does not change with time, and that the purchase price of electric buses diminishes due to battery cost reductions only. The initial battery price per kWh is assumed to be the value of $600 in 2017, as in Bloomberg New Energy Finance (2018). This price is more than that of batteries for passenger EVs because of different packaging, thermal management systems, and lower purchase volumes. To forecast future bus battery prices, we have made the same assumption as Bloomberg New Energy Finance (2018) – that is, we assume that the battery prices for electric buses decline at the same rate as those for passenger EVs. The evolution of passenger EV battery prices from 2019 to 2050 were taken from Schmidt et al. (2017), who have made such forecasts based on experience rates. The authors first used historical data regarding EV battery prices and cumulative sales to derive an expected experience rate, whch is then used to predict future prices as a function of forecasted EV sales. The expected experience rate they identified was used in our base-case scenario.

- **Salvage values**: We have assumed salvage values to be zero for all vehicles in the base-case scenario, as a result of both the difficulty of identifying reliable EV residual values and the small importance salvage values seem to play in non-electric bus replacement decisions (Laver et al., 2007).

- **Operating costs**: We have derived total operating costs (maintenance + energy) per kilometer for each combination of vehicle type, vehicle age, and period of the planning horizon. These were assumed to be the same for all

types of runs. The total operational cost incurred when performing a given type of run with a given vehicle type of a given age during a given period was then computed based on the approximate yearly distance associated with that type of run. Our assumptions and sources for maintenance and energy costs are detailed below.

- **Maintenance costs:**
  - For 60 ft diesel and hybrid buses, we have used maintenance costs based on those found by Feng and Figliozzi (2014), who have performed a regression analysis on real data from a transit agency to derive maintenance costs per mile of such vehicles as a function of age. We have assumed that maintenance costs are the same for 40 ft and 60 ft buses of the same type.
  - For electric and CNG buses, our assumptions are based on results from Blynn (2018): 1) the difference between maintenance costs of CNG buses relative to those of diesel buses ranges from -12% to 10%, so we have assumed identical maintenance costs for CNG and diesel buses; and 2) the difference between maintenance costs of electric buses relative to those of diesel buses ranges from -60% to -20%, so we have used the medium value of 40% EV maintenance savings.
- **Energy costs:**
  - We used fuel efficiencies (in miles per diesel gallon equivalent) for 40 ft and 60 ft diesel, hybrid and CNG buses based on median values from Ambrose et al. (2017) for small transit agencies with less than 300 vehicles, which is the case for the transit agency that provided us with data regarding their operations. The fuel efficiencies in miles per kWh for all 40 ft electric buses (which vary depending

on the battery size) are taken from Bloomberg New Energy Finance (2018). The efficiency of the 60 ft electric bus is estimated based on BYD's articulated electric bus (BYD, 2018), i.e., a range of 230 miles with a battery of 650 kWh. We have assumed that fuel efficiencies do not change with the age of the vehicles.

  * Yearly diesel, natural gas and electricity energy prices until 2050 for the transportation sector were taken from the U.S. Energy Information Administration's Annual Energy Outlook 2019 (US EIA, 2019) to then determine energy costs per unit of distance traveled by each vehicle type. The reference scenario identified by US EIA (2019) was used in our base-case scenario.

- **Charger types, charger purchase costs, charging powers and bus-to-charger ratios:** We have used values based on the findings of Bloomberg New Energy Finance (2018). The purchase costs and bus-to-charger ratios are exact values used in their total cost of ownership analysis. The charging power of each type of charger is based on the range of charging powers mentioned in the report for each kind of charger.

  - **Slow plug-in charger installed at a depot**: $50,000, bus-to-charger ratio of 2:1, and charging power of 50 kW. The ratio for this type of charger concerns all types of electric buses, i.e., they are all assumed to use the same type of depot charger in the base-case scenario.

  - **Fast plug-in charger installed at a line terminal**: $110,000, bus-to-charger ratio of 20:1, and charging power of 120 kW. The ratio for this type of charger only concerns the 40 ft electric bus with a 250 kWh battery using depot charging and fast plug-in charging at line terminals.

  - **Pantograph chargers installed at three bus stops**: $690,000 (i.e., $230,000 per pantograph), bus-to-charger ratio of 20:1 (i.e., 1 refers to one group

of three pantographs), 900 kW (i.e., 300 kW per pantograph). The ratio for this type of charger only concerns the 40 ft electric bus with a 110 kWh battery using depot charging and pantograph charging at bus stops.

- **Compatibility between vehicles and runs**: For a non-electric bus or an electric bus type that recharges outside the depot (at line terminals or bus stops), the compatibility was assumed to depend only on the size of the bus required for the type of run, i.e., standard (40 ft) or articulated (60 ft). For an electric bus that does not recharge outside the depot, the range of the bus on a single charge (computed based on the battery size and the efficiency of the bus in miles per kWh) must be more than the approximate daily distance of that run type, in addition to meeting the bus size requirement. We do not consider time- or load-related incompatibilities between electric bus types and runs in our case study, i.e., we assume all types of runs leave enough time for overnight charging activities, and that any articulated and standard electric bus has enough load capacity to handle the number of passengers associated with any articulated-bus and standard-bus run, respectively.

- **Demand charges**: Monthly demand charges vary considerably, with values ranging from \$0.00/kW to \$24/kW reported across the United States for commercial and industrial electricity customers (Gallo et al., 2014). We have used a medium value of \$12 per kW for monthly demand charges in our base-case scenario, which is equivalent to total yearly demand charges of \$144 per kW.

- **Electrification targets**: We assumed that 50% of the initial (entirely) diesel fleet must be electrified by 2035 in the base-case scenario. We chose a target year of 2035 in order to allow the option of keeping any initial vehicle in the fleet until the end of their lifetime, which is at most 15 years after the first period (i.e., 2019).

- **Yearly budgets and grid/space limitations for depot chargers**: We have assumed all these parameters to be unbounded in our case study, given that we could not obtain data for them or find reliable values in the literature.

- **Finance**: All identified monetary values from the literature were converted to 2018 dollars and used as such in the model. A yearly discount rate of 3% was used (Blynn, 2018).

5.5.2 Base case results

The results for the problem setting described in Section 5.5.1 are reported in Table 5.1. The fleet configuration (in terms of vehicles and EV chargers) is reported for 2020, 2025, ..., 2050, as are different cost values (in millions of dollars), as well as the solution time in seconds. The results suggest that the optimal transition plan is to 1) rely heavily on electric buses to accomplish runs that need to be performed by standard 40 ft buses; and 2) use CNG buses as a near-term diesel replacement before transitioning to electric buses for the majority of runs to be performed by articulated 60 ft buses in the long-term as well. Indeed, as soon as 2025, 30 of the 62 required standard buses consist of electric buses, and by 2035 each and every one of the 62 standard buses are electric. On the other hand, because of the hefty purchase premium of the 60 ft electric bus alternative, 60 ft CNG buses are chosen to replace aging 60 ft diesel vehicles in the initial fleet. However, with the decline of battery prices in the long term, the cost associated with the large battery of the articulated electric buses decreases significantly, and the 60 ft electric bus begins to be incorporated into the fleet between 2025 and 2030, with 12, 24 and 32 of the 38 articulated-bus runs covered by electric buses in 2035, 2040 and 2045, respectively. Neither of the 40 ft or 60 ft hybrid buses is incorporated into the fleet over the course of the entire planning horizon.

Regarding the choice among the different electric bus alternatives, the optimal replacement plan clearly suggests that among all 40 ft EV alternatives, combining the medium-sized battery of 250 kWh with fast charging at line terminals in this case is the optimal configuration. Although the 350 kWh alternative has the benefit of being compatible with 47 of 62 standard-bus runs without any investments in en route charging infrastructure, the purchase price premium resulting from the larger battery seems to outweigh the additional charging infrastructure investments at line terminals. On the other hand, the 110 kWh electric bus benefits from a low purchase cost compared to the other 40 ft EVs, but is limited in the number of runs it is compatible with due to its short driving range of approximately 90 km. It therefore requires the expensive pantograph charging configuration to grant more operational flexibility, a proposition deemed unprofitable according to the optimal replacement plan. Ultimately, the best compromise is to pay a premium for the 250 kWh battery compared to the 110 kWh battery in order to be able to employ the cheaper en route fast charging infrastructure at line terminals, all the while avoiding the most expensive 40 ft electric bus with the 350 kWh battery.

5.5.3 Sensitivity analysis for the deterministic EFTP

In order to better understand how specific problem parameters influence optimal transition plans, we have solved several variations of our case study by making incremental modifications to the base-case scenario described in Section 5.5.1. In what follows we present and discuss characteristics of optimal transition plans obtained for various scenarios concerning en route charging configurations, articulated electric bus charging infrastructure requirements, electrification targets, demand charges, future energy and battery prices, EV maintenance savings, vehicle salvage values, CNG bus-related depot upgrades, midlife costs, and charger

Table 5.1 – Optimal transition plan for the base-case scenario

Year:	2020	2025	2030	2035	2040	2045	2050
Vehicle types:							
Diesel 40 ft	58	32	21	0	0	0	0
Diesel 60 ft	38	25	14	0	0	0	0
Hybrid 40 ft	0	0	0	0	0	0	0
Hybrid 60 ft	0	0	0	0	0	0	0
CNG 40 ft	0	0	0	0	0	0	0
CNG 60 ft	0	13	21	26	14	6	6
Electric 350 kWh 40 ft DC	0	0	0	0	0	0	0
Electric 650 kWh 60 ft DC	0	0	3	12	24	32	32
Electric 250 kWh 40 ft DC	0	0	1	3	3	2	4
Electric 250 kWh 40 ft DC+FC	4	30	40	59	59	60	58
Electric 110 kWh 40 ft DC	0	0	0	0	0	0	0
Electric 110 kWh 40 ft DC+PC	0	0	0	0	0	0	0
Charger types:							
Depot plug-in charger (DC)	2	15	22	37	43	47	47
Fast plug-in charger at line terminal (FC)	1	2	2	3	3	3	3
Pantograph charger at three bus stops (PC)	0	0	0	0	0	0	0
Costs:							
Vehicle purchase costs (M$):	92.80						
Charger purchase costs (M$):	2.02						
Operating costs (M$):	95.24						
Demand charge (M$):	4.90						
End-of-horizon costs (M$):	6.78						
Total costs (M$):	201.74						
Solution time (s):	354.31						

maintenance costs. In all tables hereafter, the following abbreviations are used to refer to vehicle types:

- D-40: 40 ft diesel bus,
- D-60: 60 ft diesel bus,
- H-40: 40 ft hybrid bus,
- H-60: 60 ft hybrid bus,
- CNG-40: 40 ft CNG bus,
- CNG-60: 60 ft CNG bus,
- E350-40: 40 ft electric bus with a 350 kWh battery using depot charging exclusively,
- E650-60: 60 ft electric bus with a 650 kWh battery using depot charging exclusively,
- E250-40: 40 ft electric bus with a 250 kWh battery using depot charging exclusively,
- E250-40 FC: 40 ft electric bus with a 250 kWh battery using depot charging and fast plug-in charging at line terminals,
- E110-40: 40 ft electric bus with a 110 kWh battery using depot charging exclusively,
- E110-40 PC: 40 ft electric bus with a 110 kWh battery using depot charging and pantograph charging at bus stops,
- E110-40 WC: 40 ft electric bus with a 110 kWh battery using depot charging and wireless charging at bus stops.

5.5.3.1 En route charging configurations

While the combination of the medium-sized 250 kWh battery with fast plug-in charging at line terminals was clearly the preferred EV type for standard 40 ft buses in the base-case scenario, it is worth asking what the optimal transition plan

would resemble if such an option were not available. Indeed, fast charging at line terminals will only be possible if the distance of individual routes that are part of a given daily run can be performed on a single battery charge, and if the operating schedule allows enough time to sufficiently recharge the battery between such routes at line terminals. If either of these conditions are not met, it may be that the only feasible en route charging configurations will involve using very fast (and expensive) chargers at bus stops while passengers are boarding. Thus, in Table 5.2 we report characteristics of optimal transition plans for the base-case scenario and for two other scenarios. In the first, it is assumed that the only possible en route charging configuration is the electric bus with the 110 kWh battery to be charged at the depot with plug-in charging and at bus stops with pantograph chargers. Pantograph charging is the preferred option for charging smaller batteries at bus stops since it is cheaper and more efficient than wireless charging, the other type of charging considered to be feasible for bus stops. However, it may not always be possible to install pantograph chargers at bus stops due to space restrictions and local planning regulations, although some of these drawbacks can be overcome by opting for wireless charging (Bloomberg New Energy Finance, 2018). Thus, the second additional scenario reported in Table 5.2 assumes that the only possible en route charging configuration is an electric bus with a 110 kWh battery to be charged at the depot with plug-in charging and at bus stops with wireless chargers. An investment in a unit of wireless charging infrastructure is assumed to correspond to installing wireless chargers at five bus stops, and has the following characteristics based on Bloomberg New Energy Finance (2018):

- **Wireless chargers installed at five bus stops**: Purchase cost of $2,000,000 (i.e., $400,000 per wireless charger), bus-to-charger ratio of 20:1 (i.e., 1 refers to one group of five wireless chargers), charging power of 1000 kW (i.e., 200 kW per wireless charger).

The results indicate that when pantograph charging is the only feasible en route charging infrastructure for electric buses, the electric bus with the 110 kWh battery using depot charging and pantograph chargers at bus stops is prefered to the electric bus with the 350 kWh battery for most of the standard-bus runs with large daily distances. While the 250 kWh option with fast charging at line terminals is almost exclusively used to cover the 62 standard-bus runs in the base-case scenario, the 110 kWh option with pantograph charging is used to cover only 40 of these in the first additional scenario, with the 250 kWh battery alternative using depot charging called upon to perform approximately a third of the standard-bus runs (i.e., those it can cover with its 200 km range before being charged overnight at the depot) in the target year and beyond. The costly 350 kWh alternative with depot charging is also used to cover a few standard-bus runs with large daily distances (the 350 kWh alternative has a range of approximately 270 km) in order to avoid having to purchase more pantograph chargers. The cost breakdown shows that total discounted costs increase by about five million compared to the base-case scenario, mostly due to the larger demand charges incurred as a result of the large charging powers drawn by the pantograph chargers.

The number of standard-bus runs performed by electric buses utilizing en route charging infrastructure further drops in the second scenario investigated, due to the even more expensive wireless chargers involved. Nevertheless, the model still opts for the 110 kWh battery electric bus using the wireless chargers to cover about a third of the standard-bus runs, which in most years corresponds to about 20 fewer than were covered by the 110 kWh battery electric bus using pantograph charging in the first new scenario. Those 20 runs are now assigned to the 350 kWh alternative, whose purchase price is worth incurring to take advantage of its large driving range and to avoid the investments in more costly wireless chargers. As in the base case results, in both new scenarios approximately 75% of the fleet is electrified by the target year of 2035 despite only 50%

being required to be, and the initial 40 ft diesel vehicles are replaced entirely with electric buses.

Table 5.2 – Optimal transition plans under different en route charging assumptions

Vehicle types:	D-40	D-60	H-40	H-60	CNG-40	CNG-60	E350-40	E650-60	E250-40	E250-40 FC	E110-40	E110-40 PC	E110-40 WC
Fast plug-in charging at line terminals and pantograph charging at bus stops (base case)													
2025 fleet configuration:	32	25	0	0	0	13	0	0	0	30	0	0	N/A
2030 fleet configuration:	21	14	0	0	0	21	0	3	1	40	0	0	N/A
2035 fleet configuration:	0	0	0	0	0	26	0	12	3	59	0	0	N/A
2040 fleet configuration:	0	0	0	0	0	14	0	24	3	59	0	0	N/A
2045 fleet configuration:	0	0	0	0	0	6	0	32	2	60	0	0	N/A
2050 fleet configuration:	0	0	0	0	0	6	0	32	4	58	0	0	N/A
Vehicle purchase costs (M$): 92.80													
Charger purchase costs (M$): 2.02													
Operating costs (M$): 95.24													
Demand charge (M$): 4.90			**Total costs (M$):**			201.74							
End-of-horizon costs (M$): 6.78			**Solution time (s):**			354.31							
Pantograph charging at bus stops only													
2025 fleet configuration:	38	27	0	0	0	11	0	0	4	N/A	0	20	N/A
2030 fleet configuration:	17	14	0	0	0	21	0	3	6	N/A	0	39	N/A
2035 fleet configuration:	0	0	0	0	0	26	2	12	20	N/A	0	40	N/A
2040 fleet configuration:	0	0	0	0	0	16	3	22	19	N/A	0	40	N/A
2045 fleet configuration:	0	0	0	0	0	6	3	32	19	N/A	0	40	N/A
2050 fleet configuration:	0	0	0	0	0	6	1	32	21	N/A	0	40	N/A
Vehicle purchase costs (M$): 92.06													
Charger purchase costs (M$): 2.92													
Operating costs (M$): 96.62													
Demand charge (M$): 8.29			**Total costs (M$):**			206.73							
End-of-horizon costs (M$): 6.82			**Solution time (s):**			710.35							
Wireless charging at bus stops only													
2025 fleet configuration:	36	27	0	0	0	11	2	0	4	N/A	0	N/A	20
2030 fleet configuration:	21	14	0	0	0	21	12	3	9	N/A	0	N/A	20
2035 fleet configuration:	0	0	0	0	0	26	21	12	21	N/A	0	N/A	20
2040 fleet configuration:	0	0	0	0	0	16	30	22	17	N/A	0	N/A	15
2045 fleet configuration:	0	0	0	0	0	6	28	32	14	N/A	0	N/A	20
2050 fleet configuration:	0	0	0	0	0	6	21	32	21	N/A	0	N/A	20
Vehicle purchase costs (M$): 93.81													
Charger purchase costs (M$): 3.61													
Operating costs (M$): 97.48													
Demand charge (M$): 6.74			**Total costs (M$):**			208.58							
End-of-horizon costs (M$): 6.95			**Solution time (s)**			347.36							

5.5.3.2 Charging infrastructure requirements for articulated electric buses

Although it may seem overly optimistic to assume that the articulated electric bus with the 650 kWh battery can be charged with a 50 kW depot charger (as is the case in the base-case scenario), the range of the 650 kWh electric bus is approximately 370 km and the average daily distance of the articulated-bus runs is just over 200 km, so charging half the battery capacity each night (or charging it fully every two nights) should be sufficient for several articulated-bus runs. Nev-

ertheless, given the knowledge of the context at hand (namely regarding when overnight depot charging can occur and how much time is available for it), one could instead assume that there are different types of depot chargers that must be used by different vehicles. For example, in some contexts it may be more appropriate to consider a type of depot charger to be used specifically by the 60 ft electric buses and that is more expensive and power-consuming, or that requires a higher bus-to-charger ratio than does the type of depot charger associated with 40 ft electric buses.

In order to see whether the decision to adopt articulated electric buses in the long term is sensitive to such charging infrastructure requirements, we modified the base-case scenario so as to assume that the 60 ft electric bus with the 650 kWh battery has more stringent depot charging infrastructure requirements. We first considered a new type of depot charger that is identifical to the slow depot chargers described in Section 5.5.1, but is to be used exclusively by 60 ft electric buses with a bus-to-charger ratio of 1:1. We also considered two additional scenarios in which the 60 ft electric bus is only compatible with a new (and this time faster) type of depot charger that has the same cost and charging power characterisitcs as the fast chargers at line terminals, i.e., a purchase cost of $110,000 per charger and a charging power of 120 kW. We tested the problem setting with the faster depot chargers under two bus-to-charger ratios dictating how many of such fast depot chargers are required according to the number of 60 ft electric buses in the fleet: 2:1 and 1:1. The results for each of these three new scenarios are reported in Table 5.3 and show that the long-term profitability of the considered 60 ft electric bus is indeed sensitive to such depot charging infrastructure requirements. The first two scenarios presented in Table 5.3 have similar effects: they delay the addition of 60 ft electric buses to the fleet compared with their adoption rate in the base-case scenario, and the 60 ft electric buses represent a far smaller proportion of the fleet than they do in the base-case scenario during the second half of the

planning horizon. The scenario with fast depot chargers and a 2:1 ratio seems more detrimental to the business case of the large electric bus than the scenario with slow depot chargers and a 1:1 ratio. The last scenario with the fast depot chargers and the 1:1 ratio clearly ruins the business case of the large electric bus, which is then never added to the fleet over the entire planning horizon. The initial 60 ft diesel buses are then only replaced with 60 ft CNG buses.

Table 5.3 – Optimal transition plans under more stringent charging infrastructure requirements for articulated electric buses

Vehicle types:		D-40	D-60	H-40	H-60	CNG-40	CNG-60	E350-40	E650-60	E250-40	E250-40 FC	E110-40	E110-40 PC
Slow plug-in depot chargers for articulated electric buses with a ratio of 1:1													
2025 fleet configuration:		32	26	0	0	0	12	0	0	0	30	0	0
2030 fleet configuration:		20	14	0	0	0	24	0	0	2	40	0	0
2035 fleet configuration:		0	0	0	0	0	33	0	5	4	58	0	0
2040 fleet configuration:		0	0	0	0	0	27	0	11	4	58	0	0
2045 fleet configuration:		0	0	0	0	0	15	0	23	2	60	0	0
2050 fleet configuration:		0	0	0	0	0	11	0	27	3	59	0	0
Vehicle purchase costs (M$):	90.63												
Charger purchase costs (M$):	2.26												
Operating costs (M$):	98.08												
Demand charge (M$):	5.04			**Total costs (M$):**			202.82						
End-of-horizon costs (M$):	6.81			**Solution time (s)**			202.01						
Fast plug-in depot chargers for articulated electric buses with a ratio of 2:1													
2025 fleet configuration:		32	25	0	0	0	13	0	0	0	30	0	0
2030 fleet configuration:		16	13	0	0	0	25	0	0	1	45	0	0
2035 fleet configuration:		0	0	0	0	0	34	0	4	3	59	0	0
2040 fleet configuration:		0	0	0	0	0	30	0	8	3	59	0	0
2045 fleet configuration:		0	0	0	0	0	20	0	18	2	60	0	0
2050 fleet configuration:		0	0	0	0	0	16	0	22	5	57	0	0
Vehicle purchase costs (M$):	90.50												
Charger purchase costs (M$):	2.18												
Operating costs (M$):	98.44												
Demand charge (M$):	5.01			**Total costs (M$):**			203.06						
End-of-horizon costs (M$):	6.92			**Solution time (s)**			512.15						
Fast plug-in depot chargers for articulated electric buses with a ratio of 1:1													
2025 fleet configuration:		32	23	0	0	0	15	0	0	0	30	0	0
2030 fleet configuration:		16	11	0	0	0	27	0	0	1	45	0	0
2035 fleet configuration:		0	0	0	0	0	38	0	0	3	59	0	0
2040 fleet configuration:		0	0	0	0	0	38	0	0	3	59	0	0
2045 fleet configuration:		0	0	0	0	0	38	0	0	2	60	0	0
2050 fleet configuration:		0	0	0	0	0	38	0	0	4	58	0	0
Vehicle purchase costs (M$):	88.23												
Charger purchase costs (M$):	1.54												
Operating costs (M$):	101.19												
Demand charge (M$):	4.08			**Total costs (M$):**			203.58						
End-of-horizon costs (M$):	8.53			**Solution time (s)**			288.16						

5.5.3.3 Electrification targets

The optimal transition plan for the base-case scenario makes hefty use of electric buses (i.e., more than 70% of the fleet consists of EVs by 2035 while only 50% is required to be). Therefore, it is worth investigating how sensitive the optimal solution is to the minimal proportion P required to consist of EVs by the target year of 2035. To this end, we have solved the base-case scenario with minimal EV proportions of 0% and 100% by 2035, and presented the results in Table 5.4. First, these results show that the use of electric buses to perform the entirety of the standard-bus runs by 2035 is cost-effective even when no EVs need be incorporated into the fleet to meet a target. The solution obtained without enforcing any electrification target is nearly identical to the base case solution. Second, while it is no surprise that requiring 100% of the fleet to be electrified by 2035 results in replacing the 60 ft CNG buses used in the base-case scenario by the only EV alternative for 60 ft buses, it is interesting to note that the difference in total discounted costs between the two solutions in Table 5.4 is not that significant. Respecting ambitious electrification targets in the next decades therefore does not necessarily need to be done at the expense of incurring substantive additional costs.

For the sake of investigating how solutions may be influenced by shorter-term target years, in Table 5.5 we report characteristics of optimal transition plans under fleet electrification requirements of 50% and 100% by 2025 as well. In this case the electrification constraints (5.2) from the model of Section 5.3.1 are clearly more binding, given that exactly half of the fleet consists of EVs in 2025 in the scenario with a minimal electrification requirement of 50% of the fleet by that year. While the total discounted costs are not significantly higher for the scenario assuming an electrification target of 50% by 2025 compared to the base-case scenario, the cost increase is more notable when 100% of the fleet must be electrified by 2025. In this case, although total operational costs decrease by nearly 20% compared to

Table 5.4 – Optimal transition plans under different electrification targets to be met by 2035

Vehicle types:		D-40	D-60	H-40	H-60	CNG-40	CNG-60	E350-40	E650-60	E250-40	E250-40 FC	E110-40	E110-40 PC
100% electrification by 2035													
2025 fleet configuration:		31	30	0	0	0	0	0	8	0	31	0	0
2030 fleet configuration:		17	15	0	0	0	0	0	23	1	44	0	0
2035 fleet configuration:		0	0	0	0	0	0	0	38	3	59	0	0
2040 fleet configuration:		0	0	0	0	0	0	0	38	3	59	0	0
2045 fleet configuration:		0	0	0	0	0	0	0	38	2	60	0	0
2050 fleet configuration:		0	0	0	0	0	0	0	38	3	59	0	0
Vehicle purchase costs (M$):	98.52												
Charger purchase costs (M$):	2.26												
Operating costs (M$):	90.40												
Demand charge (M$):	5.81			**Total costs (M$):**			203.86						
End-of-horizon costs (M$):	6.86			**Solution time (s)**			152.51						
No electrification target													
2025 fleet configuration:		32	26	0	0	0	12	0	0	0	30	0	0
2030 fleet configuration:		18	13	0	0	0	21	0	4	1	43	0	0
2035 fleet configuration:		0	0	0	0	0	26	0	12	3	59	0	0
2040 fleet configuration:		0	0	0	0	0	15	0	23	3	59	0	0
2045 fleet configuration:		0	0	0	0	0	6	0	32	2	60	0	0
2050 fleet configuration:		0	0	0	0	0	6	0	32	5	57	0	0
Vehicle purchase costs (M$):	92.77												
Charger purchase costs (M$):	2.02												
Operating costs (M$):	95.20												
Demand charge (M$):	4.92			**Total costs (M$):**			201.74						
End-of-horizon costs (M$):	6.83			**Solution time (s)**			223.29						

the base-case scenario as a result of the aggressive incorporation of electric buses very early in the planning horizon, total purchase costs increase by more than 25% for the same reason (notably because 60 ft electric buses are imposed while battery prices are still high).

5.5.3.4 Demand charges

Demand charges that are based on the largest charging power retrieved from the grid over the course of each month can have a significant impact on total energy costs associated with fleet EVs (Pelletier et al., 2018; Gallo et al., 2014). However, monthly demand charges can vary significantly, with Gallo et al. (2014) reporting values ranging from \$0/kW to \$24/kW across the United States for commercial and industrial electricity consumers. In the base-case scenario, demand charges were therefore set to a medium value of 12\$/kW per month. To explore how demand charges affect EV replacement decisions in our case study,

Table 5.5 – Optimal transition plans under different electrification target to be met by 2025

Vehicle types:		D-40	D-60	H-40	H-60	CNG-40	CNG-60	E350-40	E650-60	E250-40	E250-40 FC	E110-40	E110-40 PC
50% electrification by 2025													
2025 fleet configuration:		19	21	0	0	0	10	0	7	3	40	0	0
2030 fleet configuration:		15	13	0	0	0	18	0	7	3	44	0	0
2035 fleet configuration:		0	0	0	0	0	23	0	15	3	59	0	0
2040 fleet configuration:		0	0	0	0	0	14	0	24	2	60	0	0
2045 fleet configuration:		0	0	0	0	0	6	0	32	2	60	0	0
2050 fleet configuration:		0	0	0	0	0	6	0	32	6	56	0	0
Vehicle purchase costs (M$):	96.35												
Charger purchase costs (M$):	2.08												
Operating costs (M$):	91.87												
Demand charge (M$):	5.22			**Total costs (M$):**			202.30						
End-of-horizon costs (M$):	6.79			**Solution time (s)**			288.85						
100% electrification by 2025													
2025 fleet configuration:		0	0	0	0	0	0	0	38	2	60	0	0
2030 fleet configuration:		0	0	0	0	0	0	0	38	2	60	0	0
2035 fleet configuration:		0	0	0	0	0	0	0	38	2	60	0	0
2040 fleet configuration:		0	0	0	0	0	0	0	38	2	60	0	0
2045 fleet configuration:		0	0	0	0	0	0	0	38	2	60	0	0
2050 fleet configuration:		0	0	0	0	0	0	0	38	11	51	0	0
Vehicle purchase costs (M$):	117.66												
Charger purchase costs (M$):	2.50												
Operating costs (M$):	77.97												
Demand charge (M$):	6.99			**Total costs (M$):**			212.13						
End-of-horizon costs (M$):	7.01			**Solution time (s)**			80.07						

we now solve the base-case scenario without demand charges and with high demand charges (i.e., \$24/kW). The results are shown in Table 5.6 and suggest that demand charges can indeed hinder the use of certain high-power en route chargers. While the 110 kWh electric bus using high-power pantograph chargers is never used in the base-case scenario, it is used when removing demand charges. This is done in the first half of the planning horizon when the purchase costs of EVs with larger batteries have not decreased significantly yet. Removing the demand charges incurred with the pantograph chargers seems to render the costly investments in the pantograph charging infrastructure at bus stops worthwhile. The incorporation of the 60 ft electric buses is also done at a faster rate when removing the demand charges. The opposite observations apply in the scenario assuming the highest demand charges. Nevertheless, the high demand charges are not enough to move away from the 250 kWh alternative combined with fast plug-in charging at line terminals, which remains the dominant type of vehicle

used for standard-bus runs, as in the base-case scenario.

Table 5.6 – Optimal transition plans under different demand charges

Vehicle types:		D-40	D-60	H-40	H-60	CNG-40	CNG-60	E350-40	E650-60	E250-40	E250-40 FC	E110-40	E110-40 PC
No demand charges													
2025 fleet configuration:		29	26	0	0	0	12	0	0	0	13	0	20
2030 fleet configuration:		13	13	0	0	0	16	0	9	0	29	0	20
2035 fleet configuration:		0	0	0	0	0	20	0	18	2	48	0	12
2040 fleet configuration:		0	0	0	0	0	8	0	30	2	60	0	0
2045 fleet configuration:		0	0	0	0	0	4	0	34	2	60	0	0
2050 fleet configuration:		0	1	0	0	0	3	0	34	2	60	0	0
Vehicle purchase costs (M$):	96.18												
Charger purchase costs (M$):	2.80												
Operating costs (M$):	90.87												
Demand charge (M$):	0.00			**Total costs (M$):**			196.55						
End-of-horizon costs (M$):	6.69			**Solution time (s):**			93.61						
High demand charges													
2025 fleet configuration:		36	25	0	0	0	13	0	0	0	26	0	0
2030 fleet configuration:		20	13	0	0	0	25	0	0	2	40	0	0
2035 fleet configuration:		0	0	0	0	0	32	0	6	2	60	0	0
2040 fleet configuration:		0	0	0	0	0	22	0	16	3	59	0	0
2045 fleet configuration:		0	0	0	0	0	10	0	28	2	60	0	0
2050 fleet configuration:		0	0	0	0	0	8	0	30	3	59	0	0
Vehicle purchase costs (M$):	89.97												
Charger purchase costs (M$):	1.92												
Operating costs (M$):	98.65												
Demand charge (M$):	9.02			**Total costs (M$):**			206.44						
End-of-horizon costs (M$):	6.89			**Solution time (s):**			877.31						

5.5.3.5 Energy prices

The evolution of energy prices is not only critical to the business case of fleet vehicles, but also subject to a fair amount of uncertainty. In the base-case scenario, energy prices were based on yearly diesel, natural gas and electricity price forecasts up to 2050 for the transportation sector made by the U.S. Energy Information Administration's Annual Energy Outlook 2019 (US EIA, 2019) in their reference scenario. The US EIA (2019) have also made such projections for high and low oil price scenarios, which we now use to evaluate the base case solution's sensitivity to uncertain energy price developments; the results are given in Table 5.7. The high oil price scenario, although detrimental to the diesel vehicles' business case, is actually accompanied by lower natural gas prices up to 2030 than in the reference scenario, resulting in a few extra 60 ft CNG buses being purchased early in

the planning horizon instead of electric buses. The natural gas prices are however higher beyond 2030 in the high oil price scenario than in the reference scenario, and thus by 2040 there are more 60 ft electric buses in the fleet than there are in the base-case scenario. The lower natural gas prices in the high oil price scenario up to 2030 are, however, not enough to justify replacing the 40 ft diesel buses in the initial fleets with 40 ft CNG buses, given that a dozen extra 250 kWh 40 ft electric buses using fast charging at line terminals are in the fleet in 2030 compared to the base-case scenario's 2030 fleet configuration. Because the low oil price scenario is accompanied by higher natural gas prices than in the reference scenario over the entire planning horizon, the transition to electric buses for operations required to be carried out by articulated buses is accelerated (at the expense of CNG 60 ft buses), with almost twice as many 60 ft electric buses by the target year of 2035 compared to the base-case scenario. Moreover, the lower diesel prices result in a few 60 ft diesel buses being maintained in the fleet over the entire planning horizon in this scenario. The high oil price scenario is accompanied by a total discounted costs increase of almost ten million dollars compared with the base-case scenario, while the low oil price scenario allows reducing such costs by approximately five million dollars.

5.5.3.6 Battery prices

Another important component of the business case of fleet EVs that is subject to a fair amount of uncertainty is the price of lithium-ion batteries. The rate at which these prices fall directly impacts the purchase cost premium connected to EVs. In the base-case scenario, we assumed that the battery prices for electric buses decline at the same rate as those for passenger EVs, and we used the evolution of passenger EV battery prices from 2019 to 2050 from Schmidt et al. (2017) under the expected experience rate that they derived from historical data. Schmidt et al. (2017) have also made passenger EV battery price projections that take into

Table 5.7 – Optimal transition plans under different oil price scenarios

Vehicle types:		D-40	D-60	H-40	H-60	CNG-40	CNG-60	E350-40	E650-60	E250-40	E250-40 FC	E110-40	E110-40 PC
High oil price scenario													
2025 fleet configuration:		20	11	0	0	0	27	0	0	2	40	0	0
2030 fleet configuration:		8	5	0	0	0	29	0	4	2	52	0	0
2035 fleet configuration:		0	0	0	0	0	32	0	6	4	58	0	0
2040 fleet configuration:		0	0	0	0	0	8	0	30	2	60	0	0
2045 fleet configuration:		0	0	0	0	0	6	0	32	2	60	0	0
2050 fleet configuration:		0	0	0	0	0	6	0	32	16	46	0	0
Vehicle purchase costs (M$):	105.49												
Charger purchase costs (M$):	2.15												
Operating costs (M$):	90.67												
Demand charge (M$):	5.58			**Total costs (M$):**			209.93						
End-of-horizon costs (M$):	6.05			**Solution time (s)**			430.93						
Low oil price scenario													
2025 fleet configuration:		38	32	0	0	0	6	0	0	0	24	0	0
2030 fleet configuration:		21	20	0	0	0	7	0	11	1	40	0	0
2035 fleet configuration:		0	9	0	0	0	7	0	22	2	60	0	0
2040 fleet configuration:		0	7	0	0	0	1	0	30	2	60	0	0
2045 fleet configuration:		0	4	0	0	0	0	0	34	2	60	0	0
2050 fleet configuration:		0	4	0	0	0	0	0	34	2	60	0	0
Vehicle purchase costs (M$):	91.59												
Charger purchase costs (M$):	2.07												
Operating costs (M$):	90.76												
Demand charge (M$):	5.07			**Total costs (M$):**			196.54						
End-of-horizon costs (M$):	7.06			**Solution time (s)**			337.60						

account the uncertainty surrounding the experience rate, which we use in this section to investigate how EV adoption varies under different future battery price scenarios. The authors identified a 95% confidence interval for the experience rate under expected market growth rates for EV batteries. The lowest and highest experience rates of the confidence interval are used to derive high and low battery price scenarios, respectively. The corresponding optimal transition plans are reported in Table 5.8. As with the energy price scenarios, the battery price scenarios mostly impact decisions surrounding 60 ft buses, with articulated electric buses being added to the fleet more agressively in the low battery price scenario. The battery price scenario does not seem to influence standard 40 ft bus replacement decisions.

Table 5.8 – Optimal transition plans under different battery price scenarios

Vehicle types:		D-40	D-60	H-40	H-60	CNG-40	CNG-60	E350-40	E650-60	E250-40	E250-40 FC	E110-40	E110-40 PC
High battery price scenario													
2025 fleet configuration:		32	26	0	0	0	12	0	0	0	30	0	0
2030 fleet configuration:		21	13	0	0	0	24	0	1	1	40	0	0
2035 fleet configuration:		0	0	0	0	0	32	0	6	3	59	0	0
2040 fleet configuration:		0	0	0	0	0	24	0	14	3	59	0	0
2045 fleet configuration:		0	0	0	0	0	12	0	26	2	60	0	0
2050 fleet configuration:		0	0	0	0	0	10	0	28	3	59	0	0
Vehicle purchase costs (M$):	93.24												
Charger purchase costs (M$):	1.92												
Operating costs (M$):	97.37												
Demand charge (M$):	4.62			**Total costs (M$):**			203.99						
End-of-horizon costs (M$):	6.83			**Solution time (s):**			403.38						
Low battery price scenario													
2025 fleet configuration:		32	26	0	0	0	12	0	0	0	30	0	0
2030 fleet configuration:		16	14	0	0	0	18	0	6	1	45	0	0
2035 fleet configuration:		0	0	0	0	0	22	0	16	3	59	0	0
2040 fleet configuration:		0	0	0	0	0	10	0	28	3	59	0	0
2045 fleet configuration:		0	0	0	0	0	4	0	34	2	60	0	0
2050 fleet configuration:		0	1	0	0	0	3	0	34	2	60	0	0
Vehicle purchase costs (M$):	91.85												
Charger purchase costs (M$):	2.07												
Operating costs (M$):	94.08												
Demand charge (M$):	5.08			**Total costs (M$):**			199.88						
End-of-horizon costs (M$):	6.79			**Solution time (s):**			683.33						

5.5.3.7 EV maintenance savings

Blynn (2018) reports maintenance savings for electric buses that range from 20% to 60% compared with those of diesel buses. In the base-case scenario, we assumed a middle value of 40% savings relative to diesel maintenance costs for electric buses. In Table 5.9 we report the optimal fleet replacement plans obtained when the maintenance savings of EVs are set to the low and high ends identified by Blynn (2018). As in the previous two sections, decisions surrounding standard 40 ft buses are robust to the new scenarios. Regardless of maintenance savings for EVs, the 250 kWh battery combined with fast charging at bus line terminals remains the prefered option for standard-bus runs, but the choice of vehicle types for the articulated bus requirements is sensitive to the maintenance savings scenario. Aside from scenarios considered in Section 5.5.3.2 with stringent depot charging infrastructure requirements for 60 ft electric buses, the low EV maintenance savings scenario is the only scenario considered thus far that does not

include any 60 ft electric bus in the fleet by 2035. On the other hand, 14 articulated electric buses are already in the fleet by 2030 in the high EV maintenance savings scenario, which is the highest number of 60 ft electric buses in the 2030 fleet out of all scenarios considered thus far besides those with fleet electrification targets of 100% by 2025 and 2035 considered in Section 5.5.3.3.

Table 5.9 – Optimal transition plans under different EV maintenance savings assumptions

Vehicle types:		D-40	D-60	H-40	H-60	CNG-40	CNG-60	E350-40	E650-60	E250-40	E250-40 FC	E110-40	E110-40 PC
20% maintenance savings for EVs													
2025 fleet configuration:		38	25	0	0	0	13	0	0	0	24	0	0
2030 fleet configuration:		21	13	0	0	0	25	0	0	1	40	0	0
2035 fleet configuration:		0	0	0	0	0	38	0	0	2	60	0	0
2040 fleet configuration:		0	0	0	0	0	34	0	4	2	60	0	0
2045 fleet configuration:		0	0	0	0	0	24	0	14	2	60	0	0
2050 fleet configuration:		0	0	0	0	0	18	0	20	2	60	0	0
Vehicle purchase costs (M$):	87.86												
Charger purchase costs (M$):	1.75												
Operating costs (M$):	107.09												
Demand charge (M$):	4.17			**Total costs (M$):**			209.56						
End-of-horizon costs (M$):	8.68			**Solution time (s)**			302.22						
60% maintenance savings for EVs													
2025 fleet configuration:		29	26	0	0	0	9	0	3	1	32	0	0
2030 fleet configuration:		12	14	0	0	0	10	0	14	1	49	0	0
2035 fleet configuration:		0	0	0	0	0	14	0	24	3	59	0	0
2040 fleet configuration:		0	0	0	0	0	5	0	33	2	60	0	0
2045 fleet configuration:		0	0	0	0	0	4	0	34	2	60	0	0
2050 fleet configuration:		0	1	0	0	0	3	0	34	2	60	0	0
Vehicle purchase costs (M$):	98.40												
Charger purchase costs (M$):	2.18												
Operating costs (M$):	81.21												
Demand charge (M$):	5.62			**Total costs (M$):**			192.67						
End-of-horizon costs (M$):	5.26			**Solution time (s)**			512.77						

5.5.3.8 Robustness of choice to replace 40 ft diesel buses with electric buses

The fact that electric buses are thus far consistently chosen to carry out most of the standard-bus runs raises the question of whether this would be the case even under simultaneous worst-case scenarios for demand charges, energy prices, and maintenance savings for EVs, and without requiring any minimal proportion of the fleet to consist of EVs by the target year of 2035. Because it is unclear which oil price scenario is most detrimental to EVs considering how such scenarios also influence the adoption of CNG buses, we first tested each oil price scenario with

base case electric bus-to-charger ratios, high demand charges, low EV maintenance savings, and high battery prices. The results of this experiment are reported in Table 5.10 and illustrate that even in such worst-case scenarios and without any electrification requirements, electric buses remain the prefered option to replace the 40 ft diesel buses in the initial fleet, with 60 ft electric buses being the EV type that is at the mercy of such uncertain parameters. Not a single 60 ft electric bus is added to the fleet during the entire planning horizon in the worst-case scenarios with reference and high oil prices.

The required electric bus-to-charger ratios could very well deviate from those assumed in our base-case scenario for 40 ft electric buses as well. When the same "worst-case" scenarios for EVs described above are tested while also doubling all electric bus-to-charger ratios from the base-case scenario (the results of which are reported in Table 5.11), the standard electric buses finally lose their edge at the expense of 40 ft CNG buses in the short and medium term. Nevertheless, even in this case, 40 ft electric buses represent a significant portion of the fleet near the end of the planning horizon with increasing natural gas prices and reduced battery prices in the long term.

5.5.3.9 Salvage values

The uncertainty surrounding the residual values of EVs is often cited as being a challenge to fleet operators who are thinking of incorporating them into their fleet. Cities interested in adding electric buses to their public transit fleet have also stated this to be the case (Bloomberg New Energy Finance, 2018). Although salvage revenues do not seem to be particularly impactful for replacement decisions of conventional buses (Laver et al., 2007), the strong potential of second-life applications for batteries of electric buses could result in significant revenues from reselling their batteries upon retiring vehicles. To investigate how salvage values influence optimal replacement plans, we have solved the base case from

Table 5.10 – Optimal transition plans under base case bus-to-charger ratios, worst-case scenarios for EVs in terms of demand charges, battery prices, and maintenance savings, and without electrification requirements

Vehicle types:		D-40	D-60	H-40	H-60	CNG-40	CNG-60	E350-40	E650-60	E250-40	E250-40 FC	E110-40	E110-40 PC
Reference oil price scenario with worst case demand charges, battery prices and maintenance savings for EVs													
2025 fleet configuration:		42	25	0	0	0	13	0	0	0	20	0	0
2030 fleet configuration:		20	13	0	0	0	25	0	0	2	40	0	0
2035 fleet configuration:		0	0	0	0	0	38	0	0	2	60	0	0
2040 fleet configuration:		0	0	0	0	0	38	0	0	2	60	0	0
2045 fleet configuration:		0	0	0	0	0	38	0	0	2	60	0	0
2050 fleet configuration:		0	0	0	0	0	38	0	0	2	60	0	0
Vehicle purchase costs (M$):	86.42												
Charger purchase costs (M$):	1.49												
Operating costs (M$):	109.41												
Demand charge (M$):	7.65			**Total costs (M$):**			214.91						
End-of-horizon costs (M$):	9.94			**Solution time (s):**			432.73						
High oil price scenario with worst case demand charges, battery prices and maintenance savings for EVs													
2025 fleet configuration:		26	10	0	0	2	28	0	0	0	34	0	0
2030 fleet configuration:		12	5	0	0	2	33	0	0	0	48	0	0
2035 fleet configuration:		0	0	0	0	0	38	0	0	2	60	0	0
2040 fleet configuration:		0	0	0	0	0	38	0	0	2	60	0	0
2045 fleet configuration:		0	0	0	0	0	38	0	0	2	60	0	0
2050 fleet configuration:		0	0	0	0	0	38	0	0	15	47	0	0
Vehicle purchase costs (M$):	97.71												
Charger purchase costs (M$):	1.57												
Operating costs (M$):	108.87												
Demand charge (M$):	8.45			**Total costs (M$):**			224.78						
End-of-horizon costs (M$):	8.18			**Solution time (s):**			1170.53						
Low oil price scenario with worst case demand charges, battery prices and maintenance savings for EVs													
2025 fleet configuration:		42	31	0	0	0	7	0	0	0	20	0	0
2030 fleet configuration:		21	22	0	0	0	16	0	0	2	39	0	0
2035 fleet configuration:		0	7	0	0	0	31	0	0	2	60	0	0
2040 fleet configuration:		0	3	0	0	0	31	0	4	2	60	0	0
2045 fleet configuration:		0	2	0	0	0	22	0	14	2	60	0	0
2050 fleet configuration:		0	9	0	0	0	7	0	22	2	60	0	0
Vehicle purchase costs (M$):	86.95												
Charger purchase costs (M$):	1.76												
Operating costs (M$):	105.76												
Demand charge (M$):	8.19			**Total costs (M$):**			211.65						
End-of-horizon costs (M$):	8.99			**Solution time (s):**			360.64						

Section 5.5.1 with different assumptions regarding salvage values. In both new scenarios, the salvage values of diesel and hybrid vehicles are set to $1,000 regardless of the age of the vehicle, as in Feng and Figliozzi (2014). We further assume that the CNG buses have the same salvage value due to their similar drivetrain. For the electric buses, we assume at the start of any given year, the battery can be sold in a second-hand market for a certain percentage of that year's price for a new same-sized battery. We solved the problem assuming the battery of the electric buses can be sold for 30% and 60% of the current price of a new battery

Table 5.11 – Optimal transition plans under doubled base case bus-to-charger ratios, worst-case scenarios for EVs in terms of demand charges, battery prices, and maintenance savings, and without electrification requirements

Vehicle types:	D-40	D-60	H-40	H-60	CNG-40	CNG-60	E350-40	E650-60	E250-40	E250-40 FC	E110-40	E110-40 PC
Reference oil price scenario with doubled charger ratios and worst case demand charges, battery prices and EV maintenance savings												
2025 fleet configuration:	41	25	0	0	21	13	0	0	0	0	0	0
2030 fleet configuration:	21	13	0	0	41	25	0	0	0	0	0	0
2035 fleet configuration:	0	0	0	0	61	38	0	0	1	0	0	0
2040 fleet configuration:	0	0	0	0	51	38	0	0	2	9	0	0
2045 fleet configuration:	0	0	0	0	31	38	0	0	2	29	0	0
2050 fleet configuration:	0	0	0	0	11	38	0	0	11	40	0	0
Vehicle purchase costs (M$): 88.24												
Charger purchase costs (M$): 1.47												
Operating costs (M$): 118.25												
Demand charge (M$): 3.08			**Total costs (M$):**			220.95						
End-of-horizon costs (M$): 9.91			**Solution time (s):**			114.10						
High oil price scenario with doubled charger ratios and worst case demand charges, battery prices and EV maintenance savings												
2025 fleet configuration:	31	10	0	0	31	28	0	0	0	0	0	0
2030 fleet configuration:	14	5	0	0	48	33	0	0	0	0	0	0
2035 fleet configuration:	0	0	0	0	48	38	0	0	4	10	0	0
2040 fleet configuration:	0	0	0	0	38	38	0	0	4	20	0	0
2045 fleet configuration:	0	0	0	0	21	38	0	0	4	37	0	0
2050 fleet configuration:	0	0	0	0	10	38	0	0	18	34	0	0
Vehicle purchase costs (M$): 98.66												
Charger purchase costs (M$): 1.64												
Operating costs (M$): 118.09												
Demand charge (M$): 4.64			**Total costs (M$):**			231.03						
End-of-horizon costs (M$): 8.00			**Solution time (s):**			163.64						
Low oil price scenario with doubled charger ratios and worst case demand charges, battery prices and EV maintenance savings												
2025 fleet configuration:	43	31	0	0	19	7	0	0	0	0	0	0
2030 fleet configuration:	24	23	0	0	28	15	0	0	0	10	0	0
2035 fleet configuration:	10	8	0	0	28	30	0	0	4	20	0	0
2040 fleet configuration:	17	3	0	0	9	35	0	0	6	30	0	0
2045 fleet configuration:	14	0	0	0	0	38	0	0	8	40	0	0
2050 fleet configuration:	8	9	0	0	0	23	0	6	14	40	0	0
Vehicle purchase costs (M$): 85.05												
Charger purchase costs (M$): 2.05												
Operating costs (M$): 115.35												
Demand charge (M$): 7.14			**Total costs (M$):**			219.52						
End-of-horizon costs (M$): 9.94			**Solution time (s):**			264.18						

of the same size; the results are given in Table 5.12. As for non-electric buses, the salvage values do not seem to bear much influence on optimal replacement plans. Even under the assumption that the used batteries can be sold for up to 60% of the current price of a new equivalent battery, the only difference compared to the base case replacement plan that assumes no salvage values for all vehicles is a few additional 60 ft electric buses throughout the planning horizon in place of 60 ft CNG buses, and a few extra 40 ft electric buses early on in the planning horizon in place of 40 ft diesel buses.

Table 5.12 – Optimal transition plans under different salvage value assumptions

Vehicle types:	D-40	D-60	H-40	H-60	CNG-40	CNG-60	E350-40	E650-60	E250-40	E250-40 FC	E110-40	E110-40 PC
$1,000 for non-EVs, 30% of price of a new battery for EVs												
2025 fleet configuration:	32	26	0	0	0	12	0	0	0	30	0	0
2030 fleet configuration:	21	14	0	0	0	19	0	5	1	40	0	0
2035 fleet configuration:	0	0	0	0	0	24	0	14	3	59	0	0
2040 fleet configuration:	0	0	0	0	0	13	0	25	3	59	0	0
2045 fleet configuration:	0	0	0	0	0	6	0	32	2	60	0	0
2050 fleet configuration:	0	0	0	0	0	6	0	32	4	58	0	0

Vehicle purchase costs (M$):	93.23		
Charger purchase costs (M$):	2.03		
Operating costs (M$):	94.74		
Salvage revenues (M$):	0.68		
Demand charge (M$):	4.97	**Total costs (M$):**	200.62
End-of-horizon costs (M$):	6.32	**Solution time (s):**	555.32

$1,000 for non-EVs, 60% of price of a new battery for EVs												
2025 fleet configuration:	32	26	0	0	0	12	0	0	0	30	0	0
2030 fleet configuration:	17	13	0	0	0	18	0	7	1	44	0	0
2035 fleet configuration:	0	0	0	0	0	22	0	16	3	59	0	0
2040 fleet configuration:	0	0	0	0	0	10	0	28	3	59	0	0
2045 fleet configuration:	0	0	0	0	0	4	0	34	2	60	0	0
2050 fleet configuration:	0	1	0	0	0	3	0	34	3	59	0	0

Vehicle purchase costs (M$):	93.79		
Charger purchase costs (M$):	2.07		
Operating costs (M$):	94.09		
Salvage revenues (M$):	1.31		
Demand charge (M$):	5.08	**Total costs (M$):**	199.53
End-of-horizon costs (M$):	5.81	**Solution time (s):**	553.66

5.5.3.10 Depot upgrades for CNG buses

When no CNG buses have ever been owned by a transit agency, modifications may need to be made to depots (e.g., to upgrade heating and ventilating systems and to install a CNG fueling station) before being able to operate such buses (Stasko and Gao, 2010). We did not consider such requirements in the model of Section 5.3.1 and in the base-case scenario described in Section 5.5.1 because we assume that organizations that plan to rely heavily on EVs in the future would only consider adding new CNG vehicles to their fleets if they already have the required infrastructure to accommodate them. Nevertheless, if such organizations are still willing to consider purchasing CNG vehicles despite the need for such investments, this feature can be added to the EFTP. Assuming that the cost of making such a facility upgrade at the start of period t is γ_t as in Stasko and Gao (2010), one may use binary variables λ_t equal to one if the CNG depot upgrade

is made at the start of period t, and taking a value of zero otherwise, in order to incorporate this feature into the EFTP. More precisely, the term $\sum_{t \in T} \beta^{t-1} \gamma_t \lambda_t$ should be added to objective function (5.1), and the following constraints should be added to the model of Section 5.3.1:

$$\cdot \sum_{k \in K_{CNG}} \sum_{j=0}^{\kappa^k} z_{jt}^k \leq M \cdot \sum_{\tau=1}^{t} \lambda_\tau \quad t \in T,$$

with set $K_{CNG} \subseteq K$ containing all CNG bus types and M being a sufficiently large number (e.g., the largest total number of runs to be performed in any given period). The investment associated with the depot upgrades should also be incorporated into the budget constraints (5.12).

Because 60 ft CNG buses are consistently added to the fleet in optimal transition plans obtained thus far as an intermediate solution before adopting 60 ft EVs in the long term, we tested how such decisions are affected by depot upgrades for CNG buses by adding such requirements to the base-case scenario. We used the same value for γ_t as in Stasko and Gao (2010), itself based on values provided in Clark et al. (2007). The cost of the depot upgrade for CNG buses remains constant over the course of the planning horizon and is almost three million dollars. The results are presented in Table 5.13 for three scenarios: the base-case scenario with the additional CNG depot upgrade requirement, the base-case scenario with the additional CNG depot upgrade requirement and assuming fast depot charging requirements for the 60 ft electric buses (as described in Section 5.5.3.2) with a bus-to-charger ratio of 2:1, and the base-case scenario with the additional CNG depot upgrade requirement and assuming fast depot charging requirements for the 60 ft electric buses with a bus-to-charger ratio of 1:1.

It is interesting to note that while the 60 ft CNG buses are clearly the prefered medium-term solution to ensure a smooth transition to 60 ft electric buses in the long-term in the base-case scenario, not a single CNG bus is purchased when only adding the depot upgrade requirement for CNG buses to the base-case scenario.

In this case the transition to 60 ft electric buses takes place at a much quicker pace. However, despite the required CNG bus-related depot modifications, when the 60 ft electric buses are assumed to require fast rather than slow depot chargers, the optimal transition plan reverts back to 60 ft CNG buses as replacements to the initial 60 ft diesel buses in the fleet. Articulated electric buses are still adopted in the long term when the ratio between such buses and the fast depot chargers is set to 2:1, but not a single articulated electric bus is added to the fleet over the course of the planning horizon when the ratio is 1:1, despite the depot upgrade for CNG buses.

Table 5.13 – Optimal transition plans when depot upgrades are required prior to operating CNG buses

Vehicle types:	D-40	D-60	H-40	H-60	CNG-40	CNG-60	E350-40	E650-60	E250-40	E250-40 FC	E110-40	E110-40 PC
Base-case scenario with additional depot upgrade for CNG buses												
2025 fleet configuration:	32	30	0	0	0	0	0	8	0	30	0	0
2030 fleet configuration:	15	15	0	0	0	0	0	23	1	46	0	0
2035 fleet configuration:	0	3	0	0	0	0	0	35	3	59	0	0
2040 fleet configuration:	0	3	0	0	0	0	0	35	3	59	0	0
2045 fleet configuration:	0	3	0	0	0	0	0	35	2	60	0	0
2050 fleet configuration:	0	3	0	0	0	0	0	35	3	59	0	0

Vehicle purchase costs (M$):	97.47		
Charger purchase costs + CNG depot upgrade (M$):	2.23		
Operating costs (M$):	91.07		
Demand charge (M$):	5.74	**Total costs (M$):**	203.57
End-of-horizon costs (M$):	7.06	**Solution time (s)**	1513.63

Base-case scenario with additional depot upgrade for CNG buses and fast depot chargers for 60 ft electric buses (ratio of 2:1)												
2025 fleet configuration:	32	26	0	0	0	12	0	0	0	30	0	0
2030 fleet configuration:	20	13	0	0	0	25	0	0	2	40	0	0
2035 fleet configuration:	0	0	0	0	0	34	0	4	4	58	0	0
2040 fleet configuration:	0	0	0	0	0	30	0	8	4	58	0	0
2045 fleet configuration:	0	0	0	0	0	18	0	20	2	60	0	0
2050 fleet configuration:	0	0	0	0	0	14	0	24	4	58	0	0

Vehicle purchase costs (M$):	90.58		
Charger purchase costs + CNG depot upgrade (M$):	4.87		
Operating costs (M$):	98.45		
Demand charge (M$):	5.07	**Total costs (M$):**	205.76
End-of-horizon costs (M$):	6.79	**Solution time (s)**	5815.84

Base-case scenario with additional depot upgrade for CNG buses and fast depot chargers for 60 ft electric buses (ratio of 1:1)												
2025 fleet configuration:	32	23	0	0	0	15	0	0	0	30	0	0
2030 fleet configuration:	20	11	0	0	0	27	0	0	2	40	0	0
2035 fleet configuration:	0	0	0	0	0	38	0	0	4	58	0	0
2040 fleet configuration:	0	0	0	0	0	38	0	0	4	58	0	0
2045 fleet configuration:	0	0	0	0	0	38	0	0	2	60	0	0
2050 fleet configuration:	0	0	0	0	0	38	0	0	5	57	0	0

Vehicle purchase costs (M$):	88.09		
Charger purchase costs + CNG depot upgrade (M$):	4.17		
Operating costs (M$):	101.51		
Demand charge (M$):	4.06	**Total costs (M$):**	206.28
End-of-horizon costs (M$):	8.45	**Solution time (s)**	494.17

5.5.3.11 Miscellaneous extensions

We show in this section how two simple adjustments can be made to the model of Section 5.3.1 to incorporate other cost components that may be present in the specific context at hand. For example, significant costs may need to be incurred near the midlife of vehicles for, among other things, engine overhauls and battery replacements (Blynn, 2018). Assuming a vehicle of type k is subject to midlife costs of mc_t^k when it reaches its midlife age of α^k during period t, then the following terms should be added to the objective function (5.1):

$$\sum_{t \in T} \beta^{t-1} \sum_{k \in K} mc_t^k z_{\alpha^k t}^k + \sum_{k \in K} \sum_{j=0}^{\alpha^k - 1} \beta^{t_F + \alpha^k - j - 1} mc_{t_F}^k z_{j t_F}^k.$$

The first term represents midlife costs incurred over the course of the planning horizon, while the second is to incorporate midlife costs into the end-of-horizon costs. Another possibility is that the EV chargers are associated with certain periodic maintenance costs, as indicated by an additional parameter ρ^c, in which case the term

$$\sum_{t \in T} \beta^{t-1} \sum_{c \in CT} \left(p^c u_t^c + F g^c v_t^c \right)$$

in objective function (5.1) should be changed for

$$\sum_{t \in T} \beta^{t-1} \sum_{c \in CT} \left(p^c u_t^c + (F g^c + \rho^c) v_t^c \right).$$

Results obtained with each of these extensions to the base-case scenario are presented in Table 5.14. The scenario with midlife costs assumes that such costs are incurred for vehicles when they reach an age of eight years. The midlife costs for non-EVs are taken from Blynn (2018) and represent engine overhauls. The midlife costs for EVs are assumed to represent battery replacements, and their values are therefore the price of a new battery (of the size associated with the specific EV type) with battery costs of the current period. The scenario with pe-

riodic charger maintenance costs assumes that such costs correspond to 3% of the charger's purchase costs, as in Lajunen (2018). The results obtained with the additional midlife costs suggest that such costs have similar impacts to those of other parameters studied in the sensitivity analysis: the adoption of 60 ft electric buses takes place at a slower rate than in the base-case scenario, this time due to the large fees associated with replacing the 650 kWh battery over the course of the vehicle's lifetime. The additional charger maintenance costs seem to have a fairly limited impact on the replacement plan compared with the base case results.

Table 5.14 – Optimal transition plans under miscellaneous extensions to the base-case scenario

Vehicle types:		D-40	D-60	H-40	H-60	CNG-40	CNG-60	E350-40	E650-60	E250-40	E250-40 FC	E110-40	E110-40 PC
Base-case scenario with additional midlife costs													
2025 fleet configuration:		34	23	0	0	0	15	0	0	0	28	0	0
2030 fleet configuration:		20	13	0	0	0	25	0	0	2	40	0	0
2035 fleet configuration:		0	0	0	0	0	34	0	4	3	59	0	0
2040 fleet configuration:		0	0	0	0	0	24	0	14	3	59	0	0
2045 fleet configuration:		0	0	0	0	0	14	0	24	2	60	0	0
2050 fleet configuration:		0	0	0	0	0	10	0	28	3	59	0	0
Vehicle purchase costs (M$):	90.79												
Charger purchase costs (M$):	1.90												
Operating costs (M$):	98.18												
Midlife costs (M$):	6.37												
Demand charge (M$):	4.52			**Total costs (M$):**			209.42						
End-of-horizon costs (M$):	7.65			**Solution time (s)**			767.70						
Base-case scenario with additional charger maintenance costs													
2025 fleet configuration:		34	25	0	0	0	13	0	0	0	28	0	0
2030 fleet configuration:		20	13	0	0	0	23	0	2	2	40	0	0
2035 fleet configuration:		0	0	0	0	0	28	0	10	4	58	0	0
2040 fleet configuration:		0	0	0	0	0	16	0	22	4	58	0	0
2045 fleet configuration:		0	0	0	0	0	6	0	32	2	60	0	0
2050 fleet configuration:		0	0	0	0	0	6	0	32	3	59	0	0
Vehicle purchase costs (M$):	92.37												
Charger purchase costs (M$):	2.01												
Operating costs (M$):	95.73												
Charger maintenance costs (M$):	0.99												
Demand charge (M$):	4.84			**Total costs (M$):**			202.74						
End-of-horizon costs (M$):	6.81			**Solution time (s)**			448.52						

5.5.4 The stochastic EFTP

Solving multi-period stochastic programs is notoriously difficult, not to mention the issue of designing a scenario tree that adequately represents the true distribu-

tion of uncertain parameters. While the resolution of the stochastic counterpart of the EFTP will be the focus of future work, we nevertheless briefly illustrate how the formulation stated in Section 5.4 can still be of use with a commercial solver like CPLEX if one makes assumptions that reduce the size of the problem.

To this end, we have modified the base-case scenario described in Section 5.5.1 so as to assume that 1) purchasing and task assignment decisions are made every five years (a period t thus corresponds to a time span of five years); 2) future energy and battery prices are random parameters; and 3) at least 50% of the fleet must be converted to EVs immediately (i.e., at the start of the planning horizon). The resulting stochastic problem is solved with the formulation of Section 5.4. We make no claim that the scenario tree we have devised represents realistic probabilities of transitioning from one state to another; our goal is simply to demonstrate how one may use the stochastic EFTP with a reasonably sized scenario tree and limited number of periods in the planning horizon. Since moving from a parent node to a child node represents a time span of five years, we assigned the initial vehicles in the fleet to the nearest age between zero, five, 10 and 15 years in order for all vehicle ages to remain a multiple of five at each node, and we assumed that an increment of one with age indices j in the model of Section 5.4 corresponds to an age increase of five years (so $j = 0$ corresponds to a new vehicle, $j = 1$ corresponds to an age of five years, and so on).

We assumed three possible states for energy prices in each period, and three possible states for battery prices in each period. These states correspond to the reference oil price and battery price scenarios used in the base-case scenario, as well as the high and low oil and battery price scenarios tested in Sections 5.5.3.5 and 5.5.3.6, respectively. A total of nine states are thus possible in any given period (i.e., any combination of the three energy price states with the three battery price states). The scenario tree comprises a total 1063 nodes. The first period of the planning horizon is assumed to be 2019, the second period is 2024 (five

years later), and so on until 2049; there are thus seven periods of five years each, the last of which begins in 2049. From the root node in 2019, any of the nine possible states can be reached in 2024. The probabilities are set so that the odds of ending up in the reference, high oil price, and low oil price scenarios in 2024 are 0.5, 0.25 and 0.25, respectively, and that the odds of ending up in the reference, high battery price, and low battery price scenarios in 2024 are 0.5, 0.25 and 0.25, respectively. Each of the nine nodes in 2024 also has nine children nodes in 2029, but the probabilities of reaching the nine possible states in 2029 are conditional upon the state reached in 2024. The assumption is then that the battery price scenario reached in 2029 remains the same until the end of the planning horizon, but that the energy prices are more volatile in the long term and can therefore still change. Consequently, each node in 2029 has three children nodes that could be reached in 2034, representing the three energy price states and with probabilities conditional upon the energy price state reached in 2029. The state reached in 2034 then remains the same until the end of the planning horizon. There are thus one node in 2019, nine nodes in 2024, 81 nodes in 2029, 243 nodes in 2034, 243 nodes in 2039, 243 nodes in 2044, and 243 nodes in 2049 for a total of 1063 nodes.

Energy prices (i.e., diesel, natural gas and electricity) during a given period of five years were assumed to be the values associated with the first year of the period in the realized oil price scenario. Total operational costs incurred over the course of a five-year period however took into account the yearly increases of maintenance costs as the vehicle ages over the course of the period. Characteristics of the optimal solution to the stochastic version of the EFTP described above are presented in Table 5.15. We report the fleet configuration at the root node, and the fleet configuration at each of the nine possible states in 2024 (with RO, HO, LO representing reference, high, and low oil price scenarios, respectively, and RB, HB, LB representing reference, high and low battery price scenarios, respectively). While we make no claims of insights derived from the results, they still

demonstrate how the stochastic counterpart can be used to guide immediate decisions despite uncertain future developments. For this particular configuration, the optimal solution recommends electrifying the minimum proportion required (i.e., 50% of the fleet) with eight articulated electric buses and 42 standard electric buses, and waiting to see the realized state five years later prior to making additional investments in electric buses.

Table 5.15 – Optimal solution to the assumed stochastic counterpart of the EFTP

Vehicle types:		D-40	D-60	H-40	H-60	CNG-40	CNG-60	E350-40	E650-60	E250-40	E250-40 FC	E110-40	E110-40 PC
Root node fleet configuration:		20	30	0	0	0	0	0	8	4	38	0	0
Fleet configuration after five years in RO+ RB state:		11	16	0	0	0	13	0	9	4	47	0	0
Fleet configuration after five years in RO+ HB state:		12	15	0	0	0	15	0	8	4	46	0	0
Fleet configuration after five years in RO+ LB state:		10	15	0	0	0	11	0	12	4	48	0	0
Fleet configuration after five years in HO+ RB state:		4	5	0	0	0	25	0	8	4	54	0	0
Fleet configuration after five years in HO+ HB state:		6	5	0	0	0	25	0	8	4	52	0	0
Fleet configuration after five years in HO+ LB state:		4	5	0	0	0	23	0	10	4	54	0	0
Fleet configuration after five years in LO+ RB state:		18	27	0	0	0	3	0	8	4	40	0	0
Fleet configuration after five years in LO+ HB state:		18	27	0	0	0	3	0	8	4	40	0	0
Fleet configuration after five years in LO+ LB state:		18	26	0	0	0	2	0	10	4	40	0	0
Expected costs (M$):	220.89												
Solution time (s):	13,593.30												

5.6. Conclusions

We have introduced the EFTP, whose solution provides strategic guidance to organizations having set fleet electrification targets to be met in upcoming years. We have presented deterministic and stochastic formulations of the EFTP in the form of integer and mixed integer linear programs, respectively. The formulations simultaneously take into account temporal electrification targets, vehicle purchasing and salvaging decisions, several types of EVs with different charging configurations, charger type-specific infrastructure investments and demand charges, aggregated task assignment decisions, and the mitigation of end-of-horizon effects. We have also shown how simple modifications can be made to incorporate other extensions according to the operating context, such as midlife costs, charger maintenance costs, and facility upgrades for CNG buses.

We have performed a case study inspired by real data obtained from a bus operator in France, and our numerical experiments suggest that electric buses with medium-sized batteries that are charged in depots overnight and at bus line terminals with fast plug-in chargers during the day are the optimal choice for 40 ft buses in this context. The optimal transition plan also suggested that while 60 ft electric buses present a promising business case in the longer term, articulated CNG buses are the most cost-effective intermediate alternative to articulated diesel buses until battery prices have fallen sufficiently. This is however contingent on no facility upgrade being required before incorporating CNG buses into the fleet, and on the assumed depot charging requirements for 60 ft electric buses. These findings may be of interest to other transit fleets operating in similar operational contexts (i.e., medium-sized cities with buses traveling an average of 200 km per day).

Moreover, our sensitivity analyses have shown that the choice of 40 ft electric buses to replace the initial diesel vehicles in the fleet is quite robust to parameters subject to uncertain future developments, but that such parameters can have a significant impact on the time frame associated with the incorporation of 60 ft electric buses into the fleet. No hybrid buses were used in any optimal solution, which may suggest that using such vehicles as an intermediate step towards full electrification may not be a cost-effective strategy.

Finally, we have also demonstrated that the stochastic counterpart can be solved to optimality with a reasonably sized scenario tree if purchasing decisions can be assumed to occur every five years rather than each year. We believe that interesting research avenues lie in the development of sophisticated solution methods for the stochastic counterpart of the EFTP, and in performing similar case studies for goods distribution contexts as well.

Acknowledgements

This research was partly supported by the Canadian Natural Sciences and Engineering Research Council under grants 463834-2014, 436014-2013 and 2015-06189. This support is gratefully acknowledged.

References

Ahani, P., A. Arantes, S. Melo. 2016. A portfolio approach for optimal fleet replacement toward sustainable urban freight transportation. *Transportation Research Part D: Transport and Environment* **48** 357–368.

Ambrose, H., N. Pappas, A. Kendall. 2017. Exploring the costs of electrification for California's transit agencies. Report No. UC-ITS-RR-2017-03, University of California Institute of Transportation Studies. URL `https://cloudfront.escholarship.org/dist/prd/content/qt0fn8s2jh/qt0fn8s2jh.pdf`. Last accessed May 2019.

Ansaripoor, A.H., F.S. Oliveira, A. Liret. 2016. Recursive expected conditional value at risk in the fleet renewal problem with alternative fuel vehicles. *Transportation Research Part C: Emerging Technologies* **65** 156–171.

Aronson, J.E., J.S. Aronofsky. 1983. Network generating models for equipment replacement. Technical report 83-OR-5, Department of Operations Research, Southern Methodist University, Dallas, TX.

Avere-France. 2017. Développer le transport en commun en véhicule électrique URL `http://www.avere-france.org/Site/Article/?article_id=5893`. Last accessed May 2019.

Bakır, İ. 2017. Large scale optimization methods for fleet management in long-haul transportation networks. Ph.D. thesis, Georgia Institute of Technology, Georgia.

Bektaş, T., J.F. Ehmke, H.N. Psaraftis, J. Puchinger. 2018. The role of operational research in green freight transportation. *European Journal of Operational Research* **274**(3) 807–823.

Bloomberg New Energy Finance. 2018. Electric buses in cities: Driving towards cleaner air and lower CO2. On behalf of: Financing Sustainable Cities Initiative, C40 Cities, World Resources Institute, Citi Foundation. URL `https://data.bloomberglp.com/professional/sites/24/2018/05/Electric-Buses-in-Cities-Report-BNEF-C40-Citi.pdf`. Last accessed May 2019.

Blynn, K. 2018. Accelerating bus electrification: Enabling a sustainable transition to low carbon transportation systems. M.Sc. thesis, Massachusetts Institute of Technology, Massachusetts.

BYD Motors. 2018. K11 electric transit bus. URL `https://en.byd.com/bus/k11-electric-transit-bus/`. Last accessed April 2019.

Clark, N.N., F. Zhen, W.S. Wayne, D.W. Lyons. 2007. Transit Bus Life Cycle Cost and Year 2007 Emissions Estimation. Report No. FTA WV-26-7004.2007.1, US Federal Transit Administration. URL `https://rosap.ntl.bts.gov/view/dot/29168`. Last accessed May 2019.

The Climate Group. 2018. EV100 Members. URL `https://www.theclimategroup.org/ev100-members`. Last accessed May 2019.

CNBC. 2019. Morgan Stanley: Push to electric vans and trucks will be led by Amazon and other 'megafleets'. URL `https://www.cnbc.com/2019/02/20/`

morgan-stanley-push-to-electric-vans-and-trucks-will-be-led-by-amazon-and-other-megafleets.html. Last accessed May 2019.

Feng, W., M. Figliozzi. 2013. An economic and technological analysis of the key factors affecting the competitiveness of electric commercial vehicles: A case study from the USA market. *Transportation Research Part C: Emerging Technologies* **26** 135–145.

Feng, W., M. Figliozzi. 2014. Vehicle technologies and bus fleet replacement optimization: Problem properties and sensitivity analysis utilizing real-world data. *Public Transport* **6**(1-2) 137–157.

Gallo, J.-B., T. Bloch-Rubin, J. Tomić. 2014. Peak demand charges and electric transit buses. CALSTART. URL http://calstart.org/wp-content/uploads/2018/10/Peak-Demand-Charges-and-Electric-Transit-Buses.pdf. Last accessed May 2019.

Grinold, R.C 1983. Model building techniques for the correction of end effects in multistage convex programs. *Operations Research* **31**(3) 407–431.

Islam, A. 2018. Minimization of carbon footprint of transit agencies by adopting alternative fuel technologies. M.Sc. thesis, University of Connecticut, Connecticut.

Karabakal, N., J.R. Lohmann, J.C. Bean. 1994. Parallel replacement under capital rationing constraints. *Management Science* **40**(3) 305–319.

Kleindorfer, P.R., A. Neboian, A. Roset, S Spinler. 2012. Fleet renewal with electric vehicles at La Poste. *Interfaces* **42**(5) 465–477.

Lajunen, A. 2018. Lifecycle costs and charging requirements of electric buses with different charging methods. *Jounral of Cleaner Production* **172** 56–67.

Laver, R., D. Schneck, D., Skorupski, S. Brady, L. Cham. 2007. Useful life of transit buses and vans. Report No. FTA VA-26-7229-07.1, US Federal Transit Administration.

Montreal Gazette. 2018. Montreal, Laval team up in Canada's largest order of electric buses. URL `https://montrealgazette.com/news/local-news/montreal-laval-team-up-in-canadas-largest-order-of-electric-buses`. Last accessed May 2019.

Pelletier, S., O. Jabali, G. Laporte. 2016. 50th anniversary invited article – Goods distribution with electric vehicles: Review and research perspectives. *Transportation Science* **50**(1) 3–22.

Pelletier, S., O. Jabali, G. Laporte. 2018. Charge scheduling for electric freight vehicles. *Transportation Research Part B: Methodological* **115** 246–269.

Schmidt, O., A. Hawkes, A. Gambhir, I. Staffell. 2017. The future cost of electrical energy storage based on experience rates. *Nature Energy* **2**, Article No. 17110.

Stasko, T.H., H.O. Gao. 2010. Reducing transit fleet emissions through vehicle retrofits, replacements, and usage changes over multiple time periods. *Transportation Research Part D: Transport and Environment* **15** 254–262.

U.S. Energy Information Administration. 2019. Annual Energy Outlook 2019. URL `https://www.eia.gov/outlooks/aeo/`. Last accessed May 2019.

General Conclusion

Goods distribution operations are responsible for a significant share of global polluting emissions, and EFVs have the potential to yield important societal benefits if they can be successfully incorporated into more fleets. However, because of the technological drawbacks and specific cost structure of EFVs, fleet managers must make careful decisions about purchasing, charging and routing them. The objective of this thesis was to use operations research techniques to facilitate the integration of EFVs into goods distribution schemes, thereby developing optimization-based decision making tools to support such decisions. Our main scientific contribution is thus to introduce, model and solve practical transportation problems associated with EFVs, and to identify useful managerial insights along the way. The thesis is a collection of five contributions that were written as independent scientific papers. We believe that collectively they attain the aforementioned objective.

General contributions

The first two papers of the thesis aim to gather all the relevant background information required to identify and model practical transportation problems pertaining to goods distribution with electric vehicles. We therefore began with a review of the literature related to the use of EFVs in the first paper of the thesis. Its main

contributions were to provide transportation researchers with an overview of the technological background and market penetration information needed to conduct research in this area, to present a survey of the existing research on electric vehicles in transportation science at the time of redaction, and to offer perspectives for future research. The paper clearly had an important impact on the field, as it has already been frequently quoted, and several of the research perspectives it identified were the subject of studies conducted by other researchers in the few years following its publication. Moreover, the paper was critical for identifying research directions to follow in the rest of the thesis, namely regarding the need for modeling the behaviour of electric vehicle batteries more realistically in transportation problems, and for more research dealing with issues arising in contexts in which EFVs are not recharged en route.

In the second paper of the thesis, we therefore investigated how fundamental battery degradation and behaviour characteristics could be modeled in a tractable way. Its main contribution was to provide applicable knowledge on this topic to the growing community of researchers involved in the planning of goods distribution by electric vehicles. Several existing battery models and principles were described and aggregated in order to account for fundamental battery behaviour, thereby generating practical approaches for modeling the charging, discharging and degradation of electric vehicle batteries in transportation problems. The review and analysis of battery degradation mechanisms also led to the identification of intuitive insights which should be of interest from a fleet management perspective in the context of goods distribution with electric vehicles.

Based on the aforementioned research perspectives, modeling approaches and managerial insights from the first two papers, we then introduced three relevant optimization problems pertaining to EFVs from both an operational and a strategic planning perspective: the electric freight vehicle charge scheduling problem (EFV-CSP), the electric vehicle routing problem with energy consumption uncer-

tainty (EVRP-ECU), and the electric fleet transition problem (EFTP). Each of these problems was the topic of one of the three subsequent papers in the thesis.

Operational planning problems

The third and fourth papers aimed to solve operational problems resulting from the fact that EFVs are typically charged at a central depot, and rarely use charging stations en route in urban environments. In the third paper, we considered the implications of this issue on charging decisions through the EFV-CSP, in which the charging schedule at the depot must be planned so as to allow a fleet of EFVs to complete their routes at minimal cost. We developed a comprehensive mathematical model for the EFV-CSP that incorporates a large variety of features associated with the use of EFVs. These include a realistic charging process, time-dependent energy costs, battery degradation, grid restrictions, and facility-related demand charges. Several interesting managerial insights were then derived through an extensive computational study. In the fourth paper, we focused on the routing implications of only charging EFVs at the depot by introducing the EVRP-ECU, in which EFVs must be routed so that they never get stranded along their routes regardless of the realization of energy consumption uncertainties. We used a robust optimization approach to take into account such energy consumption uncertainties, and we developed a two-phase metaheuristic based on large neighbourhood search to solve the problem. Numerical experiments illustrated the quality of the heuristic approach and the influence of several parameters on best found solutions. Several new best solutions were also identified when testing our two-phase heuristic on instances of the closely related robust capacitated vehicle routing problem (RCVRP).

Strategic planning problem

While the previous two papers concerned operational decision problems associated with EFVs (i.e., charging and routing), the fifth article of the thesis considered a strategic planning problem. More specifically, the final paper of the thesis introduced the EFTP, whose solution can provide strategic guidance to organizations having set fleet electrification targets to be met in the upcoming years. To the best of our knowledge, the EFTP is the first fleet replacement study associated with electric vehicles to take into account several types of electric vehicles with different charging configurations, charger type-specific infrastructure investments, facilities-related demand charges, and aggregated task assignment decisions. We performed an extensive public transit case study using real data, but we stress that the problem is just as applicable to goods distribution contexts as it is to public transit ones. The case study allowed us to derive meaningful insights regarding long-term transitions to electric fleets under several scenarios.

Future research

We conclude this thesis by highlighting a few interesting research avenues that are related to its contents. First, heuristic approaches could of course be considered for much larger instances of the EFV-CSP if need be. As mentioned in the conclusion of Chapter 3, we also believe that interesting research avenues lie in simultaneously optimizing the depot charging schedule and the routing of the vehicles over a multiple-day planning horizon, which would also require the development of heuristics. Second, future work related to the fourth paper could of course consider adding en route recharging into the problem to render it applicable to EVRPs in mid- and long-haul contexts, and developing new solution

methods for the EVRP-ECU in order to have more available benchmark solutions for the larger instances. Finally, with regard to the final paper of the thesis, specialized solution methods do not seem warranted for the deterministic version of the problem. However, interesting research avenues clearly lie in the development of sophisticated algorithms for the stochastic counterpart of the EFTP. Case studies similar to the one presented in Chapter 5 relative to a public transit context could also be performed for goods distribution contexts in order to derive managerial insights regarding the planning of cost-effective transitions to fleets with more EFVs.

Bibliography

Abdallah, T. 2013. The plug-in hybrid electric vehicle routing problem with time windows. Master's thesis, University of Waterloo, Canada.

Ahani, P., A. Arantes, S. Melo. 2016. A portfolio approach for optimal fleet replacement toward sustainable urban freight transportation. *Transportation Research Part D: Transport and Environment* **48** 357–368.

Ansaripoor, A.H., F.S. Oliveira, A. Liret. 2016. Recursive expected conditional value at risk in the fleet renewal problem with alternative fuel vehicles. *Transportation Research Part C: Emerging Technologies* **65** 156–171.

Arslan, O., B. Yıldız, O.E. Karaşan. 2014. Minimum cost path problem for plug-in hybrid electric vehicles. *Transportation Research Part E: Logistics and Transportation Review* **80** 123–141.

Artmeier, A., J. Haselmayr, M. Leucker, M. Sachenbacher. 2010. The shortest path problem revisited: Optimal routing for electric vehicles. R. Dillmann, J. Beyerer, U. Hanebeck, T. Schultz, eds., *KI 2010: Advances in Artificial Intelligence*. Lecture Notes in Computer Science, Vol. 6359 (Springer-Verlag, Berlin Heidelberg), 309–316.

Bakır, İ. 2017. Large scale optimization methods for fleet management in long-haul transportation networks. Ph.D. thesis, Georgia Institute of Technology, Georgia.

Basso, R., B. Kulcsár, B. Egardt, P. Lindroth, I. Sanchez-Diaz. 2019. Energy consumption estimation integrated into the electric vehicle routing problem. *Transportation Research Part D: Transport and Environment* **69** 141–167.

Bektaş, T., J.F. Ehmke, H.N. Psaraftis, J. Puchinger. 2018. The role of operational research in green freight transportation. *European Journal of Operational Research* **274**(3) 807–823.

Bongiovanni, C., M. Kaspi, N. Geroliminis. 2019. The electric autonomous dial-a-ride problem. *Transportation Research Part B: Methodological* **122** 436–456.

Breunig, U., R. Baldacci, R.F. Hartl, T. Vidal. 2019. The electric two-echelon vehicle routing problem. *Computers & Operations Research* **103** 198–210.

Bruglieri, M., S. Mancini, F. Pezzella, O. Pisacane, S. Suraci. 2017. A three-phase matheuristic for the time-effective electric vehicle routing problem with partial recharges. *Electronic Notes in Discrete Mathematics* **58** 95–102.

Dong, J., C. Liu, Z. Lin. 2014. Charging infrastructure planning for promoting battery electric vehicles: An activity-based approach using multiday travel data. *Transportation Research Part C: Emerging Technologies* **38** 44–55.

Eisner, J., S. Funke, S. Storandt. 2011. Optimal route planning for electric vehicles in large networks. W. Burgard, D. Roth, eds., *Proceedings of the Twenty-Fifth AAAI Conference on Artificial Intelligence* (AAAI, Menlo Park, CA), 1108–1113.

Erdelić, T., T. Carić. 2019. A survey on the electric vehicle routing problem: Variants and solution approaches. *Journal of Advanced Transportation*, Article ID 5075671.

Erdoğan, S., E. Miller-Hooks. 2012. A green vehicle routing problem. *Transportation Research Part E: Logistics and Transportation Review* **48**(1) 100–114.

Felipe, Á., M.T. Ortuño, G. Righini, G. Tirado. 2014. A heuristic approach for the green vehicle routing problem with multiple technologies and partial recharges. *Transportation Research Part E: Logistics and Transportation Review* **71** 111–128.

Feng, W., M. Figliozzi. 2013. An economic and technological analysis of the key factors affecting the competitiveness of electric commercial vehicles: A case study from the USA market. *Transportation Research Part C: Emerging Technologies* **26** 135–145.

Fontana, M.W. 2013. Optimal routes for electric vehicles facing uncertainty, congestion, and energy constraints. Ph.D. thesis, Massachusetts Institute of Technology, Massachusetts.

Frade, I., A. Ribeiro, G. Gonçalves, A.P. Antunes. 2011. Optimal location of charging stations for electric vehicles in a neighborhood in Lisbon, Portugal. *Transportation Research Record: Journal of the Transportation Research Board* **2252** 91–98.

Froger, A., J.E. Mendoza, O. Jabali, G. Laporte. 2017. A matheuristic for the electric vehicle routing problem with capacitated charging stations. CIRRELT Technical report, CIRRELT-2017-31.

Froger, A., J.E. Mendoza, O. Jabali, G. Laporte. 2019. Improved formulations and algorithmic components for the electric vehicle routing problem with nonlinear charging functions. *Computers & Operations Research* **104** 256–294.

Goeke, D. 2019. Granular tabu search for the pickup and delivery problem with time windows and electric vehicles. *European Journal of Operational Research*. doi.org/10.1016/j.ejor.2019.05.010. In Press.

Goeke, D., M. Schneider. 2015. Routing a mixed fleet of electric and conventional vehicles. *European Journal of Operational Research* **245**(1) 81–99.

Gonçalves, F., S.R. Cardoso, S. Relvas, A.P.F.D. Barbosa-Póvoa. 2011. Optimization of a distribution network using electric vehicles: A VRP problem. D. Cardoso, J. Clímaco, eds., *IO2011-15 Congresso da Associação Portuguesa de Investigação Operacional* (INESC, Coimbra, Portugal), 103–114.

González, J., R. Alvaro, C. Gamallo, M. Fuentes, J. Fraile-Ardanuy. 2014. Determining electric vehicle charging point locations considering drivers' daily activites. *Procedia Computer Science* **32** 647–654.

He, F., D. Wu, Y. Yin, Y. Guan. 2013. Optimal deployment of public charging stations for plug-in hybrid electric vehicles. *Transportation Research Part B: Methodological* **47** 87– 101.

Hiermann, G., J. Puchinger, S. Ropke, R.F. Hartl. 2016. The electric fleet size and mix vehicle routing problem with time windows and recharging stations. *European Journal of Operational Research* **252**(3) 995–1018.

Hiermann, G., R.F. Hartl, J. Puchinger, T. Vidal. 2019. Routing a mix of conventional, plug-in hybrid, and electric vehicles. *European Journal of Operational Research* **272**(1) 235–248.

Hof, J., M. Schneider, D. Goeke. 2017. Solving the battery swap station location-routing problem with capacitated electric vehicles using an AVNS algorithm for vehicle-routing problems with intermediate stops. *Transportation Research Part B: Methodological* **97** 102–112.

Islam, A. 2018. Minimization of carbon footprint of transit agencies by adopting alternative fuel technologies. M.Sc. thesis, University of Connecticut, Connecticut.

Jie, W., J. Yang, M. Zhang, Y. Huang. 2019. The two-echelon capacitated electric vehicle routing problem with battery swapping stations: Formulation and efficient methodology. *European Journal of Operational Research* **272**(3) 879–904.

Keskin, M., B. Çatay. 2018. A matheuristic method for the electric vehicle routing problem with time windows and fast chargers. *Computers & Operations Research* **100** 172–188.

Keskin, M., G. Laporte, B. Çatay. 2019. Electric vehicle routing problem with time-dependent waiting times at recharging stations. *Computers & Operations Research* **107** 77–94.

Kleindorfer, P.R., A. Neboian, A. Roset, S Spinler. 2012. Fleet renewal with electric vehicles at La Poste. *Interfaces* **42**(5) 465–477.

Koç, C., O. Jabali, J.E. Mendoza, G. Laporte. 2018. The electric vehicle routing problem with shared charging stations. *International Transactions in Operational Research* **26**(4) 1211–1243.

Lebeau, P., C. De Cauwer, J. Van Mierlo, C. Macharis, W. Verbeke, T. Coosemans. 2015. Conventional, hybrid, or electric vehicles: Which technology for an urban distribution centre? *The Scientific World Journal*, Article ID 302867.

Macrina, G., G. Laporte, F. Guerriero, L. Di Puglia Pugliese. 2019. An energy-efficient green-vehicle routing problem with mixed vehicle fleet, partial battery recharging and time windows. *European Journal of Operational Research* **276**(3) 971–982.

Mak, H.Y., Y. Rong, Z.J.M. Shen. 2013. Infrastructure planning for electric vehicles with battery swapping. *Management Science* **59**(7) 1557–1575.

Mancini, S. 2017. The hybrid vehicle routing problem. *Transportation Research Part C: Emerging Technologies* **78** 1–12.

Montoya, A., C. Guéret, J.E. Mendoza, J.G. Villegas. 2017. The electric vehicle routing problem with nonlinear charging function. *Transportation Research Part B: Methodological* **103** 87–110.

Nie, Y.M., M. Ghamami. 2013. A corridor-centric approach to planning electric vehicle charging infrastructure. *Transportation Research Part B: Methodological* **57** 172–190.

Preis, H., S. Frank, K. Nachtigall. 2014. Energy-optimized routing of electric vehicles in urban delivery systems. S. Helber, M. Breitner, D. Rösch, C. Schön, J-M. Graf von der Schulenburg, P. Sibbertsen, M. Steinbach, S. Weber, A. Wolter, eds., *Operations Research Proceedings 2012* (Springer International Publishing, Switzerland), 583–588.

Roberti, R., M. Wen. 2016. The electric traveling salesman problem with time windows. *Transportation Research Part E: Logistics and Transportation Review* **89** 32–52.

Rogge, M., E. van der Hurk, A. Larsen, D.U. Sauer. 2018. Electric bus fleet size and mix problem with optimization of charging infrastructure. *Applied Energy* **211** 282–295.

Sachenbacher, M., M. Leucker, A. Artmeier, J. Haselmayr. 2011. Efficient energy-optimal routing for electric vehicles. W. Burgard, D. Roth, eds., *Proceedings of the Twenty-Fifth AAAI Conference on Artificial Intelligence* (AAAI, Menlo Park, CA), 1402–1407.

Sassi, O., A. Oulamara. 2014a. Joint scheduling and optimal charging of electric vehicles problem. B. Murgante, S. Misra, A.M.A.C. Rocha, C. Torre, J.G. Rocha, M.I. Falcão, D. Taniar, B.O. Apduhan, O. Gervasi, eds., *ICCSA 2014 Proceedings, Part II*. Lecture Notes in Computer Science, vol. 8580 (Springer International Publishing, Switzerland), 76–91.

Sassi, O., A. Oulamara. 2014b. Simultaneous electric vehicles scheduling and optimal charging in the business context: Case study. *5th IET Hybrid and Electric Vehicles Conference* (IET, Stevenage, UK), 105–110.

Sassi, O., W.R. Cherif-Khettaf, A. Oulamara. 2015. Vehicle routing problem with mixed fleet of conventional and heterogenous electric vehicles and time dependent charging costs. *International Journal of Mathematical, Computational, Statistical, Natural and Physical Engineering* **9**(3) 148–158.

Schiffer, M., M. Schneider, G. Laporte. 2018. Designing sustainable mid-haul logistics networks with intra-route multi-resource facilities. *European Journal of Operational Research* **265**(2) 517–532.

Schiffer, M., G. Walther. 2017a. An adaptive large neighborhood search for the location routing problem with intraroute facilities. *Transportation Science* **52**(2) 331–352.

Schiffer, M., G. Walther. 2017b. The electric location routing problem with time windows and partial recharging. *European Journal of Operational Research* **260**(3) 995–1013.

Schiffer, M., G. Walther. 2018. Strategic planning of electric logistics networks: A robust location-routing approach. *Omega* **80** 31–42.

Schneider, M., A. Stenger, D. Goeke. 2014. The electric vehicle-routing problem with time windows and recharging stations. *Transportation Science* **48**(4) 500–520.

Strehler, M., S. Merting, C. Schwan. 2017. Energy-efficient shortest routes for electric and hybrid vehicles. *Transportation Research Part B: Methodological* **103** 111–135.

Sweda, T.M., I.S. Dolinskaya, D. Klabjan. 2016. Optimal recharging policies for electric vehicles. *Transportation Science* **51**(2) 457–479.

Sweda, T.M., I.S. Dolinskaya, D. Klabjan. 2017. Adaptive routing and recharging policies for electric vehicles. *Transportation Science* **51**(4) 1326–1348.

Touati-Moungla, N., V. Jost. 2012. Combinatorial optimization for electric vehicles management. *Journal of Energy and Power Engineering* **6**(5) 738–743.

van Duin, J.H.R., L.A. Tavasszy, H.J. Quak. 2013. Towards e(lectric)-urban freight: First promising steps in the electric vehicle revolution. *European Transport*, Issue 54, Paper no.9.

Villegas, J.G., C. Guéret, J.E. Mendoza, A. Montoya. 2018. The technician routing and scheduling problem with conventional and electric vehicles. Working paper hal-01813887. URL `https://hal.archives-ouvertes.fr/hal-01813887/document`. Last accessed May 2019.

Wang, I.-L., Y. Wang, P.C. Lin. 2016. Optimal recharging strategies for electric vehicle fleets with duration constraints. *Transportation Research Part C: Emerging Technologies* **69** 242–254.

Xu, H., S. Miao, C. Zhang, D. Shi. 2013. Optimal placement of charging infrastructures for large-scale integration of pure electric vehicles into grid. *International Journal of Electrical Power & Energy Systems* **53** 159–165.

Yang, J., H. Sun. 2015. Battery swap station location-routing problem with capacitated electric vehicles. *Computers & Operations Research* **28** 217–232.

Yıldız, B., E. Olcaytu, A. Şen. 2019. The urban recharging infrastructure design problem with stochastic demands and capacitated charging stations. *Transportation Research Part B: Methodological* **119** 22–44.

Zündorf, T. 2014. Electric vehicle routing with realistic recharging models. Master's thesis, Karlsruhe Institute of Technology, Germany.